

UNIVERSITÄT
BAYREUTH



Heterogeneous Iron Catalysts for the Chemoselective Synthesis of Primary Amines and the Hydrogenation of N-Heteroarenes

Dissertation

zur Erlangung des akademischen Grades
eines Doktors der Naturwissenschaften (Dr. rer. nat.)
an der Fakultät für Biologie, Chemie und Geowissenschaften
der Universität Bayreuth

vorgelegt von

M. Sc. Christoph Norbert Hermann Bäumler

geboren in Sulzbach-Rosenberg

Bayreuth, 2020

Die vorliegende Arbeit wurde in der Zeit von Juni 2017 bis September 2020 in Bayreuth am Lehrstuhl Anorganische Chemie II unter Betreuung von Herrn Professor Dr. Rhett Kempe angefertigt.

Vollständiger Abdruck der von der Fakultät für Biologie, Chemie und Geowissenschaften der Universität Bayreuth genehmigten Dissertation zur Erlangung des akademischen Grades eines Doktors der Naturwissenschaften (Dr. rer. nat.).

Dissertation eingereicht am: 30.09.2020

Zulassung durch Promotionskommission: 08.10.2020

Wissenschaftliches Kolloquium: 02.03.2021

Amtierender Dekan: Prof. Dr. Matthias Breuning

Prüfungsausschuss:

Prof. Dr. Rhett Kempe	(Gutachter)
-----------------------	-------------

Dr. habil. Günter Motz	(Gutachter)
------------------------	-------------

Prof. Dr. Rainer Schobert	(Vorsitz)
---------------------------	-----------

JProf. Dr. Mirjam Zobel	
-------------------------	--

Meiner Familie in Dankbarkeit gewidmet.

Table of Contents

Abbreviations	9
1. Summary/Zusammenfassung	11
1.1 Summary	11
1.2 Zusammenfassung	13
2. Introduction	17
2.1 Important role of heterogeneous earth-abundant 3d metal catalysts in organic synthesis	17
2.2 Heterogeneous catalyst systems based on polymer-derived ceramics (PDCs) as support materials.....	19
2.3 Hydrogenation of nitroarenes	20
2.4 Reductive amination of carbonyl compounds to primary amines	22
2.5 Selective hydrogenation of N-heterocycles.....	23
2.6 References	24
3. Overview over the thesis results.....	28
3.1 Synopsis	28
3.2 Individual contribution to joint publications.....	38
4. The Direct Synthesis of Imines, Benzimidazoles and Quinoxalines from Nitroarenes and Carbonyl Compounds via Selective Nitroarene Hydrogenation Employing a Reusable Iron Catalyst.....	40
4.1 Introduction	40
4.2 Results and Discussion.....	41
4.3 Acknowledgements	48
4.4 References	49
4.5 Supporting Information	52
4.5.1 General Considerations.....	52
4.5.2 Synthesis and characterization of the Fe nanocomposite.....	53
4.5.3 Catalytic studies	58

4.5.4	Characterization of isolated products	61
4.5.5	References	95
5.	The synthesis of primary amines via reductive amination employing an iron catalyst	96
5.1	Introduction	96
5.2	Results and Discussion	98
5.3	Acknowledgements	106
5.4	References	106
5.5	Supporting Information	109
5.5.1	General Considerations.....	109
5.5.2	Synthesis and characterization of the Fe/(N)SiC catalyst.....	110
5.5.3	Catalytic studies	119
5.5.4	Characterization of isolated products	123
5.5.5	References	193
6.	Hydrogenation of various N-heterocycles Employing a Heterogeneous Iron Catalyst	194
6.1	Introduction	194
6.2	Results and Discussion	196
6.3	Acknowledgements	201
6.4	References	201
6.5	Supporting Information	204
6.5.1	General considerations	204
6.5.2	General catalytic procedures	205
6.5.3	Characterization of isolated products	205
7.	List of publications	213
8.	Acknowledgements.....	215
9.	Declaration / Erklärung	217

Abbreviations

AAS	Atom absorption spectroscopy
AIBN	Azobisisobutyronitrile
Ap ^{TMS} H	4-Methyl-2-((trimethylsilyl)amino)pyridine
BET	Brunauer-Emmet-Teller
DCP	Dicumylperoxide
DFT	Density functional theory
DMF	Dimethylformamide
DMSO	Dimethyl sulfoxide
EA	Elemental analysis
EDX	Energy-dispersive X-ray spectroscopy
FFT	Fast Fourier Transformation
FTIR	Fourier-transform infrared spectroscopy
GC	Gas chromatography
GC-MS	Gas chromatography-mass spectrometry
HTT 1800	Commercially available polysilazane precursor
ICP-OES	Inductively coupled plasma optical emission spectrometry
MOF	Metal-organic framework
NP	Nanoparticle
NMR	Nuclear magnetic resonance
NLDFT	Non-linear density functional theory
OAc	Acetate
PAN	Polyacrylonitrile
PDC	Polymer derived ceramic
ppm	parts per million

PXRD	Powder X-ray diffraction spectroscopy
SEM	Scanning electron microscope
SiC	Silicon carbide
SiCN	Silicon carbonitride
SMP 10	Polycarbosilan
SQUID	Superconducting quantum interference device
TEA	Triethylamine
TEM	Transmissions electron microscopy
THF	Tetrahydrofuran
TPR	Temperature programmed reduction
TPD	Temperature programmed desorption
XPS	X-ray photoelectron spectroscopy

1. Summary/Zusammenfassung

1.1 Summary

This thesis deals with the development of reusable iron hydrogenation catalysts and their application in selective organic synthesis. The main focus of this work is the synthesis of primary amines. Follow up reactions originated from this motive and gave impulses for further catalytic applications, such as the hydrogenation of N-heteroarenes (Figure 1). The iron catalysts presented here are the product of a detailed investigation of various metal complexes, support materials and the combination of both in a constructive way as shown in Figure 1.

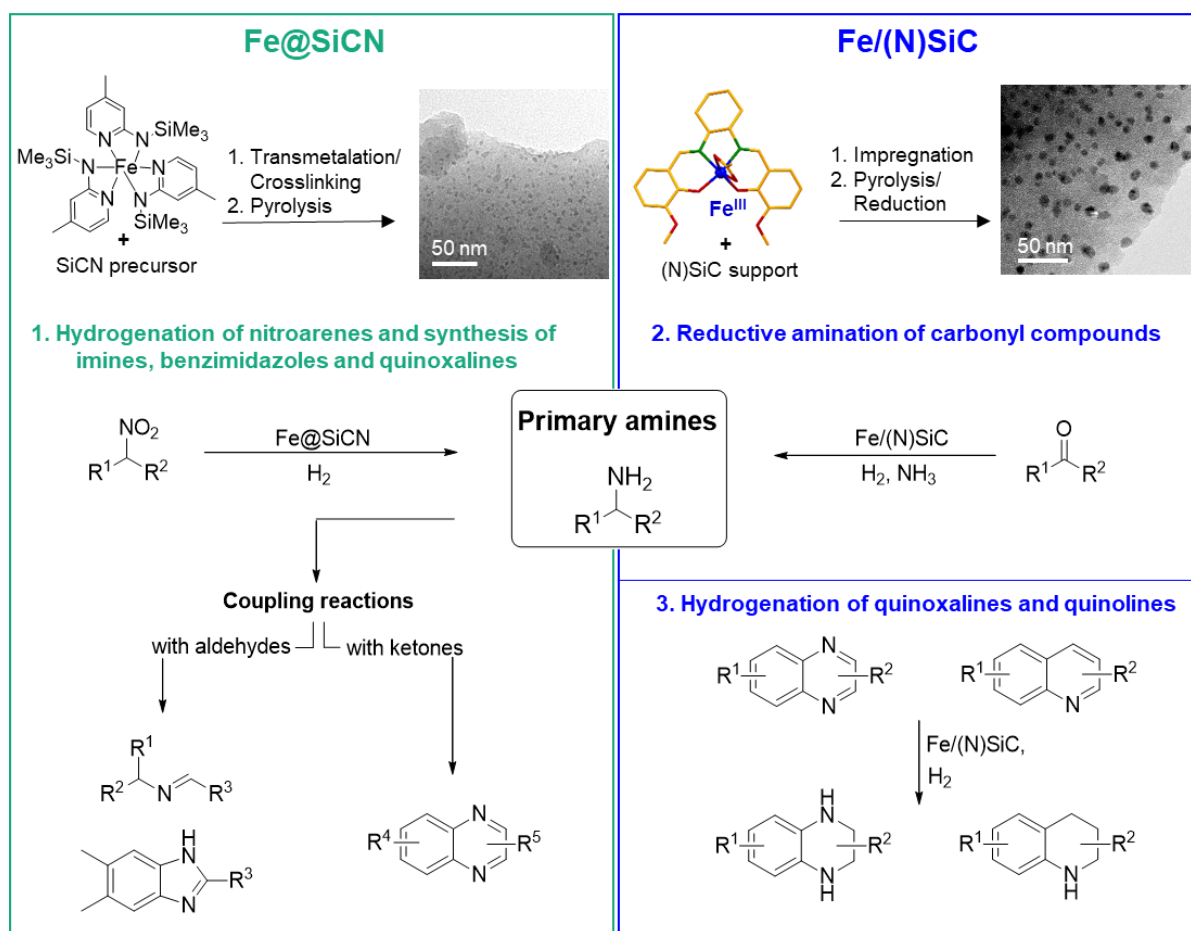


Figure 1: Overview of the two developed catalyst systems Fe@SiCN and Fe/(N)SiC and their applications in the organic synthesis via hydrogenation reactions. (Molecular structure of the complex used for the synthesis of the Fe/(N)SiC catalyst was determined by X-ray single crystal structure analysis; color code: green = N, red = O, orange = C, blue = Fe).

First, a robust and reusable Fe@SiCN catalyst with excellent properties in the chemoselective hydrogenation of nitro compounds is introduced. The generation of this mesoporous nanocomposite material was accomplished following a molecular synthesis pathway, starting with the transfer of the

iron ion from the iron complex to the preceramic polymer HTT-1800 by transmetalation. After crosslinking, the greenbody was pyrolyzed under nitrogen atmosphere at 750 °C, resulting in the amorphous Fe@SiCN catalyst. Magnetic measurements confirmed the transition from a paramagnetic behavior of Fe³⁺ ions in the greenbody to superparamagnetic properties of the pyrolyzed nanocomposite, indicating the formation of small iron nanoparticles. Further analysis via transmission electron microscopy (TEM) verified the existence of homogeneously distributed nanoparticles with an average particle size of 5 nm. X-ray photoelectron spectroscopy (XPS) indicated the presence of metallic Fe and surface iron oxide species in the as-synthesized Fe@SiCN material. Nitrogen physisorption measurements revealed that 91 % of the specific surface area of 101 m²g⁻¹ are caused by mesopores smaller than 10 nm. The Fe@SiCN catalyst proved to be highly active in the reduction of various nitroarenes to their corresponding aniline derivatives at optimized reaction conditions of 6.0 MPa hydrogen pressure, solvent mixture of 3:1 water/triethylamine and a reaction time of 20 h at 120 °C. The catalyst exhibited an impressive chemoselectivity towards functional groups, especially hydrogenation-sensitive ones such as nitriles, amides, ketones or aldehydes. Based on the tolerance of carbonyl functionalities, new protocols for the synthesis of 11 imines, 6 benzimidazoles and 6 quinoxalines from nitroarenes and aldehydes/diketones in excellent yields were introduced. Moreover, the robust and easy to handle catalyst is reusable over several runs, additionally, any loss of activity can be easily restored by temperature programmed reduction (TPR) treatment.

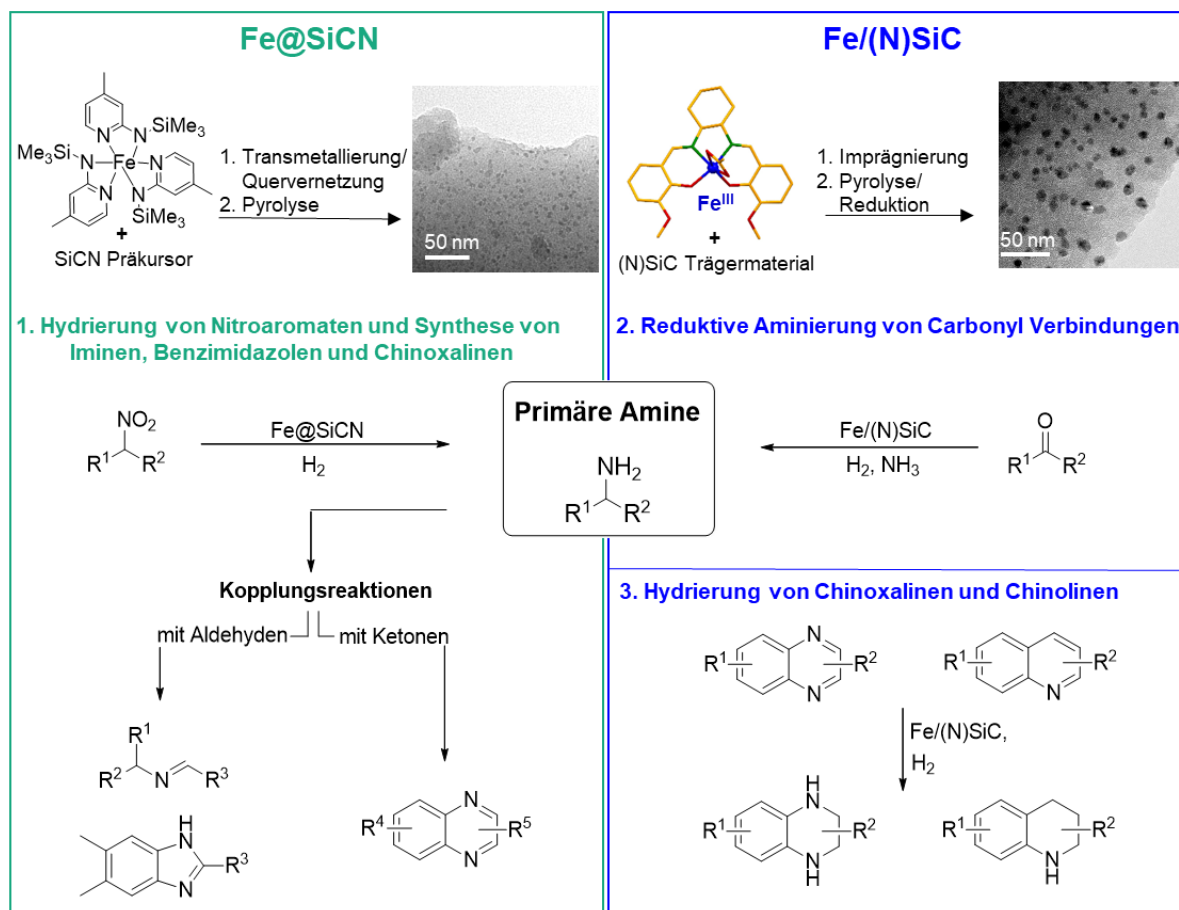
Then, a novel catalyst system was developed to enable further challenging catalytic applications like the reductive amination of carbonyl compounds to primary amines. The new catalyst was synthesized by wet impregnating a (N)SiC (N-doped SiC material) support material with a specific iron salen complex (Figure 1, top right), followed by a pyrolysis step (750 °C / N₂-atmosphere) and a reduction step (550 °C / forming gas). The generation of homogeneously distributed metallic iron nanoparticles with an average size of 10 nm was confirmed via energy-dispersed X-ray (EDX) and TEM analysis. XPS measurements indicated the presence of metallic and oxidic iron species on the catalyst surface. Further investigations of the catalyst by powder X-ray diffraction (PXRD) showed matching reflexes for cubic iron, which was also verified by High-Resolution-TEM analysis of the lattice spacing of the iron nanoparticles. Nitrogen physisorption measurements of the catalyst revealed a microporous surface area of 415 m²g⁻¹. The application of the Fe/(N)SiC in the reductive amination of carbonyl compounds yielded optimal results when 3.5 mL of 25 % aqueous ammonia and 6.5 MPa H₂ are used at 130-140 °C and the reaction was run for 20 h. The catalytic performance was excellent and various ketones, including purely aliphatic ones, aryl-alkyl, dialkyl and heterocyclic were converted into their corresponding primary amines. Furthermore, aldehydes could be reductively aminated, which tend to

undergo various of side reactions. In addition, the high potential of this catalyst in industrially relevant applications was demonstrated by the amination of pharmaceuticals, bioactive compounds and natural products. Many functional groups, such as hydroxy, methoxy, dioxol, sulfonyl and boronate esters were well tolerated. The reusability up to five consecutive runs of this easy to synthesize catalyst and the upscaling to gram-scale of the reaction has been demonstrated.

As a consequence of the high catalytic activity of the above-mentioned Fe/(N)SiC catalyst in the hydrogenation of an imine during the reductive amination, further investigations were focused on the hydrogenation of N-heteroarenes, especially quinolines and quinoxalines. The partly hydrogenated 1,2,3,4-tetrahydro-quinolines and -quinoxalines represent a class of compounds that has attracted a lot of attention due to their immense utility as building blocks and key intermediates in the synthesis of pharmaceuticals, agrochemicals, and other fine chemicals. The Fe/(N)SiC catalyst showed the best performance using 10 mol% Fe, 3 mL methanol, 150 °C and 6.5 MPa H₂ for 24 h. The high selectivity towards the hydrogenation of the heterocyclic part of the compound was demonstrated on 10 different (iso)quinoline based substrates with various functional groups such as methoxy, hydroxy or chloride. Even polycyclic N-heteroarenes like 1,10-phenanthroline could be partly hydrogenated to 1,2,3,4-tetrahydro-1,10-phenanthroline. Finally, quinoxalines were selectively converted to their corresponding tetrahydroquinoxalines. In particular, the introduction of sterically demanding substituents including a pyridine motive was achieved, which shows the great selectivity towards different types of N-heterocycles.

1.2 Zusammenfassung

Diese Dissertation beschäftigt sich mit der Entwicklung von wiederverwendbaren Eisenkatalysatoren für Hydrierungsreaktionen und deren Anwendung in der selektiven organischen Synthese. Die Herstellung von primären Aminen stellt dabei die Kernthematik dar, wodurch Anregungen für weitere katalytische Anwendungen, wie z.B. die Hydrierung von N-Heteroaromaten, resultierten. Die in Abbildung 1 dargestellten Eisenkatalysatoren basieren auf einer detaillierten Recherche verschiedener Metallkomplexe und Trägermaterialien, sowie deren sinnvoller Kombination zur Herstellung aktiver Katalysatorsysteme.



Reaktionsbedingungen von 6.0 MPa H₂, einem Lösungsmittelgemisch aus 3:1 Wasser/Triethylamin und einer Reaktionsdauer von 20 h bei 120 °C als sehr aktiv in der Reduktion verschiedener Nitroarenen zu den entsprechenden Anilinderivaten herausgestellt. Des Weiteren verfügt der Fe@SiCN Katalysator über eine besonders hohe Chemoselektivität gegenüber funktionellen Gruppen, insbesondere von hydrierempfindlichen, wie z.B. Nitrilen, Amiden, Ketonen oder Aldehyden. Basierend auf der Toleranz gegenüber Carbonylverbindungen konnten neue Syntheseprotokolle für die Herstellung von 11 Iminen, 6 Benzimidazolen und 6 Quinoxalinen ausgehend von Nitroaromaten und Aldehyden/Diketonen angewendet werden. Der robuste Fe@SiCN Katalysator überzeugt durch eine leichte Handhabung und ist mehrmals wiederverwendbar. Zudem konnte gezeigt werden, dass jeglicher Verlust an Katalysatoraktivität durch TPR Behandlung wiederherstellbar ist.

Zur Erschließung neuer anspruchsvoller katalytischer Anwendungsmöglichkeiten, wie z.B. die reduktive Aminierung von Carbonylverbindungen, wurde ein neues Katalysatorsystem entwickelt. Die Herstellung erfolgte im ersten Schritt durch die Nassimprägnierung eines (N)SiC (N-dotiertes SiC Material) Trägermaterials mit einem speziellen Eisen Salen Komplex (Abbildung 1, oben rechts). Anschließend wurde das Material bei 750 °C in N₂-Atmosphäre pyrolysiert und im Anschluss bei 550 °C reduziert. Die Generierung von homogen verteilten metallischen Eisennanopartikeln mit einer durchschnittlichen Partikelgröße von 10 nm wurde mittels EDX und TEM Analysen verifiziert. XPS Untersuchungen der Katalysatoroberfläche ergaben, dass sich sowohl metallische als auch oxidische Eisenspezies auf der Oberfläche befinden. Durch die Charakterisierung des Fe/(N)SiC Katalysators mittels PXRD konnten die erhaltenen Reflexe der einzelnen Netzebenen, denen des kubischen Eisens zugeordnet werden. Diese Ergebnisse konnten durch HR-TEM Analysen der Netzebenenabstände der Eisennanopartikel bestätigt werden. N₂-Physisorptionsmessungen zeigten, dass die spezifische Oberfläche von 415 m²g⁻¹ durch Mikroporen generiert wurde. Als optimale Bedingungen für die Anwendung in der reduktiven Aminierung von Carbonylverbindungen ergaben sich 3.5 mL einer wässrigen Ammoniaklösung (25 %) und 6.5 MPa H₂ bei 130-140 °C für 20 h. Die katalytische Performance des Katalysators war exzellent, was durch die Umsetzung verschiedener Ketone, insbesondere von aliphatischen, aryl-alkyl, dialkyl, heterozyklischen oder von Aldehyden zu den entsprechenden primären Aminen gezeigt wurde. Des Weiteren konnte durch die Aminierung von Pharmazeutika oder von biologisch aktiven Molekülen das hohe Potential des Katalysatorsystems für industrielle Anwendungen demonstriert werden. Diverse funktionelle Gruppen, wie z.B. Hydroxy-, Methoxy-, 1,3-Dioxolan-, Sulfonyl-Substituenten oder Boronsäureester konnten toleriert werden. Der Katalysator lässt sich einfach herstellen, ist wiederverwendbar und überzeugt durch eine leichte

Handhabung. Die Möglichkeit die Reaktion im Gramm Maßstab durchzuführen konnte ebenfalls demonstriert werden.

Aufgrund der hohen katalytischen Aktivität des Fe/(N)SiC Katalysators im Hydrierungsschritt der reduktiven Aminierung, wurde das Katalysatorsystem in der Reduktion von N-Heteroaromaten (Chinoline und Chinoxaline) getestet. Die selektiv hydrierten 1,2,3,4-Tetrahydrochinoline oder -chinoxaline stellen eine Klasse von Verbindungen dar, die aufgrund ihrer besonderen Nützlichkeit als Bausteine und Schlüsselzwischenprodukte bei der Herstellung von Arzneimitteln, Agrochemikalien und anderen Feinchemikalien viel Aufmerksamkeit erregt haben. Unter Verwendung von 10 mol% Fe, 3 mL Methanol, 150 °C und 6.5 MPa H₂ für 24 h, konnten die besten katalytischen Umsätze generiert werden. Die hohe Selektivität des Katalysators lediglich den heterozyklischen Teil der Verbindung zu hydrieren, wurde anhand 10 verschiedener (Iso)Chinolin Verbindungen mit unterschiedlichen funktionellen Gruppen (Hydroxy, Methoxy, Chlorid) verdeutlicht. Außerdem konnten polyzyklische N-Heteroaromaten, wie z.B. 1,10-Phenanthrolin, zum entsprechenden 1,2,3,4-Tetrahydro-1,10-phenanthrolin selektiv hydriert werden. Zuletzt wurden Chinoxaline bei erhöhter Reaktionszeit und -temperatur zu den entsprechenden Tetrahydrochinoxalinen umgesetzt. Die Einführung von sterisch anspruchsvollen Substituenten, mitunter von Pyridin basierten, zeigt die besondere Selektivität des Katalysators gegenüber verschiedener N-Heterozyklen.

2. Introduction

2.1 *Important role of heterogeneous earth-abundant 3d metal catalysts in organic synthesis*

The development of advanced sustainable and efficient processes in the synthesis of functionalized molecules is a cornerstone in the green chemistry. An important issue considering sustainability is the production of chemical compounds from biomass derived substrates and not from nonrenewable petroleum feedstocks. Therefore, the conservation of resources, especially rare metals which are commonly used in key technologies and in catalysis, is a very important target to ensure the availability of these elements for future generations. One promising approach is the replacement of catalysts based on rare noble metals like ruthenium, rhodium, iridium, platinum or palladium by earth-abundant 3d transition metal catalysts which are essential elements of living bodies with a quite less toxicity. Another advantage is that catalysts based on these abundant metals have a totally different selectivity pattern than known systems with precious metals, enabling new synthetic pathways and reactions. As depicted in Figure 2.1, one benefiting point is the higher abundance of the 3d metals like iron, cobalt, manganese or nickel in the earth's crust which leads to cheaper prices.

^[1] Relating to the active species in the heterogeneous catalyst, it is important to compare the prices per mol, which indicates the real differences between the metals including their molecular weights. Regarding the price of pig iron (0.02 €/mol; around 94 % iron content) and for example cobalt (1.77 €/mol), the difference lies at the factor of approximately 85, which is a result of the enormous abundance of iron in the earth's crust (Fe: 56300 mg/kg vs Co: 25 mg/kg). The enormous potential of iron becomes apparent by comparison with noble metals like rhodium or iridium. The relative abundances of these metals in the earth's crust are 0.001 and 0.015 mg/kg with a price per mol of 24412 €/mol for rhodium and 4500 €/mol for iridium, which reveals a completely different price level with an alarming low abundance.^[1] Regarding the relative frequency of the 3d metals in the earth's crust, especially iron, and their positive catalytic properties, a replacement of the precious metals seems to be desirable.

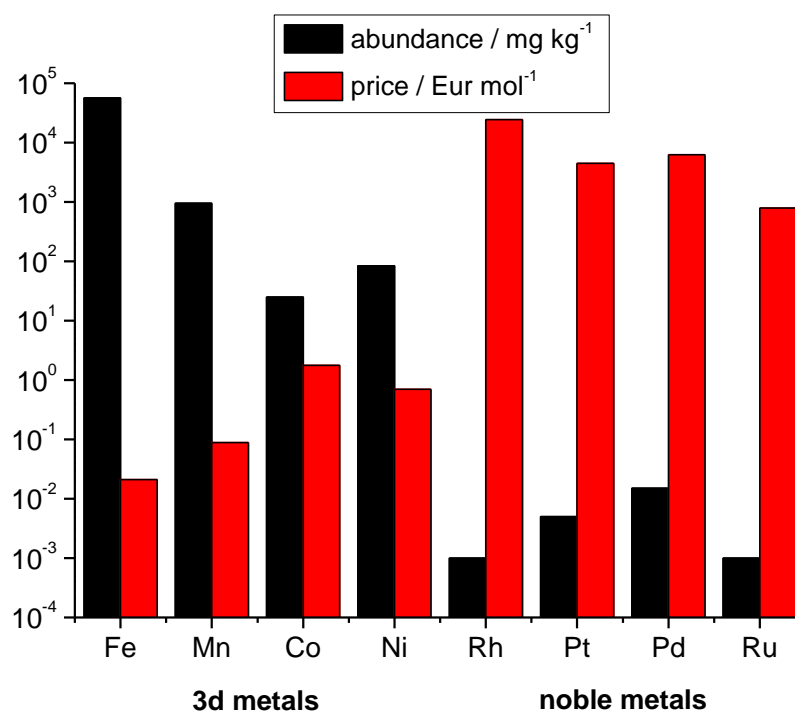


Figure 1: Comparison of the abundances and prices of different noble and earth-abundant 3d metals commonly used in catalysis.

Hence, significant progress has been made in the field of homogeneous earth-abundant 3d metal catalysis in recent years. Especially (de)hydrogenation reactions turned out to be a very promising approach for the substitution of the high-price noble metals with cobalt, iron or manganese.^[2] *Beller et al.* introduced an iron catalyst system, based on $\text{Fe}(\text{BF}_4)_2$ and a special phosphine ligand, for the liberation of H_2 from formic acid via dehydrogenation.^[3] The iron catalyzed selective anti-markovnikov alkene hydrosilylation using tertiary silanes was accomplished by *Chirik and coworkers*. Another interesting work of *Chirik and coworkers* deals with the application of a cobalt catalyst in the asymmetric alkene hydrogenation with chiral phosphine ligands.^[4] *Morris and coworkers* developed an iron-based catalyst system which enables the asymmetric transfer hydrogenation of ketones and imines.^[5] The reduction of esters and carboxylic acids to alcohols was reported by *de Bruin and coworkers* applying a catalyst system consisting of $\text{Co}(\text{BF}_4) \cdot \text{H}_2\text{O}$ and a tridentate phosphine ligand.^[6] *Kempe and coworkers* introduced a manganese-based catalyst for the selective hydrogenation of ketones and aldehydes.^[7] Also, the synthesis of pyrroles (from alcohols and aminoalcohols)^[8] and pyrimidines (from alcohols and amidines)^[9] was realized by this group.

The use of reusable nanostructured earth-abundant 3d metal catalysts for a broad applicability in complex organic synthesis is highly desirable and has been disclosed significantly less. *Beller and coworkers* started the development of efficient, highly active and selective catalyst systems based on iron and cobalt, which achieved high yields by mild conditions compared to previous works. The generation of cobalt- or iron-oxide nanoparticles on a carbon support material through impregnation

and pyrolysis led to active catalyst systems in the hydrogenation of nitroarenes. The hydrogenation of heteroarenes was achieved with a cobalt catalyst, consisting of cobalt oxide nanoparticles embedded on a α - Al_2O_3 support material. Furthermore, the impregnation of an in situ generated Co-MOF (Metal Organic Framework) on a carbon support followed by pyrolysis, generated a cobalt catalyst system for the synthesis of primary amines via reductive amination of carbonyl compounds.^[10] Another interesting work in the reductive amination of ketones and aldehydes was made by *Kempe and coworkers*, which discovered that a nickel catalyst supported by γ - Al_2O_3 and synthesized from a specific nickel complex achieved high yields under very mild conditions by employing ammonia dissolved in water.^[11]

2.2 Heterogeneous catalyst systems based on polymer-derived ceramics (PDCs) as support materials

In general, polymer derived ceramics (PDCs) were synthesized by pyrolysis of mostly silicon based preceramic polymers. There are two broad classes of PDCs which can be divided in binary systems like silicon-carbide (SiC) and ternary or higher order systems like SiCN or SiCNO. The great advantage of these materials is, that their properties are tunable due to the microstructure of the preceramic polymers and are much easier to handle regarding problems by the production of ceramics with the powder technology.^[13] Hence, significant technological breakthroughs in ceramic science including developments like ceramic fibers, coatings or high-temperature stable ceramics could be achieved. The precursor derived PDCs exhibit in general enhanced thermo-mechanical properties regarding oxidation resistance up to 1600 °C without any notable mechanical creep, stability with respect to crystallization, decomposition and corrosion resistance.^[13-15] Due to their excellent thermo-mechanical properties the application potential for catalysis is very high. Among non-oxidic ceramics SiCN and SiC materials have proven to be very suitable materials for catalyst systems, due to their robustness and high temperature stability. Synthetic strategies for these metal containing PDCs can be divided in many categories.^[16,17] The chemical approach is to mix the preceramic polymers with metal-powder or -oxides before they undergo crosslinking and pyrolysis. The molecular approach is to use metal complexes instead. Another interesting possibility is the use of the PDCs as support materials which were impregnated with metal salts or complexes followed by pyrolysis. The main difference between these approaches is, that the impregnation method mainly generates nanoparticles on the surface near term area and the chemical method directly in the nanocomposite matrix.^[16,17] Therefore, it is very important to have a great porosity to have access to the active metal centers in the nanocomposite matrix for catalytic approaches.

Our group established the introduction of a broad variety of metals via metal complexes in the ceramic precursor. *Glatz and coworkers* introduced a catalyst based on a system synthesized from a copper aminopyridinate complex and from a commercially available polysilazane precursor HTT 1800. The resulting Cu@SiCN catalyst was applied in the selective oxidation of cycloalkanes.^[17] Resultant works were published with various metal sources. *Zaheer and coworkers* developed a Pd₂Si@SiCN catalyst for the hydrogenation of aromatic ketones to alcohols, a Ni@SiCN system for the hydrogenation of alkynes and a mesoporous structured Ni@SiC catalyst for the hydrogenolysis of aryl ethers.^[18] The synthesis of pyrroles from secondary alcohols and 1,2-amino alcohols were accomplished with an Ir@SiCN catalyst.^[19] Another interesting approach was the introduction of a bimetallic Pd₂Ru@SiCN catalyst system for a novel hydrogen storage system^[20] or system consisting of three different catalysts (Ru@SiCN, Ir@SiCN, Pd@SiCN) for the synthesis of carbazoles, quinolines and acridines.^[21] Also, the introduction of earth-abundant 3d metals was further developed including Co@SiCN^[22], mesoporous structured Ni@PS₆₀SiCN^[23] and Co@N-SiC^[24] catalysts for the selective hydrogenation of nitroarenes. The combination of a SiC preceramic material with a cobalt phenanthroline complex led to a Co@N-SiC catalyst which was used for the selective hydrogenation of nitroarenes.^[25]

The use of earth-abundant metals such as iron in combination with preceramic polymers were introduced as part of this doctor thesis.^[25,26]

2.3 Hydrogenation of nitroarenes

The hydrogenation of nitroarenes is the method of choice for the synthesis of aniline derivatives, an important class of compounds.^[27] Already in 1989, Haber proposed a reaction pathway for the reduction of nitrobenzene including possible side reactions and intermediate products.^[28] Today, this proposed mechanistic pathway is generally accepted for describing the step by step reduction of nitroarene.

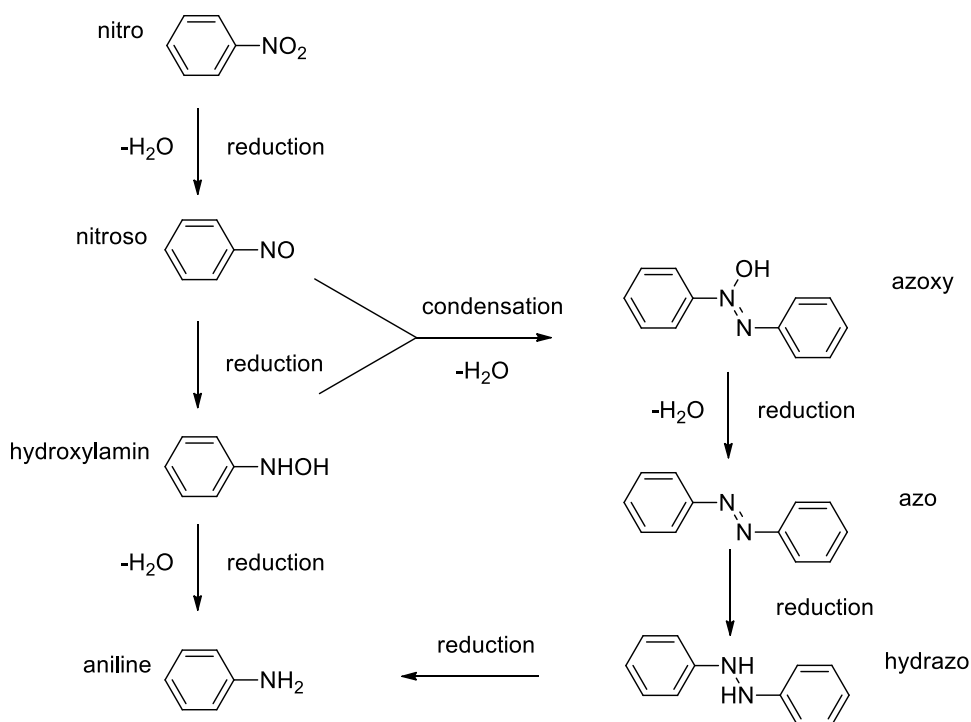


Figure 2: Proposed reaction pathway for the hydrogenation of nitroarenes by Haber.^[27]

The reaction pathway (Figure 3) shows, that the catalyst must be highly active to avoid the condensation reaction of nitroso and hydroxylamine. The reduction of hydroxylamine is the rate determining step in this reaction and depends on factors such as reaction temperature or hydrogen pressure.^[29] Therefore, the reduction step of the nitro group over the nitroso intermediate to the hydroxylamine is very fast.

Great progress in the field of the chemoselective hydrogenation of nitroarenes where made by the *group of Siegrist* 1998.^[27] Modification of commercial Pt/C catalysts with H₃PO₂ promoted by V complexes led to the toleration of bromide, iodide, carbonyl, nitrile, alkene and alkyne functional groups.^[30] *Corma et al.* made the breakthrough in the chemoselective hydrogenation with a heterogeneous gold catalyst which was supported by different materials like TiO₂. The selectivity towards functional groups like alkene, aldehyde, nitrile or amide in the presence of the nitro groups was over 95 % at conversions higher than 98 %.^[31] In the following, *Beller and coworkers* introduced works based on earth-abundant 3d metals (e.g. Fe^[32], Co^[33]) with excellent chemoselectivity and broad substrate scopes. Based on these initial works, a variety of groups developed Co based catalysts^[34] including our group, which introduced a Co@SiCN based system with great selectivity pattern against functional groups and the application of follow up reactions based on the generated amines.^[35]

2.4 Reductive amination of carbonyl compounds to primary amines

In general, the reductive amination of ketones and aldehydes is the method of choice for the synthesis of alkyl amines from inexpensive and diversely available compounds.^[36] The synthesis of primary amines by employing ammonia as the nucleophile is especially attractive and challenging.^[37] *Mignonac* showed in 1921, that the reductive amination of aldehydes or ketones to their corresponding primary amines, can be mediated by a nickel catalyst employing ammonia as nitrogen source.^[38]

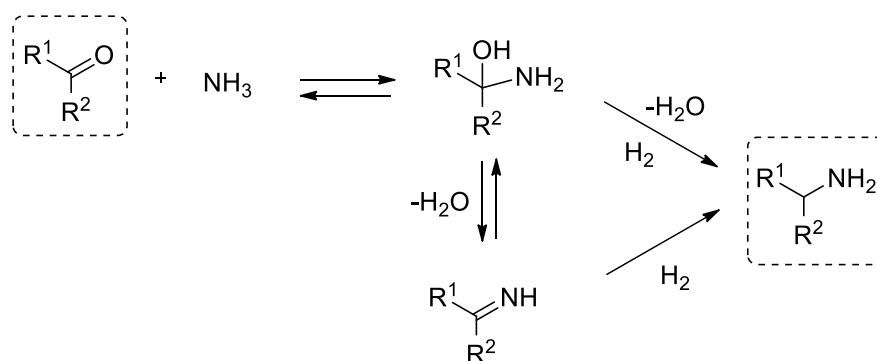


Figure 3: Proposed mechanism for the reductive amination of carbonyls by *Mignonac*.^[38]

In the first reaction step, the amine source reacts with the carbonyl group to form a hemiaminal (carbinolamine). *Mignonac* proposed that the primary amine can be either generated by direct hydrogenolysis of the hemiaminal or by hydrogenation of the formed imine. Secondary and tertiary amines can be obtained if the formed primary/secondary amine reacts directly with the remaining carbonyl compound. Another notable side reaction is the hydrogenation of the carbonyl compound to the corresponding alcohol.^[38,39] Consequently, it is extremely sophisticated to generate primary amines with high selectivity, since the afore mentioned side reactions have to be avoided.^[37-39] Most of the early works-based on Raney nickel or common noble metal catalysts show a quite low toleration of functional groups and a small substrate scope.^[40] *Beller et al.* introduced the first cobalt based catalyst for the chemoselective reductive amination of carbonyl compounds.^[41] The catalyst was prepared by the impregnation of an in situ generated cobalt MOF (Metal-organic framework) on a carbon support, followed by pyrolysis under argon atmosphere. The catalyst was highly active in the reductive amination and gave access to a very broad substrate scope including various of functional groups. *Hahn and coworkers* developed a Ni/Al₂O₃ catalyst by the impregnation of a nickel complex on γ-Al₂O₃ and pyrolysis.^[42] The catalyst performs the reductive amination by very mild conditions: 80 °C and 1.0 MPa H₂ for 20 h using a catalyst loading of 1.4 mol% Ni. Based on these initial works, further Co and Ni based catalysts were described.^[43]

2.5 Selective hydrogenation of N-heterocycles

The reduction of N-heteroarenes to their corresponding partially or completely saturated derivatives has attracted increased attention due to their immense utility as biologically active building blocks and key intermediates in the manufacture of pharmaceuticals, agrochemicals, and other fine chemicals.^[44] Catalysts that are able to hydrogenate only the nitrogen containing aromatic rings are extremely desirable in the production of complex molecules. Regarding quinoline, the motive of 1,2,3,4-tetrahydroquinolines (THQs) is part of various natural products and synthetic bioactive compounds. Well known drugs based on this motive are Oxamniquine for the treatment of *Schistosoma mansoni* infection, Nicainoprol for cardiac arrhythmias or viratmycin as an antibiotic.^[45] Substituted 1,2,3,4-tetrahydroquinoxalines (THQXs) are important structure motives for the synthesis of tetrahydrofolic acid^[46] and potent cholesteryl ester transfer protein inhibitors for different treatments like for atherosclerosis.^[47]

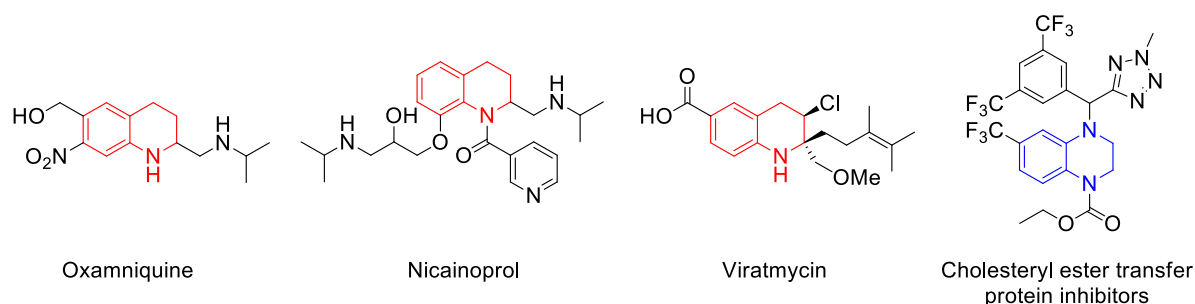


Figure 4: THQ and THQX derivatives in the application of drugs.

The first reported heterogeneous catalyst for the selective hydrogenation of quinolines was reported by Adkins et al. using Raney nickel for the synthesis of THQ.^[48] Another inspiring work was published by Shaw et al., using different metal/ Al_2O_3 catalysts (Pd, Pt, Ru, Rh, Raney Ni) for the selective hydrogenation of quinolines and indoles.^[49] Catalysts based on noble metals are well investigated although problems with stereo selectivity and functional group tolerance are known.^[50] In the last years, the focus of the researchers shifted to earth-abundant 3d base metals (e.g. Ni, Co, Fe) in regard to sustainability and environment concerns. Reports concerning the application in the hydrogenation of N-heteroarenes are quite limited so far.^[51] The first iron based heterogeneous work was published by Shaw et al., converting quinaldine at very harsh conditions at 300 °C.^[52] Also, Beller and coworkers introduced a system based on Fe with a broad substrate scope and great selectivity towards functional groups.^[53] To the best of my knowledge there is no report on iron based heterogeneous catalysts which are able to selectively convert further N-heteroarenes like quinoxalines. This novel selectivity pattern will be presented in chapter 6.

2.6 References

- [1] a) ABUNDANCE OF ELEMENTS IN THE EARTH'S CRUST AND IN THE SEA, *CRC Handbook of Chemistry and Physics*, 97th edition (**2016–2017**). b) Aktuelle Edelmetallpreise available at <https://www.gold.de/kurse/> (04.05.2020). c) Pig iron price available at <https://www.metal.com/> (04.05.2020).
- [2] a) G. A. Filonenko, R. van Putten, E. J. M. Hensen, E. A. Pidko, *Chem. Soc. Rev.* **2018**, *47*, 1459–1483. b) F. Kallmeier, R. Kempe, *Angew. Chem. Int. Ed.* **2018**, *57*, 46–60.
- [3] A. Boddien, D. Mellmann, F. Gärtner, R. Jackstell, H. Junge, P. J. Dyson, G. Laurenczy, R. Ludwig, M. Beller, *Science* **2011**, *333*, 1733–1736.
- [4] a) A. M. Tondrea, C. C. H. Atienza, K. J. Weller, S. A. Nye, K. M. Lewis, J. G. P. Delis, P. J. Chirik, *Science* **2012**, *335*, 567–570. b) M. R. Friedfeld, M. Shevlin, J. M. Hoyt, S. W. Krska, M. T. Tudge, P. J. Chirik, *Science* **2013**, *342*, 1076–1080.
- [5] W. Zuo, A. J. Lough, Y. F. Li, R. H. Morris, *Science* **2013**, *342*, 1080–1083.
- [6] T. J. Korstanje, J. I. van der Vlugt, C. J. Elsevier, B. de Bruin, *Science* **2015**, *350*, 298–302.
- [7] F. Kallmeier, T. Irrgang, T. Dietel, R. Kempe, *Angew. Chem. Int. Ed.* **2016**, *55*, 11806–11809.
- [8] F. Kallmeier, B. Dudziec, T. Irrgang, R. Kempe, *Angew. Chem. Int. Ed.* **2017**, *56*, 7261–7265.
- [9] N. Deibl, R. Kempe, *Angew. Chem. Int. Ed.* **2017**, *56*, 1663–1666.
- [10] a) F. A. Westerhaus, R. V. Jagadeesh, G. Weinhöfer, M. M. Pohl, J. Radnik, A. E. Surkus, J. Rabeah, K. Junge, H. Junge, M. Nielsen, A. Brückner, M. Beller, *Nat. Chem.* **2013**, *5*, 537–543. b) R. V. Jagadeesh, A. E. Surkus, H. Junge, M. M. Pohl, J. Radnik, J. Rabeah, H. Huan, V. Schünemann, A. Brückner, M. Beller, *Science* **2013**, *342*, 1073–1076. c) F. Cheng, A.-E. Surkus, L.-He, M.-M. Pohl, J. Radnik, C. Topf, K. Junge, M. Beller, *J. Am. Chem. Soc.* **2015**, *137*, 11718–11724. d) R. V. Jagadeesh, K. Murugesan, A. S. Alshammari, H. Neumann, M. M. Pohl, J. Radnik, M. Beller, *Science* **2017**, *358*, 326–332. e) B. Sahoo, C. Kreyenschulte, G. Agostini, H. Lund, S. Bachmann, M. Scalone, K. Junge, M. Beller, *Chem. Sci.* **2018**, *9*, 8134–8141.
- [11] G. Jaiswal, V. G. Landge, D. Jagadeesan, E. Balaraman, *Nat. Commun.* **2017**, *8*, 2147–2159.
- [12] G. Hahn, P. Kunnas, N. de Jonge and R. Kempe, *Nat. Catal.* **2019**, *2*, 71–77.
- [13] P. Colombo, *J. Am. Ceram. Soc.*, **2010**, *93*, 1805–1837.
- [14] E. Ionescu, H.-J. Kleebe, R. Riedel, *Chem. Soc. Rev.* **2012**, *41*, 5032–5052.
- [15] M. Birot, J.-P. Pillot, J. Dunogues, *Chem. Rev.* **1995**, *95*, 1443–1477.
- [16] M. Zaheer, T. Schmalz, G. Motz, R. Kempe, *Chem. Soc. Rev.* **2012**, *41*, 5102–5116.
- [17] G. Glatz, T. Schmalz, T. Kraus, F. Haarmann, G. Motz, R. Kempe, *Chem. Eur. J.* **2010**, *16*, 4231–4238.
- [18] a) M. Zaheer, G. Motz, R. Kempe, *J. Mater. Chem.* **2011**, *21*, 18825–18831. b) M. Zaheer, C. D. Keenan, J. Hermannsdörfer, E. Roessler, G. Motz, J. Senker, R. Kempe, *Chem. Mater.* **2012**,

- 24, 3952-3963. c) M. Zaheer, J. Hermannsdörfer, W. P. Kretschmer, G. Motz, R. Kempe, *ChemCatChem* **2014**, *6*, 91-95.
- [19] D. Forberg, J. Obenauf, M. Friedrich, S.-M. Hühne, W. Mader, G. Motz, R. Kempe, *Catal. Sci. Technol.* **2014**, *4*, 4188-4192.
- [20] D. Forberg, T. Schwob, M. Zaheer, M. Friedrich, N. Miyajima, R. Kempe, *Nat. Commun.* **2016**, *7*, 13201-13207.
- [21] D. Forberg, T. Schwob, R. Kempe, *Nat. Commun.* **2018**, *9*, 1751-1752
- [22] T. Schwob, R. Kempe, *Angew. Chem. Int. Ed.* **2016**, *55*, 15175-15179.
- [23] G. Hahn, J.-K. Ewert, C. Denner, D. Tilgner, R. Kempe, *ChemCatChem* **2016**, *8*, 2461-2465.
- [24] M. Eckardt, M. Zaheer, R. Kempe, *Sci. Rep.* **2018**, *8*, 2567-2572.
- [25] C. Bäuml, R. Kempe, *Chem. Eur. J.* **2018**, *24*, 8989-8993.
- [26] C. Bäuml, C. Bauer, R. Kempe, *ChemSusChem* **2020**, *13*, 3110-3114.
- [27] H.-U. Blaser, H. Steiner, M. Studer, *ChemCatChem* **2009**, *1*, 210-221.
- [28] a) F. Haber, *Z. Elektrotech. Elektrochem.* **1889**, *4*, 506-514. b) F. Haber, *Angew. Chem.* **1900**, *13*, 433-439.
- [29] E. A. Gelder, S. D. Jackson, C. M. Lok, *Chem. Commun.* **2005**, 522-524.
- [30] a) P. Baumeister, H. U. Blaser, U. Siegrist, M. Studer, *Chem. Ind.* **1998**, *75*, 207-219. b) H. U. Blaser, U. Siegrist, H. Steiner, M. Studer, *Fine Chemicals through Heterogeneous Catalysis*, Eds.: R. A. Sheldon, H. van Bekkum, Wiley-VCH, Weinheim, **2001**, p. 389.
- [31] A. Corma, P. Serna, *Science* **2006**, *313*, 332-334.
- [32] R. V. Jagadeesh, A.-E. Surkus, H. Junge, M.-M. Pohl, J. Radnik, J. Rabeah, H. Huan, V. Schunemann, A. Brückner, M. Beller, *Science* **2013**, *342*, 1073-1076. b) R. V. Jagadeesh, T. Stemmler, A.-E. Surkus, H. Junge, K. Junge, M. Beller, *Nat. Protoc.* **2015**, *10*, 548-557. c) D. Formenti, C. Topf, K. Junge, F. Ragaini, M. Beller, *Catal. Sci. Technol.* **2016**, *6*, 4473-4477.
- [33] a) F. A. Westerhaus, R. V. Jagadeesh, G. Wienhofer, M.-M. Pohl, J. Radnik, A.-E. Surkus, J. Rabeah, K. Junge, H. Junge, M. Nielsen, A. Brückner, M. Beller, *Nat. Chem.* **2013**, *5*, 537-543. b) R. V. Jagadeesh, T. Stemmler, A.-E. Surkus, M. Bauer, M.-M. Pohl, J. Radnik, K. Junge, H. Junge, A. Brückner, M. Beller, *Nat. Protoc.* **2015**, *10*, 916-926.
- [34] a) Z. Wei, J. Wang, S. Mao, D. Su, H. Jin, Y. Wang, F. Xu, H. Li, Y. Wang, *ACS Catal.* **2015**, *5*, 4783-4789; d) L. Liu, P. Concepción, A. Corma, *J. Catal.* **2016**, *340*, 1-9; b) B. Chen, F. Li, Z. Huang, G. Yuan, *ChemCatChem* **2016**, *8*, 1132-1138; c) P. Ji, K. Manna, Z. Lin, X. Feng, A. Urban, Y. Song, W. Lin, *J. Am. Chem. Soc.* **2017**, *139*, 7004-7011; d) P. Zhou, Z. Zhang, *ChemSusChem* **2017**, *10*, 1892-1897; e) H. Alex, P. Loos, T. Baramov, J. Barry, T. Godiawala, J. Hassfeldt, N. Steinfeldt, *ChemCatChem* **2017**, *9*, 16; f) I. Sorribes, L. Liu, A. Corma, *ACS Catalysis* **2017**, *7*, 2698-2708; g) F. Zhang, C. Zhao, S. Chen, H. Li, H. Yang, X.-M. Zhang, *J.*

- Catal.* **2017**, *348*, 212-222; h) L. Jiang, P. Zhou, Z. Zhang, Q. Chi, S. Jin, *New J. Chem.* **2017**, *41*, 11991-11997; i) X. Cui, K. Liang, M. Tian, Y. Zhu, J. Ma, Z. Dong, *J. Colloid Interface Sci.* **2017**, *501*, 231-240; j) B. Sahoo, D. Formenti, C. Topf, S. Bachmann, M. Scalone, K. Junge, M. Beller, *ChemSusChem* **2017**, *10*, 3035-3039; k) Li. Liu, F. Gao, P. Concepción, A. Corma, *J. Catal.* **2017**, *350*, 218-225; l) Z. Wei, S. Mao, F. Sun, J. Wang, B. Mei, Y. Chen, H. Li, Y. Wang, *Green Chem.* **2018**, *20*, 671-679; m) X. Sun, A. I. Olivos-Suarez, D. Osadchii, M. J. V. Romero, F. Kapteijn, J. Gascon, *J. Catal.* **2018**, *357*, 20-28.
- [35] T. Schwob, R. Kempe, *Angew. Chem. Int. Ed.* **2016**, *55*, 15175-15179.
- [36] W. S. Emerson, *Org. React. (N.Y.)* **1948**, *4*, 174-202.
- [37] a) J. L. Klinkenberg, J. F. Hartwig, *Angew. Chem. Int. Ed.* **2011**, *50*, 86-95. b) J. Kim, H. J. Kim, S. Chang, *Eur. J. Org. Chem.* **2013**, *16*, 3201-3213.
- [38] G. Mignonac, *Compt. Rend.* 1921, 172, 223.
- [39] S. Gomez, J. A. Peters, T. Maschmeyer, *Adv. Synth. Catal.* **2002**, *344*, 1037-1057.
- [40] a) C. F. Winans, *J. Am. Chem. Soc.* **1939**, *61*, 3566-3567. b) E. R. Alexander, A. L. Misegades, *J. Am. Chem. Soc.* **1948**, *70*, 1315-1316. c) M. V. Klyuev, M. L. Khidekel', *Russ. Chem. Rev.* **1980**, *49*, 14-27. d) P. Dolezal, O. Machalický, M. Pavelek, P. Kubec, K. Hrádková, R. Hrdina, R. Suláková, *Appl. Catal. A-Gen.* **2005**, *286*, 202-210.
- [41] R. V. Jagadeesh, K. Murugesan, A. S. Alshammari, H. Neumann, M.-M. Pohl, J. Radnik, M. Beller, *Science* **2017**, *358*, 326-332.
- [42] G. Hahn, P. Kunnas, N. de Jonge, R. Kempe, *Nat. Catal.* **2019**, *2*, 71-77.
- [43] a) Z. Yuan, B. Liu, P. Zhou, Z. Zhang, Q. Chi, *J. Catal.* **2019**, *370*, 347-356. b) Y. Zhang, H. Yang, Q. Chi, Z. Zhang, *ChemSusChem* **2019**, *12*, 1246-1255. c) K. Murugesan, M. Beller, R. V. Jagadeesh, *Angew. Chem. Int. Ed.* **2019**, *131*, 5118-5122.
- [44] a) T. J. Donohoe, R. Garg and C. A. Stevenson, *Tetrahedron: Asymmetry* **1996**, *7*, 317-344. b) A. Gualandi, D. Savoia, *RSC Adv.* **2016**, *6*, 18419-18451. c) Z. Wei, F. Shao, J. Wang, *Chin. J. Chem.* **2019**, *40*, 980-1002.
- [45] L. Tao, Q. Zhang, S. S. Li, X. Liu, Y. M. Liu, Y. Cao, *Adv. Synth. Catal.* **2015**, *357*, 753-760.
- [46] a) S. J. Benkovic, P. A. Benkovic, D. R. Comfort, *J. Am. Chem. Soc.* **1969**, *91*, 5270-5279. b) M. P. Mertes, A. J. Lin, *J. Med. Chem.* **1970**, *13*, 77-82.
- [47] C. T. Eary, Z. S. Jones, R. D. Groneberg, L. E. Burgess, D. A. Mareska, M. D. Drew, J. F. Blake, E. R. Laird, D. Balachari, M. O'Sullivan, A. Allen, V. Marsh, *Bioorg. Med. Chem. Lett.* **2007**, *17*, 2608-2613.
- [48] H. Adkins, H. R. Billica, *J. Am. Chem. Soc.* **1948**, *70*, 695-698.
- [49] J.E. Shaw, P.R. Stapp, *J. Heterocycl. Chem.* **1987**, *24*, 1477-1483.

- [50] a) N. A. Beckers, S. Huynh, X. Zhang, E. J. Luber, J. M. Buriak, *ACS Catal.* **2012**, *2*, 1524-1534. b) D. Ren, L. He, L. Yu, R.-S. Ding, Y.-M. Liu, Y. Cao, H.-Y. He, K.-N. Fan, *J. Am. Chem. Soc.* **2012**, *134*, 17592-17598. c) M. Fang, R. A. Sánchez-Delgado, *J. Catal.* **2014**, *311*, 357-368. d) A. Karakulina, A. Gopakumar, I. Akçok, B. L. Roulier, T. LaGrange, S. A. Katsyuba, S. Das, P. J. Dyson, *Angew. Chem. Int. Ed.* **2016**, *55*, 292-296. e) X. Wang, W. Chen, L. Zhang, T. Yao, W. Liu, Y. Lin, H. Ju, J. Dong, L. Zheng, W. Yan, X. Zheng, Z. Li, X. Wang, J. Yang, D. He, Y. Wang, Z. Deng, Y. Wu, Y. Li, *J. Am. Chem. Soc.* **2017**, *139*, 9419-9422. f) S. Zhang, Z. Xia, T. Ni, Z. Zhang, Y. Ma and Y. Qu, *J. Catal.* **2018**, *359*, 101-111. g) Y. Wu, H. Yu, Y. Guo, X. Jiang, Y. Qi, B. Sun, H. Li, J. Zheng, X. Li, *Chem. Sci.* **2019**, *10*, 10459-10465.
- [51] a) C. Liu, Z. Rong, Z. Sun, Y. Wang, W. Du, Y. Wang, L. Lu, *RSC Adv.* **2013**, *3*, 23984-23988. b) F. Chen, A.-E. Surkus, L. He, M.-M. Pohl, J. Radnik, C. Topf, K. Junge, M. Beller, *J. Am. Chem. Soc.* **2015**, *137*, 11718-11724. c) Z. Wei, Y. Chen, J. Wang, D. Su, M. Tang, S. Mao, Y. Wang, *ACS Catal.* **2016**, *6*, 5816-5822. d) J. Li, G. Liu, X. Long, G. Gao, J. Wu, F. Li, *J. Catal.* **2017**, *355*, 53-62. e) F. Chen, W. Li, B. Sahoo, C. Kreyenschulte, G. Agostini, H. Lund, K. Junge, M. Beller, *Angew. Chem.* **2018**, *130*, 14696-14700. f) G. Jaiswal, M. Subaramanian, M. K. Sahoo, E. Balaraman, *ChemCatChem* **2019**, *11*, 2449-2457.
- [52] J. E. Shaw and P. R. Stapp, *J. Heterocycl. Chem.* **1987**, *24*, 1477-1483.
- [53] B. Sahoo, C. Kreyenschulte, G. Agostini, H. Lund, S. Bachmann, M. Scalone, K. Junge, M. Beller, *Chem. Sci.* **2018**, *9*, 8134-8141.

3. Overview over the thesis results

This thesis contains three different publications, which were presented in detail in the chapters 4-6. The first two works were published and the third one is to be submitted. In chapter 3.1 a smart overview of the results and the correlation between the three publications is discussed. The individual contributions are explained in chapter 3.2.

3.1 *Synopsis*

In recent years, *Kempe and coworkers* focused on the synthesis of heterogeneous catalysts for the application in sustainable organic synthesis. Combinations of PDCs as support material and different metal complexes led to various highly active catalyst systems. One aspect was the development of rare noble metal catalysts and targeted issues of green chemistry like the production of chemical compounds from biomass derived substrates instead of nonrenewable petroleum feedstocks. Therefore, the synthesis of pyrroles from bio-based secondary alcohols and 1,2-amino alcohols was accomplished with an Ir@SiCN catalyst. Another inspiring approach was the use of a Pd₂Ru@SiCN catalyst system for the reversible hydrogen storage. The other promising aspect was the replacement of the rare noble metals with earth-abundant 3d metals. The conservation of resources, especially rare metals which are commonly used in key technologies and in catalysis, is a very important target to ensure the availability of these elements for future generations. The replacement is especially attractive if novel selectivity patterns are observed permitting the development of innovative coupling reactions. Therefore, a variety of catalysts for hydrogenation and oxidation reactions were introduced, such as Cu@SiCN, Co@SiCN or Ni@SiCN, which were commonly accomplished by noble metal catalysts. These works showed that novel selectivity patterns were generated through this substitution of noble metals, making this approach even more desirable. Hence, the issue of this thesis was to develop novel heterogeneous catalyst systems, considering the afore mentioned aspects of sustainability and conservation of resources, based on the cheapest and most abundant 3d metal iron.

The first publication deals with the description of a Fe@SiCN catalyst system applied in the selective hydrogenation of nitroarenes. The iron nanocomposite has been synthesized in a two-step procedure. First, a Fe aminopyridinato [Fe(Ap^{TMS})₃] complex (Figure 1, top left) and the commercially available polysilazane HTT1800 were dissolved in tetrahydrofuran (THF) and dicumylperoxid (DCP) was added to initiate crosslinking. After removal of the solvent, the generated green body undergoes pyrolysis under nitrogen atmosphere at 750 °C, resulting in a Fe@SiCN nanocomposite.

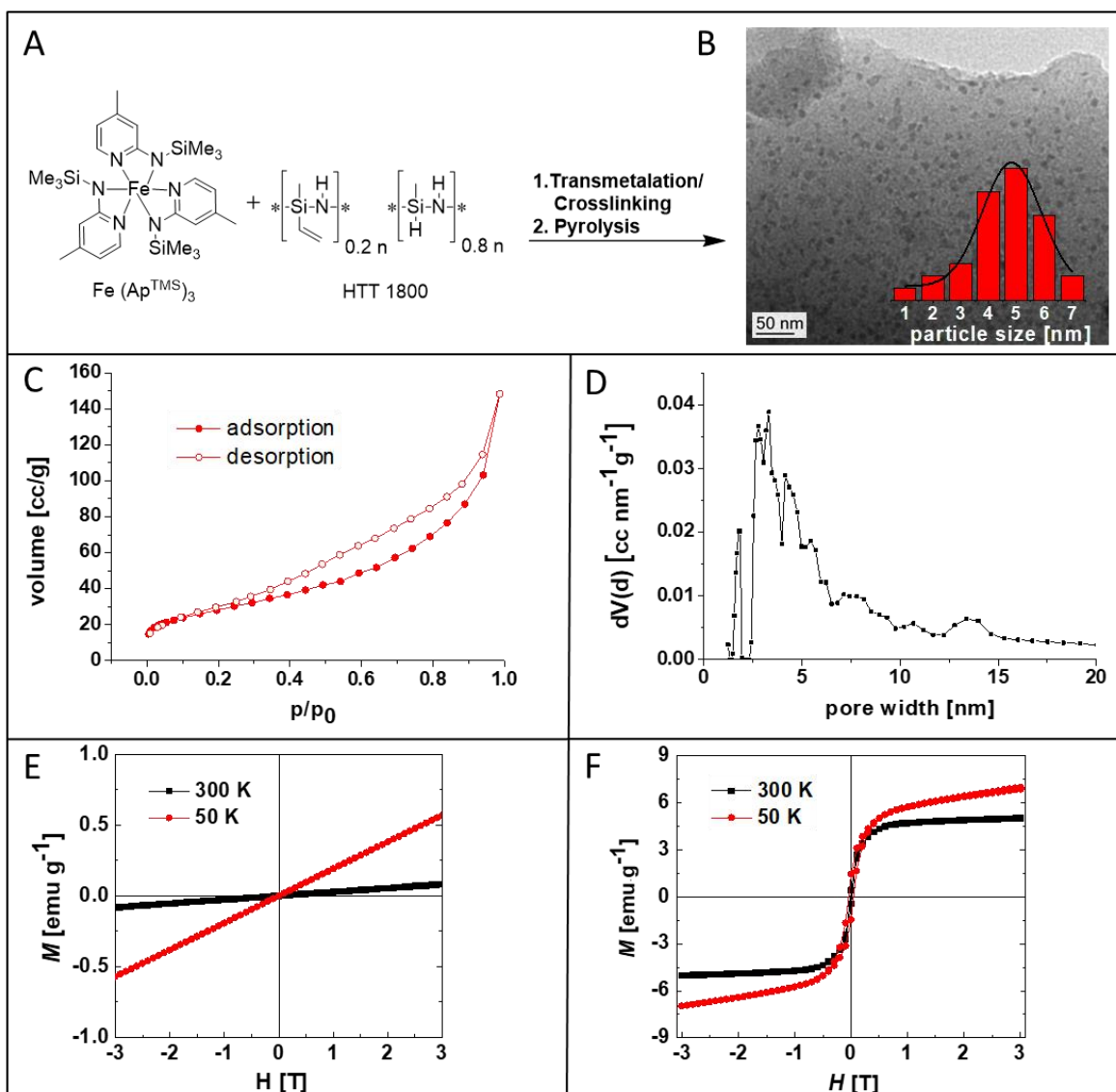


Figure 1: A: Synthesis of the novel Fe@SiCN nanocomposite. The iron complex and the commercially available polysilazane HTT 1800 are dissolved in THF, followed by crosslinking with DCP as an external initiator at 105 °C. The obtained greenbody is subjected to pyrolysis under nitrogen atmosphere at 750 °C, resulting in an amorphous Fe@SiCN nanocomposite. B: TEM analysis verified the presence of small iron nanoparticles with a homogenous particle size distribution centered at 5 nm. C: Pore characterization of the Fe@SiCN nanocomposite via nitrogen sorption measurements. D: Calculated pore-size distribution. E, F: Magnetic measurements confirm the transition of Fe³⁺ ions in the greenbody (E) to iron nanoparticles (superparamagnetic properties) in the final nanocomposite (F).

Magnetic measurements confirmed the transition of paramagnetic Fe³⁺ ions in the greenbody to superparamagnetic properties in the catalyst, indicating the presence of small iron nanoparticles (Figure 1, E,F). TEM analysis confirmed the generation of homogeneous distributed nanoparticles with an average particle size of 5 nm (Figure 1, B). Nitrogen sorption measurements of the iron catalyst indicated the presence of mainly mesopores with a calculated [Brunauer-Emmet-Teller (BET) method] specific surface area of 101 m²g⁻¹ (Figure 1, C). The calculated pore-size distribution showed that 91 % of the surface area consists of mesopores < 10 nm (Figure 1, D).

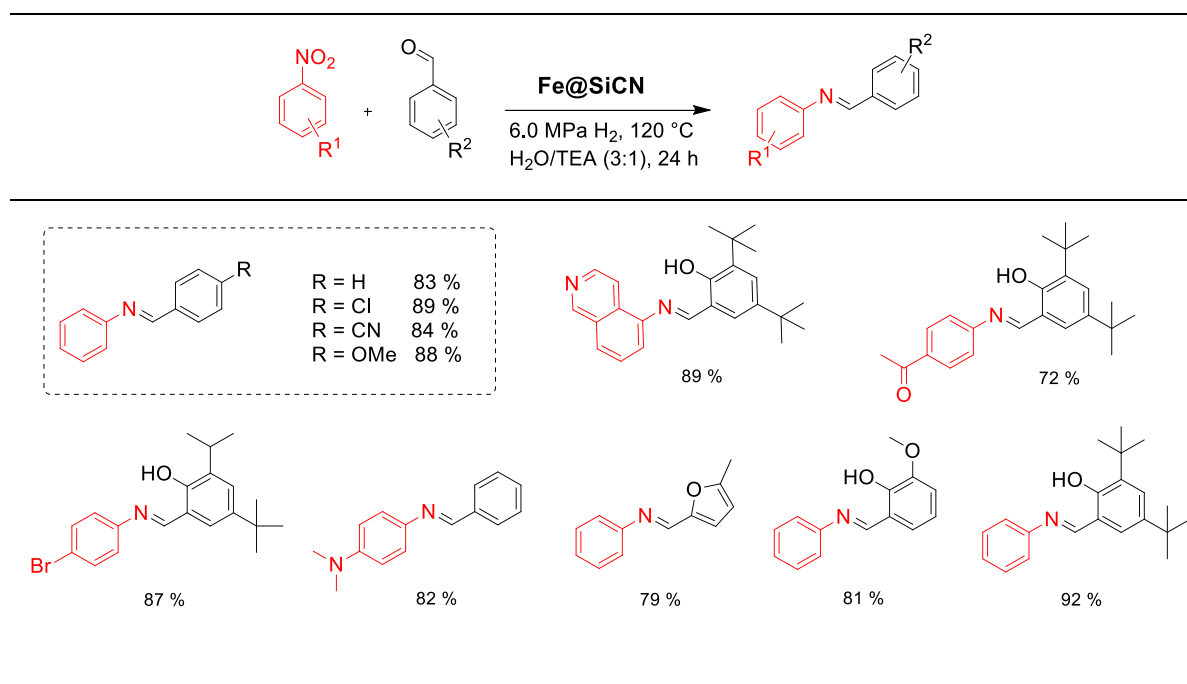
The production of aniline derivatives from easy to synthesize aromatic nitro compounds is the method of choice and very attractive. Therefore, the catalyst was applied in the reduction of nitroarenes with molecular hydrogen and showed very high activity and selectivity.

Table 1: Chemoselective hydrogenation of substituted nitroarenes; substrate scope^[a].

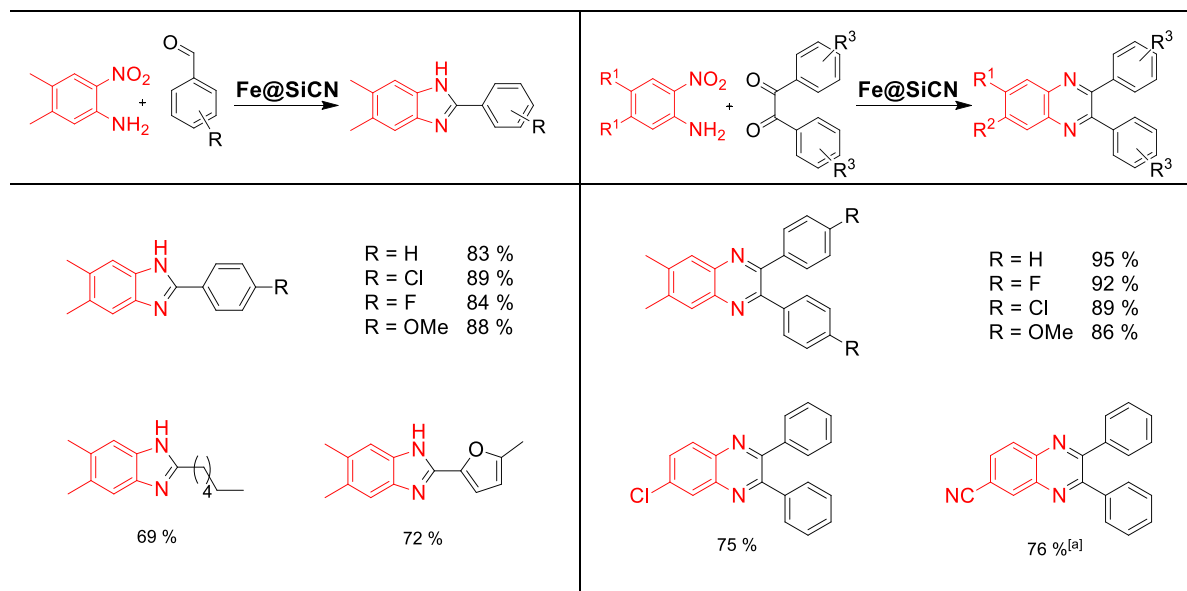
	<p>H >99 %</p> <p>4-Cl >99 %</p> <p>3-Cl >99 %</p> <p>2-Cl 91 %</p> <p>4-Br 97 %</p> <p>R = 3-Br 82 %</p> <p>2-Br 87 %</p> <p>4-F 92 %</p> <p>4-I 70 %^[b]</p> <p>3-CN 92 %^[c]</p>
<p>89 %</p>	<p>85 %</p>
<p>88 %</p>	<p>91 %</p>
<p>80 %</p>	
<p>95 %</p>	<p>94 %^[d]</p>
	<p>95 %^[d]</p>
	<p>>99 %^[d]</p>

Reaction conditions: [a] 0.5 mmol substrate, 10 mol % catalyst (2.8 mg Fe, 0.05 mmol, 70 mg), 1 mL TEA, 3 mL H₂O. [b] 100 °C, 6.5 MPa H₂, 11 mol % catalyst [c] 4 mL H₂O [d] 125 °C, 6.5 MPa, 24 h. All yields were determined by GC using *n*-dodecane as an internal standard.

Hence, a variety of functional groups, even hydrogenation-sensitive ones, could be introduced like halides (chlorides, bromides, fluorides and iodides), aldehydes, ketones, nitriles and amides. Recycling studies showed that the catalyst is active over five consecutive runs without any loss of activity. The decline of activity after the sixth run can be easily reverted by TPR treatment. The tolerance of aldehydes and ketones enabled the implementation of follow up reactions to involve further C-N and/or C-C bond formation steps. Hence, the direct synthesis of imines (Table 2), benzimidazoles (Table 3, left) and quinoxalines (Table 3, right) were accomplished in great yields with highly selectivity.

Table 2: Selective synthesis of substituted imines from nitroarenes and aldehydes; substrate scope.

Reaction conditions: 0.5 mmol nitroarene, 1.5 mmol aldehyde, 10 mol % catalyst (2.8 mg Fe, 0.05 mmol, 70 mg), 1 mL TEA, 3 mL H₂O. Yields of isolated products.

Table 3: Selective synthesis of substituted benzimidazoles and quinoxalines; substrate scope.

Reaction conditions: 0.5 mmol nitroarene, 1 mmol aldehyde or 0.5 mmol diketone, 10 mol % catalyst (2.8 mg Fe, 0.05 mmol, 70 mg), 1 mL TEA, 3 mL H₂O, 125 °C, 6.5 MPa H₂, 24 h. Yields of isolated products. [a] 4 mL H₂O, 11 mol % catalyst.

Encouraged by the great results and the excellent selectivity of the Fe@SiCN catalyst, a new selective iron-based catalyst system for the reductive amination of carbonyl compounds was developed. The reductive amination of ketones and aldehydes is the method of choice for the synthesis of alkyl amines from inexpensive and diversely available starting materials. As mentioned in chapter 2.4, the

challenge of this reaction lies in the fast transformation of the in situ formed imine to the corresponding primary amine to avoid various of side reactions. The approach was to use the wet impregnation method, to generate the active metal nanoparticles on the near surface area term for an increased accessibility of the active centers. The best results were achieved by the combination of a modified (N)SiC material, which was synthesized according to a known literature procedure by Motz, and a novel iron complex. For the catalyst synthesis, the (N)SiC material was impregnated with the iron salen complex in acetonitrile. After removal of the solvent, the sample was pyrolyzed under a nitrogen atmosphere at 750 °C followed by a reduction step at 550 °C (Figure 2, A).

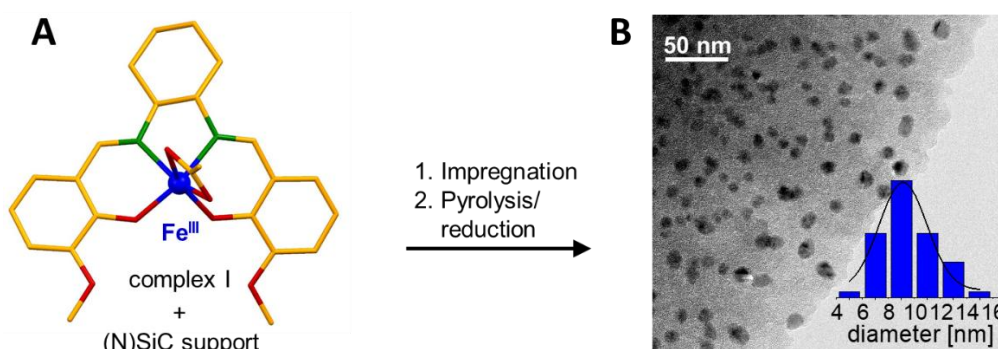


Figure 2: A) Synthesis of the iron catalyst. B) TEM analysis suggested the presence of homogeneously distributed Fe nanoparticles with an average particle size of 10 nm.

In order to find the most active catalyst, different iron sources and support materials were varied in the catalyst synthesis and applied in the reductive amination of acetophenone (Table 4).

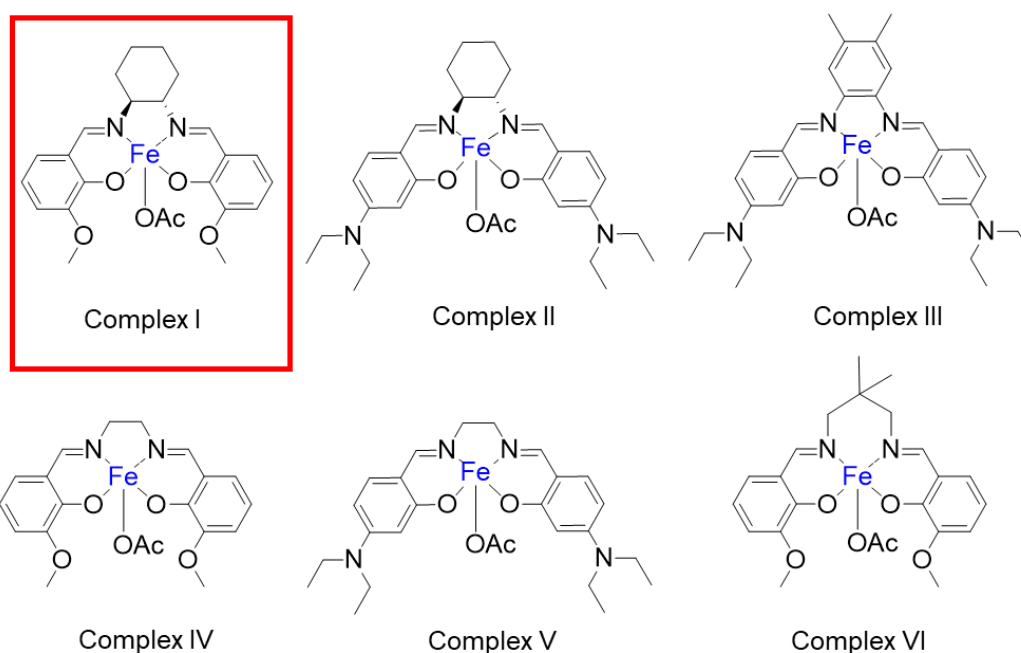
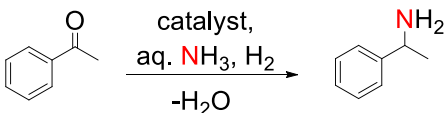


Figure 3: Different synthesized iron complexes (I-VI), used for the catalyst screening.

The use of metal oxidic support materials as well as carbon-based materials led to decreasing yields (Table 4, Entries 2-7). The combination of the (N)SiC support material and complex I provided the most active catalyst system, whereby the *ortho*-vanillin structure and the not demanding aliphatic diamino building block seem to be essential for the high activity of the catalyst based on complex I (Table 4, Entries 1, 9-13).

Table 4: Catalyst screening for the reductive amination of acetophenone.

				
Entry	Metal source	Support material	Pyrolysis temperature / °C	Yield / %
1	Complex I	(N)SiC	750	72
2	Complex I	Activated carbon	750	37
3	Complex I	SiO ₂	750	0
4	Complex I	TiO ₂	750	0
5	Complex I	CeO ₂	750	25
6	Complex I	Al ₂ O ₃	750	0
7	Complex I	Pyrolyzed PAN	750	36
8	Fe(NO ₃) ₃	(N)SiC	750	44
9	Complex II	(N)SiC	750	65
10	Complex III	(N)SiC	750	47
11	Complex VI	(N)SiC	750	68
12	Complex V	(N)SiC	750	63
13	Complex VI	(N)SiC	750	61

Reaction conditions: 8.6 mol% Fe (60 mg supported Fe catalyst with 4.0 wt% Fe loading, 0.043 mmol Fe, 2.4 mg Fe), 0.5 mmol acetophenone, 140 °C, 20 h, 6.5 MPa H₂, 3.5 mL aq. NH₃-25 %. Yields were determined by GC using *n*-dodecane as an internal standard.

Hence, the Fe/(N)SiC catalyst was characterized in more detail. TEM analysis confirmed that homogeneous distributed iron nanoparticles with an average particle size of 10 nm were generated (Figure 2, B). The nanoparticle surface was investigated by XPS measurements (Figure 4, A). The Fe 2p_{3/2} signal can be divided in two signals with the binding energies of 707.0 and 711.0 eV. The presence of metallic Fe could be identified due to its sharp line shape and its binding energies of 707.0 eV. At higher binding energies small amounts of different oxides are found. The microporous catalyst has a specific surface area of 415 m²g⁻¹, which was determined by nitrogen physisorption measurements (Figure 4, B).

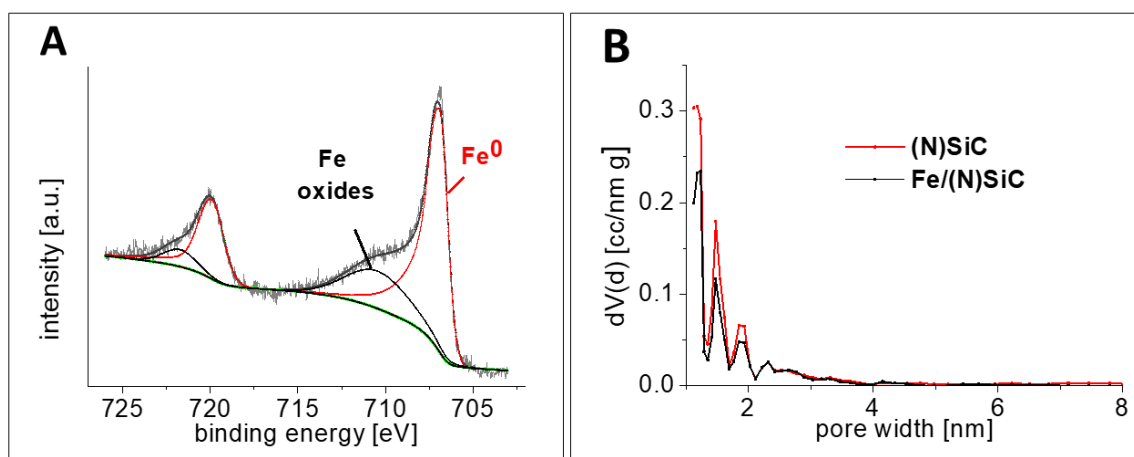
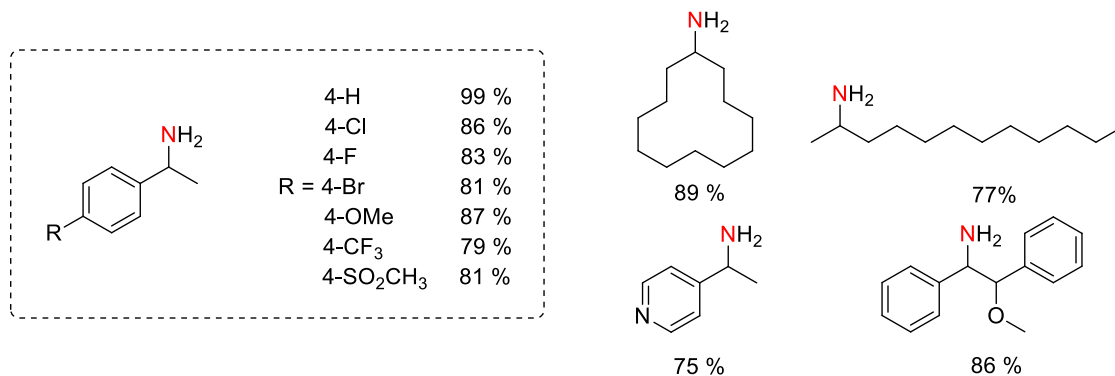


Figure 4: A) XPS analysis confirms the presence of metallic iron and iron oxide at the surface of the nanoparticles. B) Surface and pore characterization of the catalyst via nitrogen physisorption measurement.

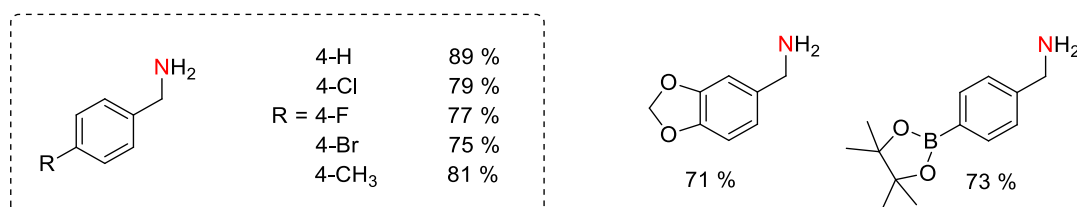
The synthesis of 1-phenylethanamine from acetophenone and aqueous ammonia was chosen as the benchmark reaction for optimizing the reaction conditions. The amount of ammonia turned out to be one of the crucial factors for high yields, because the surplus of ammonia leads to the suppression of side reactions. The best catalyst performance was achieved by applying 10 mol% Fe, 3.5 mL of 25 % aqueous ammonia, 6.5 MPa H₂ and 140 °C for 20 h. Using the optimized reaction conditions, we were interested in the broad applicability of our Fe-based catalyst system in the reductive amination of carbonyl compounds to primary amines. Aryl-alkyl ketones with various substituents (methoxy, bromide, chloride, fluoride, sulfonyl) could be converted into their corresponding primary amines in excellent isolated yields and high selectivity (Figure 5). Also, the conversion of purely aliphatic ketones was easily accomplished and was demonstrated using cycloalkyl and aliphatic substrates (Figure 5). The transformation of benzylic aldehydes was performed at 130 °C to avoid coupling reactions, which could be reduced but not completely suppressed (Figure 5).



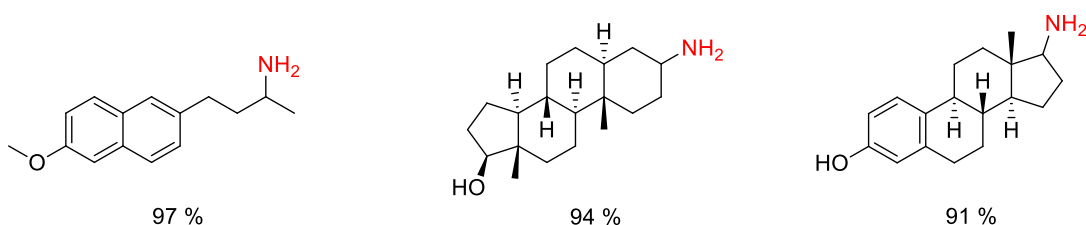
Products derived from **ketones** (21 examples)



Products derived from **aldehydes** (7 examples)



Products derived from **biologically active molecules** (4 examples)



Synthesis of **CNS stimulants** (no stereoselectivity)

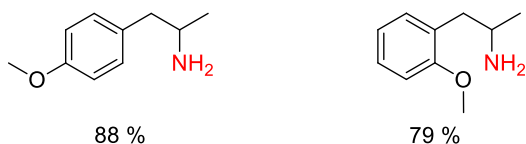


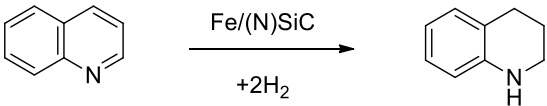
Figure 5: Excerpt of the substrate scope; isolated yields of the corresponding hydrochloride salts.

To demonstrate the excellent selectivity of the catalyst, we were interested in introducing the -NH₂ moiety in pharmaceuticals, biologically active, highly functionalized and structurally complex molecules. Another impressive approach was the successful synthesis of CNS (Central Nervous System) stimulants (Figure 5).

Recycling studies of the catalyst showed that five consecutive runs can be easily performed without any loss of activity. Moreover, an up-scaling reaction of acetophenone to 1-phenylethanamine to gram scale achieved same yields as the small-scale experiment, which outlines the great performance of the synthesized iron catalyst.

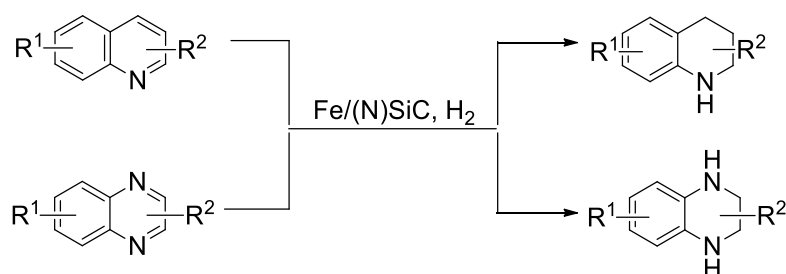
Based on the great catalytic activity of the Fe/(N)SiC catalyst in the hydrogenation of an imine during the reductive amination, we focused on the hydrogenation of N-heteroarenes, especially quinolines and quinoxalines. The partially hydrogenated 1,2,3,4-tetrahydro-quinolines and quinoxalines represent a class of compounds that possess immense utility as building blocks and key intermediates in the manufacture of pharmaceuticals, agrochemicals and other fine chemicals. The hydrogenation of quinoline to 1,2,3,4-tetrahydroquinoline was chosen as benchmark reaction for optimizing the reaction conditions. The solvent screening showed that higher yields were generated with increasing polarity of the solvent with exception of water. In summary, the catalyst showed the best performance applying 10 mol% Fe, 3 mL methanol, 150 °C and 6.5 MPa H₂ for 24 h (Table 5). Longer reaction times (48 h) achieved better results, but the reduced reaction time is more desirable concerning industrial approaches.

Table 5: Solvent screening for the reductive amination of quinolines.

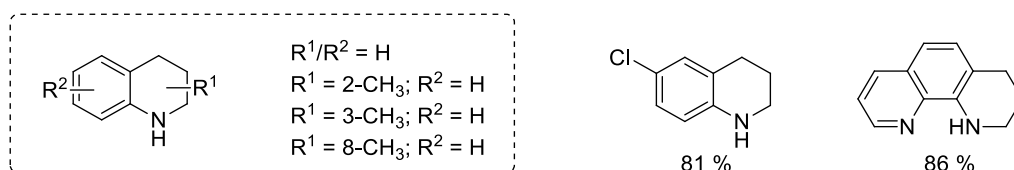
			
Solvent	Reaction time / h	Temperature / °C	Yield / %
MeOH	24	150	90
H ₂ O	24	150	56
H ₂ O/MeOH (1:1)	24	150	60
H ₂ O/MeOH (1:4)	24	150	72
EtOH	24	150	84
<i>i</i> -PrOH	24	150	77
MtBE	24	150	9
Toluol	24	150	2
THF	24	150	29
Digylme	24	150	25

Reaction conditions: 10 mol % Fe (70 mg Fe/(N)SiC, 4.0 wt% Fe, 0.05 mmol Fe, 2.8 mg Fe), 0.5 mmol quinoline, 6.5 MPa H₂, 4 mL solvent. Yields were determined by GC using *n*-dodecane as an internal standard.

With the optimized reaction conditions at hand, we focused on the substrate scope. Therefore, various substituted (iso)quinolines were hydrogenated in excellent yields. The great selectivity of the catalyst was demonstrated on 10 different substrates (Figure 6). Even polycyclic heterocycles like 1,10-phenanthroline could be selectively hydrogenated to 1,2,3,4-tetrahydro-1,10-phenanthroline. Also, functional groups like hydroxy, methoxy or chloride could be tolerated. In the next step we looked for further interesting classes of N-heterocycles which are important for applications in the pharmaceutical manufacturing, like tetrahydroquinoxalines. The reaction temperature and time had to be increased to ensure good yields.



Hydrogenated quinoline motive-based compounds (10 examples)



Hydrogenated quinoxalines

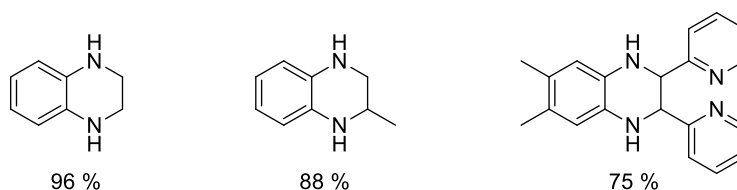


Figure 6: Excerpt of the substrate scope.

The conversion of three different quinoxalines were accomplished in very good yields. The introduction of sterically demanding substituents including a pyridine motive was also successful (Figure 6), which shows the great selectivity towards different types of N-heterocycles.

3.2 Individual contribution to joint publications

The results presented in this thesis were obtained in collaboration with others and are published or to be submitted as indicated below. The contributions of all the co-authors to the respective publications are specified in the following. The corresponding author is denoted by an asterisk (*).

Chapter 4

This work was published in Chemistry - A European Journal (*Chem. Eur. J.* **2018**, *24*, 8989-8993.) with the title:

“The Direct Synthesis of Imines, Benzimidazoles and Quinoxalines from Nitroarenes and Carbonyl Compounds by Selective Nitroarene Hydrogenation Employing a Reusable Iron Catalyst”

Authors: Christoph Bäumlér, Rhett Kempe*

I synthesized and characterized the catalyst and performed the catalytic reactions and the related analytics. Rhett Kempe and I designed the experiments and co-wrote the manuscript. Rhett Kempe supervised the work presented in this paper and was involved in the scientific discussions.

Chapter 5

This work was published in ChemSusChem – Chemistry Europe (*ChemSusChem* **2020**, *13*, 3110-3114.) with the title:

“The Synthesis of Primary Amines through Reductive Amination Employing an Iron Catalyst”

Authors: Christoph Bäumlér, Christof Bauer, Rhett Kempe*

I synthesized and characterized the catalyst and performed the catalytic reactions and the related analytics. Christof Bauer carried out some of the substrate screening reactions during his bachelor thesis. Rhett Kempe and I designed the experiments and co-wrote the manuscript. Rhett Kempe supervised the work presented in this paper and was involved in the scientific discussions.

Chapter 6

This work is to be submitted with the title:

"Hydrogenation of various N-heterocycles Employing a Heterogeneous Iron Catalyst"

Authors: Christoph Bäumlér, Rhett Kempe*

I synthesized and characterized the catalyst and performed the catalytic reactions and the related analytics. Rhett Kempe and I designed the experiments and I wrote the manuscript. Rhett Kempe supervised the work presented in this paper and was involved in the scientific discussions.

4. The Direct Synthesis of Imines, Benzimidazoles and Quinoxalines from Nitroarenes and Carbonyl Compounds via Selective Nitroarene Hydrogenation Employing a Reusable Iron Catalyst

Christoph Bäumler^[a], and Rhett Kempe^{*[a]}

[a] Anorganische Chemie II – Katalysatordesign, Universität Bayreuth, 95440 Bayreuth.

Published in *Chem. Eur. J.* **2018**, *24*, 8989-8993.

Abstract: The “replacement” of noble metals by earth-abundant metals is a desirable aim in catalysis and a possible way of conserving rare elements. The “replacement” is especially attractive if novel selectivity patterns are observed permitting the development of novel coupling reactions. Herein, we report on a novel, robust and reusable iron catalyst, which permits the selective hydrogenation of nitroarenes in the presence of hydrogenation-sensitive functional groups. Based on the selectivity pattern observed, the direct iron catalyzed synthesis of imines and benzimidazoles from nitroarenes and aldehydes becomes feasible. In addition, we introduce the direct synthesis of quinoxalines from nitroarenes and diketones applying our catalyst.

4.1 Introduction

The conservation of our rare element resources is of fundamental importance to guarantee attractive living conditions for future generations. The replacement of noble metals by earth-abundant metals in key technologies, such as catalysis, is one of the options and especially attractive if the “replacement” permits novel selectivity patterns and/or even novel catalytic transformations. Hydrogenation reactions play an important role in catalysis and, thus, are of high interest to the chemical industry and academic research.^[1] The hydrogenation of aromatic nitro compounds is the method of choice for the production or synthesis of aniline derivatives, an important class of compounds.^[2] In 2006, Corma and coworkers reported a

breakthrough regarding the tolerance of functional groups applying heterogeneous gold catalysts.^[3] Recently, Beller and coworkers could show that heterogeneous catalysts based on abundantly available transition metals, such as iron^[4] and cobalt^[5], can also mediate the highly selective hydrogenation of nitroarenes. Based on these initial findings, a variety of groups developed Co catalysts for the selective and efficient hydrogenation of nitroarenes.^[6-8] Efficient and selective iron catalysts are essentially unknown beside the initial key contributions.^[4]

Herein, we report on a novel reusable and robust silicon carbonitride (SiCN)-based Fe catalyst. Our catalyst permits the selective hydrogenation of nitroarenes in the presence of iodo, aldehyde, ketone and nitrile functional groups. Based on the tolerance of carbonyl compounds, our catalyst can mediate the direct synthesis of imines and benzimidazoles from nitroarenes and aldehydes. Furthermore, we introduce the direct synthesis of quinoxalines from nitroarenes and diketones.

Imines are important compounds and have been used extensively as ligands^[9] and for the synthesis of materials^[10], fragrances, fungicides, pharmaceuticals and agricultural chemicals.^[11] Thus, the development of novel imine synthesis protocols is of high interest.^[7,12,13] Benzimidazoles^[7,14] and quinoxalines^[15] are similarly important as well as the development of protocols for their synthesis. We have recently introduced a variety of SiCN-metal nanocomposite catalysts^[16] and have, very recently, introduced highly active, selective and reusable cobalt catalysts.^[7,8]

4.2 Results and Discussion

Our iron nanocomposite catalyst has been synthesized in a two-step procedure. A Fe aminopyridinato complex (Figure 1, top left) and the commercially available polysilazane HTT 1800 were dissolved in tetrahydrofuran (THF) and dicumylperoxid (DCP) was added to initiate crosslinking. After removal of the solvent, the generated green body undergoes pyrolysis under nitrogen atmosphere at 750 °C, resulting in a Fe@SiCN nanocomposite. Magnetic measurements confirmed the superparamagnetic properties of the pyrolyzed nanocomposite (Figure 1, bottom right) indicating the presence of small iron nanoparticles (NP). Prior to pyrolysis, Fe³⁺ have been identified via magnetic measurements (Figure 1, bottom left). The generation of iron NPs was also verified by transmission electron microscopy (TEM; Figure 1, top right). Homogeneously distributed particles with an average particle size of 5 nm could be detected. The synthesized Fe@SiCN catalyst was washed with an aqueous basic solution, followed by a temperature-programmed reduction (TPR; Figure S3). The first TPR run indicated the presence of iron oxide species, due to the increased H₂ uptake between 350-600 °C. X-ray photoelectron spectroscopy (XPS) verified the presence of metallic Fe and iron oxide species (Figure S4) with about a 1 to 2 ratio in the as synthesized Fe@SiCN material. Nitrogen sorption measurements (Figure 1, center left) of the Fe@SiCN nanocomposite indicated the

presence of mesopores. A specific surface area of $101 \text{ m}^2\text{g}^{-1}$ was calculated by the Brunauer-Emmet-Teller (BET) method. The pore-size distribution calculated exhibited the presence of micro- and mesopores, whereby 91 % of the surface area is caused by mesopores < 10 nm (Figure 1, center right).

Next, we were interested in applying our Fe catalyst in the reduction of nitroarenes. The reduction of nitrobenzene was chosen as the benchmark reaction. Therefore, various reaction parameters such as pressure, temperature, solvent and catalyst loading were varied to find conditions for a complete conversion to aniline. A 3:1 water/TEA (triethylamine) mixture, 6.0 MPa hydrogen pressure and 120 °C (Figure S5, Table S1) were found to be optimal. Our catalyst needs more drastic conditions for the nitroarene hydrogenation than the Fe catalyst developed by Beller and coworker^[4], which works well with 4.5 mol% catalyst loading, 90 to 120 °C and 3 to 5 MPa H₂ pressure. Investigation of the substrate scope revealed a broad applicability of our Fe catalyst. Various substituents, e.g. all halogenides were tolerated (Table 1; Entries 2-9). The reaction conditions for 1-iodo-4-nitrobenzene (Table 1; Entry 9), had to be modified slightly. Other hydrogenation-sensitive functional groups, such as aldehyde, amide, ketone and nitrile, could be tolerated too (Table 1). The temperature and the pressure were slightly increased to ensure full conversion of sterically more demanding substrates (Table 1; Entries 15-17). We also investigated (E)-(2-nitrovinyl)benzene but observed a mixture of products since the C-C double bond was hydrogenated. Heterocyclic nitro compounds work as demonstrated for isoquinolin-5-amine (Table 1, Entry 18).

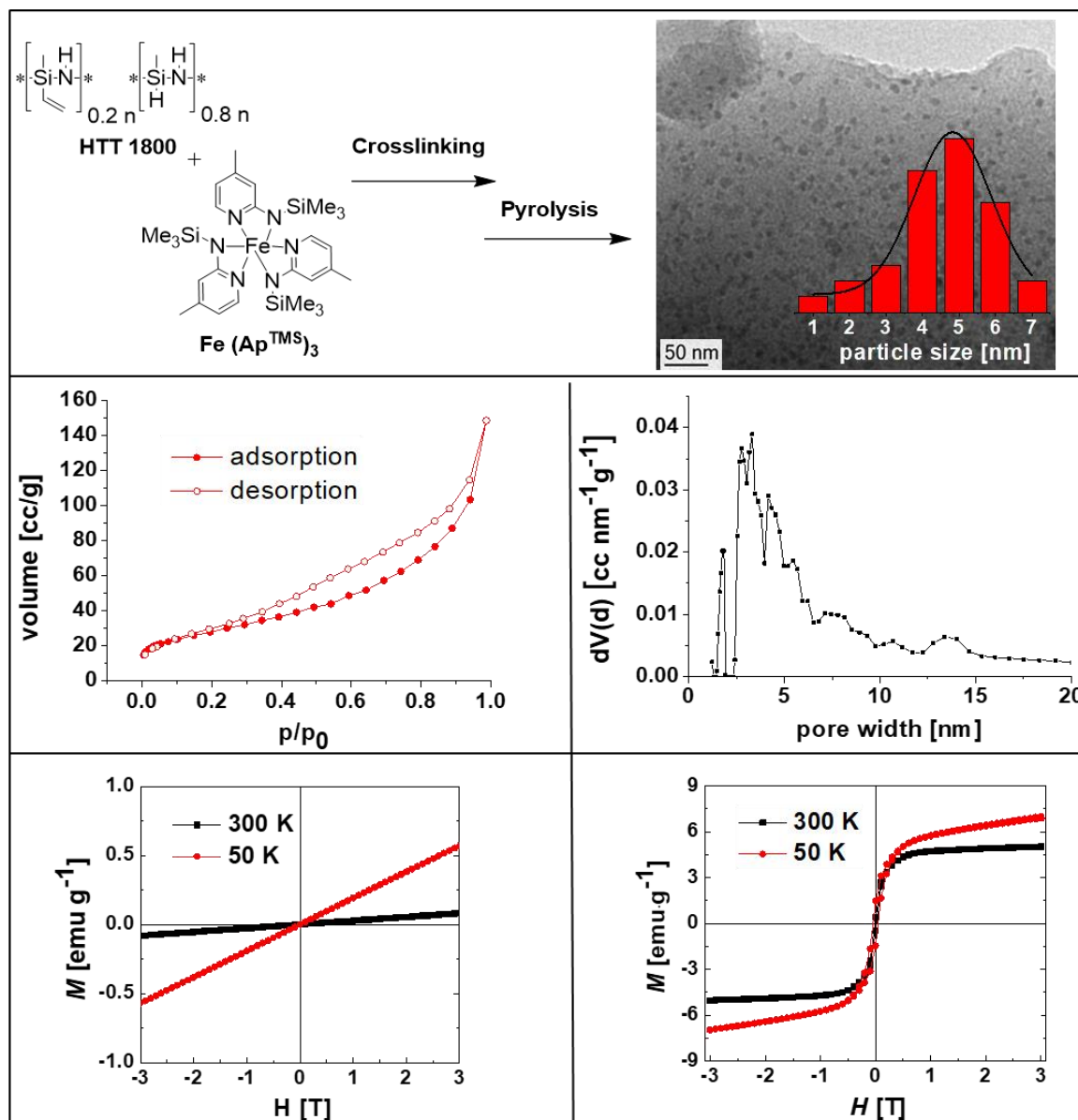


Figure 1: Top (left): Synthesis of the novel Fe@SiCN nanocomposite. The iron complex and the commercial available polysilazane HTT 1800 are dissolved in THF, followed by crosslinking with DCP as an external initiator at 105 °C. The greenbody obtained undergoes pyrolysis under nitrogen atmosphere at 750 °C, resulting in an amorphous Fe@SiCN nanocomposite. Top (right): TEM analysis verified the presence of small iron nanoparticles with a homogenous particle size distribution centered at 5 nm. Center left: Pore characterization of the Fe@SiCN nanocomposite via nitrogen sorption measurements. Center right: Calculated pore-size distribution. Bottom: Magnetic measurements confirm the transition of Fe^{3+} ions in the greenbody (left) to iron nanoparticles (superparamagnetic properties) in the final nanocomposite (right).

Six consecutive runs were performed (conditions for 80 % yield) to confirm the recyclability of our catalyst. The catalytic activity declines after the fifth run but can be regained the TPR treatment (Figure 2). We propose the formation of inactive oxide species during catalyst separation and handling. Routinely, we used TPR activation not prior to each use but after three or four times use of a catalyst sample.

Next, we looked for catalytic transformations that include a nitroarene hydrogenation step but involve further C-N and/or C-C bond formation steps for direct syntheses based on the selectivity

patterns discovered above, here especially the tolerance of carbonyl compounds. The direct synthesis of imines from nitroarenes and aldehydes was investigated first and we discover that the condition optimal for the hydrogenation of nitroarenes work for the imine synthesis as well. We see up to 8 % aryl-alkyl amine by-product formation, which reduces the (isolated) yields of the imines. Various aldehydes and nitroarenes were linked directly. Halogenated substrates (Table 2, Entries 1c, 2b) achieved isolated yields between 87 and 89 %. Keto and nitrile functionalities were investigated to confirm the tolerance of hydrogenation sensitive functional groups. The resulting imines were obtained in 72 and 84 % isolated yield, respectively. In addition, sterically demanding substituents had no negative effect on the direct imine synthesis (Table 2, Entries 2a,b, 5-7).

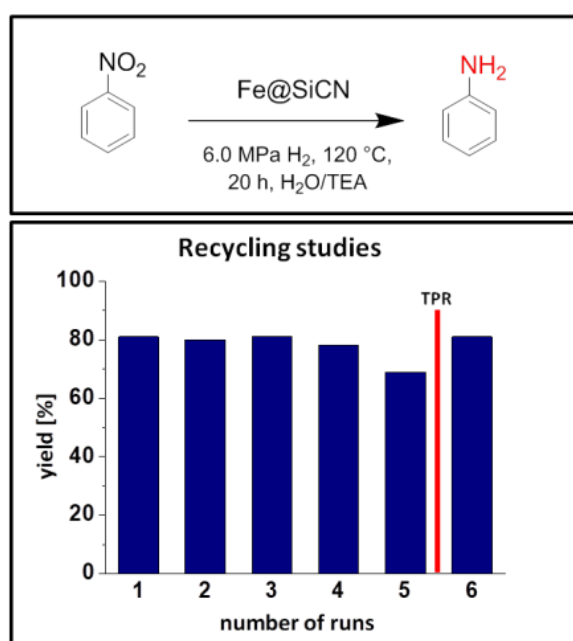


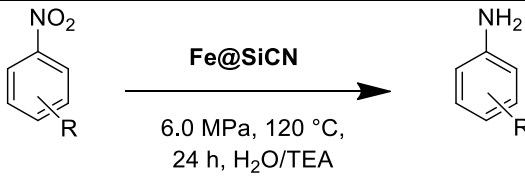
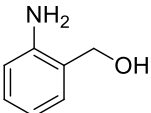
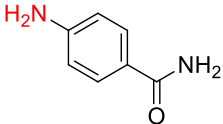
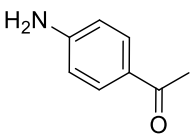
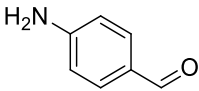
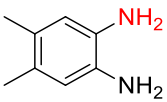
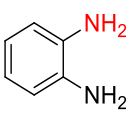
Figure 2: Top: Benchmark reaction with optimized reaction conditions. Bottom: Recycling of the Fe@SiCN catalyst over six consecutive runs (conditions for 80 % yield). The activity could be restored completely through TPR treatment.

The direct synthesis of benzimidazoles from nitroarenes and aldehydes was investigated next (Table 3) with the reductive coupling of 4,5-dimethyl-2-nitroaniline and benzaldehyde as the benchmark reaction. The corresponding benzimidazole was obtained in 87 % isolated yield under optimized reaction conditions (Table 3, Entry 1a). Aryl halide as well as heterocyclic based aldehydes gave similarly high yields (Table 3, Entries 1c,d, 2) and even aliphatic aldehyde can be employed (Table 3, Entry 3).

Finally, the direct synthesis of quinoxalines from nitroarenes and diketones was investigated (Table 4). The formation of 6,7-dimethyl-2,3-diphenylquinoxaline from 4,5-dimethyl-2-nitroaniline and benzil was used as the benchmark reaction. Some of the quinoxalines synthesized were obtained

in isolated yields > 90 % (Table 4, Entry 1a and c). Again, an attractive functional group tolerance including a hydrogenation sensitive substituent, nitrile, was observed.

Table 1: Chemoselective hydrogenation of substituted nitroarenes; substrate scope^[a].

<div style="text-align: center;">  </div>		
Entry	Product	Yield ^[b] [%]
1	R = H	> 99
2	R = 2-Cl	91
3	R = 3-Cl	> 99
4	R = 4-Cl	> 99
5	R = 2-Br	87
6	R = 3-Br	92
7	R = 4-Br	97
8	R = 4-F	92
9	R = 4-I	70 ^[c]
10	R = 3-CN	92 ^[d]
11		80
12		85
13		95
14		89
13		> 99 ^[e]
14		95 ^[e]

4. The Direct Synthesis of Imines, Benzimidazoles and Quinoxalines from Nitroarenes and Carbonyl Compounds via Selective Nitroarene Hydrogenation Employing a Reusable Iron Catalyst

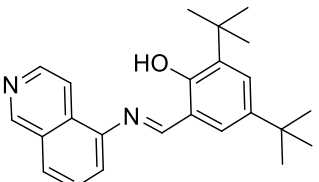
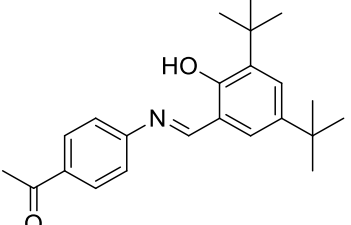
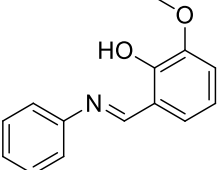
15		94 ^[e]
16		89
17		88

[a] Reaction conditions: 0.5 mmol substrate, 120 °C, 6.0 MPa H₂, 10 mol % catalyst (2.8 mg Fe, 0.05 mmol, 70 mg), 1 mL TEA, 3 mL H₂O, 20 h. [b] Yields were determined by GC using *n*-dodecane as an internal standard. [c] 100 °C, 6.5 MPa, 11 mol % catalyst. [d] 4 mL H₂O. [e] 125 °C, 6.5 MPa, 24 h.

Table 2: Selective synthesis of substituted imines from nitroarenes and aldehydes; substrate scope^[a].

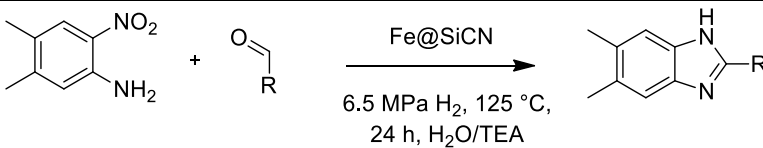
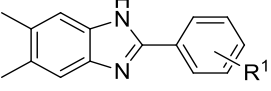
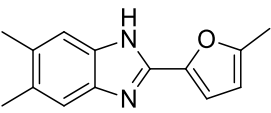
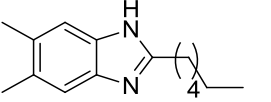
Entry	Product		Yield ^[b] [%]
1		1a: R ¹ = H 1b: R ¹ = OMe 1c: R ¹ = Cl 1d: R ¹ = CN	83 88 89 84 ^[c]
2		2a: R ² = H 2b: R ² = Br	92 87
3			82
4			79

4. The Direct Synthesis of Imines, Benzimidazoles and Quinoxalines from Nitroarenes and Carbonyl Compounds via Selective Nitroarene Hydrogenation Employing a Reusable Iron Catalyst

5		89
6		72
7		81

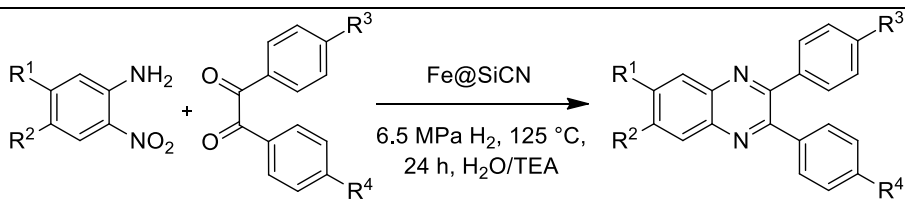
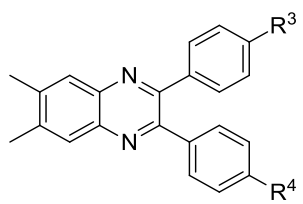
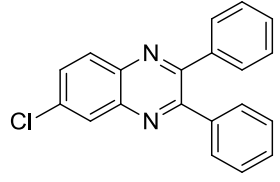
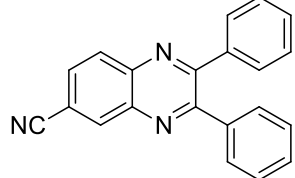
[a] Reaction conditions: 0.5 mmol substrate, 120 °C, 6.0 MPa H₂, 10 mol % catalyst (2.8 mg Fe, 0.05 mmol, 70 mg), 1 mL TEA, 3 mL H₂O, 20 h. [b] Yields of isolated product. [c] 4 mL H₂O.

Table 3: Selective synthesis of substituted benzimidazoles; substrate scope^[a].

			
Entry	Product		Yield ^[b] [%]
1		1a: R ¹ = H	87
		1b: R ¹ = 4-OMe	81
		1c: R ¹ = 4-F	84
		1d: R ¹ = 4-Cl	83
2			72
3			69

[a] Reaction conditions: 0.5 mmol substrate, 125 °C, 6.5 MPa H₂, 10 mol % catalyst (2.8 mg Fe, 0.05 mmol, 70 mg), 1 mL TEA, 3 mL H₂O, 24 h. [b] Yields of isolated product.

Table 4: Selective synthesis of substituted quinoxalines; substrate scope^[a].

			
Entry	Product		Yield ^[b] [%]
1		1a: R ^{3/4} = H	95
		1b: R ^{3/4} = 4-OMe	86
		1c: R ^{3/4} = 4-F	92
		1d: R ^{3/4} = 4-Cl	89
2			75
3			76 ^[c]

[a] Reaction conditions: 0.5 mmol substrate, 125 °C, 6.5 MPa H₂, 10 mol % catalyst (2.8 mg Fe, 0.05 mmol, 70 mg), 1 mL TEA, 3 mL H₂O, 24 h. [b] Yields of isolated product. [c] 4 mL H₂O, 11 mol % catalyst.

In summary, we have developed a novel, robust, reusable, easy to synthesize and easy to handle iron catalyst. The Fe-SiCN nanocomposite catalyst is highly selective in the hydrogenation of nitroarenes in the presence of hydrogen-sensitive functional groups. The tolerance of aldehydes permits the direct iron catalyzed synthesis of imines and benzimidazoles from nitroarenes and aldehydes. Again, hydrogenation sensitive functional groups can be tolerated. The direct synthesis of quinoxalines from nitroarenes and diketones is a novel way of accessing this important class of N-heterocyclic compound.

4.3 Acknowledgements

We thank Katja Dankhoff and Prof. Dr. Birgit Weber for magnetic measurements, John Kannan Mohanraj and Dr. Sven Hüttner for XPS analysis, Tobias Schwob and Gabriela Hahn for TEM analysis. We thank the Deutsche Forschungsgemeinschaft, SFB 840, B1 for financial support.

Keywords: iron • quinoxalines • benzimidazoles • imines • nitroarene hydrogenation

4.4 References

- [1] B. Cornils, W. A. Hermann, R. Schlögle, C.H. Wong (Eds.), *Catalysis from A to Z, 2nd edition*, Wiley-VCH, Weinheim, **2002**.
- [2] a) H.-U. Blaser, H. Steiner, M. Studer, *ChemCatChem*. **2009**, *1*, 210-221.
- [3] a) A. Corma, P. Serna, P. Concepcion, J. J. Calvino, *J. Am. Chem. Soc.* **2008**, *130*, 8748-8753; b) A. Corma, P. Serna, *Science* **2006**, *313*, 332-334.
- [4] a) R. V. Jagadeesh, A.-E. Surkus, H. Junge, M.-M. Pohl, J. Radnik, J. Rabeah, H. Huan, V. Schunemann, A. Brückner, M. Beller, *Science* **2013**, *342*, 1073-1076; b) R. V. Jagadeesh, T. Stemmler, A.-E. Surkus, H. Junge, K. Junge, M. Beller, *Nat. Protoc.* **2015**, *10*, 548-557; c) D. Formenti, C. Topf, K. Junge, F. Ragaini, M. Beller, *Catal. Sci. Technol.* **2016**, *6*, 4473-4477.
- [5] a) F. A. Westerhaus, R. V. Jagadeesh, G. Wienhofer, M.-M. Pohl, J. Radnik, A.-E. Surkus, J. Rabeah, K. Junge, H. Junge, M. Nielsen, A. Brückner, M. Beller, *Nat. Chem.* **2013**, *5*, 537-543; b) R. V. Jagadeesh, T. Stemmler, A.-E. Surkus, M. Bauer, M.-M. Pohl, J. Radnik, K. Junge, H. Junge, A. Brückner, M. Beller, *Nat. Protoc.* **2015**, *10*, 916-926.
- [6] For selected examples see: a) Z. Wei, J. Wang, S. Mao, D. Su, H. Jin, Y. Wang, F. Xu, H. Li, Y. Wang, *ACS Catal.* **2015**, *5*, 4783-4789; d) L. Liu, P. Concepción, A. Corma, *J. Catal.* **2016**, *340*, 1-9; b) B. Chen, F. Li, Z. Huang, G. Yuan, *ChemCatChem*. **2016**, *8*, 1132-1138; c) P. Ji, K. Manna, Z. Lin, X. Feng, A. Urban, Y. Song, W. Lin, *J. Am. Chem. Soc.* **2017**, *139*, 7004-7011; d) P. Zhou, Z. Zhang, *ChemSusChem* **2017**, *10*, 1892-1897; e) H. Alex, P. Loos, T. Baramov, J. Barry, T. Godiawala, J. Hassfeld, N. Steinfeldt, *ChemCatChem* **2017**, *9*, 16; f) I. Sorribes, L. Liu, A. Corma, *ACS Catalysis* **2017**, *7*, 2698-2708; g) F. Zhang, C. Zhao, S. Chen, H. Li, H. Yang, X.-M. Zhang, *J. Catal.* **2017**, *348*, 212-222; h) L. Jiang, P. Zhou, Z. Zhang, Q. Chi, S. Jin, *New J. Chem.* **2017**, *41*, 11991-11997; i) X. Cui, K. Liang, M. Tian, Y. Zhu, J. Ma, Z. Dong, *J. Colloid Interface Sci.* **2017**, *501*, 231-240; j) B. Sahoo, D. Formenti, C. Topf, S. Bachmann, M. Scalone, K. Junge, M. Beller, *ChemSusChem* **2017**, *10*, 3035-3039; k) L. Liu, F. Gao, P. Concepción, A. Corma, *J. Catal.* **2017**, *350*, 218-225; l) Z. Wei, S. Mao, F. Sun, J. Wang, B. Mei, Y. Chen, H. Li, Y. Wang, *Green Chem.* **2018**, *20*, 671-679; m) X. Sun, A. I. Olivos-Suarez, D. Osadchii, M. J. V. Romero, F. Kapteijn, J. Gascon, *J. Catal.* **2018**, *357*, 20-28.
- [7] T. Schwob, R. Kempe, *Angew. Chem. Int. Ed.* **2016**, *55*, 15175-15179.
- [8] M. Eckardt, M. Zaheer, R. Kempe, *Sci. Rep.* **2018**, *8*, 2567-2572.
- [9] V. C. Gibson, S. K. Spitzmesser, *Chem. Rev.* **2003**, *103*, 283-315.
- [10] A. W. Bosman, H. M. Janssen, E. W. Meijer, *Chem. Rev.* **1999**, *99*, 1665-1688.
- [11] D. J. Hadjipavlou-Litina, A. A. Geronikaki, *Drug Des. Discov.* **1998**, *15*, 199-206.

- [12] For selected examples of catalytic imine syntheses, please see: (oxidation of amines) a) H. Yuan, W.-J. Yoo, H. Miyamura, S. Kobayashi, *J. Am. Chem. Soc.* **2012**, *134*, 13970-13973; b) T. Sonobe, K. Oisaki, M. Kanai, *Chem. Sci.* **2012**, *3*, 3249-3255. (self-condensation of primary amines upon oxidation) c) F. Su, S. C. Mathew, L. Mohlmann, M. Antonietti, X. Wang, S. Blechert, *Angew. Chem. Int. Ed.* **2011**, *50*, 657-660; d) B. Chen, L. Wang, S. Gao, *ACS Catal.* **2015**, *5*, 5851-5876; e) B. Chen, L. Wang, W. Dai, S. Shang, Y. Lv, S. Gao, *ACS Catal.* **2015**, *5*, 2788-2794. (oxidative coupling of alcohols and amines) f) M. Tamura, K. Tomishige, *Angew. Chem. Int. Ed.* **2015**, *54*, 864-867; g) L. Geng, J. Song, Y. Zhou, Y. Xie, J. Huang, W. Zhang, L. Peng, G. Liu, *Chem. Commun.* **2016**, *52*, 13495-13498; h) B. Chen, S. Shang, L. Wang, Y. Zhang, S. Gao, *Chem. Commun.* **2016**, *52*, 471-484; i) X. Huang, L. Liu, H. Gao, W. Dong, M. Yang, G. Wang, *Green Chem.* **2017**, *19*, 769-777. (acceptorless dehydrogenative coupling of alcohols and amines) j) B. Gnanaprakasam, J. Zhang, D. Milstein, *Angew. Chem. Int. Ed.* **2010**, *122*, 1510-1513; k) L. Tang, H. Sun, Y. Li, Z. Zha, Z. Wang, *Green Chem.* **2012**, *14*, 3423-3428; l) S. Ruch, T. Irrgang, R. Kempe, *Chem. Eur. J.* **2014**, *20*, 13279-13285; m) J. Bain, P. Cho, A. Voutchkova-Kostal, *Green Chem.* **2015**, *17*, 2271-2280; n) A. Mukherjee, A. Nerush, G. Leitius, L. J. W. Shimon, Y. Ben David, N. A. Espinosa Jalapa, D. Milstein, *J. Am. Chem. Soc.* **2016**, *138*, 4298-4301; o) M. Mastalir, M. Glatz, N. Gorgas, B. Stoger, E. Pittenauer, G. Allmaier, L. Veiros, K. Kirchner, *Chem. Eur. J.* **2016**, *22*, 12316-12320; p) D.-W. Tan, H.-X. Li, M.J. Zhang, J.-L. Yao, J.-P. Lang, *ChemCatChem* **2017**, *9*, 1113-1118. (hydrogenative cross-coupling of nitriles and amines) q) S. Chakraborty, G. Leitius, D. Milstein, *Angew. Chem. Int. Ed.* **2017**, *56*, 2074-2078. (hydrogenation of nitriles to imines) r) S. Chakraborty, D. Milstein, *ACS Catal.* **2017**, *7*, 3968-3972.
- [13] For selected examples for the reductive synthesis of imines from nitroarenes and aldehydes, please see: a) Y. Zheng, K. Ma, H. Li, J. Li, J. He, X. Sun, R. Li, J. Ma, *Catal. Lett.* **2009**, *128*, 465-474; b) L. L. Santos, P. Serna, A. Corma, *Chem. Eur. J.* **2009**, *15*, 8196-8203; c) F. G. Cirujano, A. Leyva-Pérez, A. Corma, F. X. Llabrés i Xamena, *ChemCatChem* **2013**, *5*, 538-549; d) Y.-Z. Chen, Y.-X. Zhou, H. Wang, J. Lu, T. Uchida, Q. Xu, S.-H. Yu, H.-L. Jiang, *ACS Catal.* **2015**, *5*, 2062-2069.
- [14] Selected examples of recent publications reporting catalytic syntheses of benzimidazoles: a) N. T. Jui, S. L. Buchwald, *Angew. Chem. Int. Ed.* **2013**, *52*, 11624-11627; b) K. Bahrami, M. M. Khodaei, A. Nejati, *Green Chem.* **2013**, *12*, 1237-1241; c) T. B. Nguyen, L. Ermolenko, A. Al-Mourabit, *J. Am. Chem. Soc.* **2013**, *135*, 118-121; d) T. Hille, T. Irrgang, R. Kempe, *Chem. Eur. J.* **2014**, *20*, 5569-5572; e) C. Xu, Z.-Q. Xiao, H.-M. Li, X. Han, Z.-Q. Wang, W.-J. Fu, B.-M. Ji, X.-Q. Hao, M.-P. Song, *Eur. J. Org. Chem.* **2015**, 7427-7432; f) C. Chaudhari, S. H. Siddiki, K.-i. Shimizu, *Tetrahedron Lett.* **2015**, *56*, 4885-4888; g) Z. Sun, G. Bottari, K. Barta, *Green Chem.*

- 2015**, *17*, 5172-5181; h) D. Mahesh, P. Sadhu, T. Punniyamurthy, *J. Org. Chem.* **2016**, *81*, 3227-3234; i) X. Cui, K. Liang, M. Tian, Y. Zhu, J. Ma, Z. Dong, *J. Colloid Interface Sci.* **2017**, *501*, 231-240.
- [15] Selected examples of recent publications reporting catalytic syntheses of quinoxalines: a) D. J. Klein, D. A. Modarelli, F. W. Harris, *Macromolecules* **2001**, *34*, 2427-2437; b) K. M. Evans, A. M. Z. Slawin, T. Lebl, D. Philp, N. J. Westwood, *J. Org. Chem.* **2007**, *72*, 3186-3193; c) A. Go, G. Lee, J. Kim, S. Bae, B. M. Lee, B. H. Kim, *Tetrahedron* **2015**, *71*, 1215-1226; d) B. Roy, S. Ghosh, P. Ghosh, B. Basu, *Tetrahedron Lett.* **2015**, *56*, 6762-6767; e) N. Kolmer-Anderl, A. Kolmer, C. M. Thiele, M. Rehahn, *Chem. Eur. J.* **2016**, *22*, 5277-5287.
- [16] For selected examples, please see: a) D. Forberg, T. Schwob, M. Zaheer, M. Friedrich, N. Miyajima, R. Kempe, *Nature Commun.* **2016**, DOI: 10.1038/ncomms13201. b) S. Sachau, M. Zaheer, A. Lale, M. Friedrich, C. Denner, U. B. Demirci, S. Bernard, G. Motz, R. Kempe, *Chem. Eur. J.* **2016**, *43*, 15508-15512; c) G. Hahn, J.-K. Ewert, C. Denner, D. Tilgner, R. Kempe, *ChemCatChem* **2016**, *8*, 2461-2465; d) J.-K. Ewert, D. Weingarth, C. Denner, M. Friedrich, M. Zeiger, A. Schreiber, N. Jäckel, V. Presser, R. Kempe, *J. Mater. Chem. A* **2015**, *3*, 18906-18912; e) M. Zaheer, J. Hermannsdörfer, W. P. Kretschmer, G. Motz, R. Kempe, *ChemCatChem* **2014**, *6*, 91-95; f) D. Forberg, J. Obenauf, M. Friedrich, S.-M. Hühne, W. Mader, G. Motz, R. Kempe, *Catal. Sci. Technol.* **2014**, *4*, 4188-4192; g) M. Zaheer, T. Schmalz, G. Motz, R. Kempe, *Chem. Soc. Rev.* **2012**, *41*, 5102-5116.
- [17] T. Stemmler, F. A. Westerhaus, A.-E. Surkus, M.-M. Pohl, K. Junge, M. Beller, *Green Chem.* **2014**, *16*, 4535-4540.

4.5 Supporting Information

4.5.1 General Considerations

All air- and moisture sensitive reactions were performed under dry argon or nitrogen atmosphere using standard Schlenk and glove box techniques. All dried solvents were obtained from a solvent purification system (activated alumina cartridges) or purchased from Acros. Deuterated solvents were dried via molecular sieves. All chemicals were acquired from commercial sources with purity over 95 % and used without further purification. The precursor KION HTT 1800 was purchased from Clariant Advanced Materials GmbH, Frankfurt (Germany) and was degassed with argon before use. The ceramization was performed under argon atmosphere in a high temperature furnace (Gero, Berlin, Germany). Transmission electron microscopy (TEM) was carried out by using a Variant LEO 9220 (200 kV) and a JEOL JEM 2200FS (200 kV) device. For the sample preparation the ceramic was suspended in chloroform and sonicated for 5 min. For analysis a CF200-Cu grid was used. Pore characterizations were carried out via nitrogen sorption measurements using a Nova2000e (Quantachrome) device. The pore size distribution was computed via DFT calculations [calculation model: N₂ at -196.15 °C on carbon (slit/cylindrical pore, NLDFT equilibrium model)]. The specific surface area was calculated by using p/p_0 values from 0.05-0.31 (BET). Hydrogen chemisorption measurements were performed by using a ChemBET Pulsar TPR/TPD instrument from Quantachrome. X-ray photoelectron spectroscopy (XPS) was performed using a PHI Versa Probe III instrument of Physical Electronics. As X-ray source a monochromatic Al K α with a spot size of 100 μ m (24.5 W) was used. The kinetic pass energy of the photoelectrons was determined with a hemispheric analyzer (45°) set to pass energy of 26 eV for high-resolution spectra.

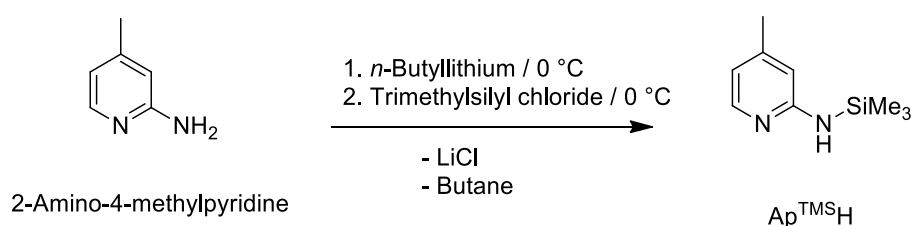
Magnetic measurements were performed with a SQUID MPMS-XL5 device from Quantum Design with the field range of -3 to 3 T in hysteresis mode. The sample was prepared in a gelatin capsule held in a plastic straw under protective atmosphere. The raw data were corrected for the diamagnetic part of the sample holder. NMR measurements were carried out with a Varian INOVA 300 (300 MHz for ¹H, 75 MHz for ¹³C) at 296 K. Chemical shifts are reported in ppm relative to the residual solvent signal (CDCl₃: 7.26 ppm (¹H), 77.16 ppm (¹³C); DMSO-d₆: 2.50 ppm (¹H), 39.51 ppm (¹³C)), coupling constants (J) are reported in Hz. EDX (energy dispersive X-ray spectroscopy) measurements were performed by using a LEO

1530 GEMINI with an acceleration voltage of 1-5 kV. All tested reactions were determined via GC and GC-MS analysis. GC analyses were carried out on an Agilent 6890N Network GC system equipped with a HP-5 column (30 m x 0.32 mm x 0.25 μ m). GC-MS analyses were carried out on an Agilent 7890A GC system equipped with a HP-5MS column (30 m x 0.32 mm x 0.25 μ m) and a 5975C inert MSD. The hydrogenation experiments were carried out with Parr Instrument stainless steel autoclaves N-MT5 300 mL equipped with heating mantles and temperature controller.

4.5.2 Synthesis and characterization of the Fe nanocomposite

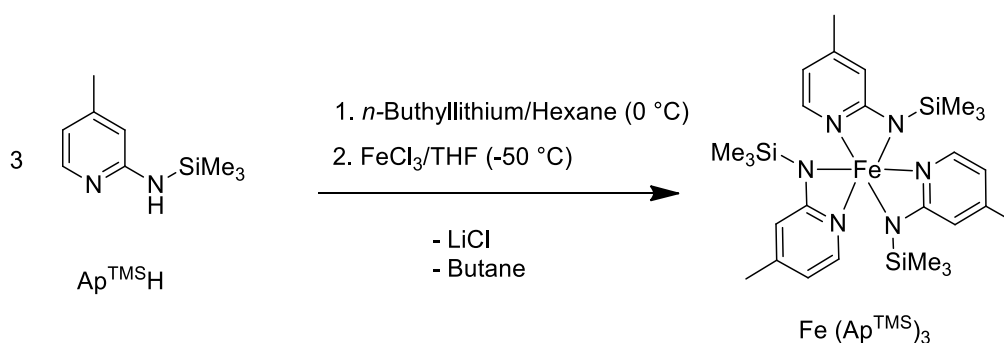
Synthesis of 4-methyl-2-((trimethylsilyl)amino)pyridine (Ap^{TMS}H)

The 4-methyl-2-((trimethylsilyl)amino)pyridine compound was synthesized according to a known literature.^[1]



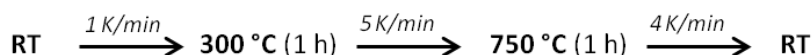
Complex synthesis

The Fe(Ap^{TMS})₃ complex was also synthesized according to known literature.^[2]



Ceramization

In a vial placed in a Schlenk tube, 12 mg dicumylperoxid (5 wt.-% HTT 1800) and 99.7 mg (0.17 mmol) $\text{Fe}(\text{Ap}^{\text{TMS}})_3$ were dissolved in 2 mL tetrahydrofuran. Under vigorous stirring, 250 μl (3.36 mmol) HTT 1800 was added dropwise to the solution. After crosslinking at 110 °C for 24 h, the solvent was removed and the greenbody was pyrolyzed under nitrogen atmosphere with the following pyrolysis program:



The ceramic yield was 73 % after the ceramization process. Finally, the received nanocomposite was milled for 20 min and washed by stirring in an aqueous solution of 5 mL NaOH ($c = 1\text{ mol/l}$) and 1 mL MeOH at 60 °C for 12 h under aerobic conditions.

ICP-OES analysis

25 mg of the catalyst were solved in 1.5 mL HNO_3 (65 %, distilled), 4.5 mL HCl (32 %, p.a.) and 1 mL HF (40 %) and heated in a microwave up to 170 °C for 7 min (80 % power), at 180 °C for 7 min (85 % power) and at 195 °C for 20 min (90 % power).

Results:

- as synthesized: 3.0 wt.-% Fe
- after washing procedure: 4.0 wt.-% Fe

Leaching experiment: A mixture of 70 mg Fe catalyst, 1 mL triethylamine and 3 mL H_2O were stirred at 120 °C and 6.0 MPa H_2 pressure for 20 h. The catalyst was removed and the resulting solution was analyzed by ICP-OES. A total Fe amount of 0.02 % of was found.

TEM analysis

TEM analysis verifies a homogenous distribution of the Fe nanoparticles in the amorphous SiCN matrix.

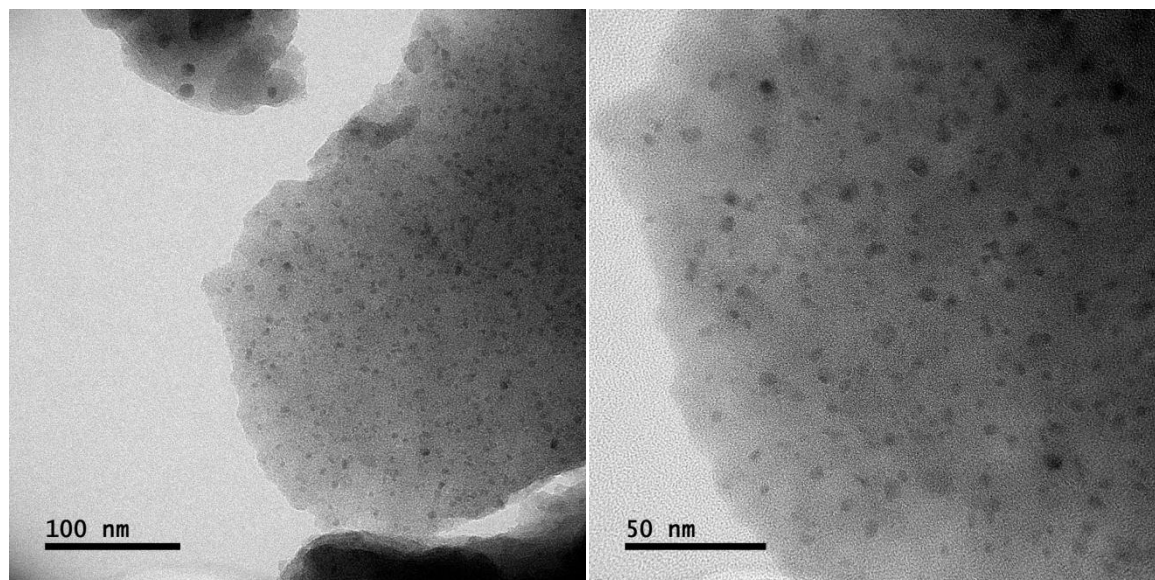


Figure S 1: TEM analysis of the Fe@SiCN nanocomposite.

Energy dispersive X-ray analysis

EDX measurements were carried out to get an inside in the surface of the catalyst. Silicon, carbon and nitrogen were associated with the precursor. The used FeCl_3 gave peaks at 0.71 and 6.40 keV for Fe and 2.62 keV for the Cl. The detected oxygen is assigned to the use of the radical initiator (dicumylperoxid) in the cross-linking process.

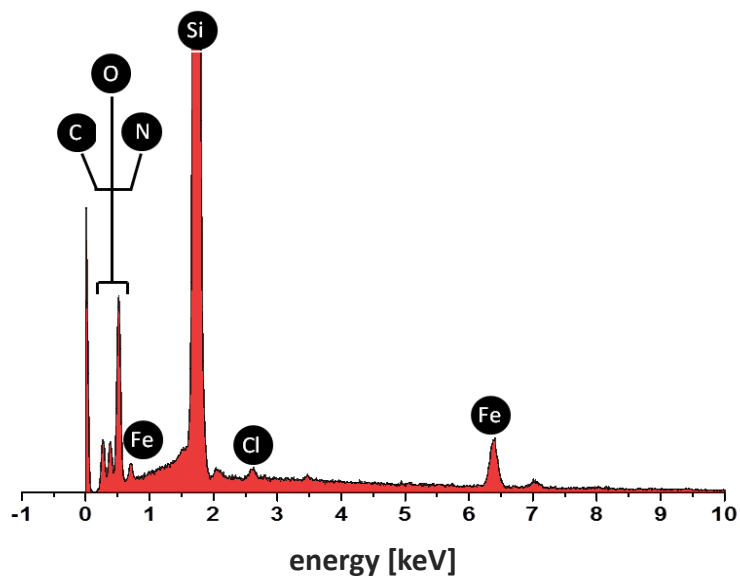


Figure S 2: Energy dispersive X-ray analysis of the catalyst surface.

Temperature programmed reduction (TPR)

High-temperature hydrogen treatment (temperature-programmed reduction (TPR)) was carried out after the washing procedure. The sample was heated up to 600 °C with 5 K/min under reductive atmosphere (95 % N₂, 5 % H₂). The first TPR run (red) was performed directly after the washing procedure. The second run was accomplished subsequently after the first TPR (black). H₂ uptake between 350 and 600 °C indicates partial oxidation of the NP during the purifying procedure. No H₂ signal was detected during the second run (black) indicating a complete reduction of the iron oxide species.

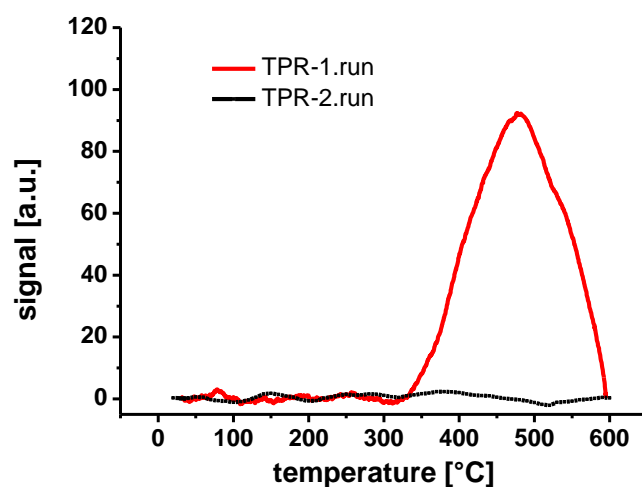


Figure S 3: Temperature programmed reduction of the washed Fe catalyst.

X-ray photoelectron spectroscopy (XPS)

XPS-measurements were carried out after the washing procedure. In **Figure S 4** the Fe 2p region is depicted.

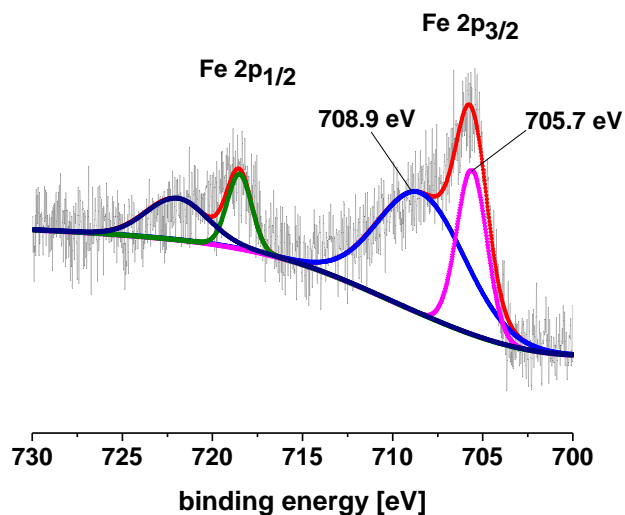


Figure S 4: XP spectra of the pretreated Fe@SiCN catalyst.

The Fe 2p_{3/2} signal can be divided in two signals with the binding energies of 705.7 and 708.9 eV. The presence of metallic Fe could be identified due to its sharp line shape and its binding energies of 705.7 eV. At higher binding energies different oxides (FeO, Fe₂O₃) are found that cannot be distinguished in the analysis.

4.5.3 Catalytic studies

Selective hydrogenation of nitrobenzene – screening experiments

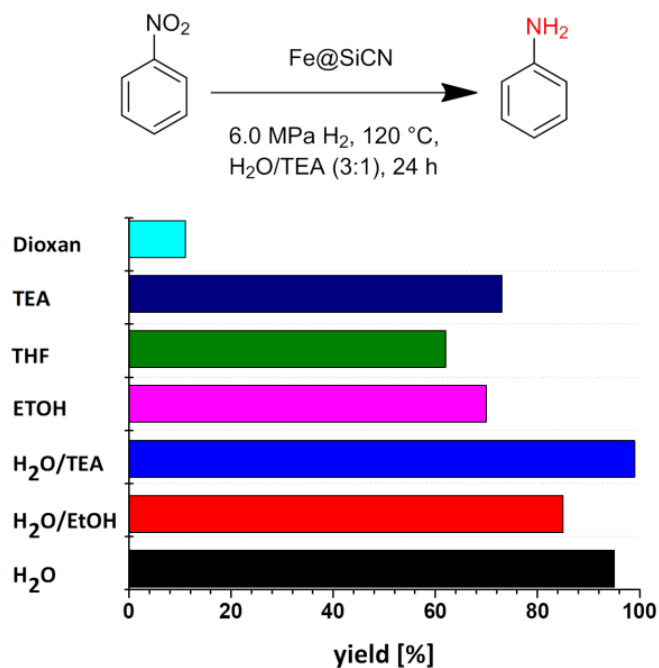


Figure S 5: Solvent screening - Selective hydrogenation of nitrobenzene; 120 °C, 6.0 MPa H₂, 10 mol% catalyst (2.8 mg Fe, 0.05 mmol, 70 mg), 4 mL solvent, 20 h.

Table S 1: Selective hydrogenation of nitrobenzene - optimization of the reaction parameters.

Entry	Fe:SiCN [ratio]	Catalyst loading [mol %]	Temperature [°C]	Pressure [MPa]	GC-yield [%]
1	1:20	10	120	6.0	> 99
2	1:20	10	110	6.0	87
3	1:20	10	100	6.5	73
4	1:10	10	120	5.0	70

General catalytic procedures

Selective hydrogenation of nitroarenes – general procedure

A magnetic stirring bar, 0.5 mmol nitro derivative, 3 mL H₂O, 1 mL triethylamine and 10 mol % Fe catalyst (2.8 mg Fe, 0.05 mmol, 70 mg) were filled in a 5 mL reaction vial. The vial was placed in a high-pressure autoclave (Parr Instruments) and the autoclave was flushed three times with 2.0 MPa of hydrogen. The autoclave was pressured with 6.0 MPa of hydrogen and the reaction was stirred for 20 h at 120 °C. The autoclave was cooled to room temperature and the hydrogen pressure was released. Then, n-dodecane was added and the solution was extracted with ethyl acetate and dried over Na₂SO₄. The yields were determined via GC and GC-MS analysis.

Selective synthesis of substituted aldimines – general procedure

A magnetic stirring bar, 1 mmol nitro derivative, 2 mmol aldehyde, 3 mL H₂O, 1 mL triethylamine and 10 mol % Fe catalyst (5.6 mg Fe, 0.1 mmol, 140 mg) were filled in a 5 mL reaction vial. The vial was placed in a high-pressure autoclave (Parr Instruments) and the autoclave was flushed three times with 2.0 MPa of hydrogen. The autoclave was pressured with 6.0 MPa of hydrogen and the reaction was stirred for 20 h at 120 °C. The autoclave was cooled to room temperature and the hydrogen pressure was released. Then, n-dodecane was added and the solution was extracted with ethyl acetate, dried over Na₂SO₄ and subsequently analyzed via GC and GC-MS.

After removal of the catalyst by centrifugation, the solvent was removed under reduced pressure. The pure product was achieved by crystallization or column chromatography. All synthesized aldimines were analyzed by NMR spectroscopy.

Selective synthesis of substituted benzimidazoles – general procedure

A magnetic stirring bar, 1 mmol 4,5-dimethyl-2-nitroaniline, 2 mmol aldehyde, 3 mL H₂O, 1 mL triethylamine and 10 mol % Fe catalyst (5.6 mg Fe, 0.1 mmol, 140 mg) were filled in a 5 mL reaction vial. The vial was placed in a high-pressure autoclave (Parr Instruments) and the autoclave was flushed three times with 2.0 MPa of hydrogen. The autoclave was pressured with 6.5 MPa of hydrogen and the reaction was stirred for 24 h at 125 °C. After that the autoclave was cooled to room temperature and the hydrogen pressure was released. Then, n-dodecane was added and the solution was extracted with ethyl acetate, dried over Na₂SO₄ and subsequently analyzed via GC and GC-MS. After removal of the catalyst by centrifugation, the solvent was removed under reduced pressure. The pure product was achieved by crystallization or column chromatography. All synthesized benzimidazoles were analyzed by NMR spectroscopy.

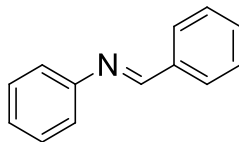
Selective synthesis of substituted quinoxalines – general procedure

A magnetic stirring bar, 1 mmol 4,5-dimethyl-2-nitroaniline, 2 mmol diketone, 3 mL H₂O, 1 mL triethylamine and 10 mol % Fe catalyst (5.6 mg Fe, 0.1 mmol, 140 mg) were filled in a 5 mL reaction vial. The vial was placed in a high-pressure autoclave (Parr Instruments) and the autoclave was flushed three times with 2.0 MPa of hydrogen. The autoclave was pressured with 6.5 MPa of hydrogen and the reaction was stirred for 24 h at 125 °C. After that the autoclave was cooled to room temperature and the hydrogen pressure was released. Then, n-dodecane was added and the solution was extracted with ethyl acetate, dried over Na₂SO₄ and subsequently analyzed via GC and GC-MS. After removal of the catalyst by centrifugation, the solvent was removed under reduced pressure. The pure product was achieved by crystallization or column chromatography. All synthesized quinoxalines were analyzed by NMR spectroscopy.

4.5.4 Characterization of isolated products

Imines

1a:



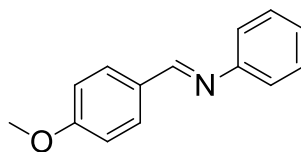
N-benzylideneaniline

[C₁₃H₁₁N] 180.1 g/mol (M)

¹H NMR (300 MHz, CDCl₃, 296 K): δ = 8.50 (s, 1H), 7.97-7.94 (m, 2H), 7.53-7.51 (m, 3H), 7.47-7.43 (m, 2H), 7.30-7.26 (m, 3H) ppm.

¹³C NMR (75 MHz, CDCl₃, 296 K): δ = 160.42, 151.98, 136.13, 131.35, 129.11, 128.77, 125.90, 120.84 ppm.

1b:



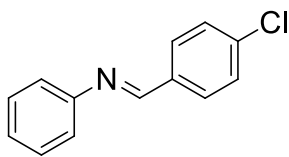
N-(4-methoxybenzylidene)aniline

[C₁₄H₁₃NO] 211.1 g/mol (M)

¹H NMR (300 MHz, CDCl₃, 296 K): δ = 8.43 (s, 1H), 7.93-7.90 (m, 2H), 7.48-7.42 (d, J = 9 Hz, 2H), 7.30-7.26 (m, 3H), 7.05-7.02 (d, J = 9 Hz, 2H), 3.89 (s, 3H) ppm.

¹³C NMR (75 MHz, CDCl₃, 296 K): δ = 161.67, 159.14, 151.77, 129.96, 128.56, 125.02, 120.33, 113.60, 54.81 ppm.

1c:



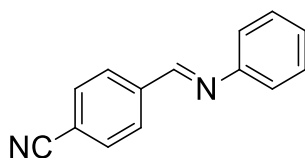
N-(4-chlorobenzylidene)aniline

[C₁₃H₁₀ClN] 215.1 g/mol (M)

¹H NMR (300 MHz, CDCl₃, 296 K): δ = 8.46 (s, 1H), 7.90-7.87 (m, 2H), 7.51-7.42 (m, 4H), 7.27-7.25 (m, 3H) ppm.

¹³C NMR (75 MHz, CDCl₃, 296 K): δ = 158.37, 151.18, 136.90, 134.22, 129.50, 128.74, 128.62, 125.75, 120.39 ppm.

1d:



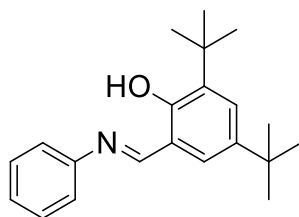
(E)-4-((phenylimino)methyl)benzonitrile

[C₁₄H₁₀N₂] 206.1 g/mol (M)

¹H NMR (300 MHz, CDCl₃, 296 K): δ = 8.52 (s, 1H), 8.04-8.02 (m, 2H), 7.79-7.77 (m, 2H), 7.46-7.42 (m, 2H), 7.32-7.25 (m, 3H) ppm.

¹³C NMR (75 MHz, CDCl₃, 296 K): δ = 157.80, 150.95, 139.90, 132.49, 129.26, 129.06, 126.88, 120.89, 118.41, 114.34 ppm.

2a:



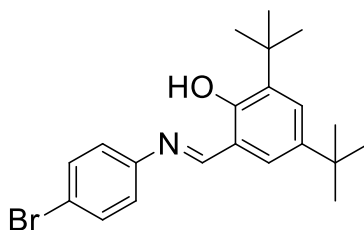
(E)-2,4-di-tert-butyl-6-((phenylimino)methyl)phenol

[C₂₁H₂₇NO] 309.2 g/mol (M)

¹H NMR (300 MHz, CDCl₃, 296 K): δ = 13.76 (s, 1H), 8.69 (s, 1H), 7.51-7.44 (m, 3H), 7.35-7.27 (m, 4H), 1.53 (s, 9H), 1.38 (s, 9H) ppm.

¹³C NMR (75 MHz, CDCl₃, 296 K): δ = 164.22, 158.66, 149.13, 140.96, 137.38, 129.73, 128.41, 127.22, 126.94, 121.58, 118.70, 35.53, 34.61, 31.90, 29.85 ppm.

2b:



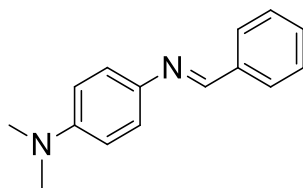
(E)-2-(((4-bromophenyl)imino)methyl)-4,6-di-tert-butylphenol

[C₂₁H₂₆BrNO] 387.1 g/mol (M)

¹H NMR (300 MHz, CDCl₃, 296 K): δ = 13.50 (s, 1H), 8.64 (s, 1H), 7.56-7.53 (m, 2H), 7.51-7.50 (m, 1H), 7.25-7.25 (m, 1H), 7.20-7.17 (m, 2H), 1.51 (s, 9H), 1.36 (s, 9H) ppm.

¹³C NMR (75 MHz, CDCl₃, 296 K): δ = 164.13, 158.24, 147.69, 140.73, 137.04, 132.39, 128.36, 126.91, 122.81, 119.94, 118.12 ppm.

3:



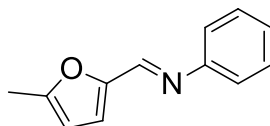
(E)-N1-benzylidene-N4,N4-dimethylbenzene-1,4-diamine

[C₁₅H₁₆N₂] 224.1 g/mol (M)

¹H NMR (300 MHz, CDCl₃, 296 K): δ = 8.34 (s, 1H), 7.81-7.78 (m, 2H), 7.41-7.36 (m, 2H), 7.22-7.20 (m, 3H), 6.77-6.74 (m, 2H), 3.07 (s, 6H) ppm.

¹³C NMR (75 MHz, CDCl₃, 296 K): δ = 160.02, 152.93, 152.42, 130.37, 128.97, 124.91, 124.36, 120.90, 111.50, 40.12 ppm.

4:



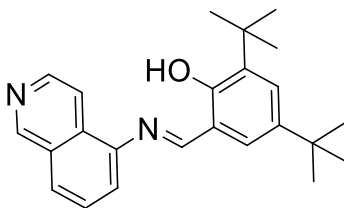
(E)-N-((5-methylfuran-2-yl)methylene)aniline

[C₁₂H₁₁NO] 185.1 g/mol (M)

¹H NMR (300 MHz, CDCl₃, 296 K): δ = 8.19 (s, 1H), 7.42-7.37 (m, 2H), 7.27-7.21 (m, 3H), 6.85-6.84 (d, J = 3 Hz, 1H), 6.19-6.18 (d, J = 3 Hz, 1H), 2.45 (s, 3H) ppm.

¹³C NMR (75 MHz, CDCl₃, 296 K): δ = 156.19, 151.16, 150.10, 146.97, 128.51, 125.26, 120.44, 118.24, 108.22, 13.46 ppm.

5:



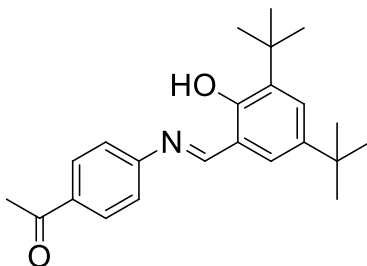
(E)-2,4-di-tert-butyl-6-((isoquinolin-5-ylimino)methyl)phenol

[C₂₄H₂₈BrN₂O] 360.2 g/mol (M)

¹H NMR (300 MHz, CDCl₃, 296 K): δ = 13.51 (s, 1H), 9.28 (s, 1H), 8.74 (s, 1H), 8.63-8.61 (d, J = 5.86 Hz, 1H), 8.08-8.06 (d, J = 5.86 Hz, 1H), 7.88-7.86 (d, J = 8.2 Hz, 1H), 7.65-7.59 (m, 1H), 7.56-7.56 (m, 1H), 7.41-7.38 (m, 1H), 7.32-7.31 (d, J = 7.03 Hz, 1H), 1.55 (s, 9H), 1.37 (s, 9H) ppm.

¹³C NMR (75 MHz, CDCl₃, 296 K): δ = 165.59, 158.37, 152.18, 145.33, 143.47, 140.89, 137.16, 131.06, 128.92, 128.74, 127.06, 125.72, 118.35, 117.85, 116.15, 35.12, 34.15, 31.39, 29.39 ppm.

6:



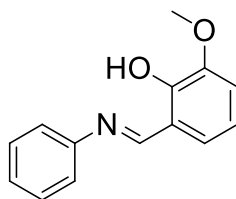
(E)-1-(4-((3,5-di-tert-butyl-2-hydroxybenzylidene)amino)phenyl)ethanone

[C₂₃H₂₉BrNO₂] 351.2 g/mol (M)

¹H NMR (300 MHz, CDCl₃, 296 K): δ = 13.42 (s, 1H), 8.69 (s, 1H), 8.06-8.04 (m, 2H), 7.52 (m, 1H), 7.37-7.35 (m, 2H), 7.28-7.27 (m, 1H), 2.65 (s, 3H) 1.50 (s, 9H), 1.36 (s, 9H) ppm.

¹³C NMR (75 MHz, CDCl₃, 296 K): δ = 196.70, 164.83, 158.02, 152.36, 140.46, 136.74, 134.60, 129.43, 128.41, 126.71, 120.90, 117.65, 34.67, 33.77, 31.00, 28.95, 26.17 ppm.

7:



(E)-2-methoxy-6-((phenylimino)methyl)phenol

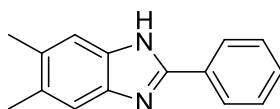
[C₁₄H₁₃NO₂] 227.1 g/mol (M)

¹H NMR (300 MHz, CDCl₃, 296 K): δ = 13.71 (s, 1H), 8.64 (s, 1H), 7.46-7.41 (m, 2H), 7.31-7.28 (m, 3H), 7.02-6.99 (m, 2H), 6.92-6.89 (m, 1H), 3.95 (s, 3H) ppm.

¹³C NMR (75 MHz, CDCl₃, 296 K): δ = 162.57, 151.40, 148.44, 148.10, 129.37, 126.94, 123.72, 121.13, 118.47, 114.67, 56.14 ppm.

Benzimidazoles

1a:



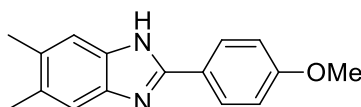
5,6-dimethyl-2-phenyl-1H-benzo[d]imidazole

[C₁₅H₁₄N₂] 222.1 g/mol (M)

¹H NMR (300 MHz, CDCl₃, 296 K): δ = 12.63 (s, 1H), 8.15-8.12 (d, 2H), 7.55-7.43 (m, 4H), 7.29 (s, 1H), 2.33-2.31 (d, 6H) ppm.

¹³C NMR (75 MHz, CDCl₃, 296 K): δ = 150.30, 142.50, 133.50, 131.14, 130.43, 129.88, 129.44, 128.85, 126.18, 118.91, 111.30, 20.03 ppm.

1b:



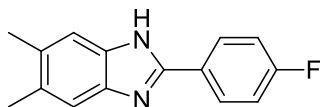
2-(4-methoxyphenyl)-5,6-dimethyl-1H-benzo[d]imidazole

[C₁₆H₁₆N₂O] 252.1 g/mol (M)

¹H NMR (300 MHz, CDCl₃, 296 K): δ = 12.48 (s, 1H), 8.10-8.07 (m, 2H), 7.33 (m, 2H), 7.10-7.07 (m, 2H), 3.82 (s, 3H), 2.31 (s, 6H) ppm.

^{13}C NMR (75 MHz, CDCl_3 , 296 K): δ = 160.10, 150.15, 129.88, 127.52, 122.61, 114.55, 114.00, 55.03, 19.74 ppm.

1c:



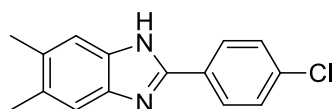
2-(4-fluorophenyl)-5,6-dimethyl-1H-benzo[d]imidazole

$[\text{C}_{15}\text{H}_{13}\text{FN}_2]$ 240.1 g/mol (M)

^1H NMR (300 MHz, CDCl_3 , 296 K): δ = 12.66 (s, 1H), 8.18 (m, 2H), 7.36 (m, 4H), 2.31 (s, 6H) ppm.

^{13}C NMR (75 MHz, CDCl_3 , 296 K): δ = 164.53, 161.25, 149.57, 130.71, 128.56, 128.43, 127.14, 116.07, 115.78, 20.04 ppm.

1d:



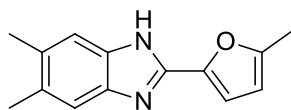
2-(4-chlorophenyl)-5,6-dimethyl-1H-benzo[d]imidazole

$[\text{C}_{15}\text{H}_{13}\text{ClN}_2]$ 256.1 g/mol (M)

^1H NMR (300 MHz, CDCl_3 , 296 K): δ = 12.72 (s, 1H), 8.16-8.13 (d, J = 8.8 Hz, 2H), 7.60-7.57 (d, J = 8.8 Hz, 2H), 7.43-7.30 (m, 2H), 2.31 (s, 6H) ppm.

^{13}C NMR (75 MHz, CDCl_3 , 296 K): δ = 149.28, 134.09, 128.98, 127.91, 20.06 ppm.

2:



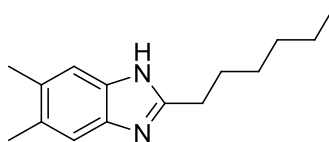
5,6-dimethyl-2-(5-methylfuran-2-yl)-1H-benzo[d]imidazole

[C₁₄H₁₄N₂O] 226.1 g/mol (M)

¹H NMR (300 MHz, CDCl₃, 296 K): δ = 7.29 (m, 2H), 7.01-7.00 (m, 1H), 6.31-6.30 (m, 1H), 2.39 (s, 3H), 2.30 (s, 6H) ppm.

¹³C NMR (75 MHz, CDCl₃, 296 K): δ = 153.44, 144.49, 143.20, 130.62, 111.00, 108.61, 20.18, 13.64 ppm.

3:



2-hexyl-5,6-dimethyl-1H-benzo[d]imidazole

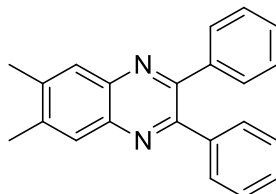
[C₁₅H₂₂N₂] 230.2 g/mol (M)

¹H NMR (300 MHz, CDCl₃, 296 K): δ = 7.21 (s, 2H), 2.76-2.71 (m, 2H), 2.26 (s, 6H), 1.72-1.69 (m, 2H), 1.26 (m, 6H), 0.83 (m, 3H) ppm.

¹³C NMR (75 MHz, CDCl₃, 296 K): δ = 154.56, 142.42, 133.19, 129.92, 118.68, 111.23, 31.45, 28.99, 28.82, 28.09, 22.48, 20.38, 14.40 ppm.

Quinoxalines

1a:



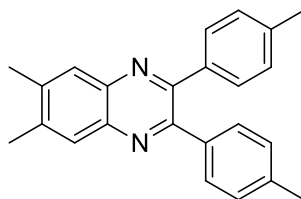
6,7-dimethyl-2,3-diphenylquinoxaline

[C₂₂H₁₈N₂] 310.2 g/mol (M)

¹H NMR (300 MHz, CDCl₃, 296 K): δ = 7.94 (m, 2H), 7.53-7.50 (m, 4H), 7.35-7.33 (m, 6H), 2.53 (s, 6H) ppm.

¹³C NMR (75 MHz, CDCl₃, 296 K): δ = 152.41, 140.47, 140.12, 139.28, 129.78, 128.47, 128.13, 20.39 ppm.

1b:



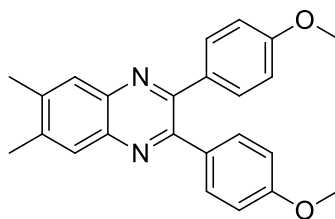
6,7-dimethyl-2,3-di-*p*-tolylquinoxaline

[C₂₄H₂₂N₂] 338.2 g/mol (M)

¹H NMR (300 MHz, CDCl₃, 296 K): δ = 7.91 (m, 2H), 7.44-7.41 (m, 4H), 7.16-7.13 (m, 4H), 2.51 (s, 6H), 2.38 (s, 6H) ppm.

¹³C NMR (75 MHz, CDCl₃, 296 K): δ = 152.53, 140.16, 138.41, 136.68, 129.72, 128.92, 128.15, 21.35, 20.41 ppm.

1c:



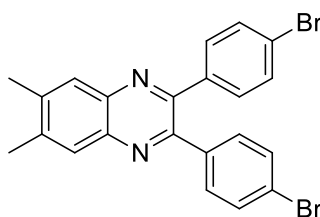
2,3-bis(4-methoxyphenyl)-6,7-dimethylquinoxaline

[C₂₄H₂₂N₂O₂] 370.2 g/mol (M)

¹H NMR (300 MHz, CDCl₃, 296 K): δ = 7.88 (m, 2H), 7.49-7.46 (m, 4H), 6.88-6.85 (m, 4H), 3.82 (s, 6H), 2.50 (s, 6H) ppm.

¹³C NMR (75 MHz, CDCl₃, 296 K): δ = 159.87, 151.96, 139.96, 131.90, 131.14, 127.95, 113.62, 55.21, 20.33 ppm.

1d:



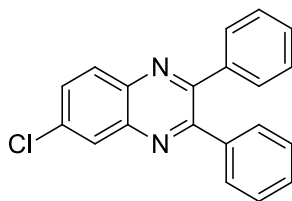
2,3-bis(4-bromophenyl)-6,7-dimethylquinoxaline

[C₂₂H₁₆Br₂N₂] 466.0 g/mol (M)

¹H NMR (300 MHz, CDCl₃, 296 K): δ = 7.89 (m, 2H), 7.50-7.47 (m, 4H), 7.39-7.36 (m, 4H), 2.52 (s, 6H) ppm.

¹³C NMR (75 MHz, CDCl₃, 296 K): δ = 150.90, 141.12, 140.25, 137.98, 131.59, 128.15, 123.36, 20.49 ppm.

2:



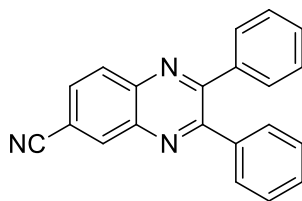
6-chloro-2,3-diphenylquinoxaline

[C₂₀H₁₃ClN₂] 316.1 g/mol (M)

¹H NMR (300 MHz, CDCl₃, 296 K): δ = 8.19-8.18 (m, 1H), 8.13-8.10 (m, 1H), 7.74-7.73 (m, 1H), 7.54-7.51 (m, 4H), 7.40-7.35 (m, 6H) ppm.

¹³C NMR (75 MHz, CDCl₃, 296 K): δ = 153.81, 153.14, 140.99, 138.22, 138.14, 135.18, 130.50, 129.95, 129.32, 128.63, 128.56, 127.86, 127.58 ppm.

3



2,3-diphenylquinoxaline-6-carbonitrile

[C₂₁H₁₃N₃] 307.1 g/mol (M)

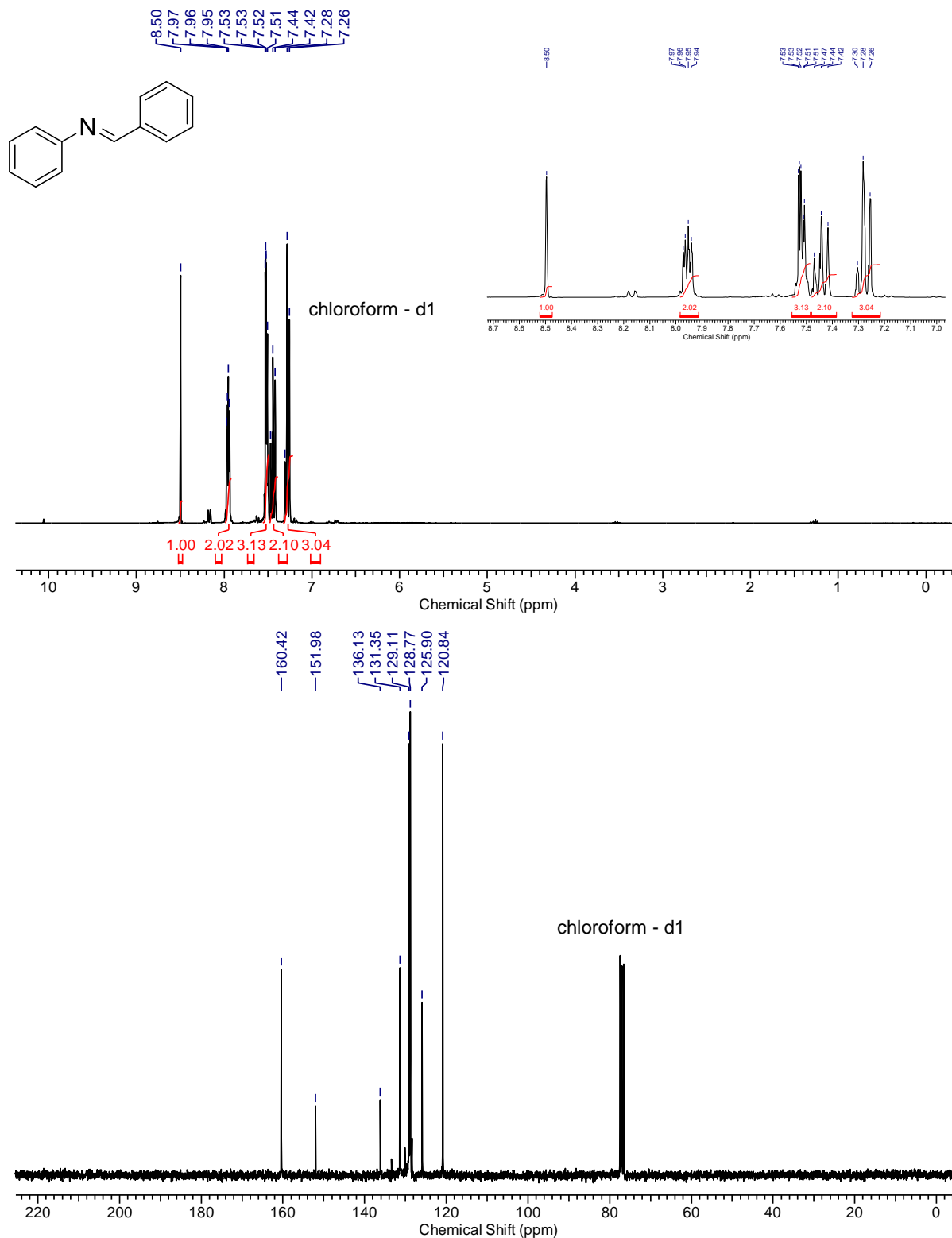
¹H NMR (300 MHz, CDCl₃, 296 K): δ = 8.72-8.71 (m, 1H), 8.28-8.25 (m, 1H), 8.12 (m, 1H), 7.49-7.37 (m, 10H) ppm.

¹³C NMR (75 MHz, CDCl₃, 296 K): δ = 155.23, 154.57, 141.66, 139.21, 137.74, 134.65, 130.89, 130.17, 129.41, 129.11, 128.98, 127.83, 117.89, 112.20 ppm.

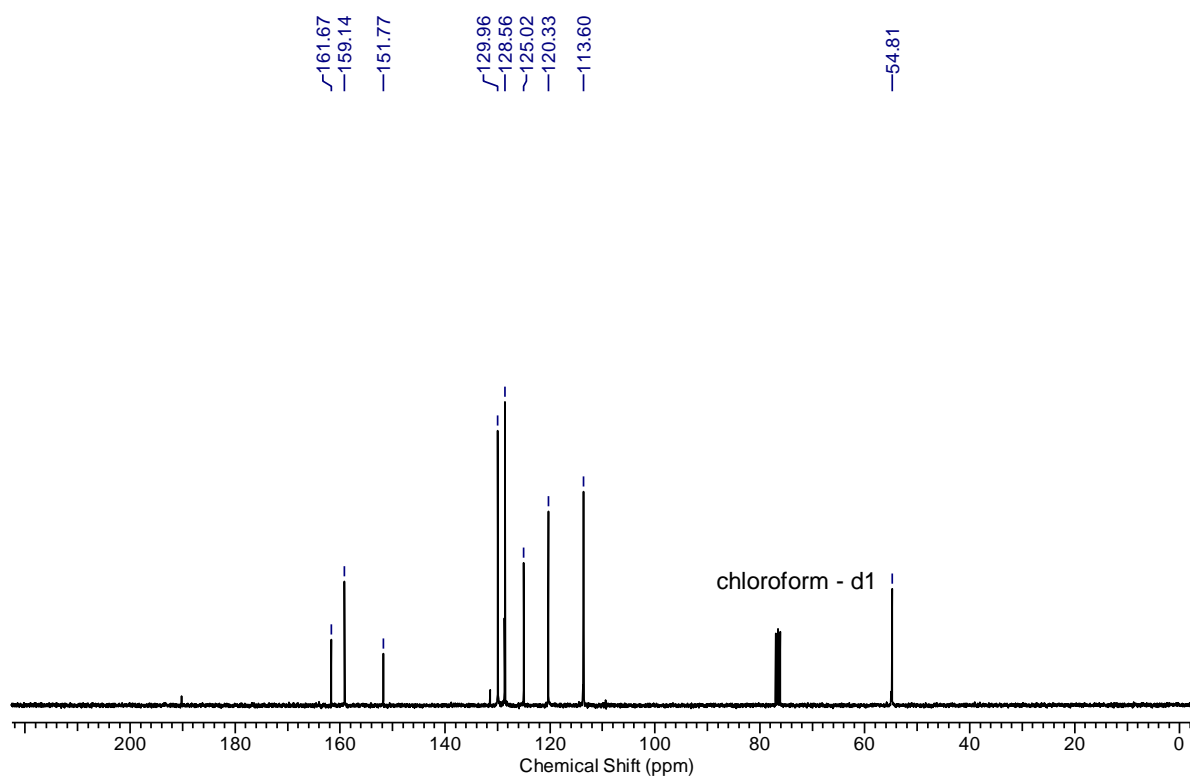
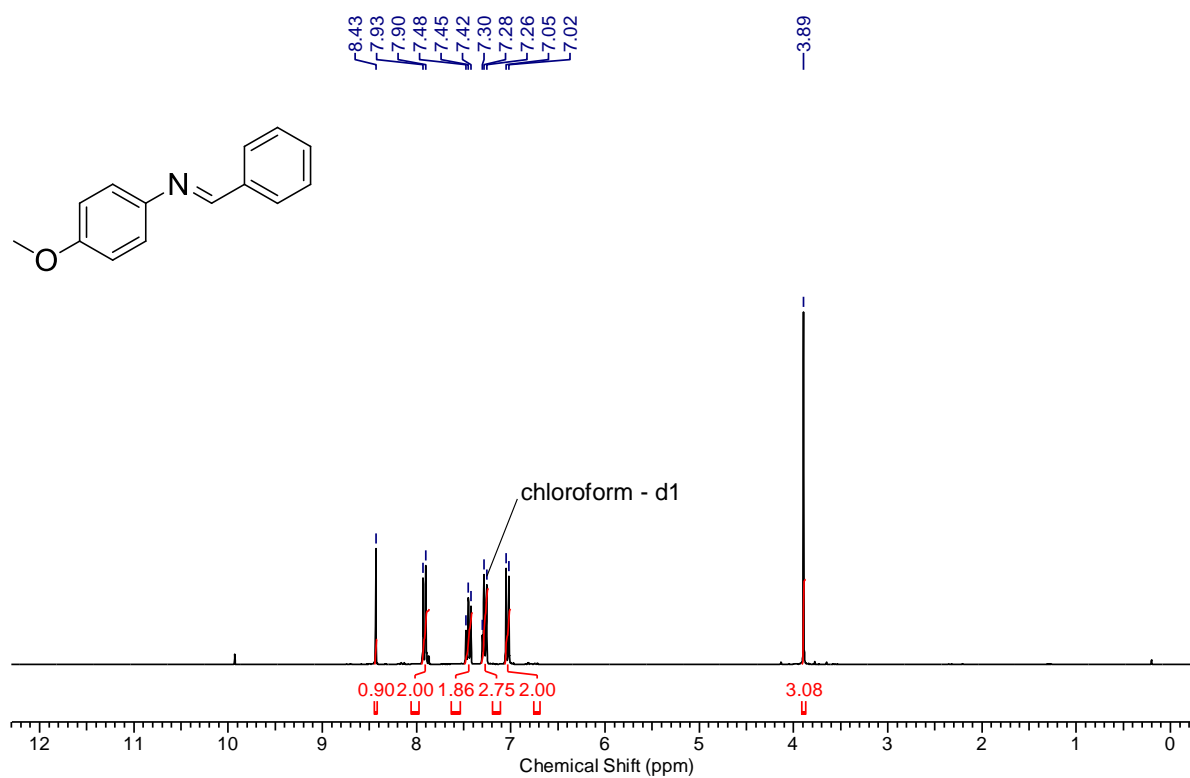
NMR spectra

Imines

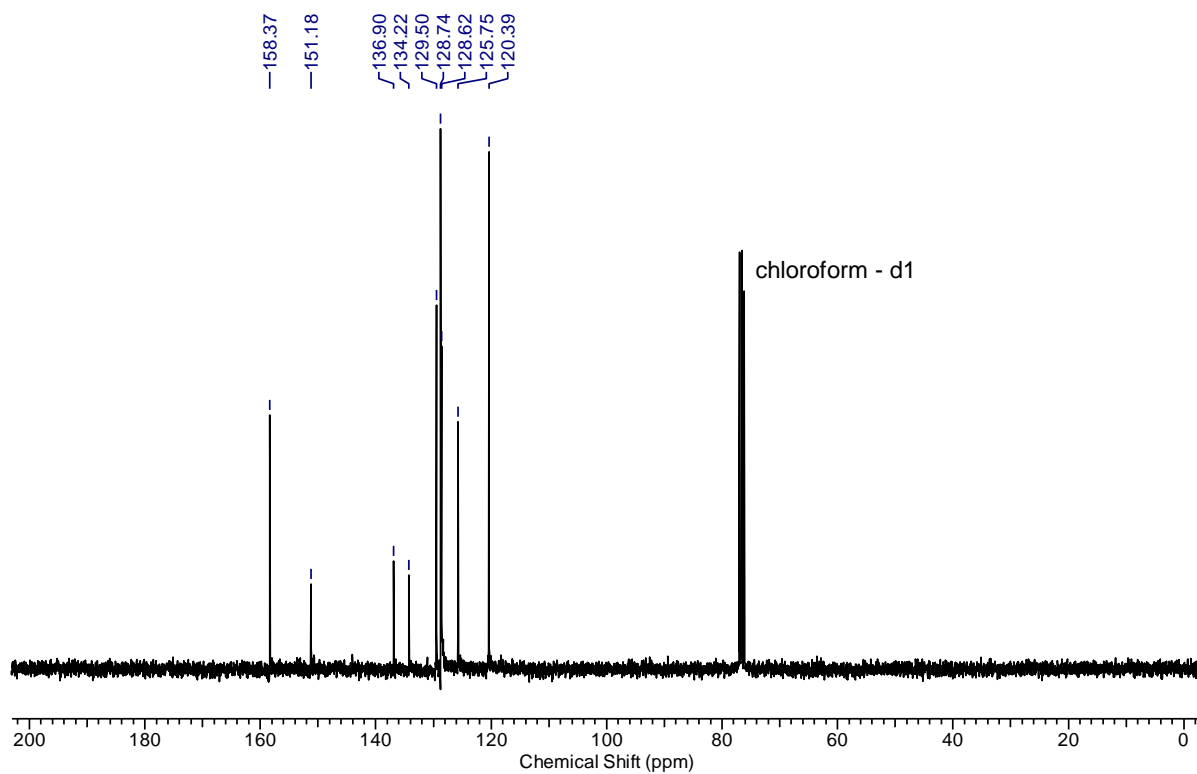
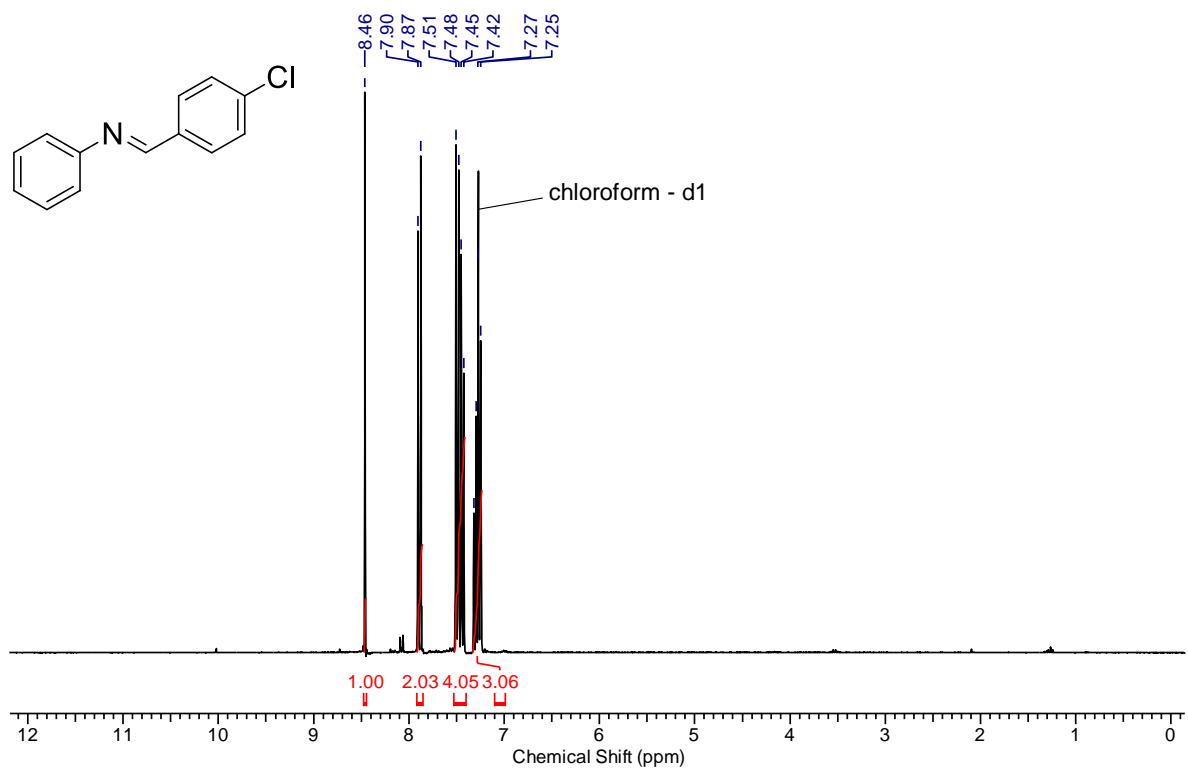
1a:



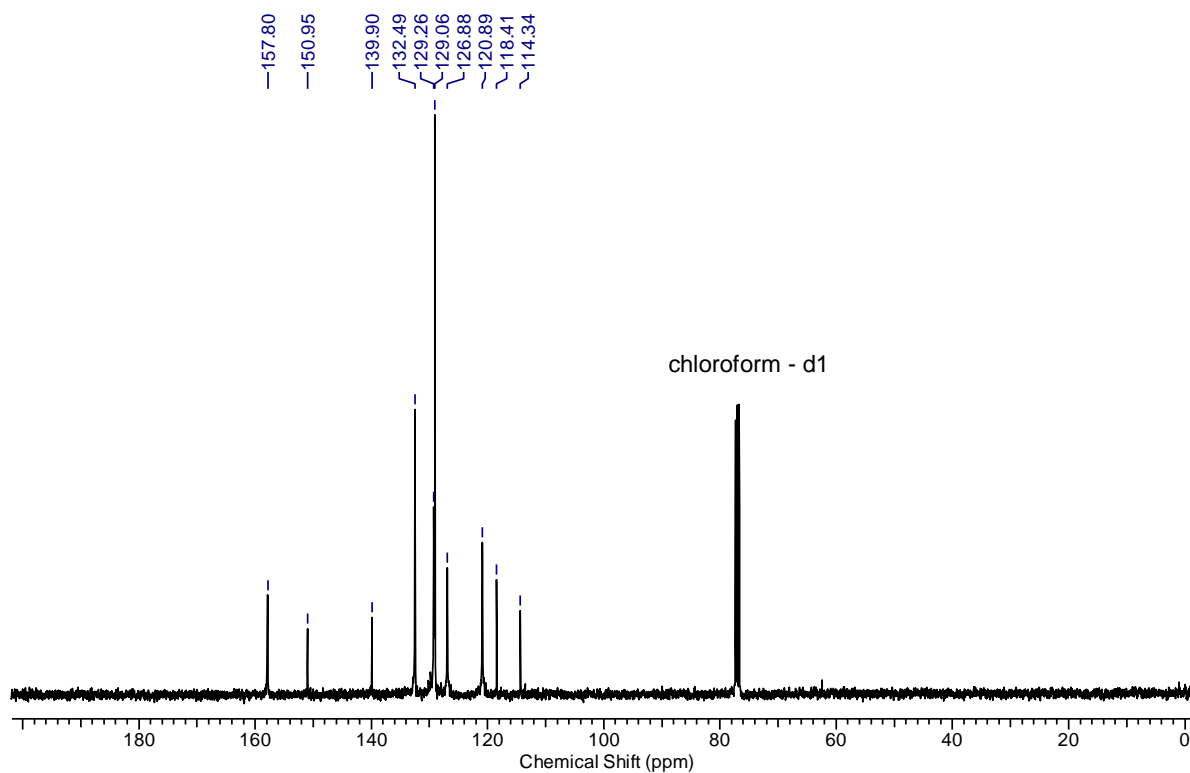
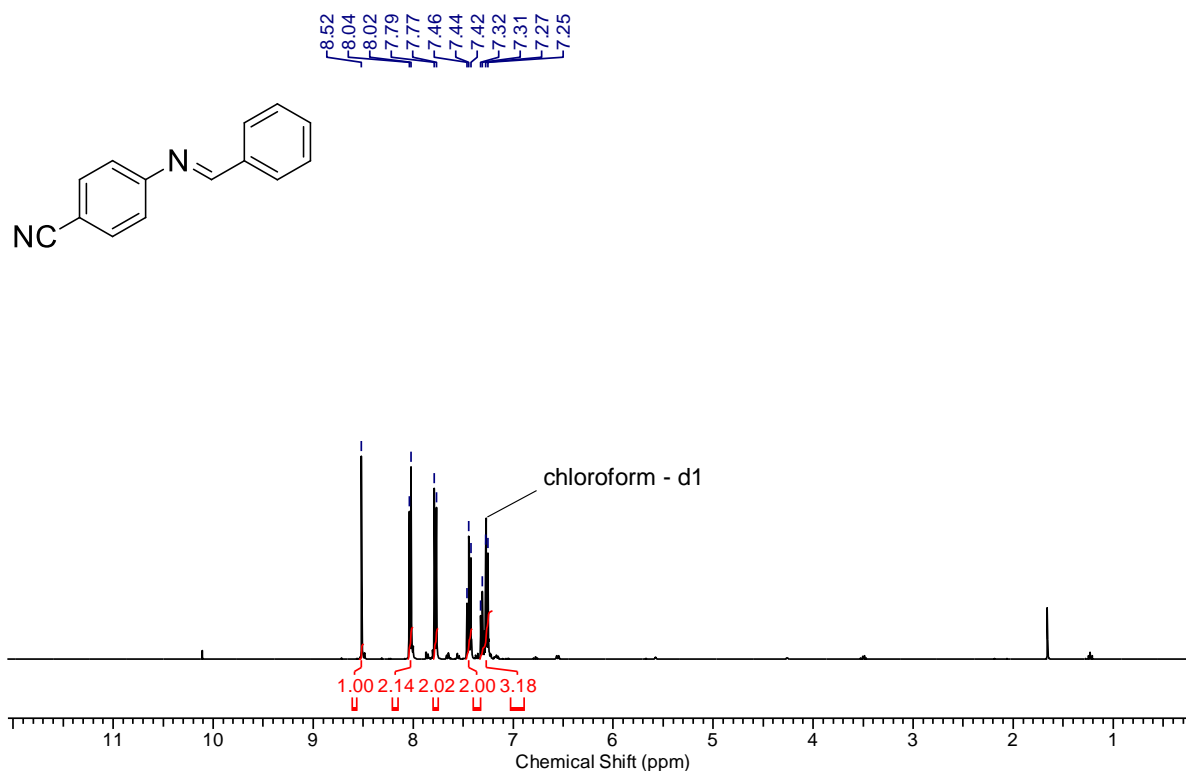
1b:



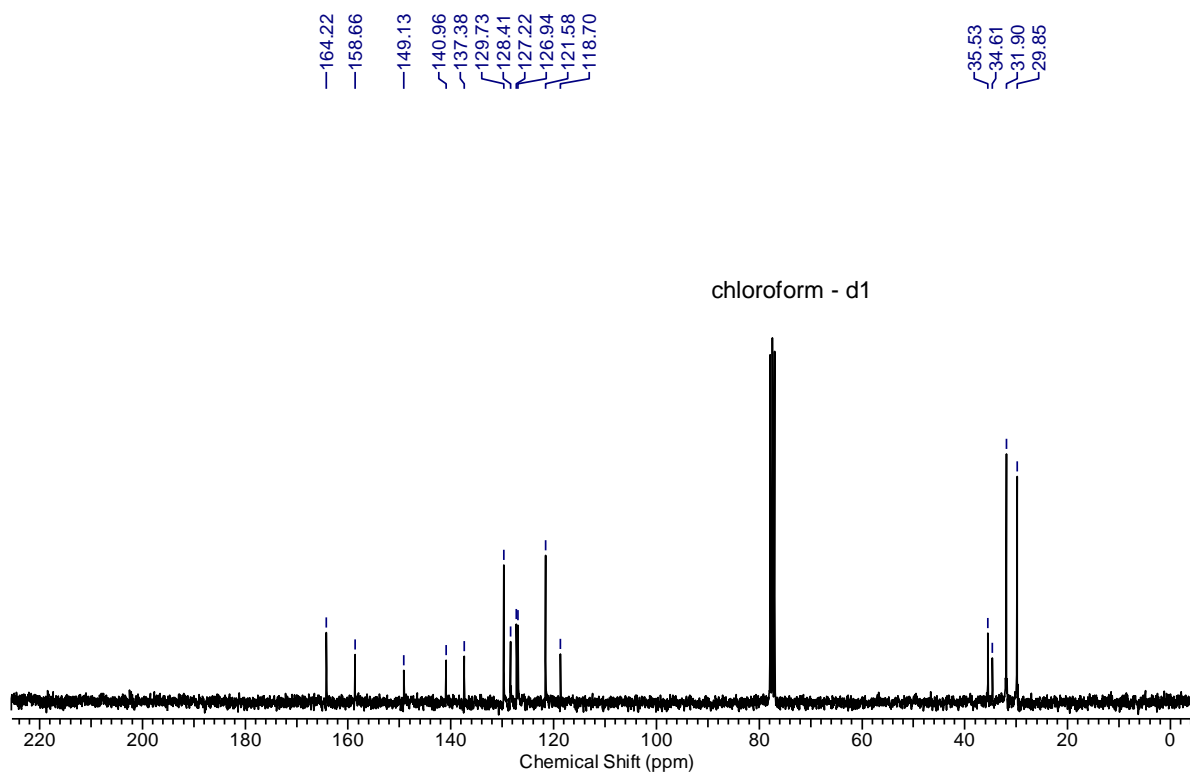
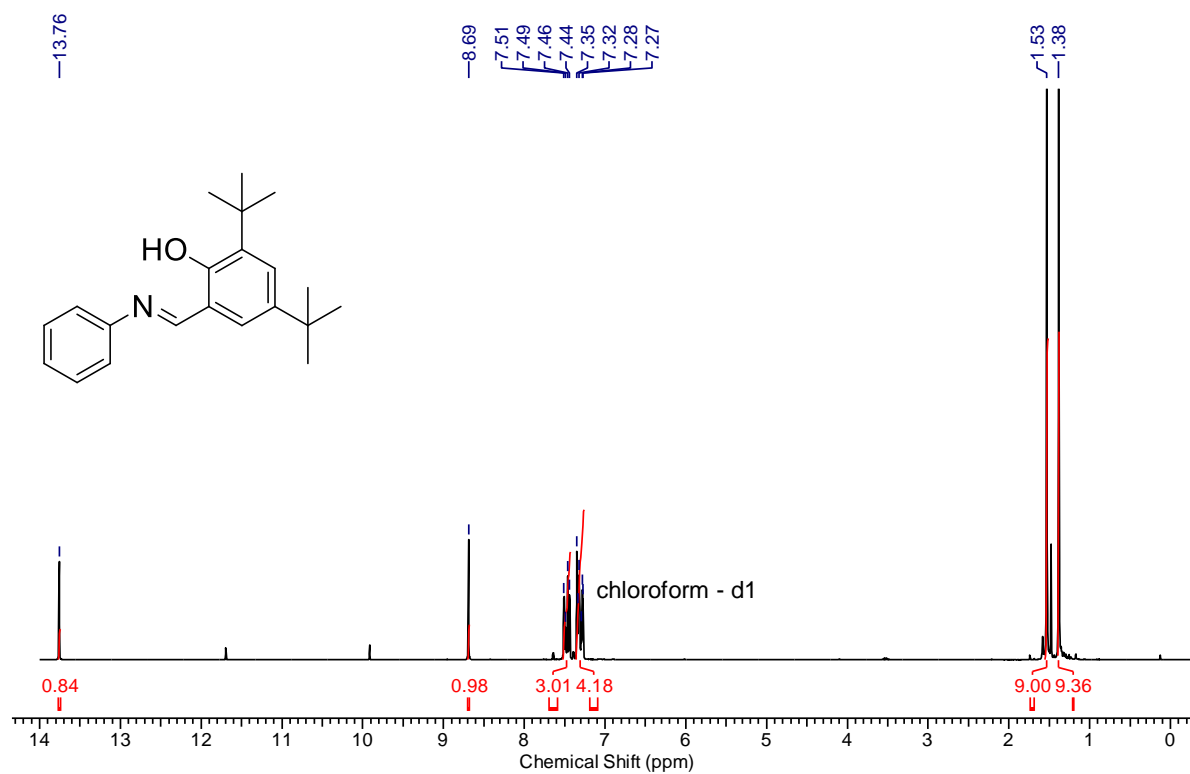
1c:



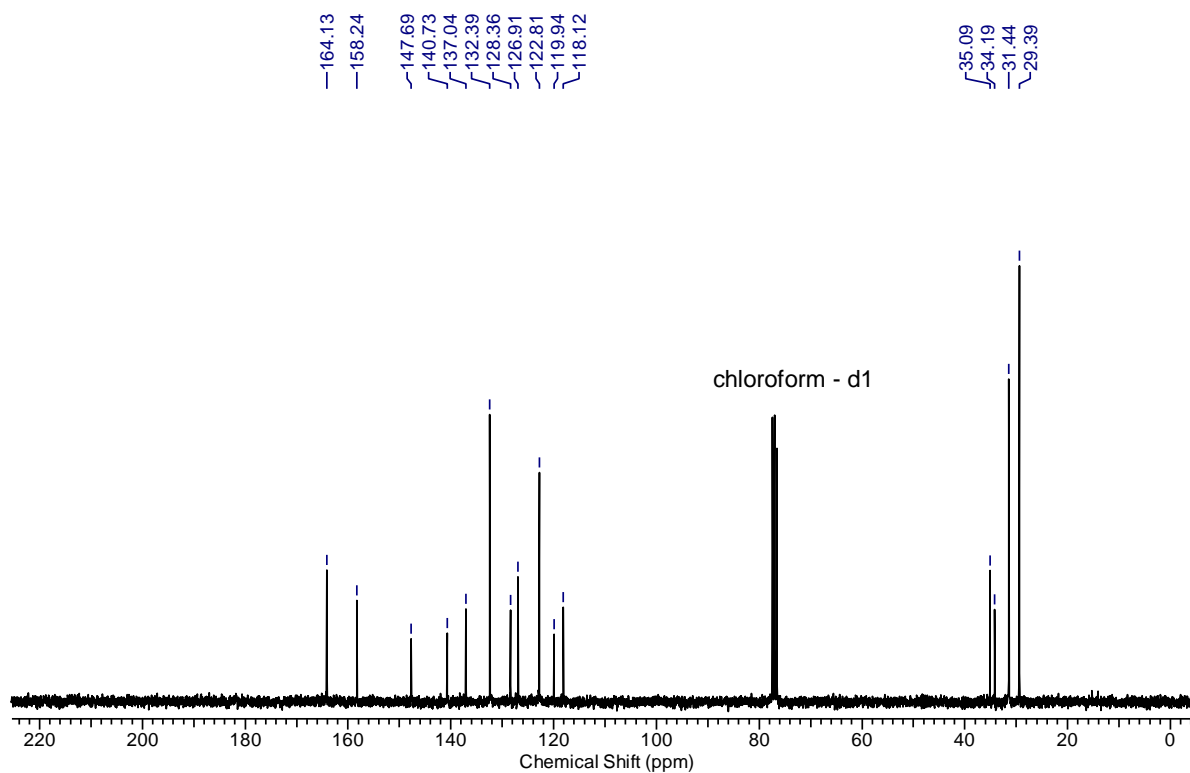
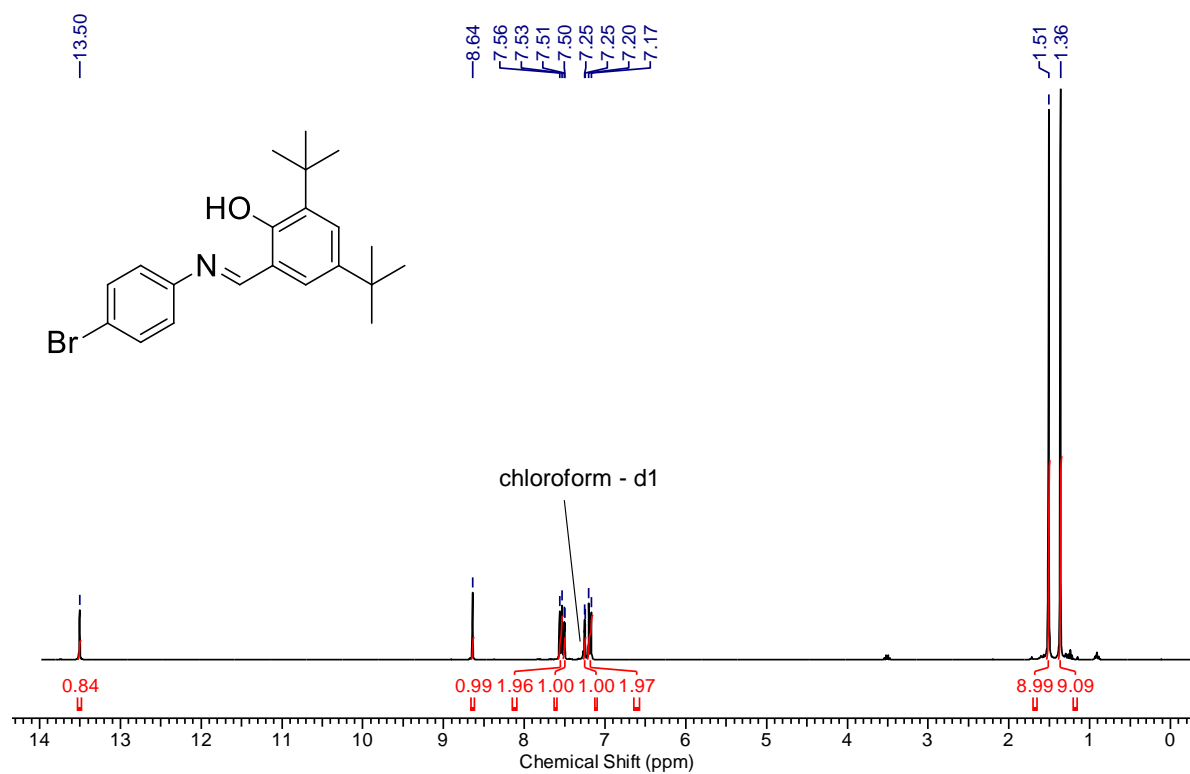
1d:



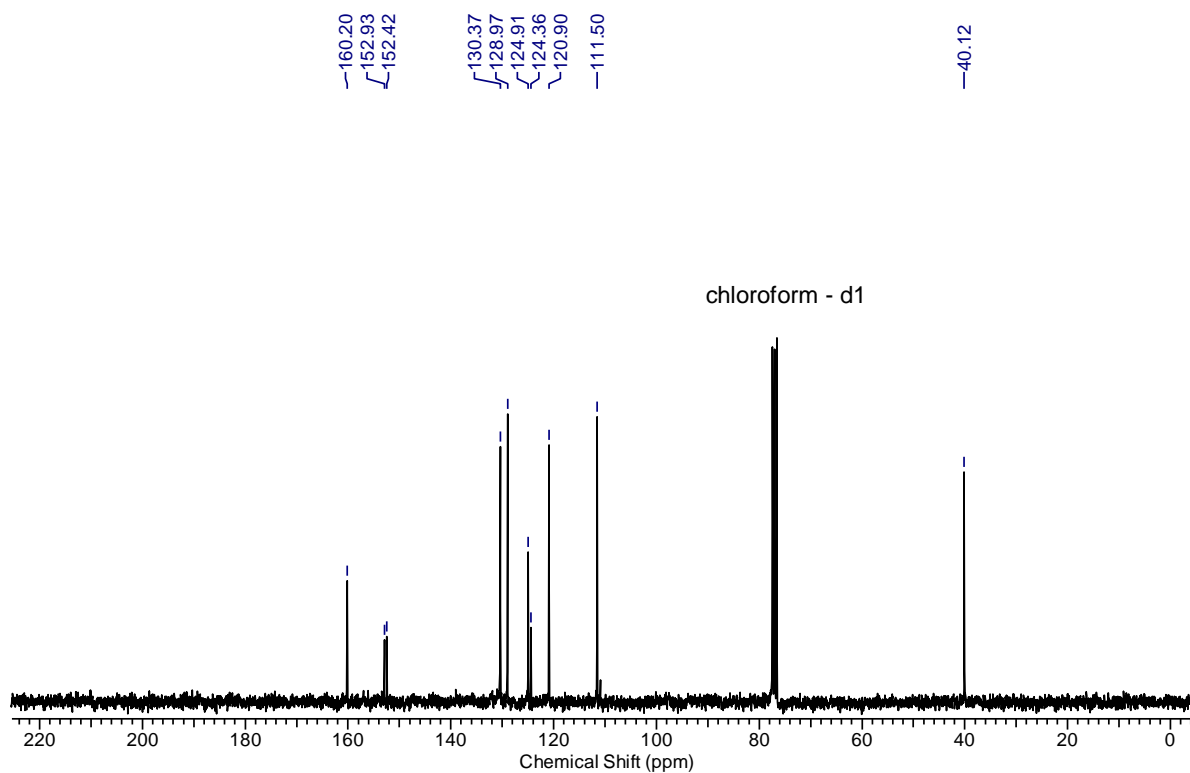
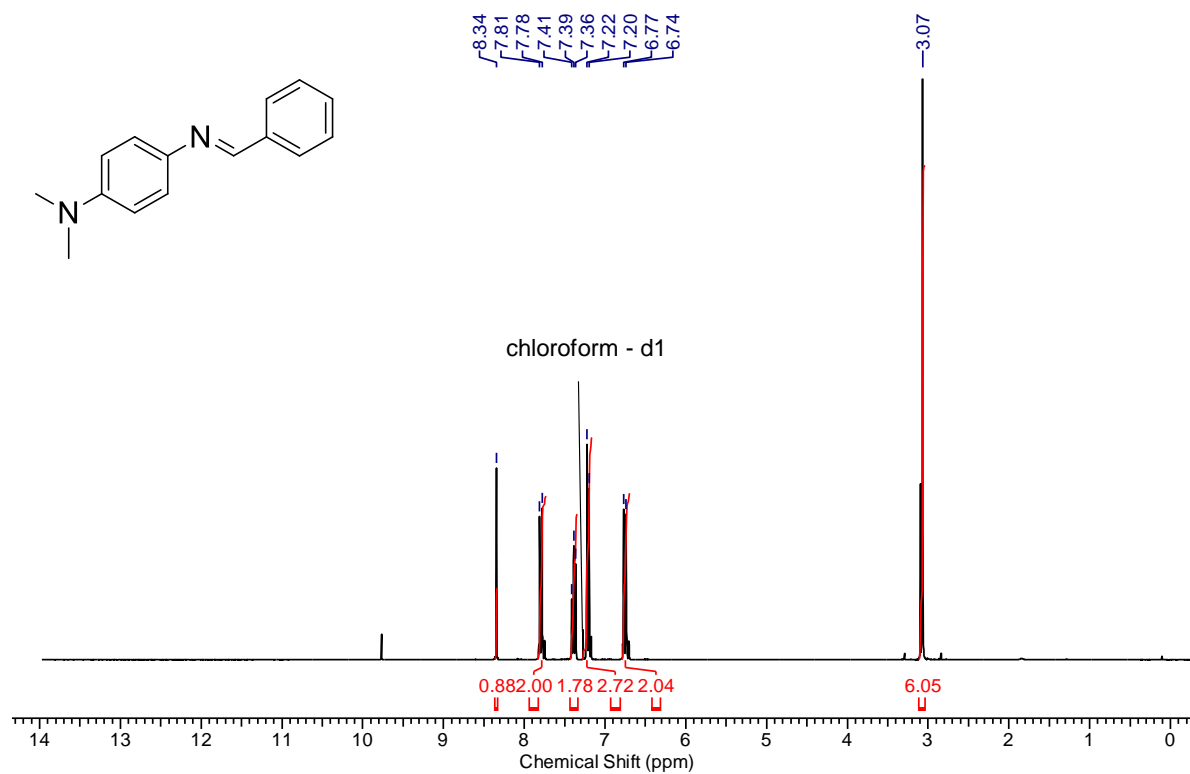
2a:



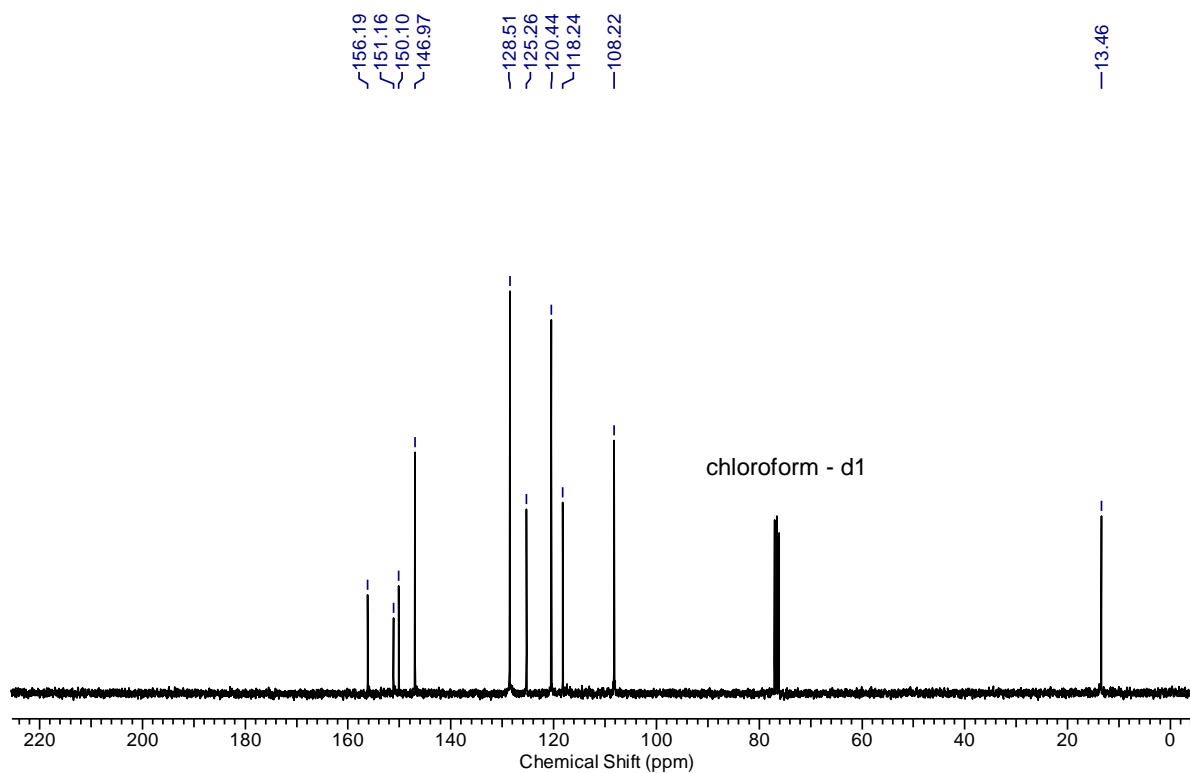
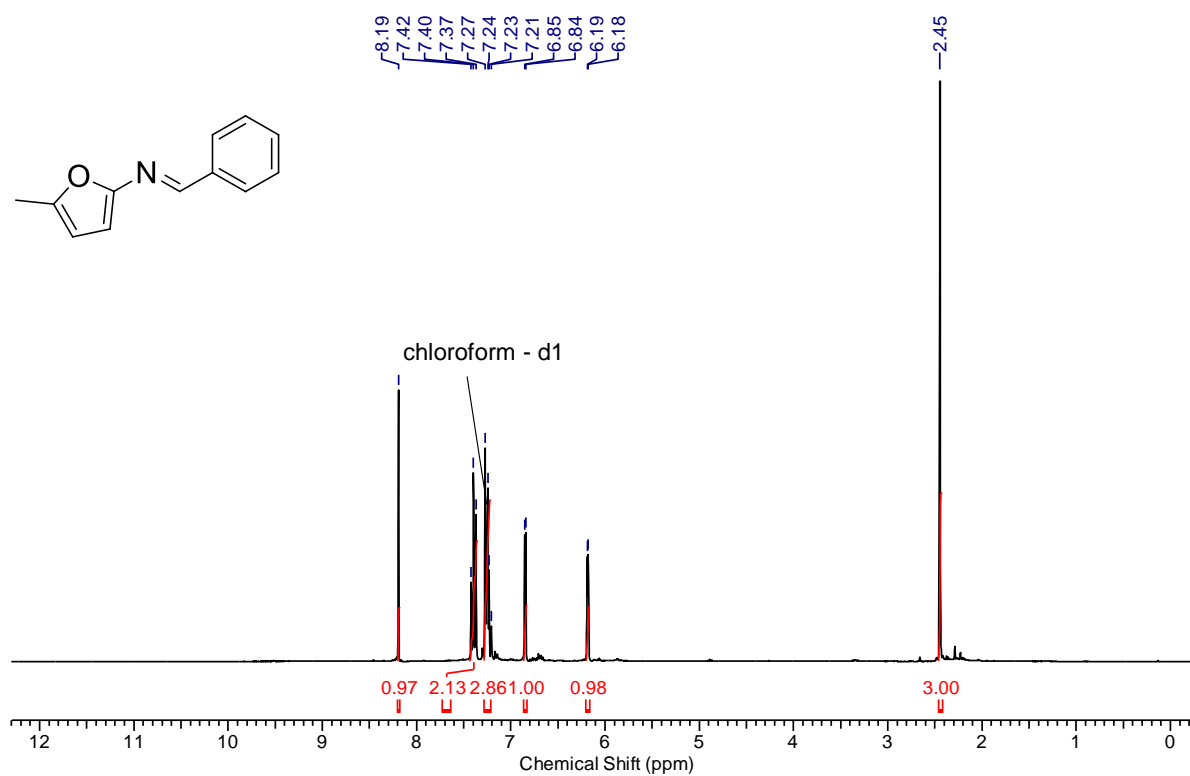
2b:



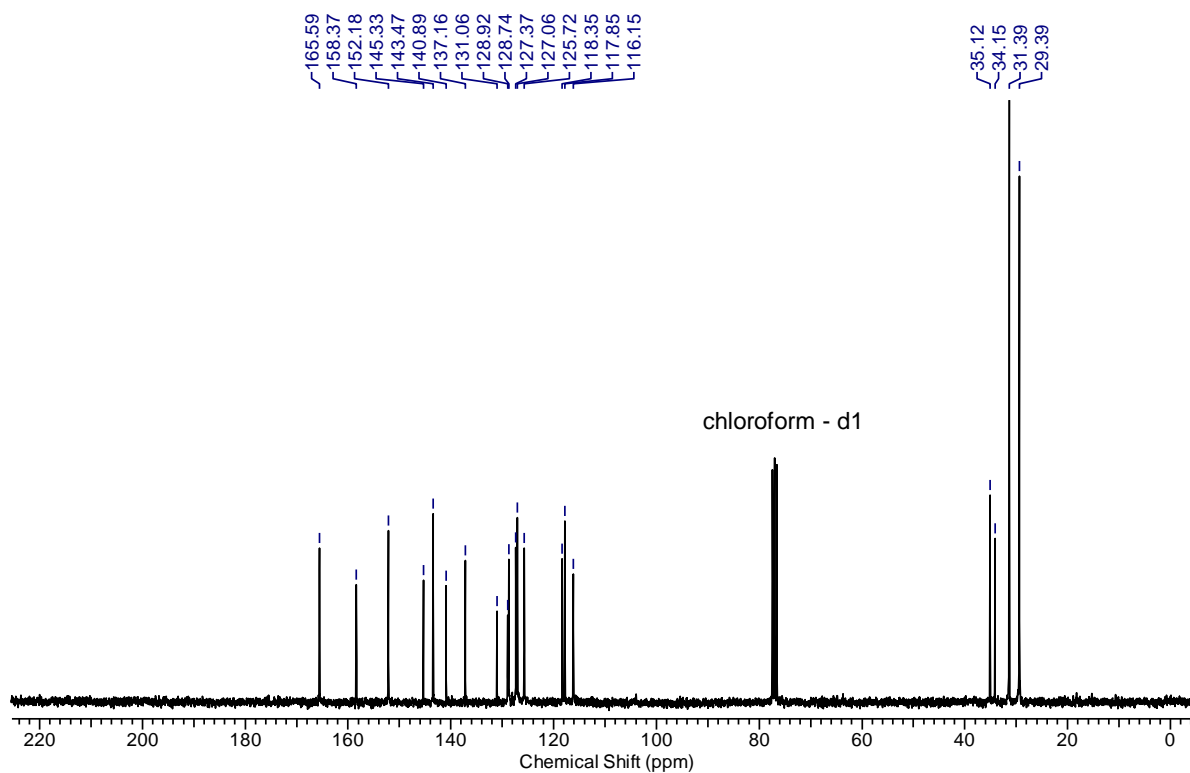
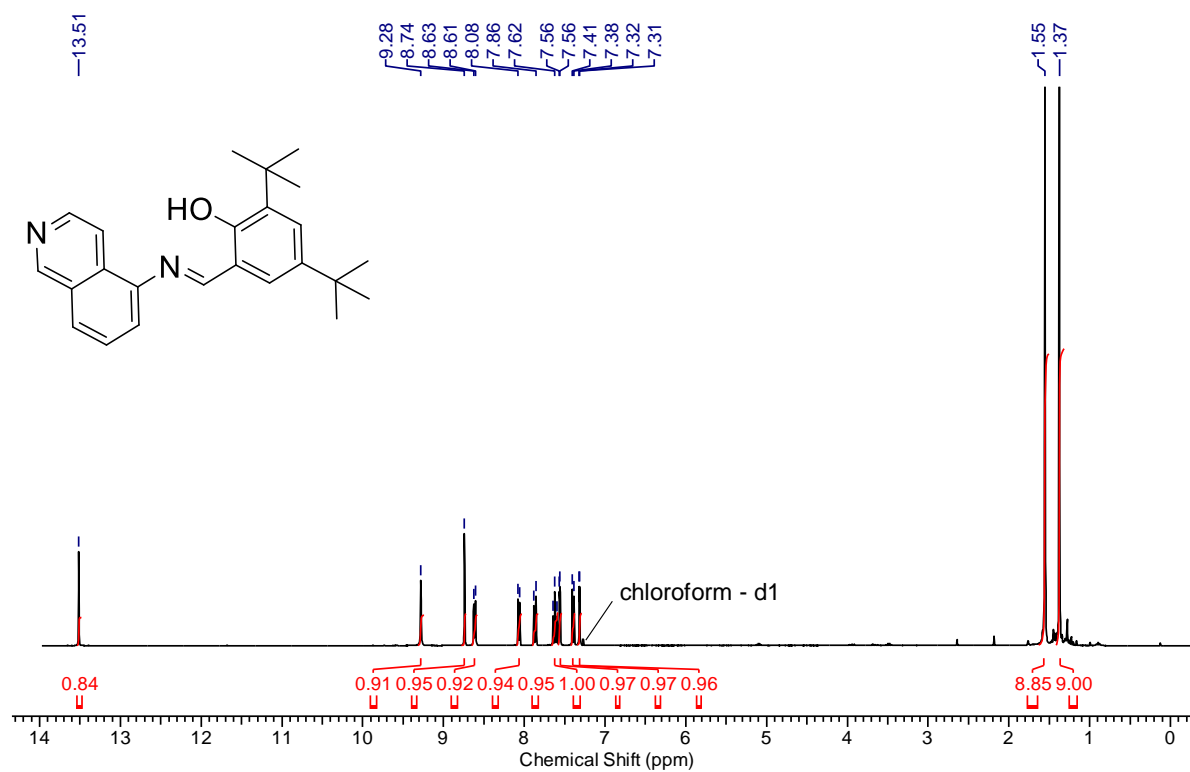
3:



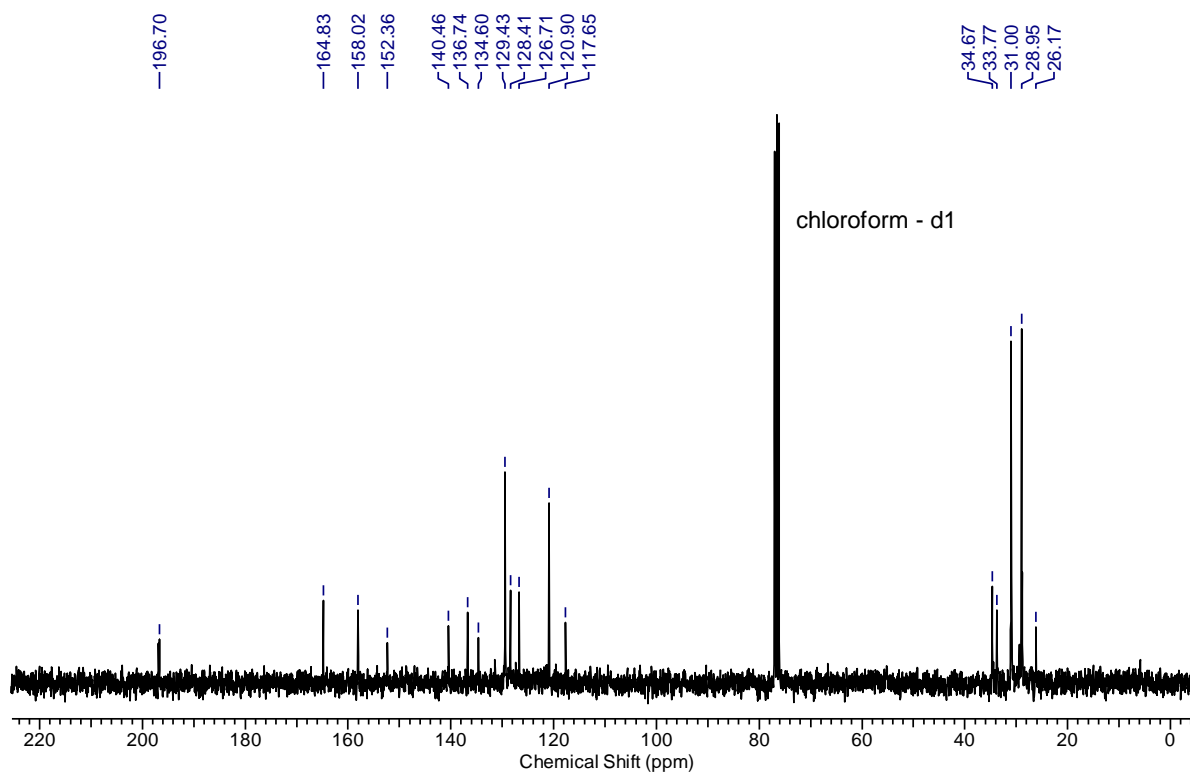
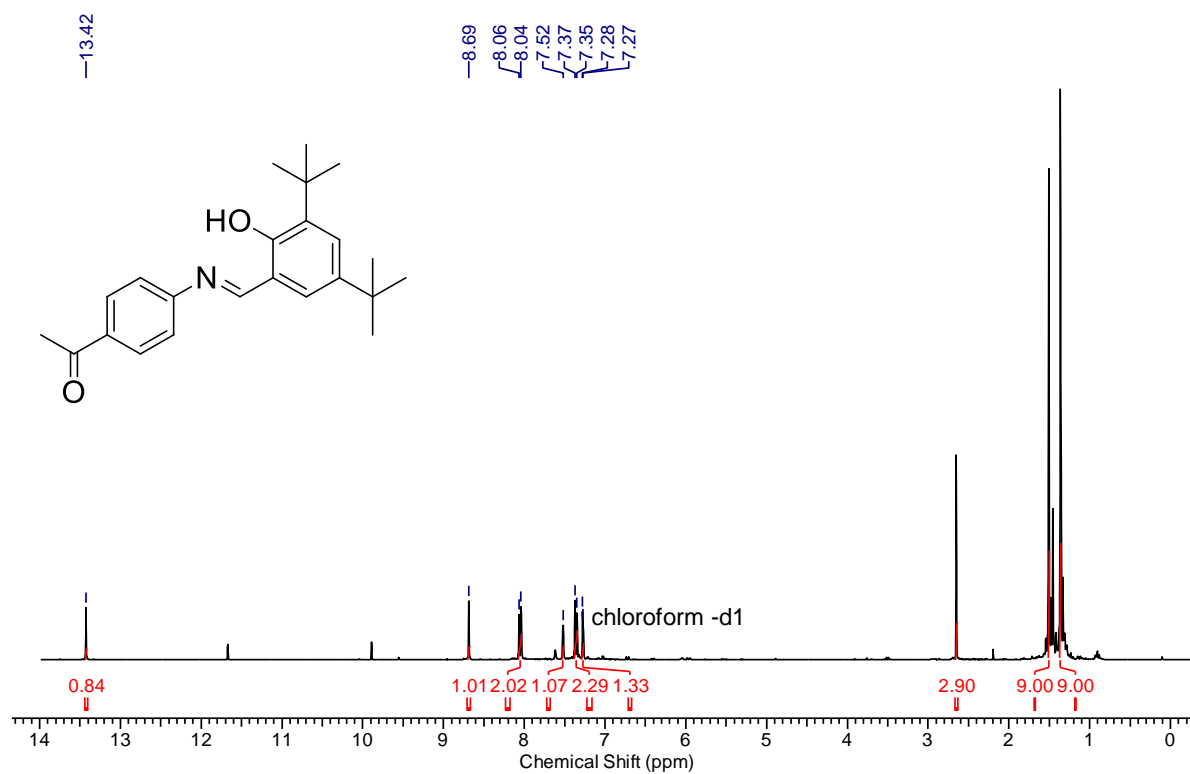
4:



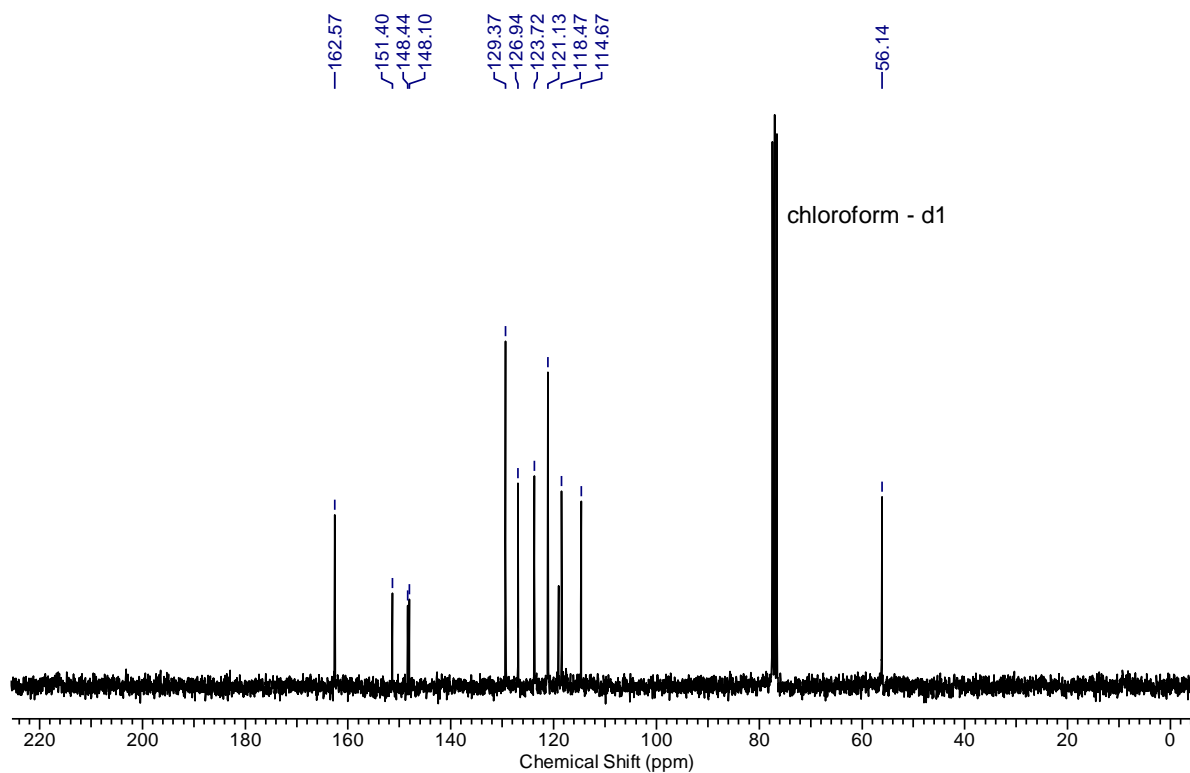
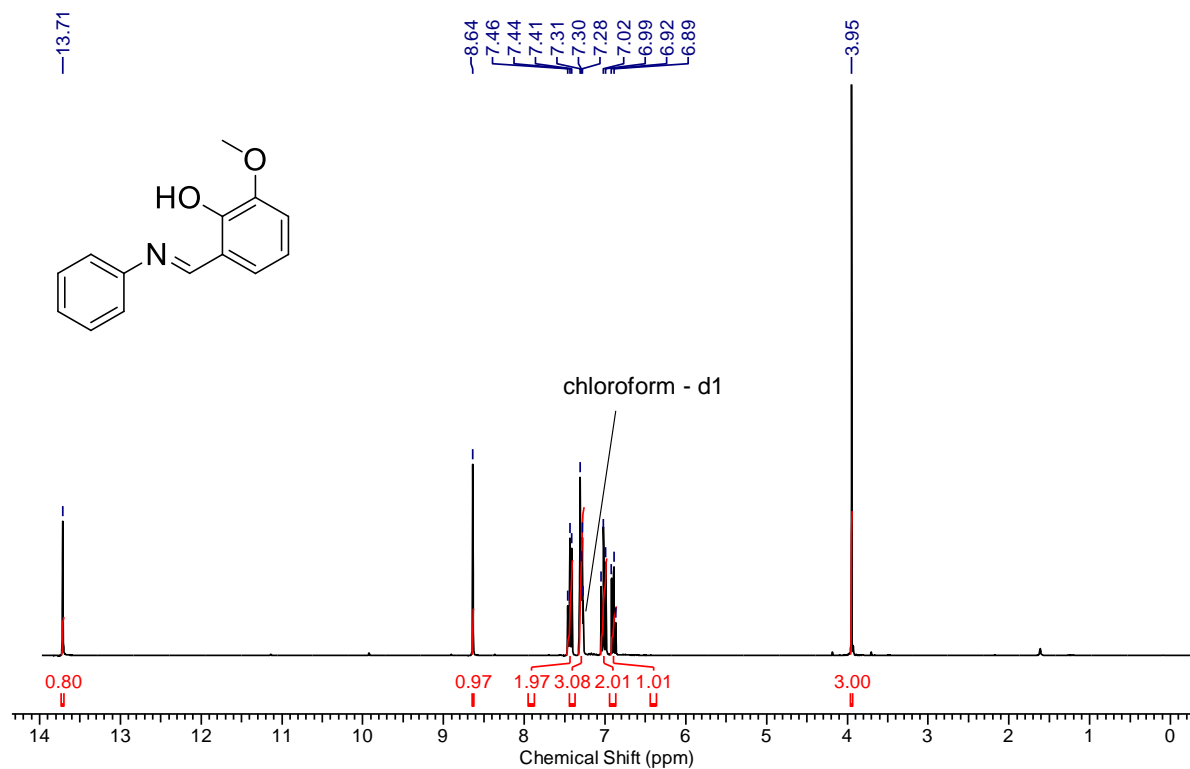
5:



6:

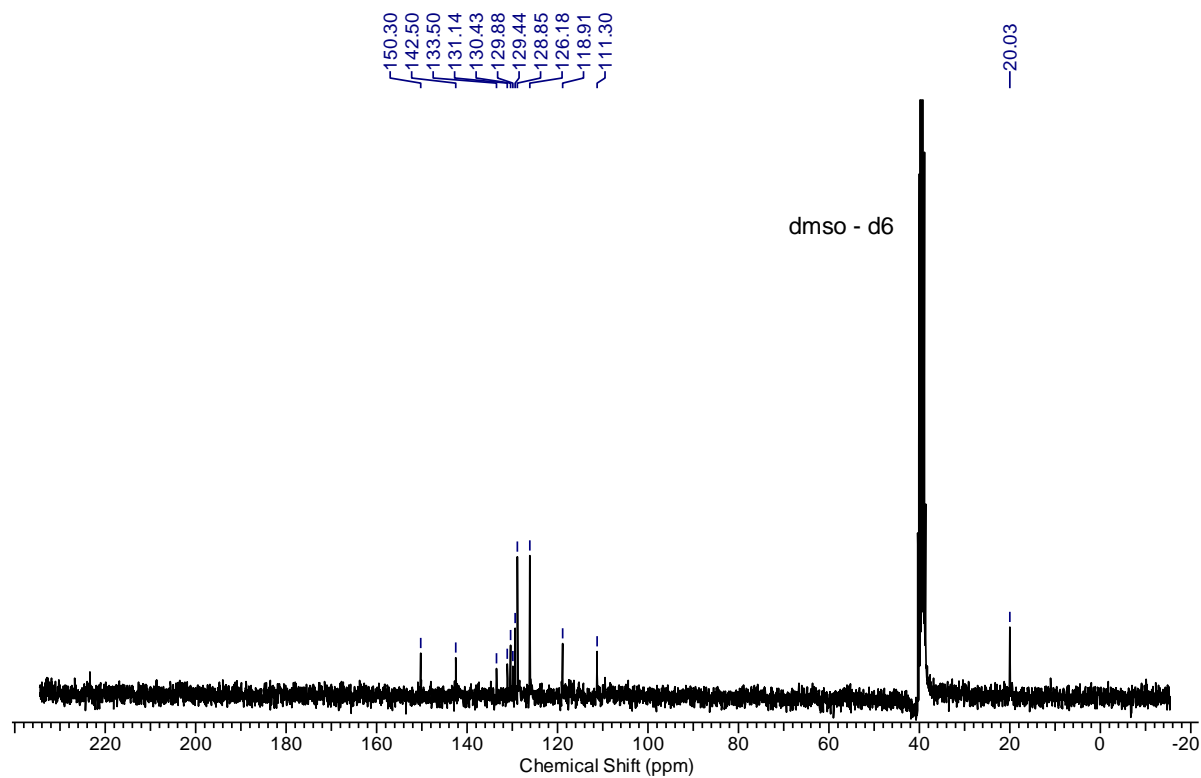
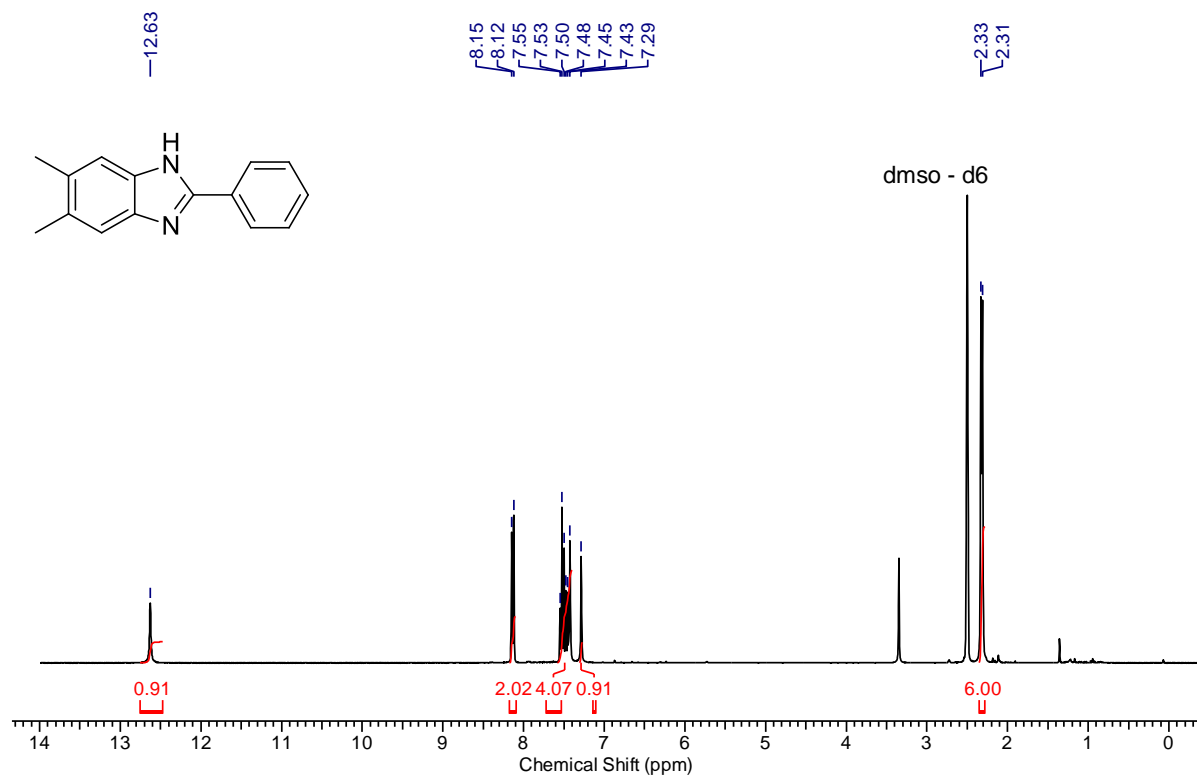


7:

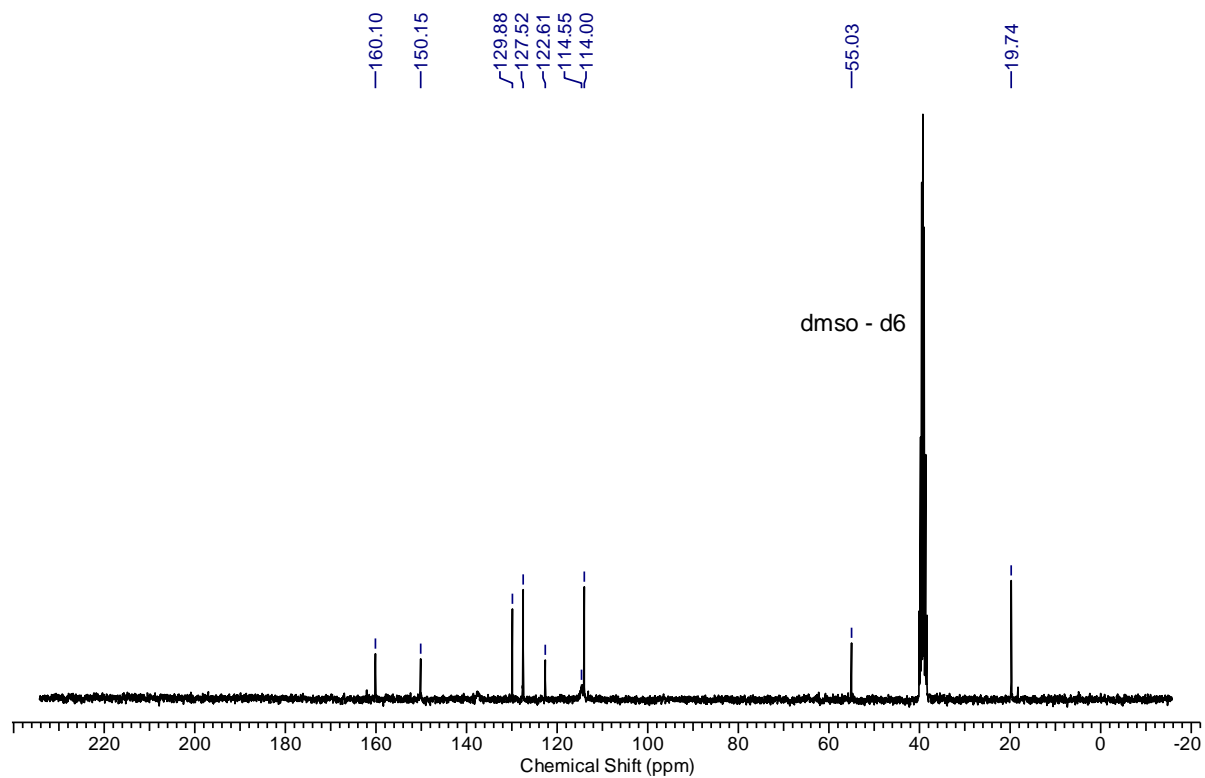
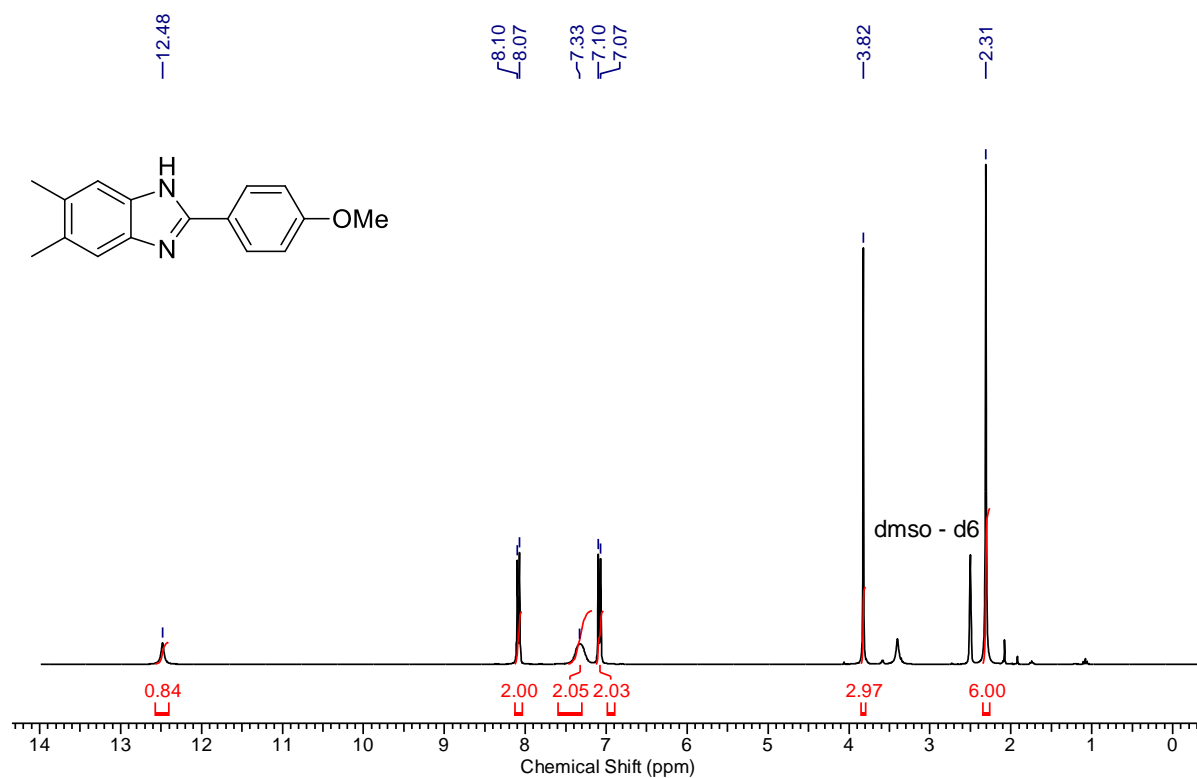


Benzimidazoles

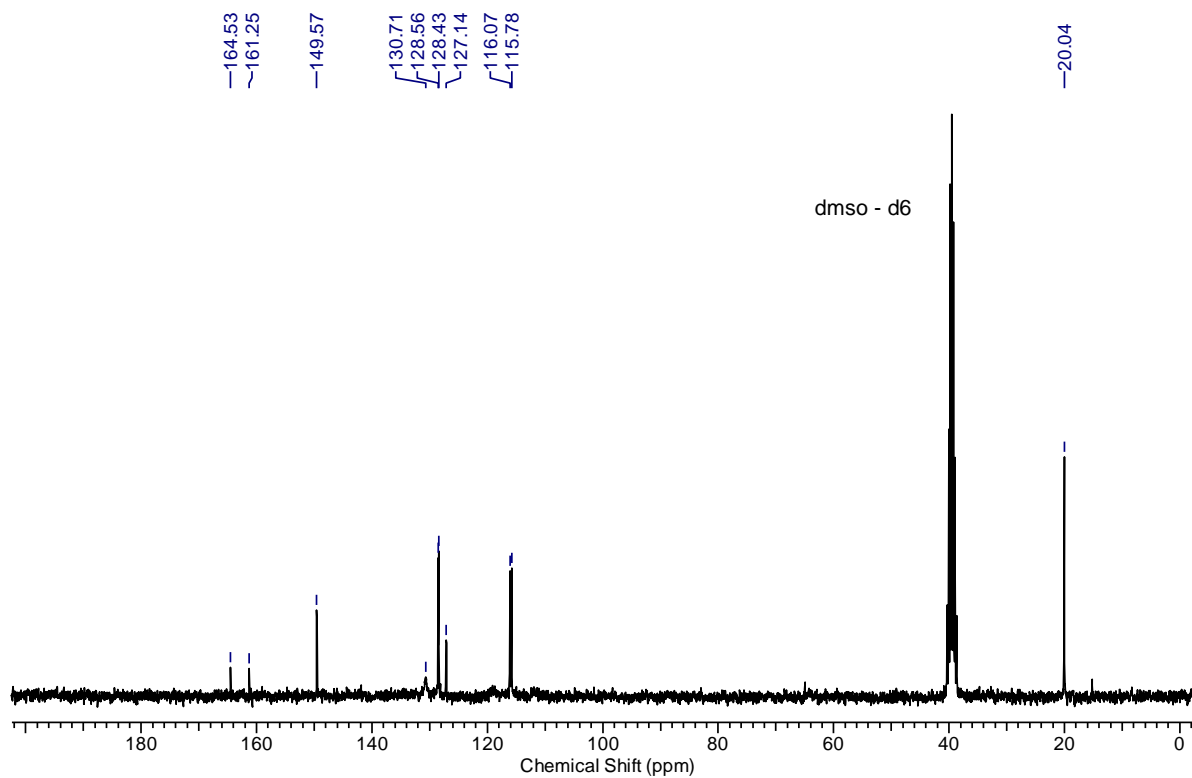
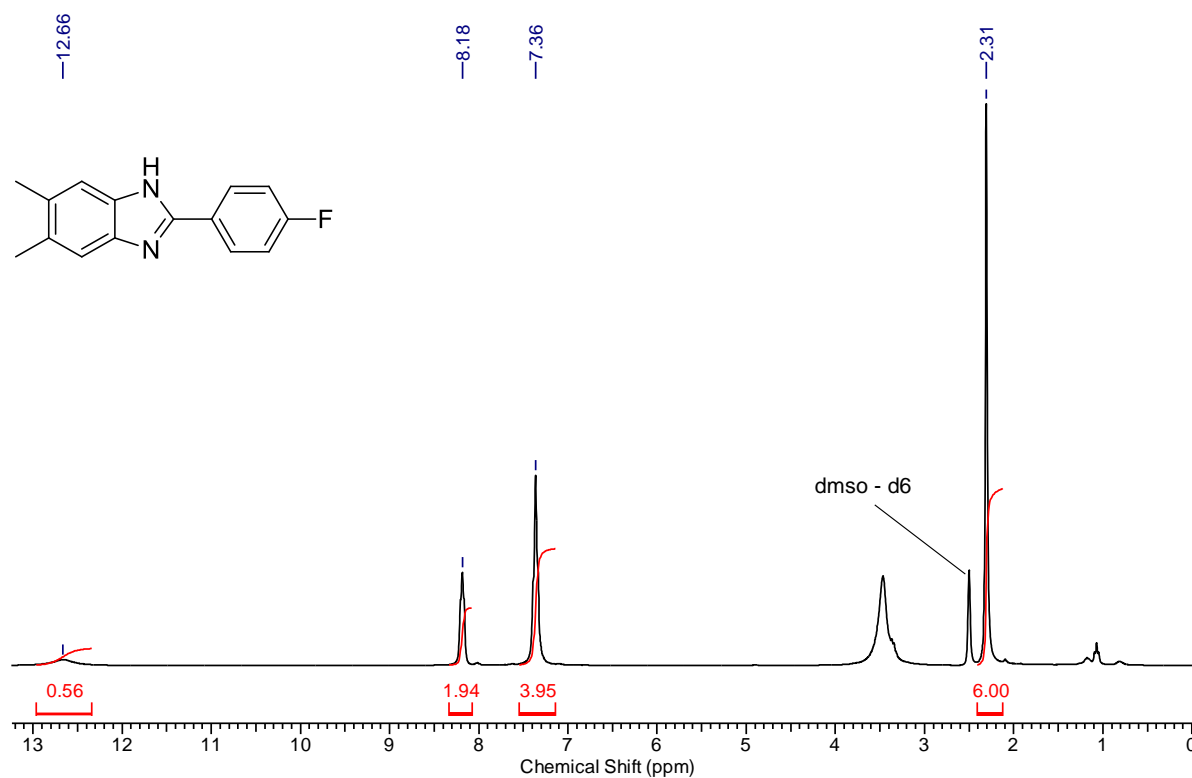
1a:



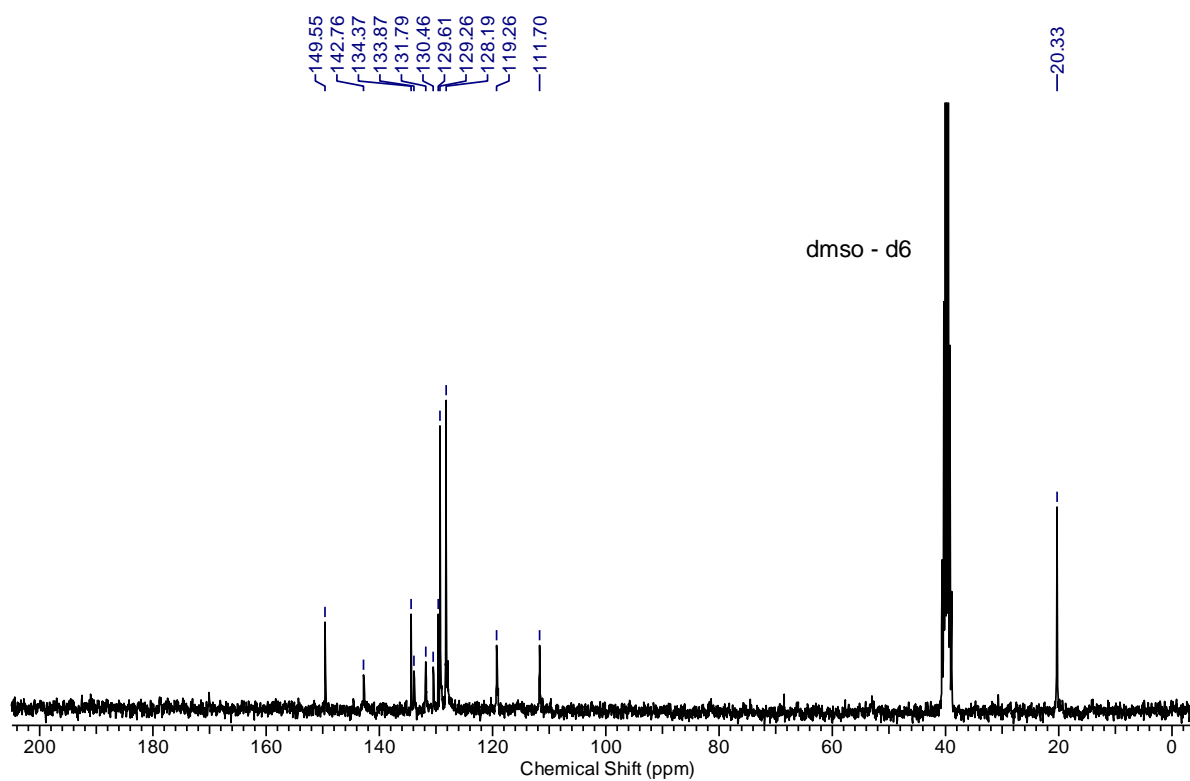
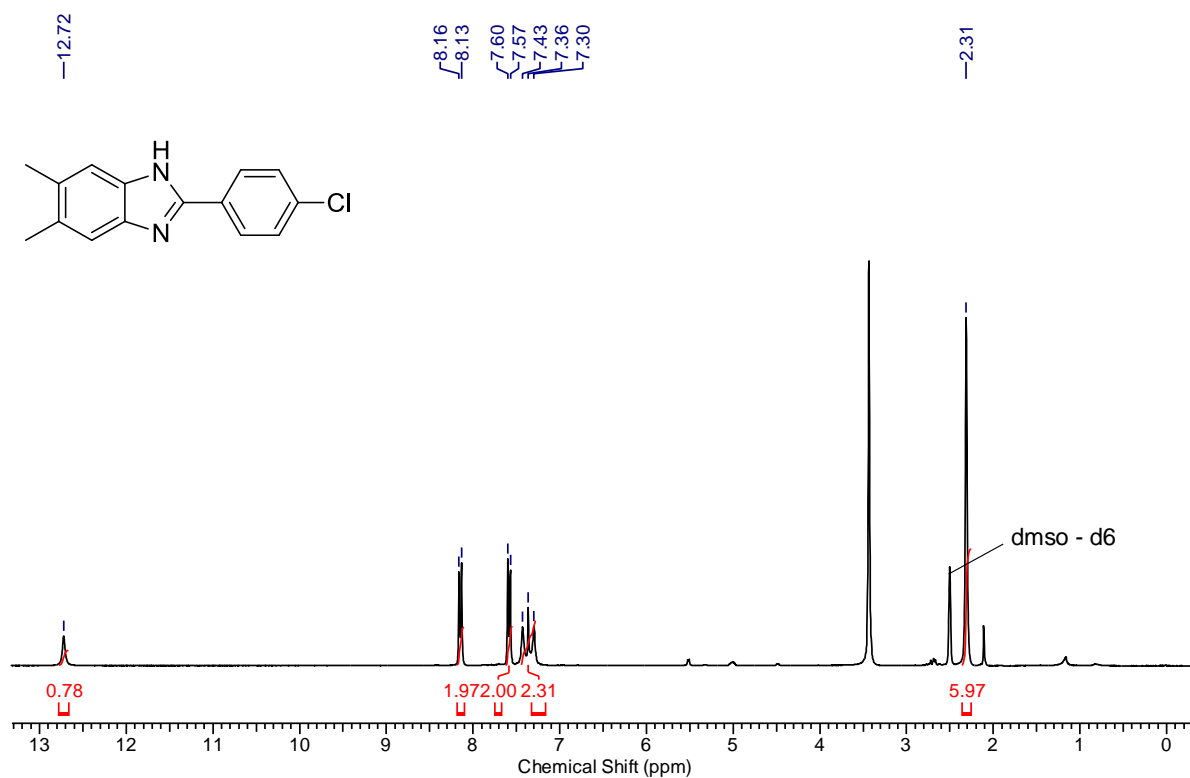
1b:



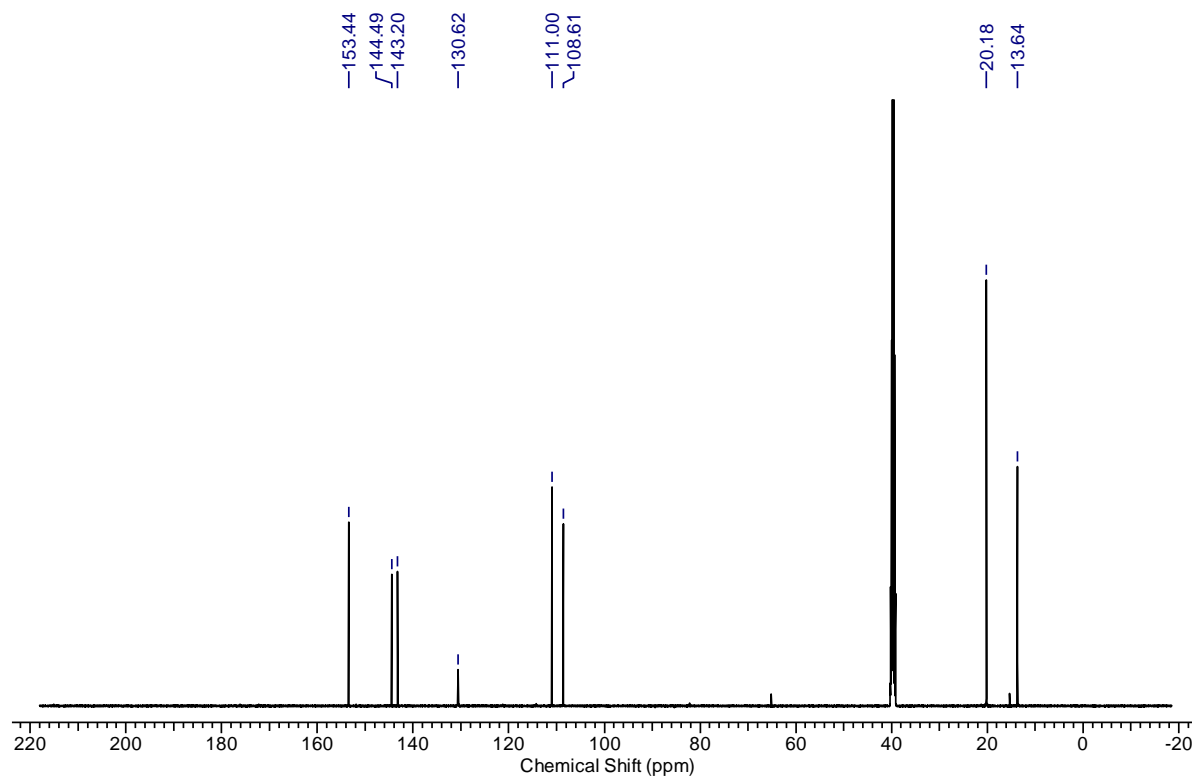
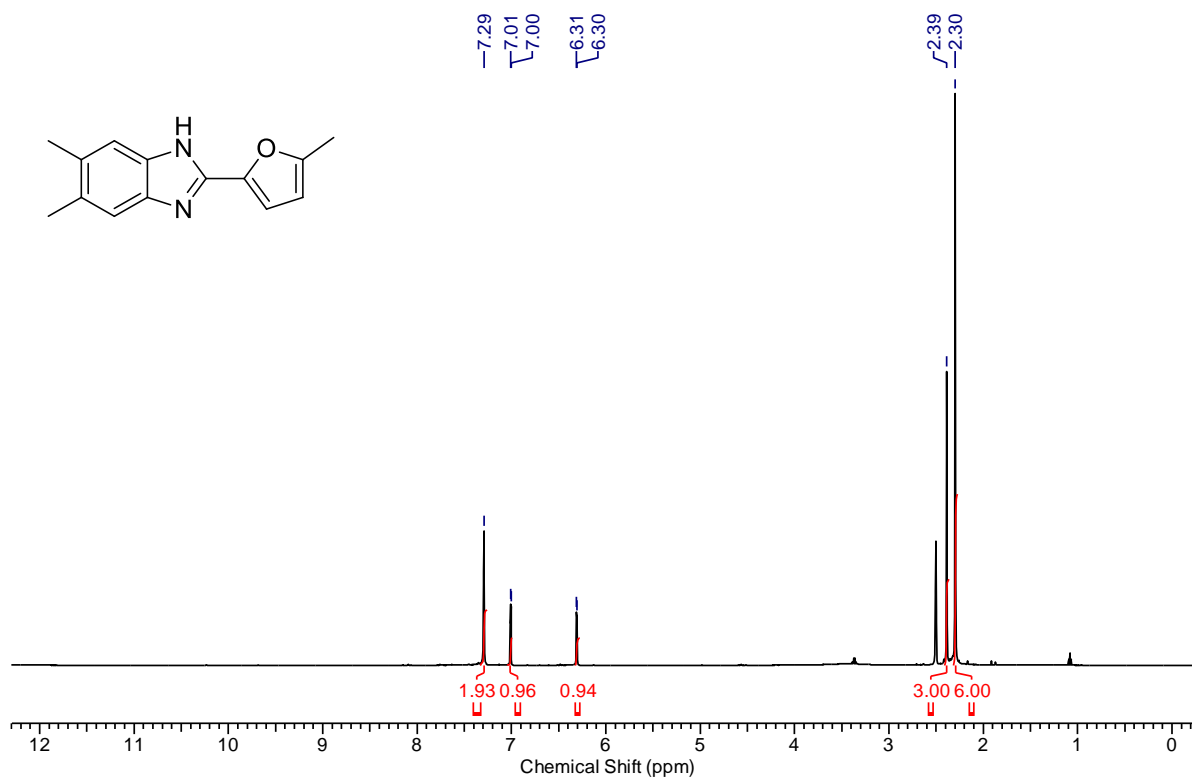
1c:



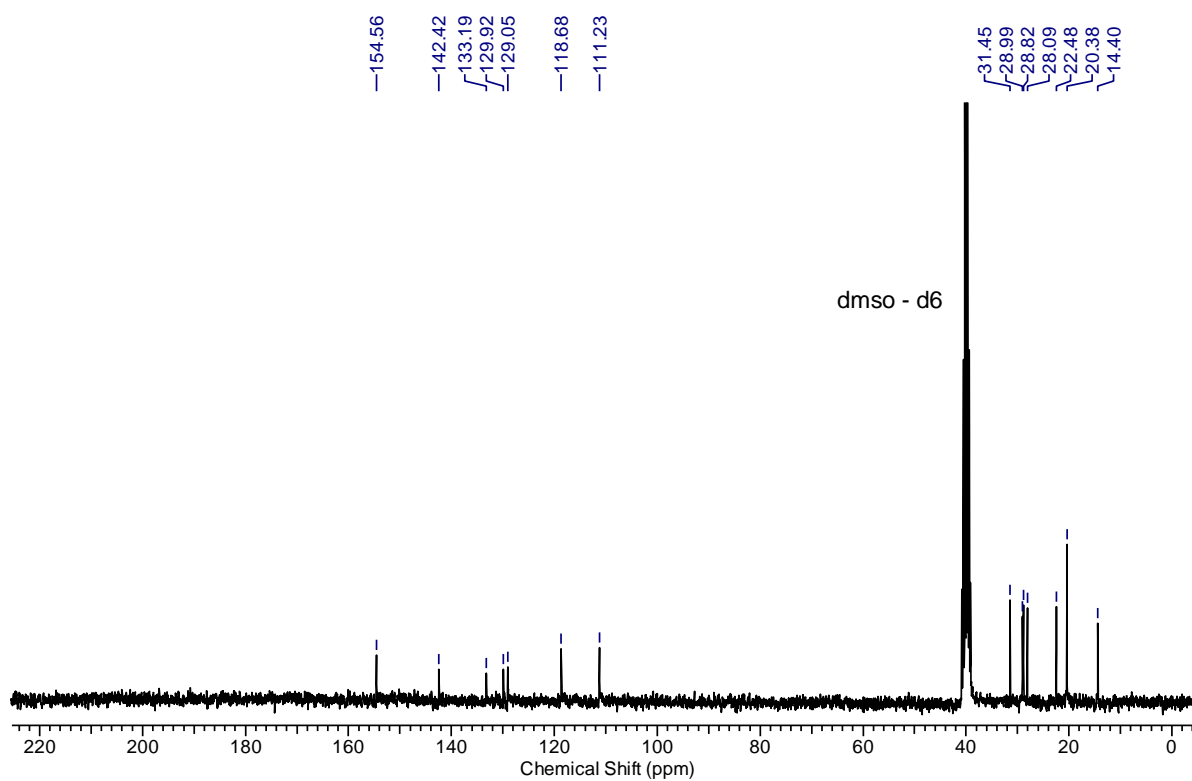
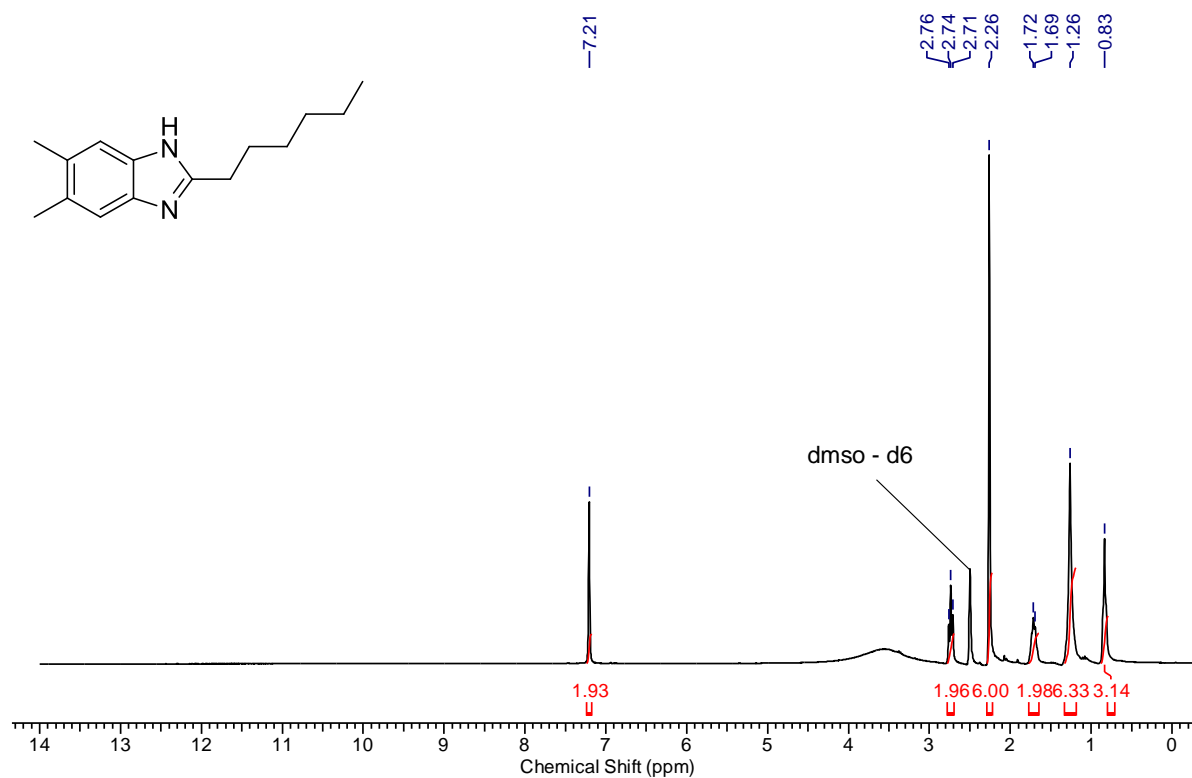
1d:



2:

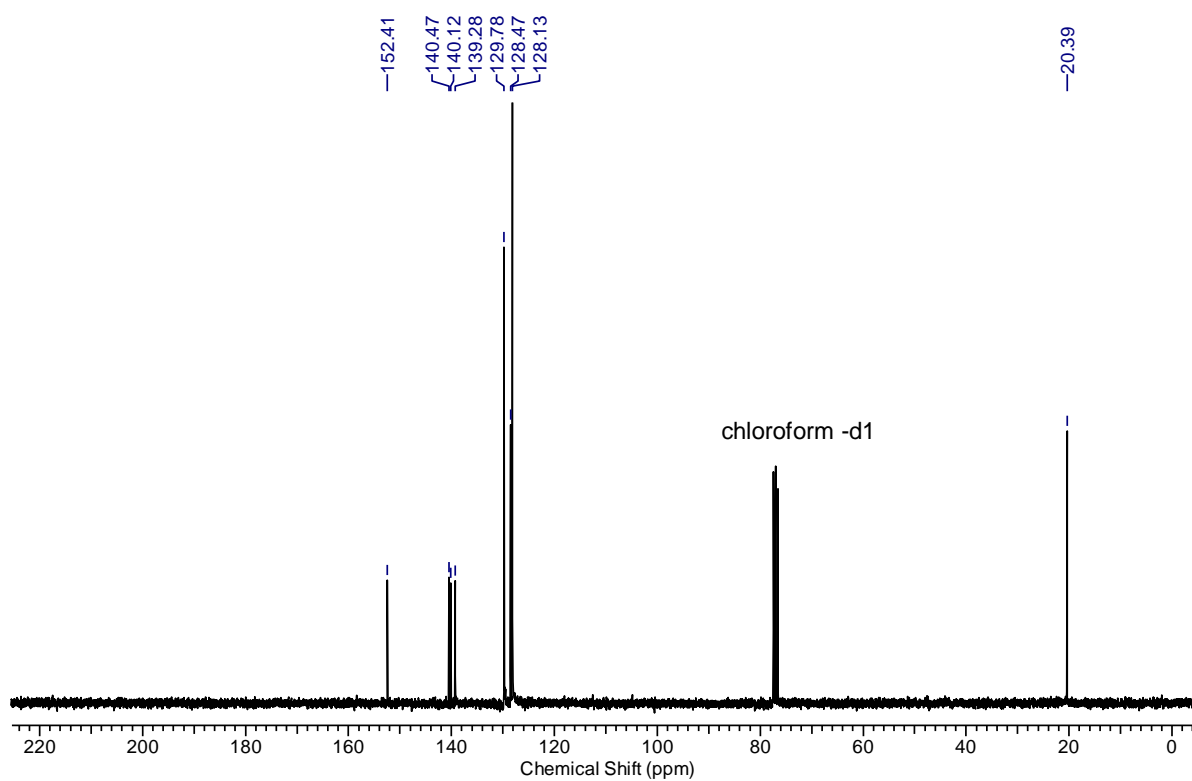
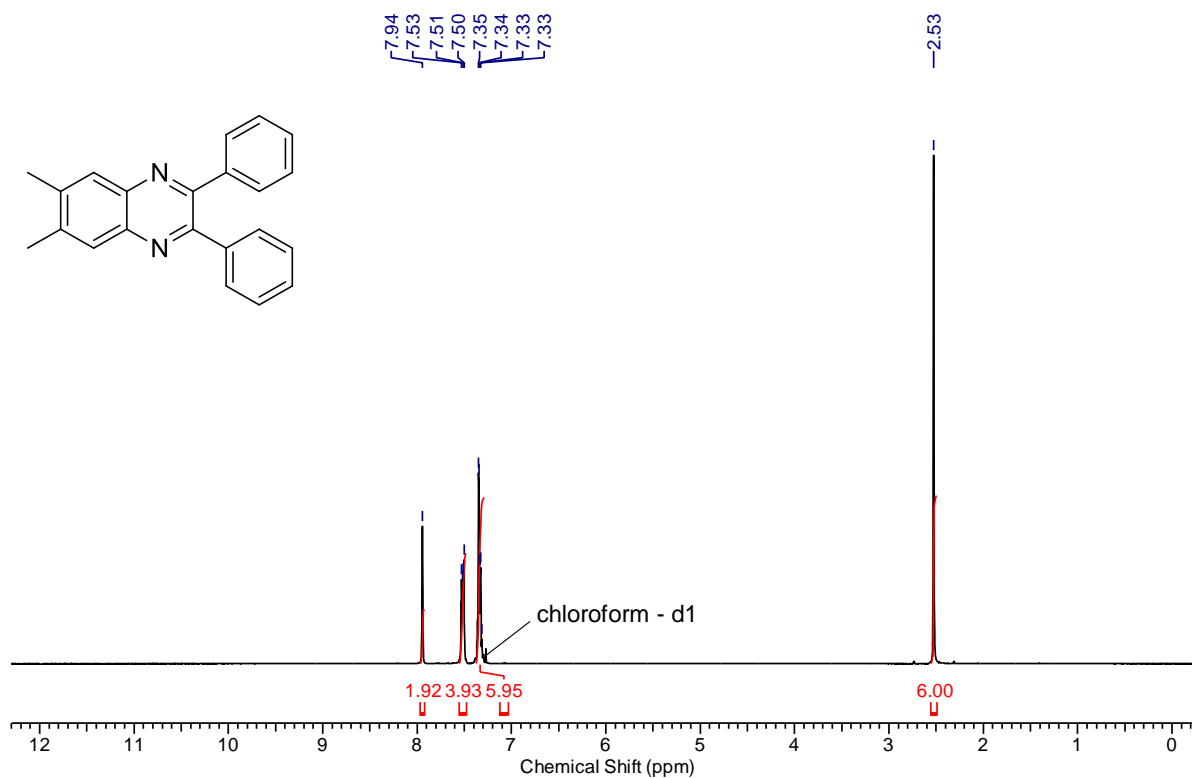


3:

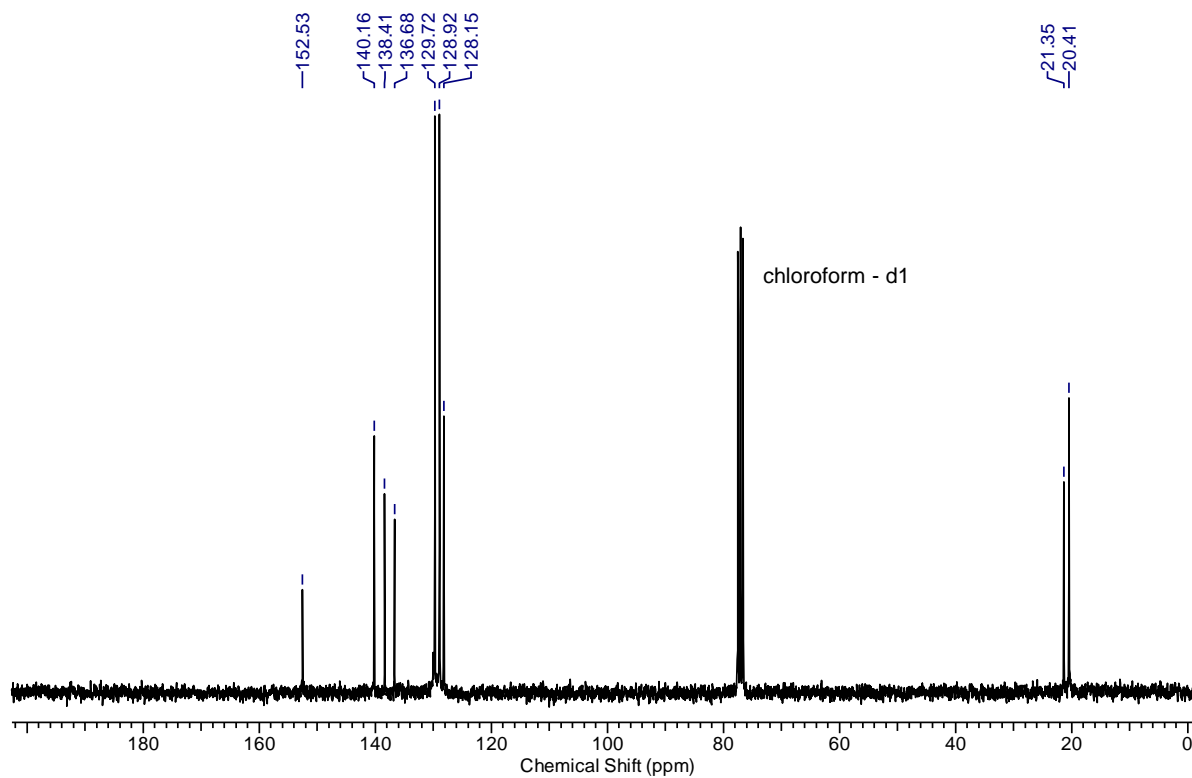
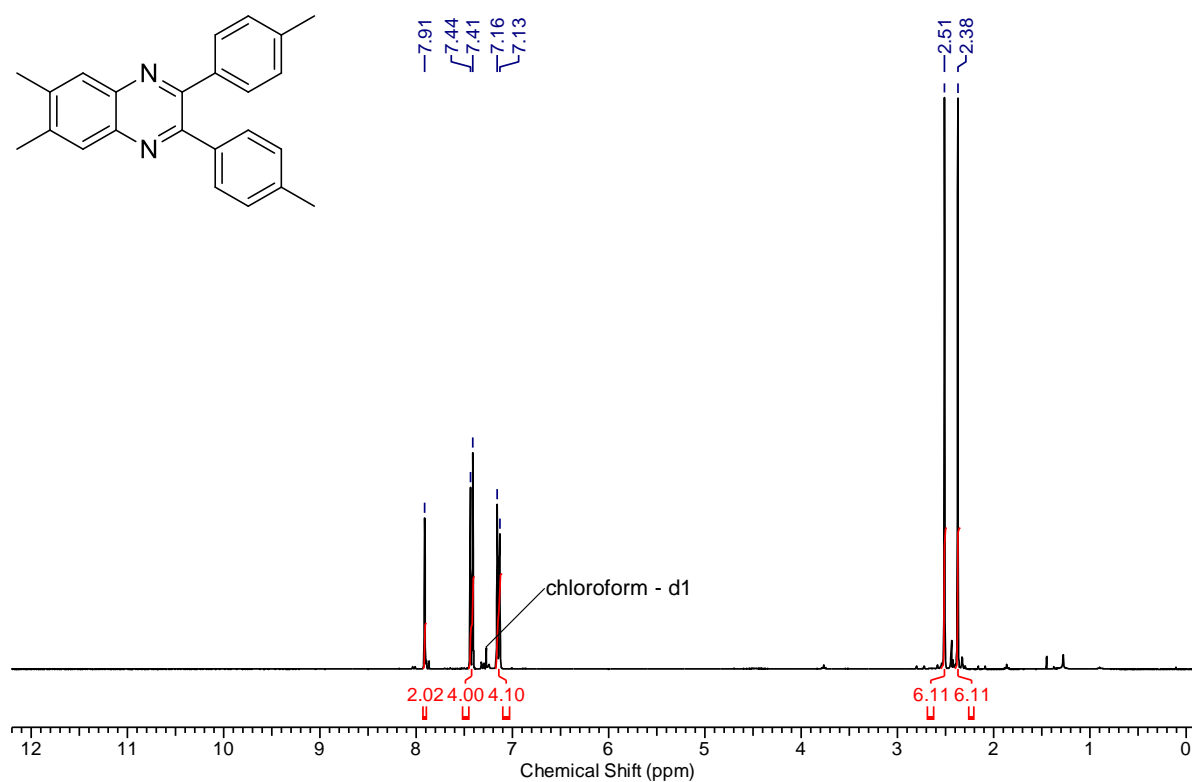


Quinoxalines

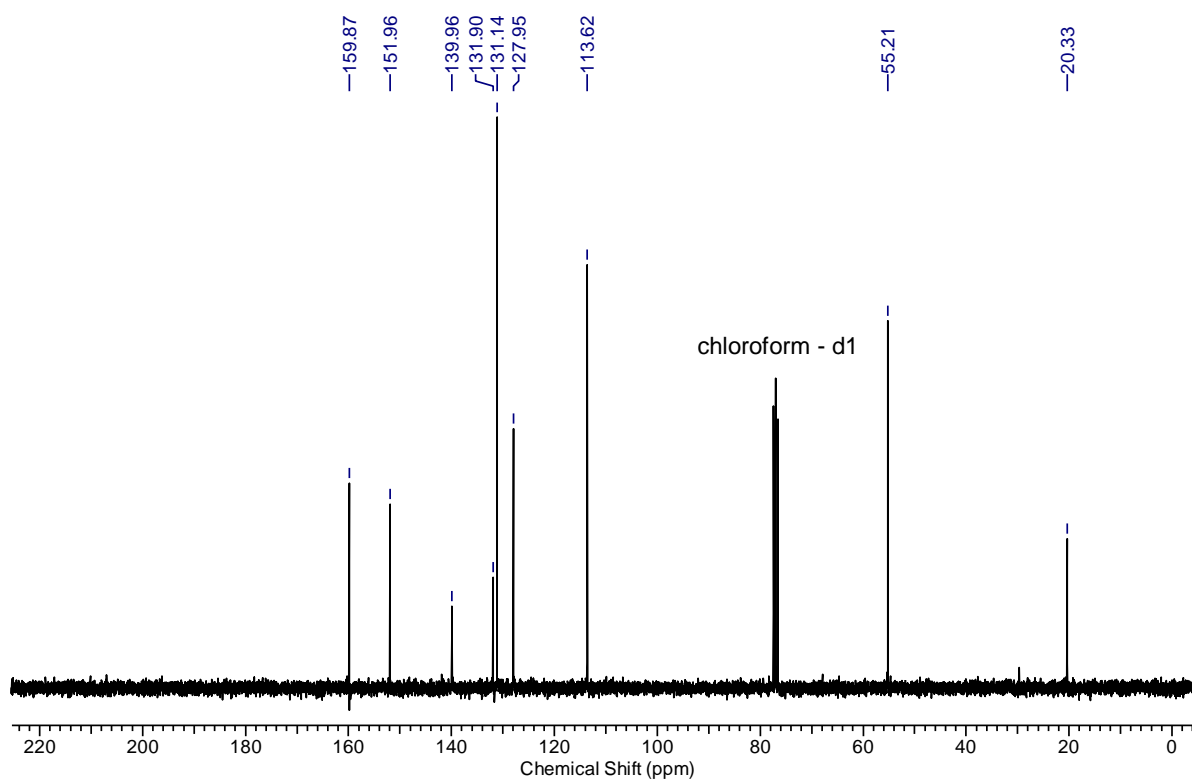
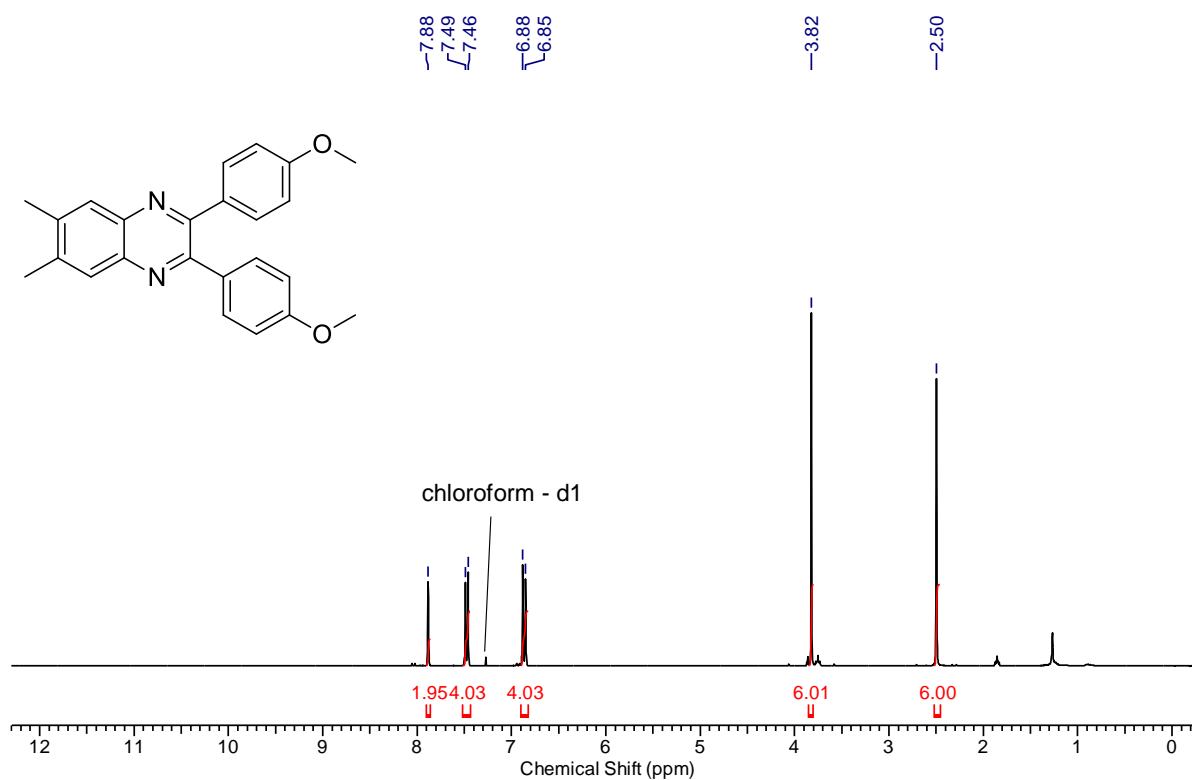
1a:



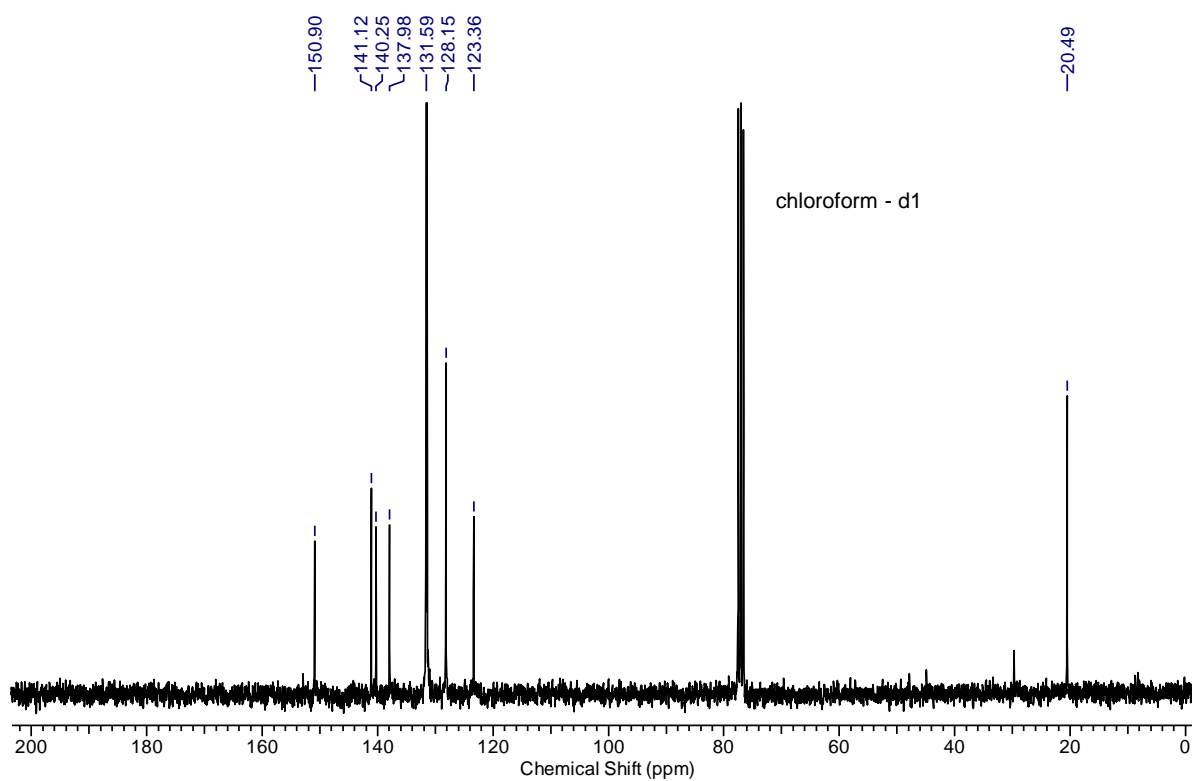
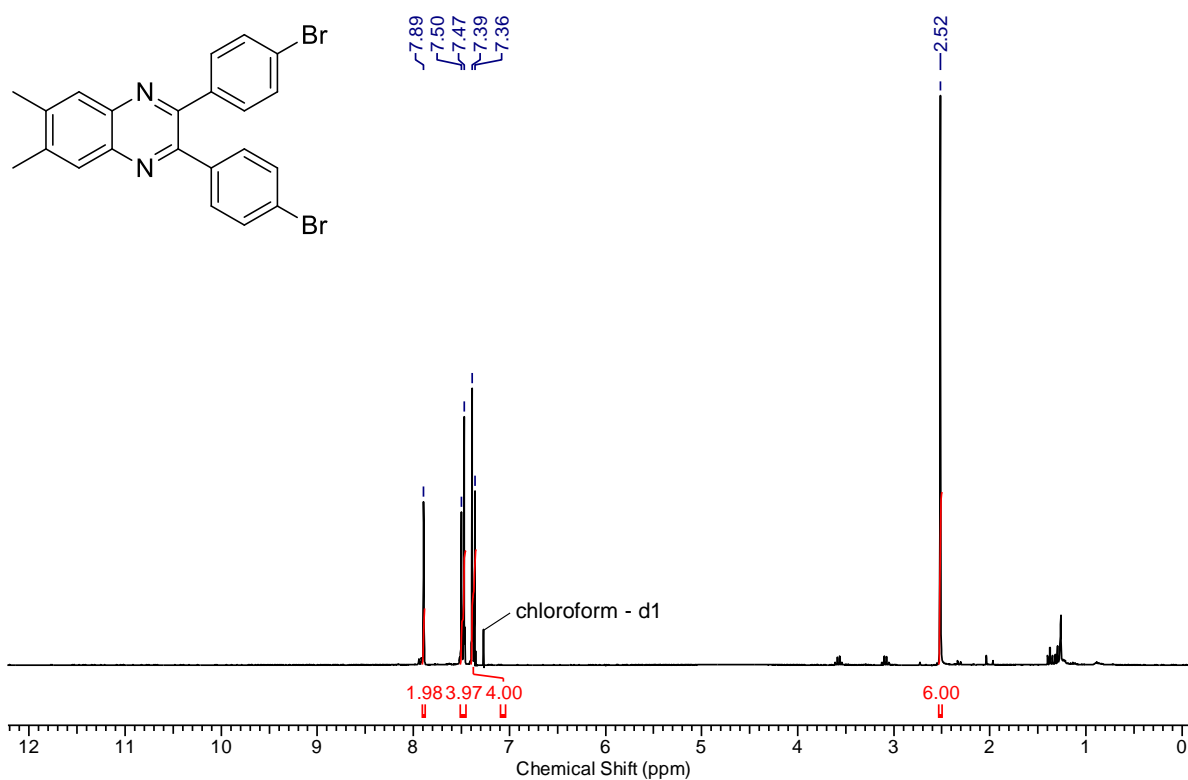
1b:



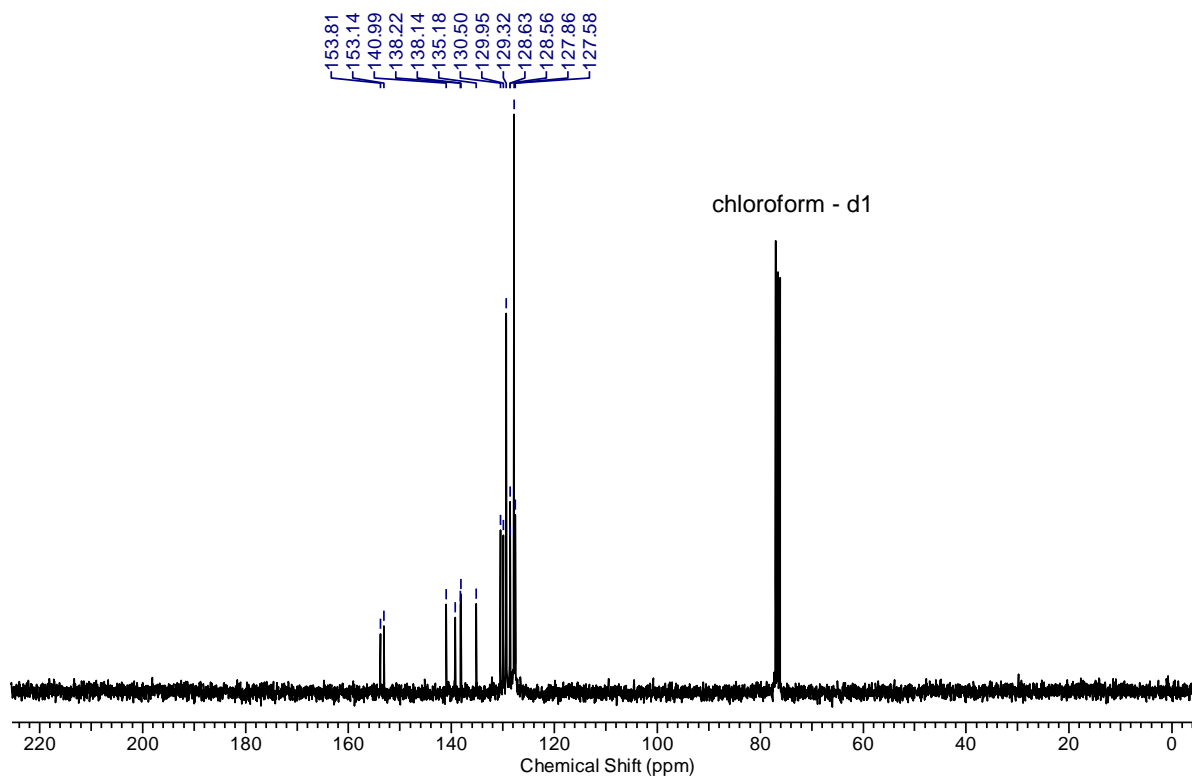
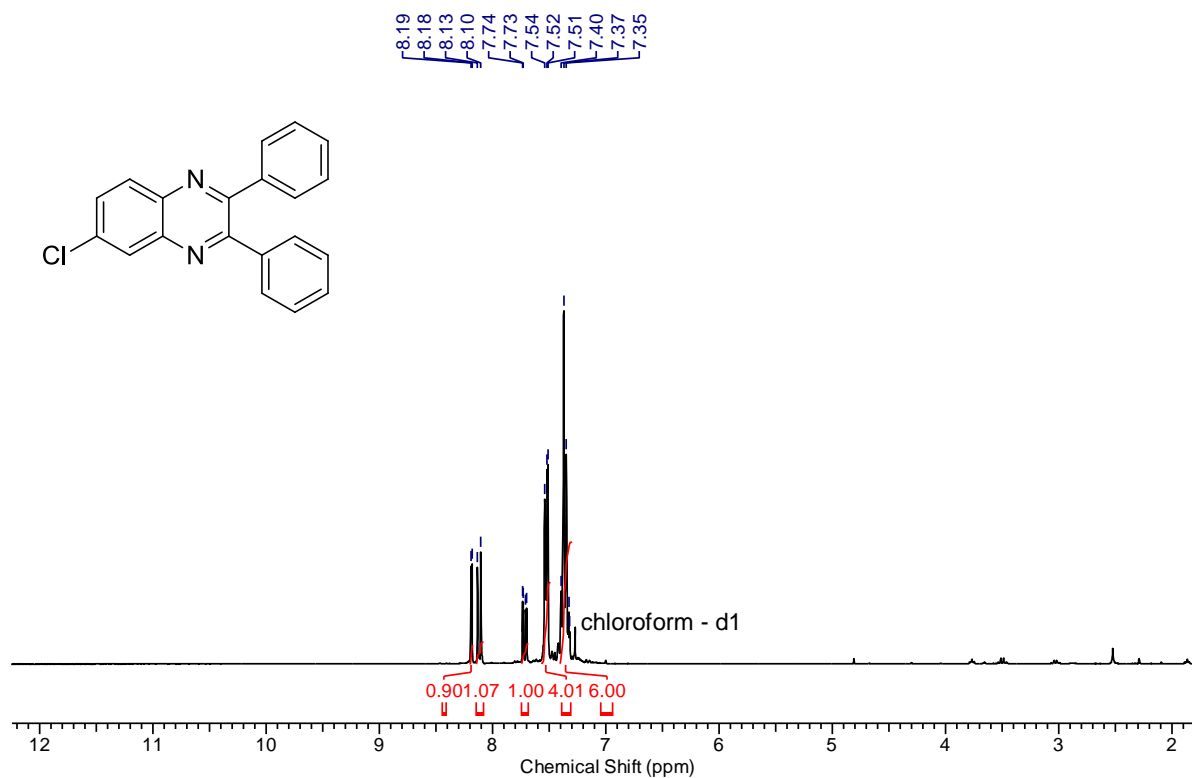
1c:



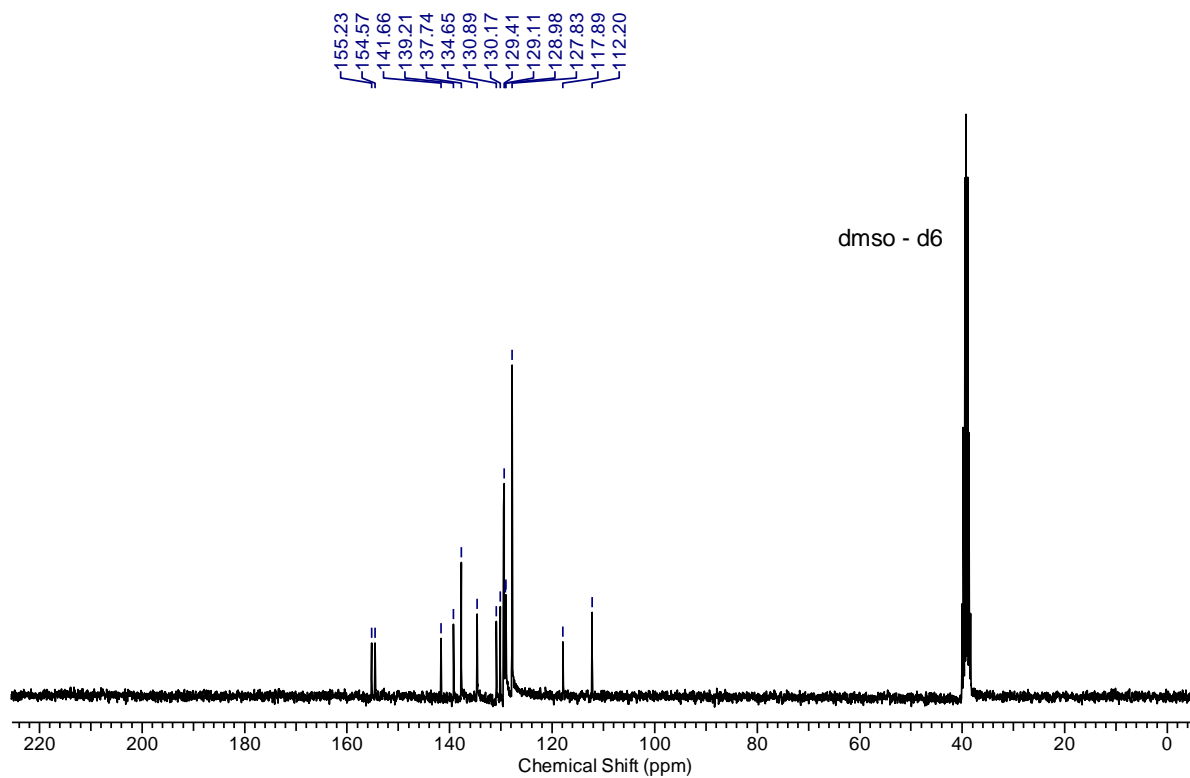
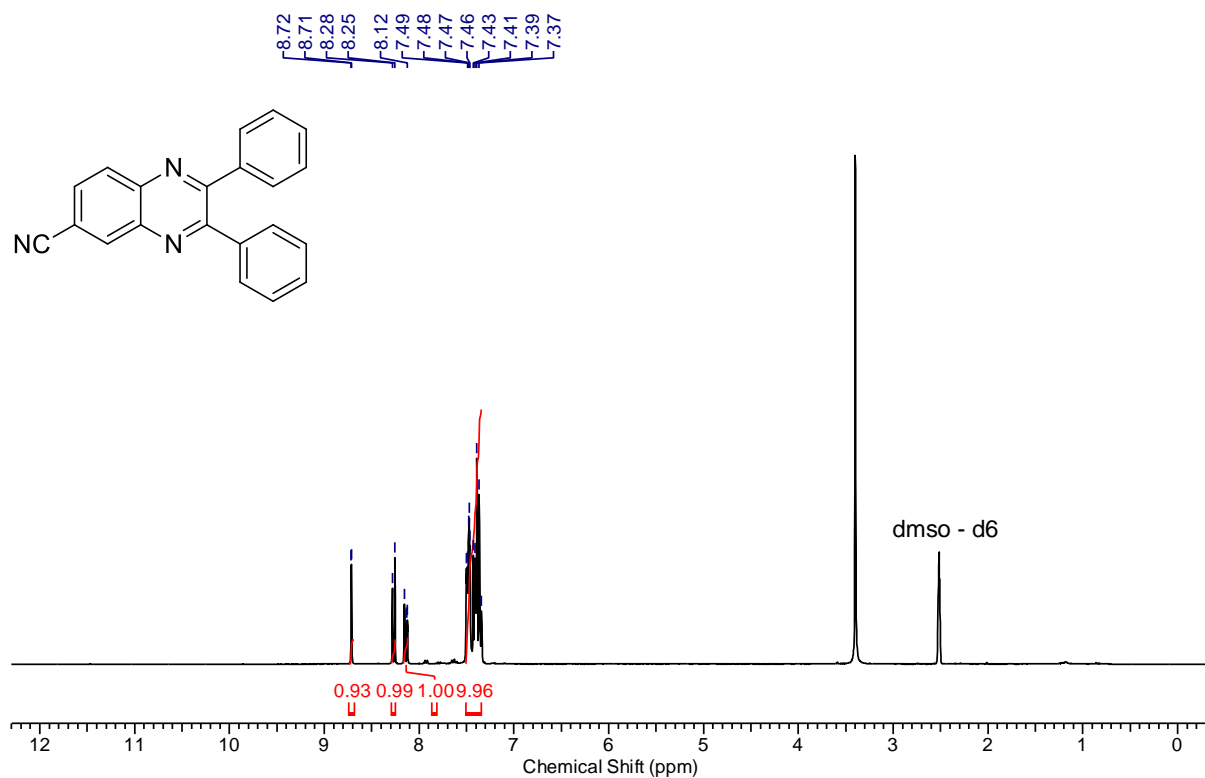
1d:



2:



3



4.5.5 References

- [1] R. Kempe, P. Arndt, *Inorg. Chem.* **1996**, *35*, 2644-2649.
- [2] G. Glatz, S. Demeshko, G. Motz, R. Kempe, *Eur. J. Inorg. Chem.* **2009**, 1385-1392.

5. The synthesis of primary amines via reductive amination employing an iron catalyst

Christoph Bäumler^[a], Christof Bauer^[a] and Rhett Kempe^{*[a]}

[a] Anorganische Chemie II – Katalysatordesign, Universität Bayreuth, 95440 Bayreuth.

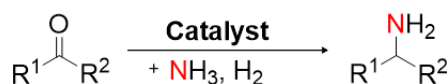
Published in *ChemSusChem* **2020**, *13*, 3110-3114.

Abstract: The reductive amination of ketones and aldehydes by ammonia is a highly attractive method for the synthesis of primary amines. The use of catalysts, especially reusable catalysts, based on earth-abundant metals is similarly appealing. We report on the iron-catalyzed synthesis of primary amines via reductive amination. We observe a broad scope and a very good tolerance of functional groups. Ketones, including purely aliphatic ones, aryl-alkyl, dialkyl, heterocyclic and aldehydes can be converted smoothly into their corresponding primary amines. In addition, the amination of pharmaceuticals, bioactive compounds and natural products has been demonstrated. Many functional groups, such as hydroxy, methoxy, dioxol, sulfonyl and boronate ester substituents, are tolerated. Our catalyst is easy to handle, selective and reusable, and ammonia dissolved in water could be employed as the nitrogen source. The key is the use of a specific Fe complex for the catalyst synthesis and a N-doped SiC material as catalyst support.

5.1 Introduction

The reductive amination of ketones and aldehydes is the method of choice for the synthesis of alkyl amines from inexpensive and diversely available educts.^[1] The synthesis of primary amines by employing ammonia as the nucleophile is especially attractive and challenging (Scheme 1, top).^[1] Amines are a very important class of chemical compounds and key functional groups in many bulk and fine chemicals,^[2] drugs^[3] and materials.^[4] The use of catalysts based on earth-abundant metals in reactions classically mediated by noble metals is also attractive and challenging. Significant progress has been made in the field of homogeneous earth-abundant 3d metal catalysis in recent years.^[5-7] The use of reusable nanostructured earth-abundant 3d metal catalysts for a broad applicability in complex organic synthesis is highly desirable and has been disclosed significantly less.^[8,10] Beller and coworkers recently introduced a reusable cobalt catalyst for the general synthesis of primary amines from aldehydes or ketones and ammonia^[9] (Scheme 1), and we discovered that a nickel catalyst supported by γ -Al₂O₃ and synthesized from a specific nickel complex can be used under

very mild conditions by employing ammonia dissolved in water. Aqueous ammonia is an attractive and easy to handle source of ammonia and has been used for the synthesis of primary amines in other catalytic reactions, such as hydroaminomethylation,^[11] telomerization of ammonia and butadiene,^[12] allylic substitutions,^[13,14] cross couplings,^[15] benzene oxyamination^[16] and amine alkylation.^[17] Murugesan and coworkers recently disclosed a different Ni catalyst for the general synthesis of primary amines via reductive amination.^[18] In addition, other reusable Co catalysts were described.^[19] A reusable iron catalyst for the synthesis of primary amines via reductive amination of ketones and aldehydes has not yet been disclosed. A reusable iron-based catalyst system for the synthesis of secondary aryl-alkyl amines^[20] and homogeneous iron catalysts for the reductive amination are known.^[21]



Previous works using reusable 3d-metal catalysts with broad scope:

- Co (Beller 2017^[9])
- Ni (Kempe^[10], Beller 2019^[18])

This work:

- Fe catalyst
- Broad substrate scope and functional group tolerance
- Reusable and easy to synthesize catalyst

Scheme 1: Reusable 3d metal catalyst developments with a broad scope in reductive amination of aldehydes and ketones to primary amines employing ammonia and hydrogen (R¹ and R² are aryl, alkyl substituents and, in the case of aldehydes, one of them represents a hydrogen atom).

We have recently introduced a variety of homogeneous earth-abundant metal catalysts^[22,23] and reusable nanostructured catalysts for energy storage^[24] and novel organic reactions,^[25] and earth-abundant metal catalysts with a broad applicability in organic synthesis.^[10,26] Herein, we report on a reusable and nanostructured iron catalyst for the general synthesis of primary amines from ketones or aldehydes via reductive amination. We employ easy to handle ammonia dissolved in water, observe a broad scope and find that many functional groups can be tolerated. Ketones, including purely aliphatic ones, aryl-alkyl, dialkyl, heterocyclic and aldehydes can be converted smoothly into their corresponding primary amines. In addition, the amination of pharmaceuticals, bioactive compounds and natural products has been demonstrated. Many functional groups, such as hydroxy, methoxy, dioxol, sulfonyl and boronate ester substituents, are tolerated. Our catalyst is easy to handle, selective and reusable. The key is the use of a specific Fe complex and a N-doped SiC material as the catalyst support. N-doping leads to a stronger metal support interaction during catalyst

synthesis and performance in comparison to non-doped materials. The stronger metal support interaction could enhance long time stability and reusability of the catalyst.^[27]

5.2 Results and Discussion

Catalyst synthesis and characterization. Our novel iron catalyst was synthesized in a two-step procedure (impregnation and pyrolysis) using a (N)SiC support (Figure 1A), which was prepared by modifying a known literature procedure.^[28] (N)SiC support synthesis: the commercially available polycarbosilane SMP 10 and acrylonitrile were dissolved in dimethylformamide, crosslinked with AIBN (azobisisobutyronitrile) as a radical initiator for crosslinking and pyrolyzed at 1000 °C under a nitrogen atmosphere (see Supporting Information (SI) for more details). Catalyst synthesis: the resulting (N)SiC support was impregnated with the Fe complex I (Figure 1A) in acetonitrile. After removal of the solvent, the sample was pyrolyzed under a nitrogen atmosphere at 750 °C followed by a reduction step (N₂/H₂ 90/10) at 550 °C (SI). Atom absorption spectroscopy (AAS) revealed an iron content of 4.0 wt% in the Fe/(N)SiC catalyst. Nitrogen physisorption measurements (SI Figure S3) of the (N)SiC support material and the catalyst showed a moderate decrease in the specific surface area [Brunauer-Emmett-Teller (BET) method] from 485 to 415 m²g⁻¹.

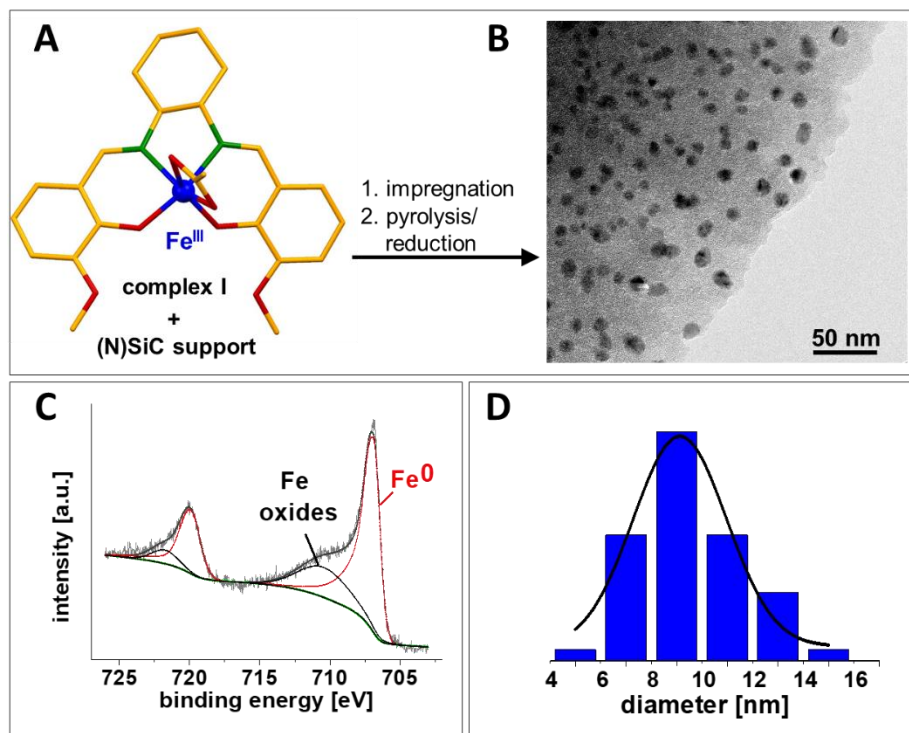


Figure 1: Synthesis and characterization of the Fe catalyst: A) Synthesis of the iron catalyst by wet impregnation of complex I (molecular structure determined by X-ray single crystal structure analysis, color code: green = N, red = O, orange = C) on the (N)SiC support, followed by pyrolysis and hydrogen treatment (reduction). B) TEM analysis suggested the presence of homogeneously distributed Fe nanoparticles. C) XPS analysis confirms the presence of metallic iron and iron oxide at the surface of the nanoparticles. D) Size distributions revealed an average iron nanoparticle size of 10 nm.

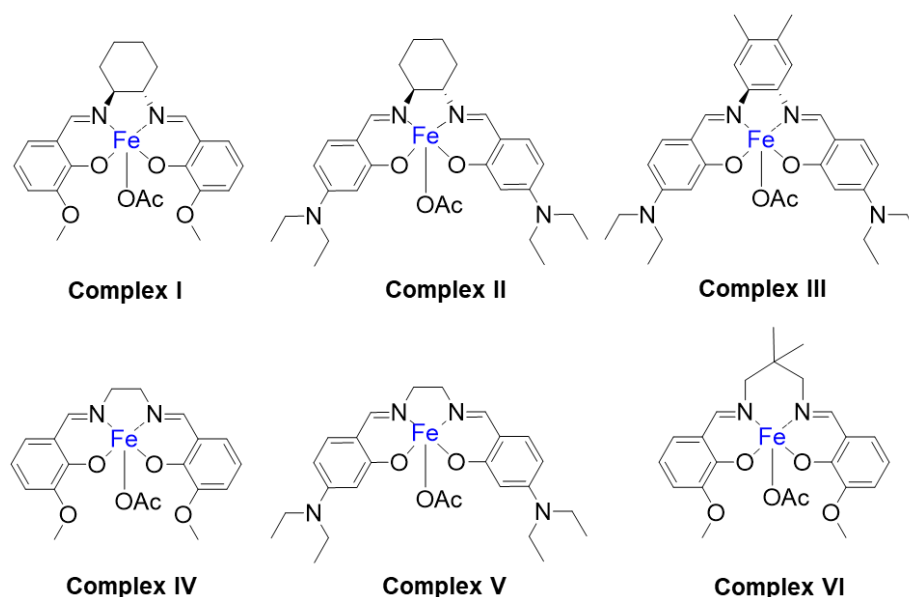


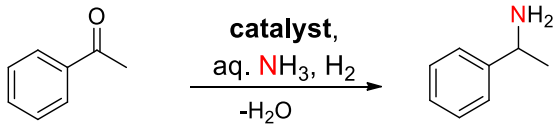
Figure 2: Different synthesized iron complexes used as metal source for the catalyst screening; (OAc = acetate).

The calculated pore-size distributions were almost identical and exhibited the presence of mainly micropores (92 %). The existence of metallic iron nanoparticles (cubic iron metal phase) was

confirmed by powder X-ray diffraction (PXRD, SI Figure S9). Transmission electron microscopy (TEM) showed a homogeneous distribution of the iron nanoparticles over the (N)SiC support with an average particle size of 10 nm (Figure 1B,D). The lattice spacing of an iron nanoparticle was investigated by High-Resolution-TEM analysis in order to additionally verify the presence of metallic iron (SI Figure S10). The averaged lattice plane distance of the nanoparticle was determined to be 0.2022 nm, which is in good agreement with the literature values. Additionally, the Fe/(N)SiC catalyst was investigated by X-ray photoelectron spectroscopy (XPS), indicating the presence of metallic and oxidic iron species on the nanoparticle surface (Figure 1C). Further investigations were carried out by scanning energy microscopy (SEM) combined with energy dispersed X-ray (EDX) element maps and revealed that the iron nanoparticles are homogeneously distributed over the entire support material (SI Figure S4).

Optimization of the reaction parameters. The synthesis of 1-phenylethanamine from acetophenone and aqueous ammonia was chosen as the benchmark reaction for optimizing the reaction conditions. The solvent screening showed a higher yield with increasing polarity (SI Table S2), consequently, water was chosen as the best solvent. Next, the amount of ammonia was screened. It was found that the quantity of ammonia strongly influences the yield by reducing self-coupling reactions of the carbonyl compound (SI Table S3/S4). In summary, the optimized conditions for the Fe/(N)SiC catalyst are 3.5 mL of 25 % aqueous ammonia, 6.5 MPa H₂ and 140 °C (SI Table S5). Various commercially available supports and iron sources were tested in the amination of acetophenone to ensure that our combination of support material and metal complex is the most effective catalyst system in the reductive amination of carbonyl compounds to primary amines (Table 1). Surprisingly, catalysts based on support materials recently applied successfully for nickel catalysts (Al₂O₃, SiO₂) showed no activity.

Table 1: Catalyst screening for the reductive amination of acetophenone.

				
Entry	Metal source	Support material	Pyrolysis temperature [°C]	Yield [%]
1 ^[a]	Complex I	(N)SiC	750	99
2	Complex I	(N)SiC	650	54
3	Complex I	(N)SiC	750	72
4	Complex I	(N)SiC	850	51
5	Complex II	(N)SiC	750	65
6	Complex III	(N)SiC	750	47
7	Complex IV	(N)SiC	750	68
8	Complex V	(N)SiC	750	63

9	Complex VI	(N)SiC	750	61
10	Complex I	Activated carbon	750	37
11	Complex I	SiO ₂	750	0
12	Complex I	TiO ₂	750	0
13	Complex I	CeO ₂	750	25
14	Complex I	Al ₂ O ₃	750	0
15	Complex I	Pyrolyzed PAN	750	36
16 ^[b]	-	(N)SiC	1000	0
17	Fe(acacH) ₃	(N)SiC	750	42
18	Fe(NO ₃) ₃	(N)SiC	750	44

Reaction conditions: 8.6 mol% Fe (60 mg supported Fe catalyst with 4.0 wt% Fe loading, 0.043 mmol Fe, 2.4 mg Fe), 0.5 mmol acetophenone, 140 °C, 20 h, 6.5 MPa H₂, 3.5 mL aq. NH₃-25 %. Yields were determined by GC using n-dodecane as an internal standard. [a] 10 mol% Fe (70 mg Fe/(N)SiC with 4.0 wt% Fe loading, 0.05 mmol Fe, 2.8 mg Fe). [b] 60 mg (N)SiC; (acacH = (Z)-4-hydroxypent-3-en-2-one).

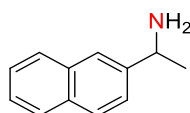
Catalysts based on activated carbon, CeO₂ and pyrolyzed PAN (polyacrylonitrile) showed low activity, whereas TiO₂ is not suitable at all for this reaction. The complexes (see Supporting Information (SI) for more details) in Figure 2 were tested as metal sources for the Fe/(N)SiC synthesis and showed also good yields, up to 68 % in case of complex IV. It seems that the *ortho*-vanillin structure in combination with a sterically undemanding aliphatic diamino-building block is essential. Therefore, complex I generated the highest active catalyst-system with a yield of 72 % (Table 1, Entries 3, 5-9). A decrease of the yield was observed compared to complex I by replacing the metal source with a commercially available iron complex Fe(acac)₃ (acacH = (Z)-4-hydroxypent-3-en-2-one) or an common salt Fe(III) nitrate (Fe(NO₃)₃·9H₂O). TEM investigations of all catalysts based on (N)SiC in combination with the different complexes and of complex I in combination with the different supports, see SI, revealed that the combination of complex I and (N)SiC gave rise to a rather well defined nanostructured catalyst. All other catalysts are significantly less well defined.

Substrate scope. We were next interested in the broad applicability of our Fe-based catalyst system in the reductive amination of carbonyl compounds to primary amines. All yields of primary amines are isolated yields for the corresponding hydrochloride salts. Aryl-alkyl ketones with various substituents were aminated in good to excellent yields. Ketones with electron-donating substituents (e.g. methoxy, methyl) on the aromatic ring could be smoothly converted in isolated yields up to 96 % (Table 2, Entries 2–4, 8, 11, 14).

Table 2: Reductive amination of ketones to primary amines.^{[a][b]}

$ \begin{array}{c} \text{O} \\ \parallel \\ \text{R}^1-\text{C}-\text{R}^2 \end{array} \xrightarrow[\text{-H}_2\text{O}]{\text{Fe/(N)SiC, aq. NH}_3, \text{ 6.5 MPa H}_2, \text{ 140 }^\circ\text{C}} \begin{array}{c} \text{NH}_2 \\ \\ \text{R}^1-\text{CH}-\text{R}^2 \end{array} $			
Entry		Product	Yield [%]
1		R = H	99
2		R = 4-CH ₃	96
3		R = 3-CH ₃	90
4		R = 2-CH ₃	82
5		R = 4-Cl	86
6		R = 4-Br	81
7		R = 4-F	83
8		R = 4-OCH ₃	87
9		R = 4-CF ₃	79
10		R = 4-SO ₂ CH ₃	81
11		R = 3,4-di-CH ₃	83
12		R = H	93
13		R = 4-CH ₃	91
14		R = 4-OCH ₃	82
15		R = 4-Cl	89
16			75 ^[c]
17			86 ^[c]
18			87
19			85
20			79 ^[c]

21



91

[a] Reaction conditions: 10 mol% Fe (70 mg Fe/(N)SiC with 4.0 wt% Fe loading, 0.05 mmol Fe, 2.8 mg Fe), 0.5 mmol ketone, 140 °C, 20 h, 6.5 MPa H₂, 3.5 mL aq. NH₃-25 %. [b] Isolated yields of the corresponding hydrochloride salts. [c] 150 °C.

Table 3: Reductive amination of aldehydes to primary amines.^{[a][b]}

<div style="text-align: center;"> </div>			
Entry		Product	Yield [%]
22		R = H	89
23		R = 4-Cl	79
24		R = 4-Br	75
25		R = 4-F	77
26		R = 4-CH ₃	81
27			71 ^[c]
28			73 ^[c]

[a] Reaction conditions: 10 mol% Fe (70 mg Fe/(N)SiC with 4.0 wt% Fe loading, 0.05 mmol Fe, 2.8 mg Fe), 0.5 mmol aldehyde, 130 °C, 20 h, 6.5 MPa H₂, 3.5 mL aq. NH₃-25 %. [b] Isolated yields of the corresponding hydrochloride salts. [c] 12 mol% Fe, 120 °C.

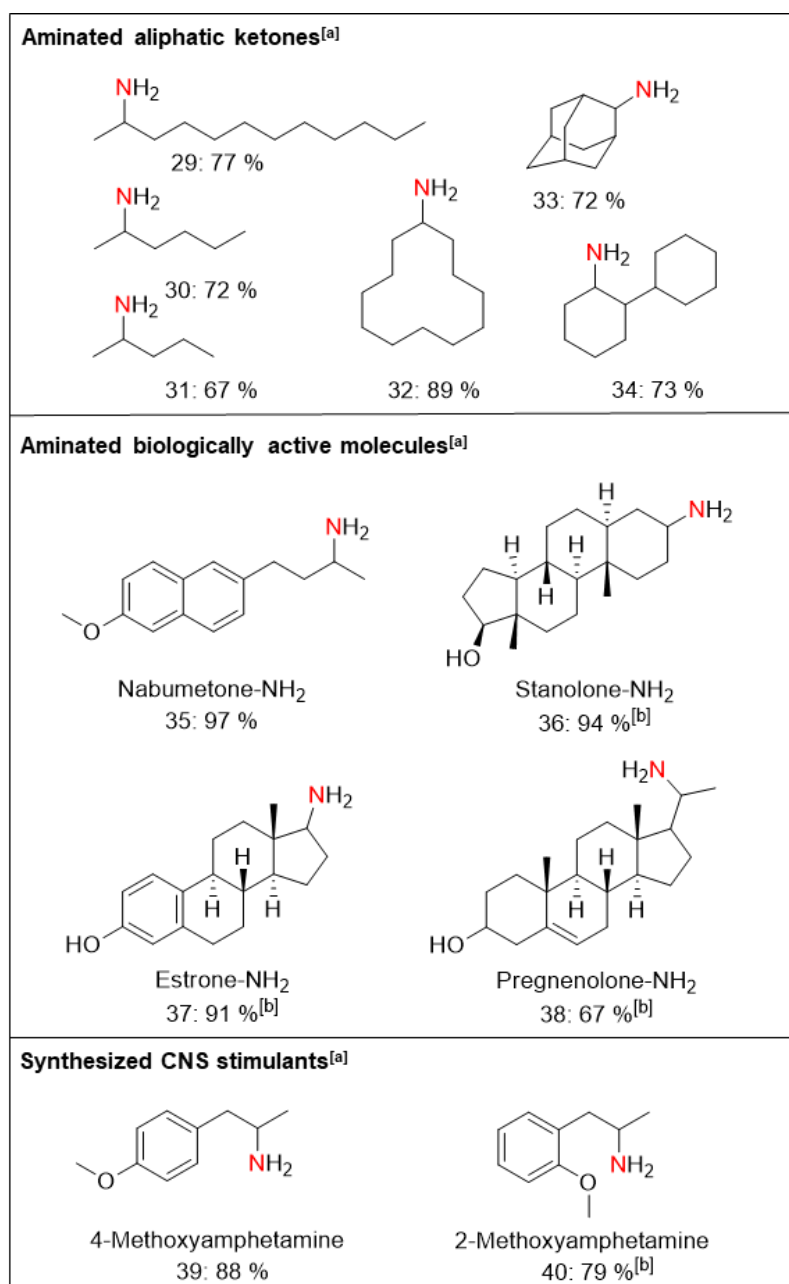


Figure 3: Reductive amination of purely aliphatic ketones and biologically active molecules. [a] Reaction conditions: 10 mol% Fe (70 mg Fe/(N)SiC with 4.0 wt% Fe loading, 0.05 mmol Fe, 2.8 mg Fe), 0.5 mmol ketone, 140 °C, 20 h, 6.5 MPa H₂, 3.5 mL aq. NH₃-25 %. Isolated yields of the corresponding hydrochloride salts. [b] 150 °C.

The position of the substituent played a decisive role. *ortho*-Substituted ketones were more difficult to aminate to the corresponding primary amines than the *meta*- and *para*-substituted, most likely due to the increasing steric hindrance (Table 2, Entries 2–4). Electron-withdrawing substituents, such as halogens and sulfonyl (Table 2, Entry 10), were well-tolerated. Therefore, different substituted chloro-, fluoro-, CF₃- and bromo-ketones were converted into their corresponding amines in good yields with only traces of dehalogenation (Table 2, Entries 5–7, 9, 15). The reductive amination of a heteroaromatic ketone containing nitrogen was accomplished with a good yield of 75 % (Table 2, Entry 16). Additionally, sterically demanding aryl-alkyl ketones, such as 2-methoxy-1,2-

diphenylethanamine, could be isolated in very good yield (Table 2, Entry 17). Moreover, the necessity of the α -carbon (C_α) position of the aromatic ring next to the carbonyl group was investigated. The amination of 4-phenylbutan-2-one showed that ketones with a phenyl ring at the γ -carbon position can be transformed with an impressive isolated yield (87 %, Table 2, Entry 18). Aryl-alkyl ketones with a long alkyl chain can be converted with our synthesis protocol (Table 2, Entry 19, $C_{n=7}$), albeit with a slightly lower yield: 85 vs. 93 % (Table 2, Entry 12, $C_{n=3}$). The amination of a naphthalene-based ketone proceeded smoothly, whereas the biphenyl-substituted ketone required higher temperatures for attractive conversion (Table 2, Entries 20, 21).

The transformation of benzylic aldehydes was performed under milder conditions; thus, the self-coupling reactions were reduced but not completely suppressed. Therefore, yields are slightly lower than for ketones. Halogenated aldehydes, including bromides, chlorides and fluorides, were converted with good yields >75 % (Table 3, Entries 23–25). The toleration of an electron-donating methyl substituent was also accomplished with good yields recorded (Table 3, Entry 26). Synthetically useful functionalities, such as 4,4,5,5-tetramethyl-1,3,2-dioxaborolanyl or dioxol, could be tolerated, albeit under milder reaction conditions and with higher catalyst loadings (Table 3, Entries 27–28).

In addition, we tested purely aliphatic ketones in the reductive amination. Both aliphatic (Figure 3, Entries 29–31) and cycloalkyl ketones (Figure 3, Entries 32–34) of various length and ring sizes could be converted to the corresponding primary amines in yields up to 89 %. Finally, we were interested in introducing the $-NH_2$ moiety in pharmaceuticals, biologically active, highly functionalized and structurally complex molecules. The selective conversion of nabumetone, estrone and stanolone to primary amines was achieved with yields over 91 % (Figure 3, Entries 35–37). The C-C double bond functionality of pregnenolone was tolerated and the corresponding amine was isolated in 67 % yield (Figure 3, Entry 38). Finally, the synthesis of CNS (Central Nervous System) stimulants was realized. 4- and 2-methoxyamphetamine were obtained in good yields up to 88 % (Figure 3, Entries 39–40).

Regarding reusability and upscaling, finally, five consecutive runs without any loss of activity were performed (conditions for 99 % yield) to confirm the recyclability of our catalyst (SI Figure S 12). An up-scaling reaction of acetophenone to 1-phenylethanamine to gram scale was also carried out with the same yield as the small-scale experiment (SI).

In summary, we report on a selective reusable iron-based catalyst system for the synthesis of primary amines via reductive amination employing ammonia dissolved in water. Ketones, including purely aliphatic ones, aryl-alkyl, dialkyl, heterocyclic and aldehydes can be converted smoothly into their corresponding primary amines. In addition, the amination of pharmaceuticals, bioactive compounds and natural products has been demonstrated. Many functional groups, such as hydroxy, methoxy, dioxol, sulfonyl and boronate ester substituents, are tolerated. Our catalyst is easy to synthesize and

handle. It is reusable and upscaling has been demonstrated. The key is the use of a specific Fe complex and a N-doped SiC material as a support to observe catalytic activity.

5.3 Acknowledgements

We thank the DFG for financial support (KE 756/33-1) and Christine Denner for SEM measurements.

Keywords: Reductive amination • primary amines • iron catalyst • ketones • aldehydes

5.4 References

- [1] W. S. Emerson, *Org. React.* (N.Y.) **1948**, *4*, 174–202.
- [2] K. Weissermel, H.-J. Arpe, *Industrial Organic Chemistry*, 3rd ed., Wiley-VCH, Weinheim, **2008**.
- [3] R. Vardanyan, V. Hruby, *Synthesis of Best-Seller Drugs*, 1st ed., Academic Press, Amsterdam, **2016**.
- [4] S. A. Lawrence, *Amines: Synthesis, Properties and Applications*, Cambridge University Press, Cambridge, UK, New York, **2004**.
- [5] a) A. Boddien, D. Mellmann, F. Gärtner, R. Jackstell, H. Junge, P. J. Dyson, G. Laurenczy, R. Ludwig, M. Beller, *Science* **2011**, *333*, 1733–1736. b) A. M. Tondrea, C. C. H. Atienza, K. J. Weller, S. A. Nye, K. M. Lewis, J. G. P. Delis, P. J. Chirik, *Science* **2012**, *335*, 567–570. c) M. R. Friedfeld, M. Shevlin, J. M. Hoyt, S. W. Krska, M. T. Tudge, P. J. Chirik, *Science* **2013**, *342*, 1076–1080. d) W. Zuo, A. J. Lough, Y. F. Li, R. H. Morris, *Science* **2013**, *342*, 1080–1083. e) J. M. Hoyt, V. A. Schmidt, A. M. Tondreau, P. J. Chirik, *Science* **2015**, *349*, 960–963. f) T. J. Korstanje, J. I. van der Vlugt, C. J. Elsevier, B. de Bruin, B. *Science* **2015**, *350*, 298–302. g) R. P. Yu, D. Hesk, N. Rivera, I. Pelczer, P. J. Chirik, *Nature* **2016**, *529*, 195–199. h) M. R. Friedfeld, H. Zhong, R. T. Ruck, M. Shevlin, P. J. Chirik, *Science* **2018**, *360*, 888–893.
- [6] G. A. Filonenko, R. van Putten, E. J. M. Hensen, E. A. Pidko, *Chem. Soc. Rev.* **2018**, *47*, 1459–1483.
- [7] F. Kallmeier, R. Kempe, *Angew. Chem. Int. Ed.* **2018**, *57*, 46–60.
- [8] a) R. V. Jagadeesh, A. E. Surkus, H. Junge, M. M. Pohl, J. Radnik, J. Rabeah, H. Huan, V. Schünemann, A. Brückner, M. Beller, *Science* **2013**, *342*, 1073–1076. b) F. A. Westerhaus, R. V. Jagadeesh, G. Weinhöfer, M. M. Pohl, J. Radnik, A. E. Surkus, J. Rabeah, K. Junge, H. Junge, M. Nielsen, A. Brückner, M. Beller, *Nat. Chem.* **2013**, *5*, 537–543.
- [9] R. V. Jagadeesh, K. Murugesan, A. S. Alshammari, H. Neumann, M. M. Pohl, J. Radnik, M. Beller, *Science* **2017**, *358*, 326–332.
- [10] G. Hahn, P. Kunnas, N. de Jonge and R. Kempe, *Nat. Catal.* **2019**, *2*, 71–77.

- [11] B. Zimmermann, J. Herwig, M. Beller, *Angew. Chem. Int. Ed.* **1999**, *38*, 2372–2375.
- [12] T. Prinz, B. Driessen-Hölscher, *Chem. Eur. J.* **1999**, *5*, 2069–2076.
- [13] T. Nagano, S. Kobayashi, *J. Am. Chem. Soc.* **2009**, *131*, 4200–4201.
- [14] K. Das, R. Shibuya, Y. Nakahara, N. Germain, T. Ohshima, K. Mashima, *Angew. Chem. Int. Ed.* **2012**, *51*, 150–154.
- [15] J. Schranck, A. Tilili, *ACS. Catal.* **2018**, *8*, 405–418.
- [16] B. Guo, Q. Zhang, G. Li, J. Yao, C. Hu. *Green Chem.* **2012**, *14*, 1880–1883.
- [17] K.-I. Fujita, S. Furukawa, N. Morishima, M. Shimizu, R. Yamaguchi, *ChemCatChem* **2018**, *10*, 1993–1997.
- [18] K. Murugesan, M. Beller, R. V. Jagadeesh, *Angew. Chem. Int. Ed.* **2019**, *131*, 5118–5122.
- [19] a) Z. Yuan, B. Liu, P. Zhou, Z. Zhang, Q. Chi, *J. Catal.* **2019**, *370*, 347–356.
b) Y. Zhang, H. Yang, Q. Chi, Z. Zhang, *ChemSusChem* **2019**, *12*, 1246–1255.
10.1002/cssc.201802459.
- [20] T. Stemmler, A. E. Surkus, M. M. Pohl, K. Junge, M. Beller, *ChemSusChem* **2014**, *7*, 3012–3016.
- [21] a) Y. Watanabe, M. Yamashita, T.-A. Mitsudo, M. Tanaka, Y. Takegami, *Tetrahedron Lett.* **1974**, *15*, 1879–1880. b) M. D. Bhor, M. J. Bhanushali, N. S. Nandurkar, B. M. Bhanage, *Tetrahedron Lett.* **2008**, *49*, 965–969. c) S. Enthaler, *ChemCatChem* **2010**, *2*, 1411–1415. d) S. Fleischer, S. Zhou, K. Junge, M. Beller, *Chem. Asian. J.* **2011**, *6*, 2240–2245. e) A. Pagnoux-Ozherelyeva, N. Pannetier, M. D. Mbaye, S. Gaillard, J. L. Renaud, *Angew. Chem. Int. Ed.* **2012**, *51*, 4976–4980. f) S. Moulin, H. Dentel, A. Pagnoux-Ozherelyeva, S. Gaillard, A. Poater, L. Cavallo, J. F. Lohier, J. L. Renaud, *Chem. Eur. J.* **2013**, *19*, 17881–17890. g) S. Fleischer, S. Zhou, S. Werkmeister, K. Junge, M. Beller, *Chem. Eur. J.* **2013**, *19*, 4997–5003. h) S. Zhou, S. Fleischer, H. Jiao, K. Junge, M. Beller, *Adv. Synth. Catal.* **2014**, *356*, 3451–3455. i) T. T. Thai, D. S. Mérel, A. Poater, S. Gaillard, J. L. Renaud, *Chem. Eur. J.* **2015**, *21*, 7066–7070.
- [22] a) S. Rösler, J. Obenauf, R. Kempe, *J. Am. Chem. Soc.* **2015**, *137*, 7998–8001. b) S. Rösler, M. Ertl, T. Irrgang, R. Kempe, *Angew. Chem. Int. Ed.* **2015**, *54*, 15046–15050. c) N. Deibl, R. Kempe, *J. Am. Chem. Soc.* **2016**, *138*, 10786–10789.
- [23] a) F. Kallmeier, T. Irrgang, T. Dietel, R. Kempe, *Angew. Chem. Int. Ed.* **2016**, *55*, 11806–11809. b) N. Deibl, R. Kempe, *Angew. Chem. Int. Ed.* **2017**, *56*, 1663–1666. c) F. Kallmeier, B. Dudziec, T. Irrgang, R. Kempe, *Angew. Chem. Int. Ed.* **2017**, *56*, 7261–7265. d) G. Zhang, T. Irrgang, T. Dietel, F. Kallmeier, R. Kempe, *Angew. Chem. Int. Ed.* **2018**, DOI: 10.1002/anie.201801573. e) F. Freitag, T. Irrgang, R. Kempe, *J. Am. Chem. Soc.* **2019**, *141*, 11677–11685. f) R. Fertig, T. Irrgang, F. Freitag, J. Zander, R. Kempe, *ACS Catal.* **2018**, *8*, 8525–8530.
- [24] D. Forberg, T. Schwob, M. Zaheer, M. Friedrich, N. M. Iyajima, R. Kempe, *Nat. Commun.* **2016**, *7*, 13201–13206.

- [25] D. Forberg, T. Schwob, R. Kempe, *Nat. Commun.* **2018**, *9*, 1751–1757.
- [26] a) T. Schwob, R. Kempe, *Angew. Chem. Int. Ed.* **2016**, *55*, 15175–15179. b) T. Schwob, M. Ade, R. Kempe, *ChemSusChem* **2019**, *12*, 3013–3017. c) C. Bäuml, R. Kempe, *Chem. Eur. J.* **2018**, *24*, 8989–8993.
- [27] a) Z. Ma, T. Song, Y. Yuan, Y. Yang, *Chem. Sci.* **2019**, *10*, 10283–10289. b) T. Song, Z. Ma, P. Ren, Y. Yuan, J. Xiao, Y. Yang, *ACS Catal.* **2020**, *10*, 4617–4629.
- [28] L. F. B. Ribeiro, O. Flores, P. Furtat, C. Gervais, R. Kempe, R. A. F. Machado and G. Motz, *J. Mater. Chem. A* **2017**, *5*, 720–729.

5.5 *Supporting Information*

5.5.1 General Considerations

All air- and moisture sensitive reactions were performed under dry argon or nitrogen atmosphere using standard Schlenk and glove box techniques. All dried solvents were obtained from a solvent purification system (activated alumina cartridges) or purchased from Acros. Deuterated solvents were dried via molecular sieves. All chemicals were acquired from commercial sources with purity over 95 % and used without further purification. The precursor SMP 10 was purchased from Starfire Systems, New York, USA.

Hydrogen chemisorption measurements were performed by using a ChemBET Pulsar TPR/TPD instrument from Quantachrome.

Pyrolysis and reduction were performed under nitrogen or forming gas (90/10) atmosphere in a high temperature furnace (EHA 12/450B200, Carbolite) or in a ChemBET Pulsar TPR/TPD instrument from Quantachrome.

Transmission electron microscopy (TEM) was carried out by using a Variant LEO 9220 (200 kV) and a JEOL JEM 2200FS (200 kV) device. For the sample preparation the ceramic was suspended in chloroform and sonicated for 5 min. For analysis a LC200-Cu and a CF200-Cu grid were used.

Pore characterizations were carried out via nitrogen sorption measurements using a Nova2000e (Quantachrome) device. The pore size distribution was computed via DFT calculations [calculation model: N₂ at -196.15 °C on carbon (slit/cylindrical pore, NLDFT equilibrium model)]. The specific surface area was calculated by using p/p_0 values from 0.05-0.31 (BET).

Powder X-ray diffractograms (PXRD) were detected by a Panalytical Empyrean (Cu K α radiation, 1.5405980 Å) instrument with a PIXcel1D-Medipix3 detector. The reference codes for comparison are 00-006-0696 for cubic iron and 01-075-1621 for graphite.

X-ray photoelectron spectroscopy (XPS) was performed using a PHI Versa Probe III instrument of Physical Electronics. As X-ray source a monochromatic Al K α with a spot size of 100 μ m (24.5 W) was used. The kinetic pass energy of the photoelectrons was determined with a hemispheric analyzer (45°) set to pass energy of 26 eV for high-resolution spectra. Fourier transform infrared (FTIR) spectroscopy measurements were performed with a Cary 630 FTIR spectrometer (Agilent Technologies) over a range from 2000 cm⁻¹ to 700 cm⁻¹.

Atom absorption spectroscopy (AAS) was performed with a Varian Spectr AA. 100 instrument.

Inductively coupled plasma optical emission spectrometry (ICP-OES) measurements were carried out on a Varian Vista-pro instrument. The digestion was performed in a Berghof Speed Wave 4 microwave. The carbon amount was determined by combustion analysis with a carbon analyzer Leco

C-200 using SiC as standard and the nitrogen and oxygen content by hot gas extraction with a Leco TC-436 N/O analyzer using TiN and WO₃ as standards. The silicon amount was calculated.

SEM (scanning electron microscopy) and EDX (energy dispersive X-ray spectroscopy) were performed by using a Zeiss Ultra plus microscope with an acceleration voltage of 15 kV.

NMR measurements were carried out with a Varian INOVA 300 and 400 (300 MHz for ¹H, 75 MHz for ¹³C; 400 MHz for ¹H, 100 MHz for ¹³C) at 296 K. Chemical shifts are reported in ppm relative to the residual solvent signal (DMSO-d₆: 7.26 ppm (1H), 77.16 ppm (¹³C); DMSO-d₆: 2.50 ppm (¹H), 39.51 ppm (¹³C)), coupling constants (J) are reported in Hz.

All tested reactions were determined via GC and GC-MS analysis. GC analyses were carried out on an Agilent 6850 GC system equipped with an Optima 17 column (30 m x 0.32 mm x 0.25 μm). GC-MS analyses were carried out on an Agilent 7890A GC system equipped with a HP-5MS column (30 m x 0.32 mm x 0.25 μm) and a 5975C inert MSD.

The hydrogenation experiments were carried out with Parr Instrument stainless steel autoclaves N-MT5 300 mL equipped with heating mantles and temperature controller.

5.5.2 Synthesis and characterization of the Fe/(N)SiC catalyst

Synthesis of the Fe salen complexes

The Fe salen complex I was synthesized in a two-step procedure.

First, the 6,6'-((1E,1'E) - ((1S,2S) - cyclohexane - 1,2 - diylbis (azanylylidene)) bis (methanylylidene)) bis (2-methoxyphenol) ligand was synthesized according to known literature procedure and characterized by NMR and IR and EA (calculated for C₂₂H₂₆N₂O₄: C, 69.09; H, 6.85; N, 7.32; found: C, 69.10; H, 7.04; N, 7.50).^[1a]

Next, complex I was synthesized according to a known literature procedure^[1b] and characterized by IR and EA (calculated for C₂₄H₂₇FeN₂O₆: C, 58.20; H, 5.49; N, 5.66; found: C, 57.17; H, 5.69; N, 5.41) and additionally characterized via X-ray single crystal structure analysis. 1.15 g (3 mmol) of the ligand was dissolved in 40 mL acetone while stirring. 521 mg (3mmol) Fe(II) acetate were added. Then, the solution was stirred under aerobic conditions for 24 h. The solvent was partially removed under reduced pressure and a purple precipitation was formed. The solution was filtered and washed with ethanol and acetone. Finally, a purple powder was obtained (1.5 g, 82 %).

(C₂₄H₂₇FeN₂O₆, 495.12 g/mol)

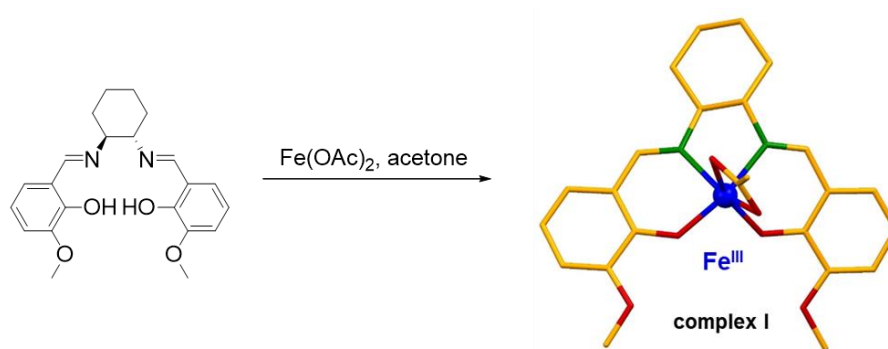
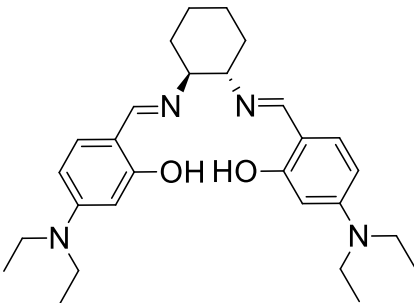
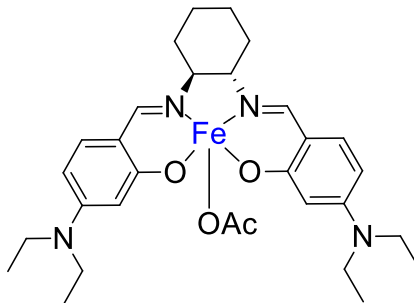
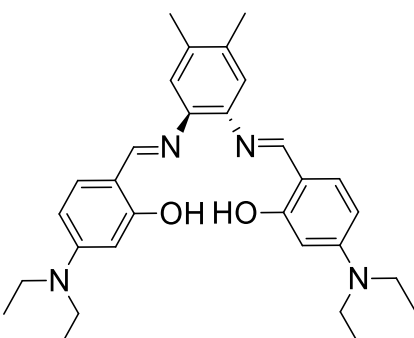
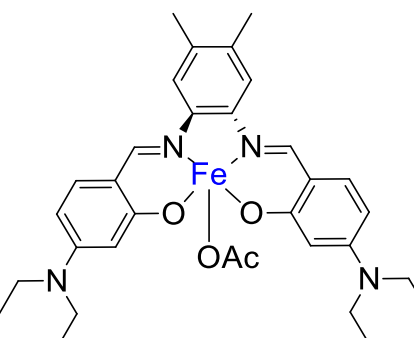
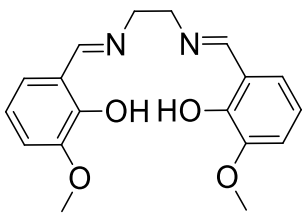
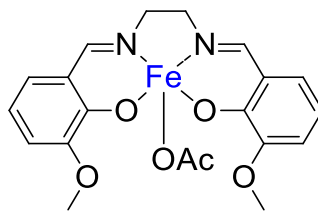
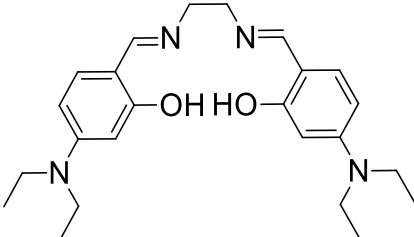
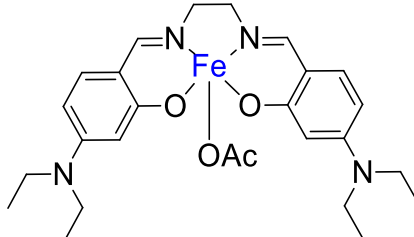
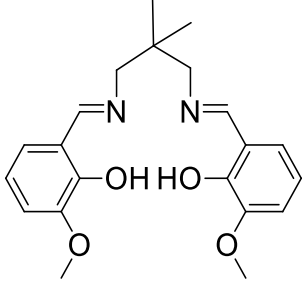
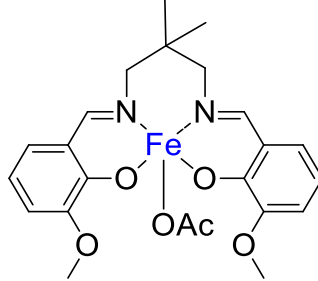


Figure S 1: Synthesis of the specific Fe complex I in the presence of air. The molecular structure of complex I was determined by X-ray single crystal structure analysis.

The synthesis of the complexes II-VI was accomplished in the same way as complex I. The ligands were characterized by EA and NMR analysis and the complexes by EA and IR analysis.

Table S 1: Synthesis of various Fe salen complexes.

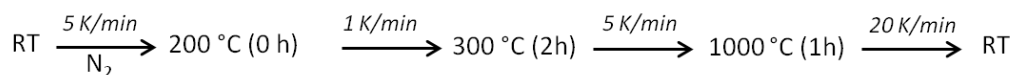
Ligand II	Complex II
	
6,6'-((1E,1'E)-((1S,2S)-cyclohexane-1,2-diylbis(azanylylidene))bis(methanylylidene))bis(3-(diethylamino)phenol) M: 464.32 g/mol (yellow-brown) C ₂₈ H ₄₀ N ₄ O ₂	M: 577.25 g/mol (brown-purple) C ₃₀ H ₄₁ FeN ₄ O ₄
EA: calc: C: 72.38; H: 8.68; N: 12.06 found: C: 71.99; H: 8.74; N: 11.84	EA: calc: C: 62.39; H: 7.16; N: 9.70 found: C: 61.98; H: 7.72; N: 9.85
Ligand III	Complex III
	
6,6'-((1E,1'E)-((4,5-dimethyl-1,2-phenylene)bis(azanylylidene))bis(methanylylidene))bis(3-(diethylamino)phenol) M: 486.30 g/mol (orange-brown)/C ₃₀ H ₃₈ N ₄ O ₂	M: 599.23 g/mol (purple) C ₃₂ H ₃₉ FeN ₄ O ₄
EA: calc: C: 74.04; H: 7.87; N: 11.51 found: C: 73.35; H: 8.15; N: 11.62	EA: calc: C: 64.11; H: 6.56; N: 9.35 found: C: 64.62; H: 7.26; N: 9.27
Ligand IV	Complex IV
	
6,6'-((1E,1'E)-(ethane-1,2-diylbis(azanylylidene))bis(methanylylidene))bis(2-methoxyphenol) M: 328.14 g/mol (yellow)/ C ₁₈ H ₂₀ N ₂ O ₄	M: 441.07 g/mol (purple) C ₂₀ H ₂₁ FeN ₂ O ₆

EA: calc: C: 65.84; H: 6.14; N: 8.53 found: C: 65.89; H: 6.09; N: 8.26	EA: calc: C: 54.44; H: 4.80; N: 6.35 found: C: 54.00; H: 4.87; N: 6.06
Ligand V	Complex V
	
6,6'-((1E,1'E)-(ethane-1,2-diylbis(azanylylidene))bis(methanylylidene))bis(3-(diethylamino)phenol) M: 410.27 g/mol (brown)// $C_{24}H_{34}N_4O_2$	M: 523.20 g/mol (dark purple) $C_{26}H_{35}FeN_4O_4$
EA: calc: C: 70.21; H: 8.35; N: 13.65 found: C: 69.63; H: 8.73; N: 13.61	EA: calc: C: 59.66; H: 6.74; N: 10.70 found: C: 59.46; H: 7.03; N: 10.94
Ligand VI	Complex VI
	
6,6'-((1E,1'E)-((2,2-dimethylpropane-1,3-diyl)bis(azanylylidene))bis(methanylylidene))bis(2-methoxyphenol) M: 370.19 g/mol (yellow)// $C_{21}H_{26}N_2O_4$	M: 483.12 g/mol (purple) $C_{23}H_{27}FeN_2O_6$
EA: calc: C: 68.09; H: 7.07; N: 7.56 found: C: 67.60; H: 7.14; N: 7.39	EA: calc: C: 57.16; H: 5.63; N: 5.80 found: C: 56.50; H: 5.62; N: 5.91

Synthesis of the support material

The (N)SiC material was prepared by modifying a known literature procedure.^[2]

0.200 g SMP-10 (StarPCS™), 0.988 mL (0.800 g, 15.08 mmol) acrylonitrile (AN) and 0.075 g (0.46 mmol) azobisisobutyronitrile (AIBN) were dissolved in 4 mL dimethylformamide (DMF). After polymerization and crosslinking at 75 °C, the solvent was removed under reduced pressure. The obtained greenbody was pyrolyzed at 1000 °C under nitrogen atmosphere.



The mass loss after pyrolysis was 45%. After ball milling for 20 minutes, 500 mg catalyst were washed by stirring in an aqueous solution of 6.7 mL NaOH ($c = 1 \text{ mol/l}$) and 5 mL MeOH at 80 °C for 20 h under aerobic conditions. Afterwards the material was washed neutral and dried.

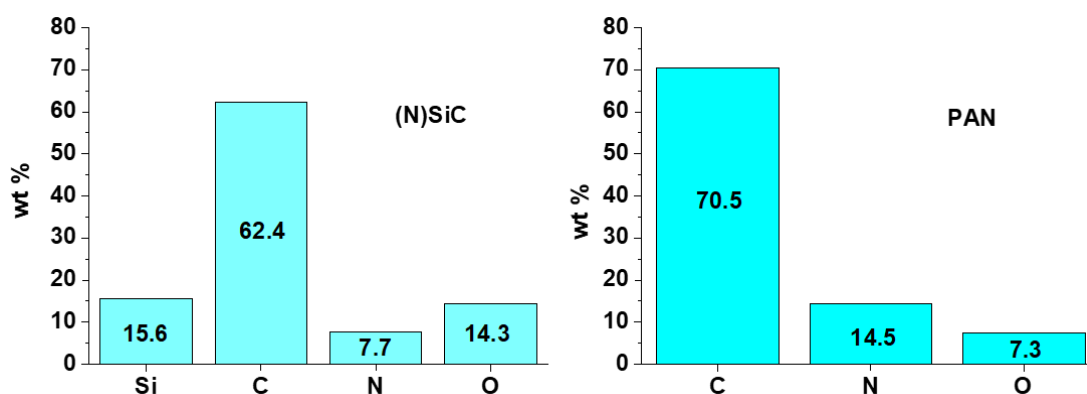
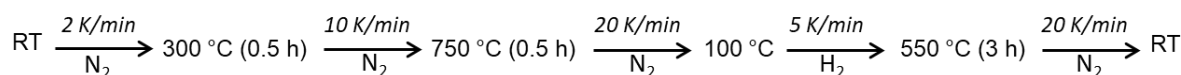


Figure S 2: Elemental analysis of the (N)SiC support and pyrolyzed polyacrylonitrile (PAN) as reference. As a result of the copolymerization of acrylonitrile and SiC, the nitrogen content is reduced. The high oxygen content is due to the polymerization in air atmosphere and the solvent DMF.

Catalyst synthesis

1.0 g (N)SiC were impregnated with 0.44 g **complex I** in 17 mL acetonitrile. After removal of the solvent, the sample was pyrolyzed under a nitrogen atmosphere at 750 °C followed by a treatment under a reductive atmosphere (N_2/H_2 90/10) at 550 °C.



Catalyst characterization**AAS analysis of the catalyst:**

Theoretical Fe content: 5.0 wt%

Measured Fe content: 4.0 wt%

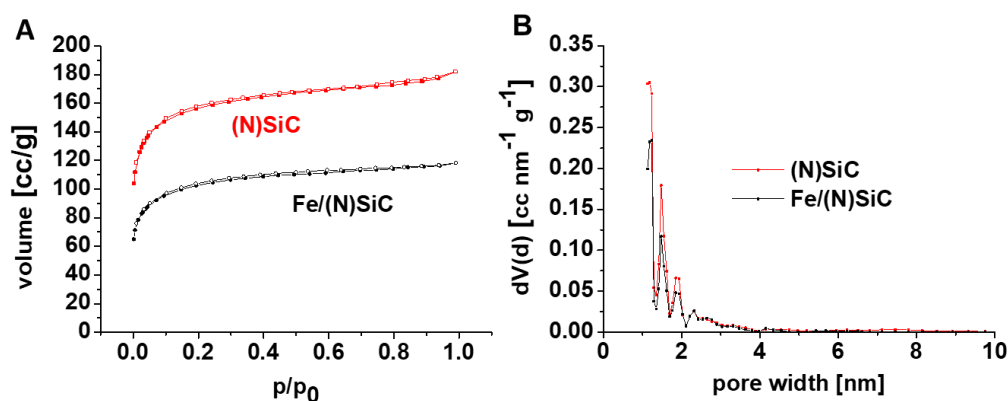


Figure S 3: Nitrogen physisorption measurements of the Fe catalyst and the (N)SiC support material. A: Isotherms of both materials. The course of the two isotherms indicates the presence of mainly micropores. A specific surface area of $485 \text{ m}^2\text{g}^{-1}$ [(N)SiC] and $415 \text{ m}^2\text{g}^{-1}$ (Fe catalyst) was calculated by the Brunauer-Emmett-Teller (BET) method. The lower surface area of the catalyst is due to the process of impregnation on the support material. B: The pore-size distributions show that micropores are responsible for the main part of the resulting surface areas [Calculation model: N_2 at 77 K on carbon (cylindr. pores, NLDFT equilibrium model)]. Both materials show a similar process in both isothermal and pore-size distributions.

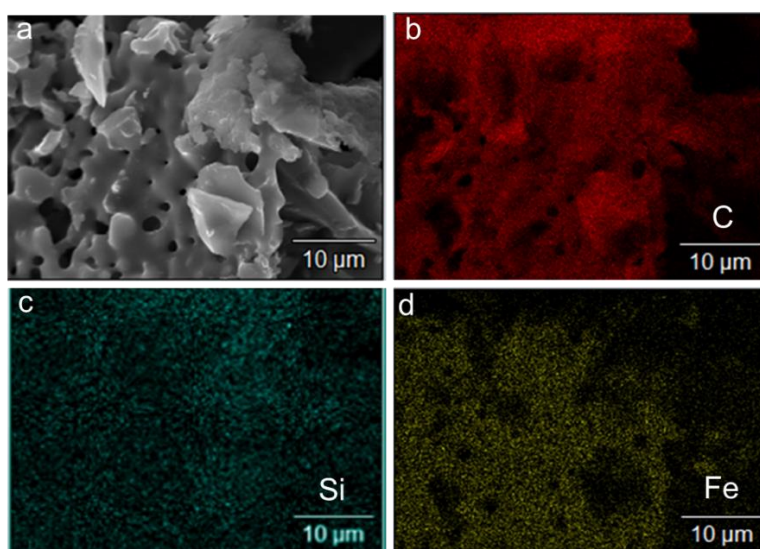


Figure S 4: Scanning electron microscopy (SEM, a) combined with energy-dispersive X-ray (EDX, b-c) element maps. The iron nanoparticles have a homogeneous distribution on the surface. In addition, the individual elements of the carrier material are also very evenly distributed.

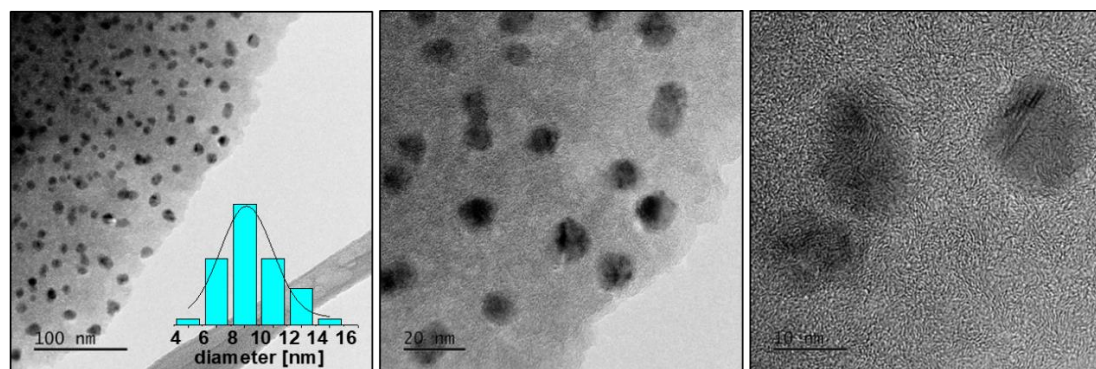


Figure S 5: Transmission electron microscopy (TEM) analysis of the Fe/(N)SiC catalyst surface. TEM analysis verifies a homogenous distribution of the Fe nanoparticles on the (N)SiC matrix. An average particle size of 10 nm could be determined.

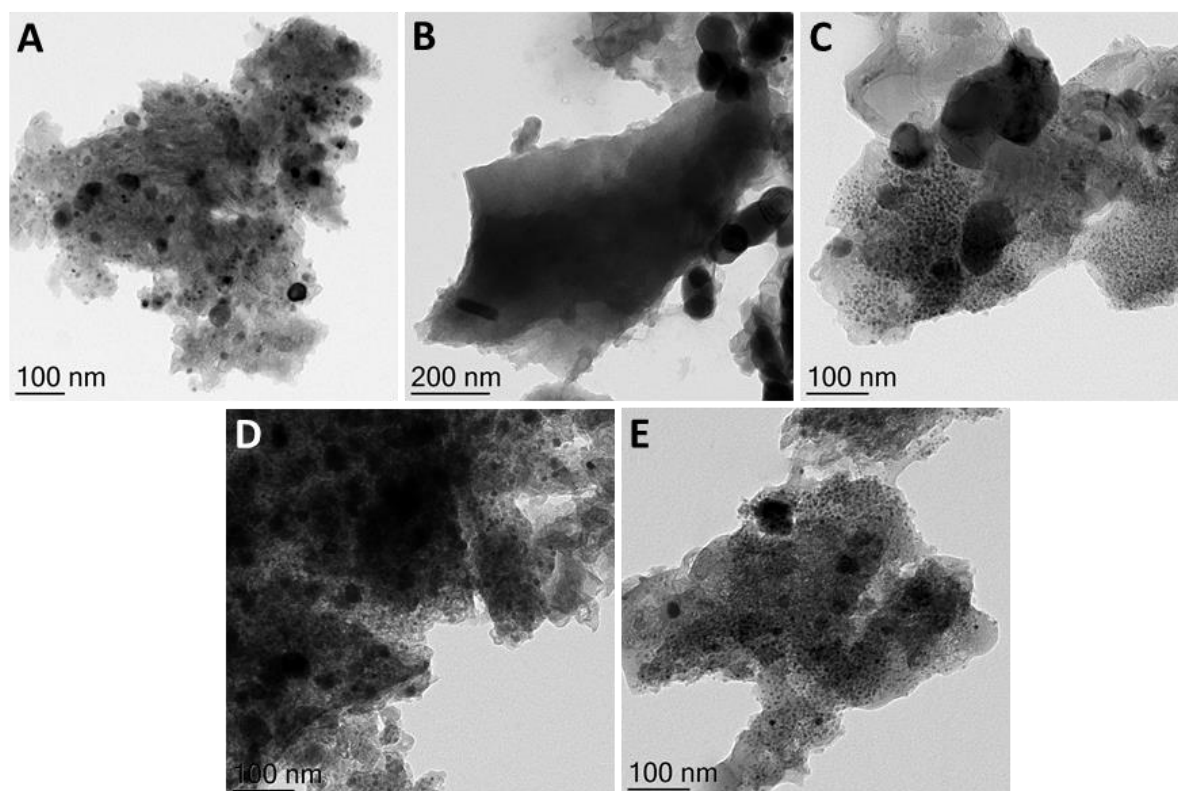


Figure S 6: TEM characterization of different catalysts used for the catalyst screening in the reductive amination of carbonyl compounds. Variation of the iron-salen complexes as metal source for the synthesis of various Fe/(N)SiC catalysts; A) Complex II; B) Complex III; C) Complex IV; D) Complex V; E) Complex VI.

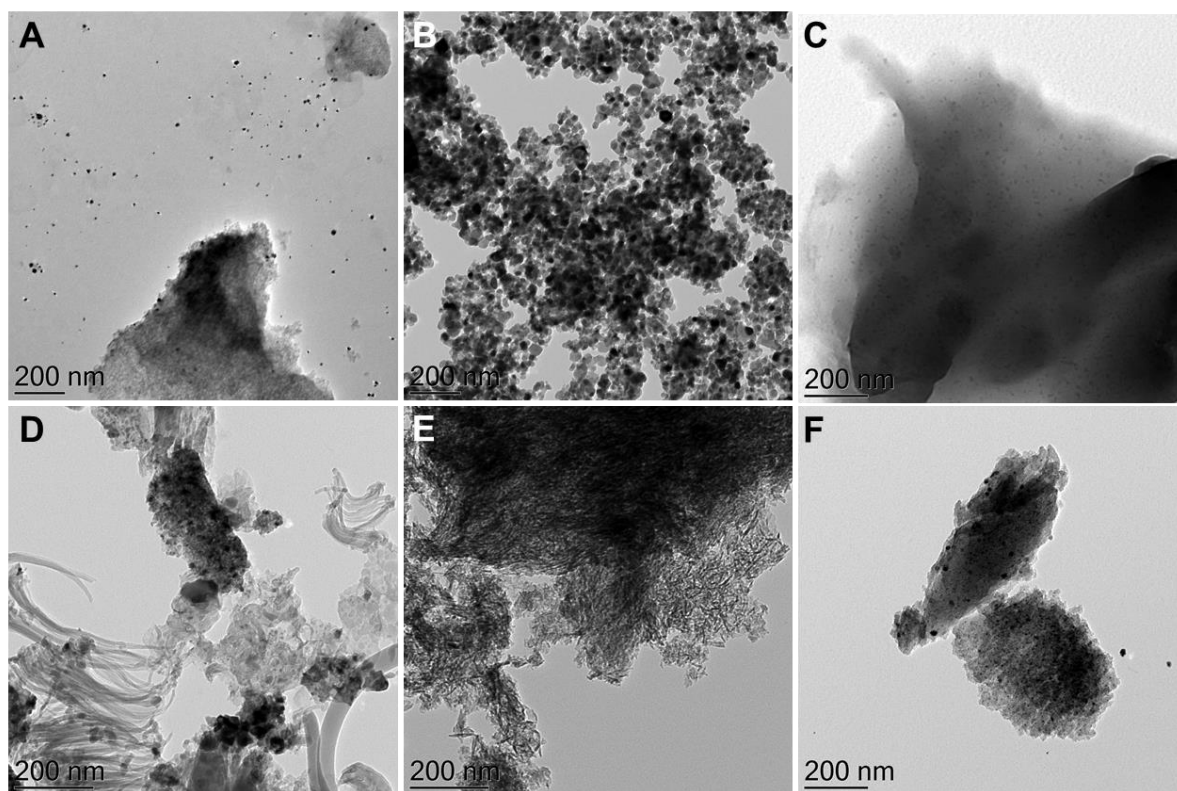


Figure S 7: TEM characterization of different catalysts used for the catalyst screening in the reductive amination of carbonyl compounds. Variation of the support material by using complex I as metal source; A) Fe/TiO₂; B) Fe/SiO₂; C) Fe/pyrolyzed PAN; D) Fe/CeO₂; E) Fe/Al₂O₃; F) Fe/active carbon.

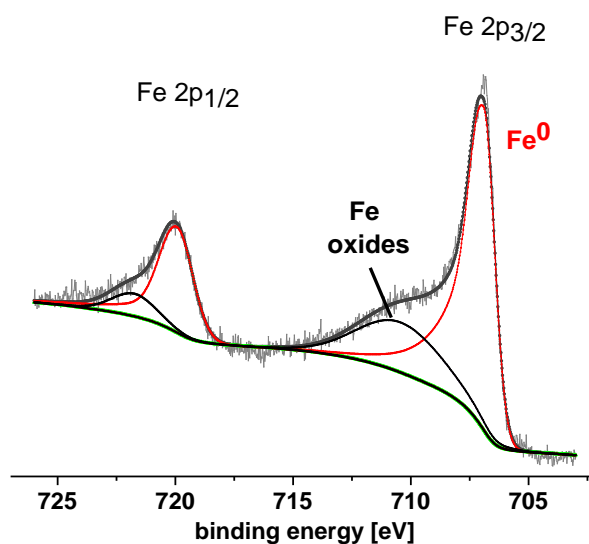


Figure S 8: XP spectrum of the catalyst. The Fe 2p_{3/2} signal can be divided in two signals with the binding energies of 707.0 and 711.0 eV. The presence of metallic Fe could be identified due to its sharp line shape and its binding energies of 707.0 eV. At higher binding energies small amounts of different oxides (e.g. FeO, Fe₂O₃) are found that cannot be distinguished in the analysis.

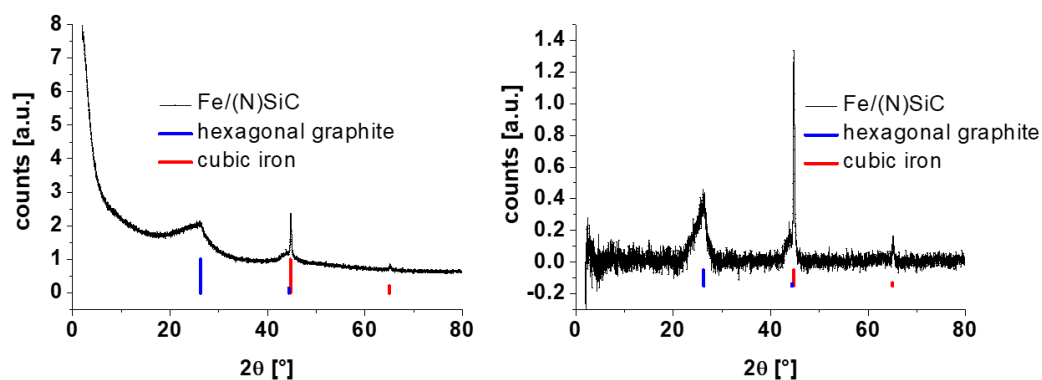


Figure S 9: Powder X-ray diffraction of the catalyst. The reflexes at the 2θ value of 44.67° and 65.02° can be assigned to the (110) and (200) reflexes of cubic iron (red). The reflexes at the 2θ value of 26.23° and 44.37° can be assigned to the (002) and (101) reflexes of hexagonal carbon (blue, graphite), what indicates a graphitic like structure what might be caused by the pyrolysis of polyacrylonitrile.

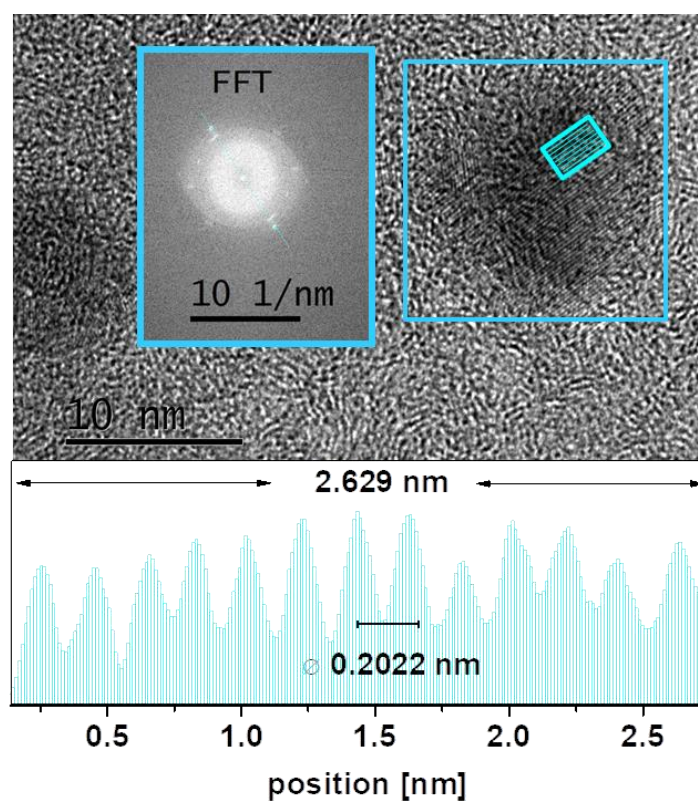
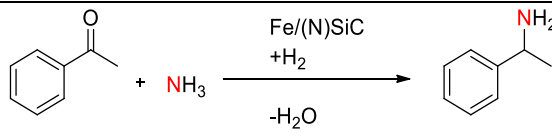


Figure S 10: HR-TEM analysis with focus on lattice spacing distances of the iron nanoparticles. Previous PXRD patterns showed matching reflections for cubic iron at $2\theta = 44.67^\circ$ with a lattice spacing of 0.2027 (110) nm. The FFT (Fast Fourier Transform) of the investigated nanoparticle, resulted in an averaged lattice plane distance of 0.2022 nm, which is in good agreement with the literature values.

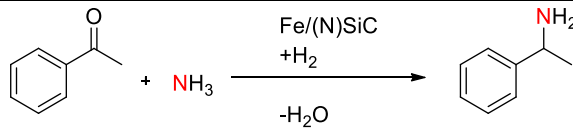
5.5.3 Catalytic studies

Table S 2: Solvent screening for the reductive amination of acetophenone.

	
Solvent [2.0 mL]	Yield [%]
H₂O	65
Methanol	40
Ethanol	33
Toluene	15
Dioxane	32
Tetrahydrofuran	27

Reaction conditions: 10 mol% Fe (70 mg Fe/(N)SiC, 4.0 wt% Fe, 0.05 mmol Fe, 2.8 mg Fe), 0.5 mmol acetophenone, 140 °C, 20 h 6.5 MPa H₂, 1.5 mL aq. NH₃-25%. Yields were determined by GC using *n*-dodecane as an internal standard.

Table S 3: Screening of the NH₃ amount for the reductive amination of acetophenone.

			
H ₂ O	aq. NH ₃ -25 %	Volume	Yield
[mL]	[mL]	[mL]	[%]
3.5	0.5 (6.7 mmol)	4.0	32
3.0	1.0 (13.4 mmol)	4.0	35
2.5	1.5 (20.0 mmol)	4.0	36
2.0	2.0 (26.7 mmol)	4.0	40
1.0	3.0 (40.1 mmol)	4.0	50
0	3.0 (40.1 mmol)	3.0	56
0	3.5 (46.7 mmol)	3.5	60
0	4.0 (53.4 mmol)	4.0	57
0	5.0 (66.8 mmol)	5.0	53

Reaction conditions: 10 mol% Fe (70 mg Fe/(N)SiC, 4.0 wt% Fe, 0.05 mmol Fe, 2.8 mg Fe), 0.5 mmol acetophenone, 130 °C, 20 h, 6.5 MPa H₂. Yields were determined by GC using *n*-dodecane as an internal standard.

Table S 4: Screening of the NH₃ amount for the reductive amination of benzaldehyde.

<div style="display: flex; justify-content: space-around; align-items: center;"> <div style="text-align: center;">a</div> <div style="text-align: center;">b</div> <div style="text-align: center;">c</div> </div>				
aq. NH ₃ -25 % [mL]	Volume [mL]	Yield ^[a] [%]		
		a	b	c
2.0 (26.7 mmol)	2.0	45	40	13
3.0 (40.1 mmol)	3.0	55	30	14
3.5 (46.7 mmol)	3.5	63	18	18
4.0 (53.4 mmol)	4.0	64	16	19
5.0 (66.8 mmol)	5.0	63	15	21

Reaction conditions: 8.6 mol% Fe (60 mg Fe/(N)SiC, 4.0 wt% Fe, 0.043 mmol Fe, 2.4 mg Fe), 0.5 mmol benzaldehyde, 125 °C, 20 h, 6.5 MPa H₂. Yields were determined by GC using *n*-dodecane as an internal standard.

Table S 5: Reductive amination of acetophenone / Optimization of the reaction parameters.

Entry	Catalyst loading [mol %]	Temperature [°C]	Pressure [MPa]	Time [h]	GC-yield [%]
1	8.6	120	6.5	20	32
2	10	120	6.5	20	39
3	8.6	130	6.5	20	46
4	10	130	6.5	20	60
5	8.6	140	5.0	20	54
6	10	140	5.0	20	76
7	8.6	140	6.5	20	72
8	10	140	6.5	2	11
9	10	140	6.5	4	27
10	10	140	6.5	16	87
11	10	140	6.5	20	99

Reaction conditions: 0.5 mmol acetophenone, 3.5 mL aq. NH₃-25%. Yields were determined by GC using *n*-dodecane as an internal standard.

Up-scaling of the reaction

In order to prove the usefulness of the catalyst, an up-scaling reaction to gram scale was carried out. Acetophenone was chosen as representative carbonyl substrate for this reaction. The optimized reaction conditions were scaled up for 10 mmol substrate (1.4 g Fe/(N)SiC, 10 mmol acetophenone, 140 °C, 20 h, 6.5 MPa H₂, 70 mL aq. NH₃-25%). The reaction was carried out in a 250 mL high pressure autoclave (Parr Instruments) in the same way as the 0.5 mmol reactions.

Isolated yield of 1-phenylethanaminium chloride: 1.544 g, 98 %

Recycling studies

The recycling studies were accomplished with the optimized reaction conditions. Therefore, the Fe/(N)SiC catalyst was separated after each run via centrifugation, washed with ethyl acetate, dried under vacuum and used again without any reactivation. For determining the initial rate of each run, a recycling study with a run time of 4 h and the same reaction parameters were accomplished. The yields of 1-phenylethylamine were determined via GC using *n*-dodecane as an internal standard.

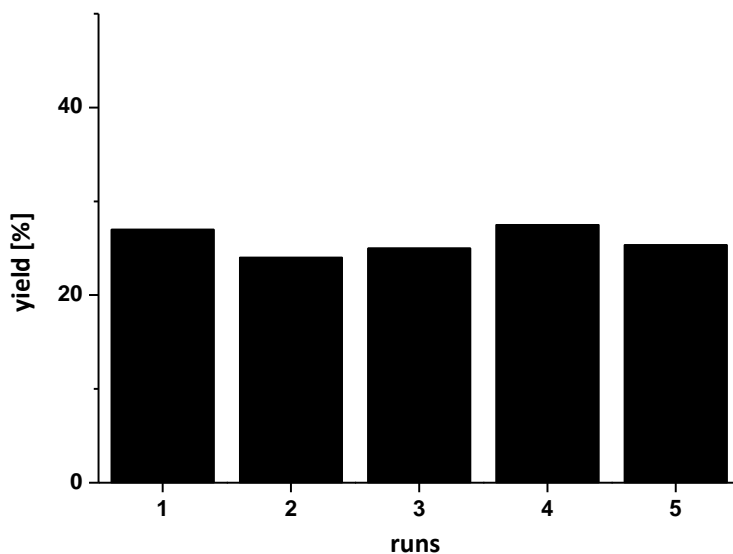


Figure S 11: Recycling study of the Fe/(N)SiC catalyst over 5 consecutive runs (4 h reaction time), for calculating the initial rate. Reaction conditions: 10 mol% Fe (70 mg Fe/(N)SiC with 4.0 wt% Fe loading, 0.05 mmol Fe, 2.8 mg Fe), 0.5 mmol acetophenone, 140 °C, 4 h, 6.5 MPa H₂, 3.5 mL aq. NH₃-25%. Yields were determined by GC using *n*-dodecane as an internal standard.

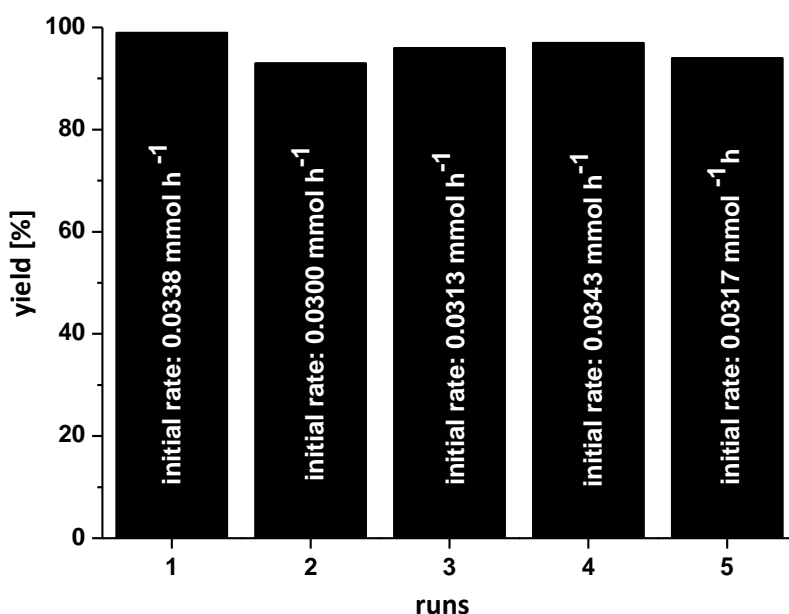


Figure S 12: Recycling study of the Fe/(N)SiC catalyst over 5 consecutive runs (conditions for 99 % yield), including initial rates. Reaction conditions: 10 mol% Fe (70 mg Fe/(N)SiC with 4.0 wt% Fe loading, 0.05 mmol Fe, 2.8 mg Fe), 0.5 mmol acetophenone, 140 °C, 20 h, 6.5 MPa H₂, 3.5 mL aq. NH₃-25%. Yields were determined by GC using *n*-dodecane as an internal standard.

General catalytic procedures

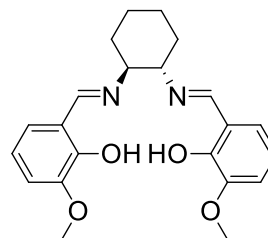
Reductive amination of aldehydes and ketones

A magnetic stirring bar, 0.5 mmol substrate, 3.5 mL aq. NH₃-25% and 10 mol % Fe catalyst (2.8 mg Fe, 0.05 mmol, 70 mg) were filled in a 5 mL reaction vial. The vial was placed in a high-pressure autoclave (Parr Instruments) and the autoclave was flushed three times with 2.0 MPa of hydrogen. The autoclave was pressured with 6.5 MPa of hydrogen and the reaction was stirred for 20 h at 130 °C for aldehydes and 140 °C for ketones. The autoclave was cooled to room temperature and the hydrogen pressure was released. Then, the solution was extracted with Methyl *tert*-butyl ether, dried over Na₂SO₄, filtered and the solvent was removed under reduced pressure. In case of primary amines based on aldehydes, column chromatography (silica, ethyl acetate-methanol mixture as eluent) was executed for purification and for isolating the primary amine. All amines were converted into their corresponding hydrochloride salts via HCl in Ether (0.7 mmol HCl) for further purification. The solvent was removed under reduced pressure and the salt was washed with ethyl acetate again twice. The obtained hydrochloride salts were further analyzed by ¹H and ¹³C spectroscopy.

5.5.4 Characterization of isolated products

Ligand I:

6,6'-((1E,1'E)-((1S,2S)-cyclohexane-1,2-diylbis(azanylylidene))bis(methanylylidene))bis(2-methoxyphenol)
 $[C_{22}H_{26}N_2O_4]$ 382.19 g/mol (M)

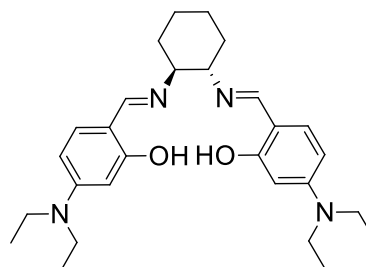


1H NMR (400 MHz, $CDCl_3$, 296 K): δ = 13.85 (s, 2H), 8.24 (s, 2H), 6.85-6.83 (m, 2H), 6.79-6.77 (m, 2H), 6.73-6.69 (m, 2H), 3.85 (s, 6H), 3.32-3.29 (m, 2H), 1.95-1.85 (m, 4H), 1.74-1.66 (m, 2H), 1.52-1.44 (m, 2H) ppm.

^{13}C NMR (100 MHz, $CDCl_3$, 296 K): δ = 164.63, 151.42, 148.10, 123.02, 118.25, 117.76, 113.68, 72.28, 55.89, 32.90, 23.92 ppm.

Ligand II:

6,6'-((1E,1'E)-((1S,2S)-cyclohexane-1,2-diylbis(azanylylidene))bis(methanylylidene))bis(3-(diethylamino)phenol)
 $[C_{28}H_{40}N_4O_2]$ 464.32 g/mol (M)

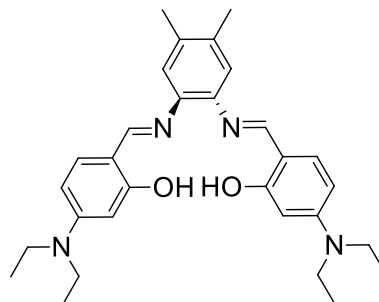


1H NMR (400 MHz, $CDCl_3$, 296 K): δ = 7.94 (s, 2H), 6.90-6.88 (m, 2H), 6.08-6.03 (m, 4H), 3.35-3.30 (q, J = 7.03 Hz, 8H), 3.17-3.14 (m, 2H), 1.96-1.92 (m, 2H), 1.84-1.82 (m, 2H), 1.65-1.62 (m, 2H), 1.44-1.39 (m, 2H), 1.16-1.13 (t, J = 7.03 Hz, 12H) ppm.

^{13}C NMR (100 MHz, $CDCl_3$, 296 K): δ = 166.09, 162.63, 151.37, 108.16, 102.84, 98.06, 70.66, 44.38, 33.19, 24.28, 12.66 ppm.

Ligand III:

6,6'-((1E,1'E)-((4,5-dimethyl-1,2-phenylene)bis(azanylylidene))
bis(methanylylidene))bis(3-(diethylamino)phenol)
[C₃₀H₃₈N₄O₂] 486.30 g/mol (M)

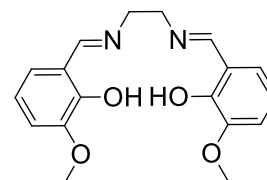


¹H NMR (400 MHz, CDCl₃, 296 K): δ = 8.41 (s, 2H), 7.14-7.12 (m, 2H), 6.98 (s, 2H) 6.24-6.20 (m, 4H) 3.41-3.36 (q, J=7.03 Hz, 8H), 2.30 (s, 6H), 1.21-1.18 (t, J=7.03 Hz, 12H) ppm.

¹³C NMR (100 MHz, CDCl₃, 296 K): δ = 164.77, 159.89, 151.69, 139.57, 134.45, 133.54, 120.17, 109.51, 103.47, 98.21, 44.52, 19.47, 12.72 ppm.

Ligand IV:

6,6'-((1E,1'E)-(ethane-1,2-
diylbis(azanylylidene))bis(methanylylidene))bis(2-methoxyphenol)
[C₁₈H₂₀N₂O₄] 328.14 g/mol (M)

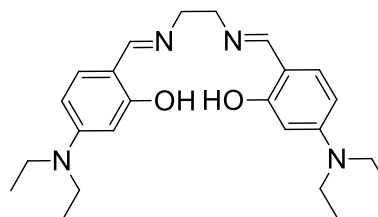


¹H NMR (400 MHz, CDCl₃, 296 K): δ = 13.55 (s, 2H), 8.32 (s, 2H), 6.90-6.75 (m, 6H), 3.94 (s, 4H), 3.88 (s, 6H) ppm.

¹³C NMR (100 MHz, CDCl₃, 296 K): δ = 166.57, 151.34, 148.19, 123.07, 118.32, 117.96, 113.96, 59.37, 55.94 ppm.

Ligand V:

6,6'-((1E,1'E)-(ethane-1,2-
diylbis(azanylylidene))bis(methanylylidene))bis(3-
(diethylamino)phenol)
[C₂₄H₃₄N₄O₂] 410.27 g/mol (M)

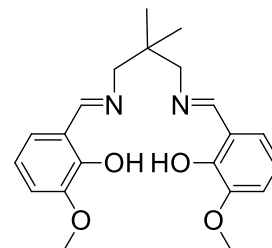


¹H NMR (400 MHz, CDCl₃, 296 K): δ = 8.02 (s, 2H), 6.98-6.95 (m, 2H), 6.14-6.09 (m, 4H) 3.75 (s, 4H), 3.38-3.33 (q, J=7.03 Hz, 6H), 1.19-1.15 (t, J=7.03 Hz, 12H) ppm.

¹³C NMR (100 MHz, CDCl₃, 296 K): δ = 165.83, 164.27, 151.48, 132.95, 108.23, 102.99, 98.08, 58.09, 44.42, 12.68 ppm.

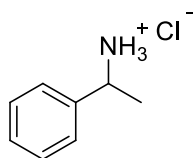
Ligand VI:

6,6'-((1E,1'E)-((2,2-dimethylpropane-1,3-diyl)bis(azanylylidene))bis(methanylylidene))bis(2-methoxyphenol)
 [C₂₁H₂₆N₂O₄] 370.19 g/mol (M)



¹H NMR (400 MHz, CDCl₃, 296 K): δ = 8.32 (s, 2H), 6.94-6.87 (m, 4H), 6.82-6.78 (m, 2H), 3.91 (s, 6H), 3.49 (s, 4H), 1.07 (s, 6H) ppm.

¹³C NMR (100 MHz, CDCl₃, 296 K): δ = 165.72, 152.00, 148.39, 122.84, 118.29, 117.81, 113.70, 67.19, 55.93, 36.08, 24.16 ppm.

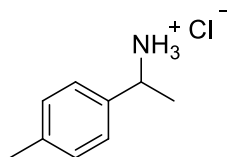
1:

1-Phenylethanaminium chloride

[C₈H₁₂ClN] 157.64 g/mol (M)

¹H NMR (300 MHz, DMSO-d₆, 296 K): δ = 8.78 (s, 3H), 7.57-7.55 (d, J = 7.03 Hz, 2H), 7.41-7.33 (m, 3H), 4.38-4.32 (q, J = 6.44 Hz, 1H), 1.54-1.51 (d, J = 6.44 Hz, 3H) ppm.

¹³C NMR (75 MHz, DMSO-d₆, 296 K): δ = 139.54, 128.63, 128.28, 126.92, 50.10, 20.93 ppm.

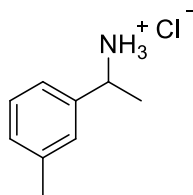
2:

1-(p-Tolyl)ethanaminium chloride

[C₉H₁₄ClN] 171.67g/mol (M)

¹H NMR (300 MHz, DMSO-d₆, 296 K): δ = 8.68 (s, 3H), 7.43-7.41 (d, J = 8.2 Hz, 2H), 7.21-7.19 (d, J = 7.81 Hz, 2H), 4.32-4.29 (m, 1H), 2.29 (s, 3H), 1.51-1.49 (d, J = 6.64 Hz, 3H) ppm.

¹³C NMR (75 MHz, DMSO-d₆, 296 K): δ = 137.95, 136.92, 129.49, 127.20, 50.16, 21.22, 21.10 ppm.

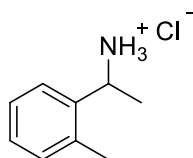
3:

1-(m-Tolyl)ethanaminium chloride

[C₉H₁₄ClN] 171.67g/mol (M)

¹H NMR (300 MHz, DMSO-d₆, 296 K): δ = 8.75 (s, 3H), 7.36-7.16 (m, 4H), 4.30 (m, 1H), 2.30 (s, 3H), 1.51 (m, 3H) ppm.

¹³C NMR (75 MHz, DMSO-d₆, 296 K): δ = 139.49, 137.74, 128.82, 128.55, 127.52, 123.92, 50.09, 21.07, 20.94 ppm.

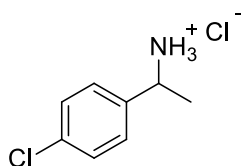
4:

1-(o-Tolyl)ethanaminium chloride

[C₉H₁₄ClN] 171.67g/mol (M)

¹H NMR (300 MHz, DMSO-d₆, 296 K): δ = 8.67 (s, 3H), 7.64-7.22 (m, 4H), 4.50 (m, 1H), 2.34 (s, 3H), 1.49-1.48 (d, J = 6.25 Hz, 3H) ppm.

¹³C NMR (75 MHz, DMSO-d₆, 296 K): δ = 137.87, 135.04, 130.49, 128.01, 126.47, 125.45, 46.16, 20.37, 18.80 ppm.

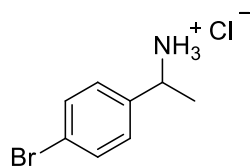
5:

1-(4-Chlorophenyl)ethanaminium chloride

[C₈H₁₁Cl₂N] 192.02 g/mol (M)

¹H NMR (300 MHz, DMSO-d₆, 296 K): δ = 8.70 (s, 3H), 7.58-7.47 (m, 4H), 4.38-4.32 (m, 1H), 1.51 (m, 3H) ppm.

¹³C NMR (75 MHz, DMSO-d₆, 296 K): δ = 138.48, 132.91, 129.00, 128.57, 49.37, 20.68 ppm.

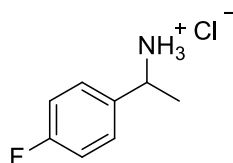
6:

1-(4-Bromophenyl)ethanaminium chloride

[C₈H₁₁BrClN] 236.54 g/mol (M)

¹H NMR (300 MHz, DMSO-d₆, 296 K): δ = 8.63 (s, 3H), 7.64-7.62(m, 2H), 7.51-7.48 (m, 2H), 4.39 (m, 1H), 1.50-1.49 (d, J = 6.63 Hz, 3H) ppm.

¹³C NMR (75 MHz, DMSO-d₆, 296 K): δ = 138.78, 131.56, 129.21, 121.57, 49.36, 20.57 ppm.

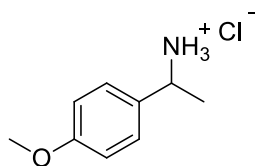
7:

1-(4-Fluorophenyl)ethanaminium chloride

[C₈H₁₁ClFN] 175.63 g/mol (M)

¹H NMR (300 MHz, DMSO-d₆, 296 K): δ = 8.75 (s, 3H), 7.64-7.60 (m, 2H), 7.27-7.21 (m, 2H), 4.43-4.36 (q, J = 6.44 Hz, 1H), 1.52-1.50 (d, J = 6.44 Hz, 3H) ppm.

¹³C NMR (75 MHz, DMSO-d₆, 296 K): δ = 163.51, 160.28, 135.74, 129.31, 129.20, 115.54, 115.25, 49.34, 20.79 ppm.

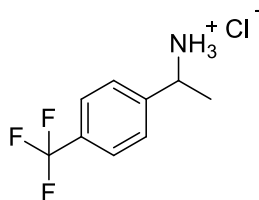
8:

1-(4-Methoxyphenyl)ethanaminium chloride

[C₉H₁₄ClNO] 187.67 g/mol (M)

¹H NMR (300 MHz, DMSO-d₆, 296 K): δ = 8.54 (s, 3H), 7.47-7.44 (m, 2H), 6.97-6.94 (m, 2H), 4.31-4.29 (m, 1H), 3.75 (s, 3H), 1.52-1.50 (d, J = 6.44 Hz, 3H) ppm.

¹³C NMR (75 MHz, DMSO-d₆, 296 K): δ = 159.26, 131.36, 128.33, 114.00, 55.26, 49.53, 20.76 ppm.

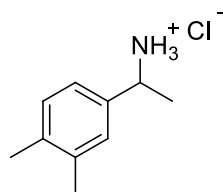
9:

1-(4-(Trifluoromethyl)phenyl)ethanaminium chloride

[C₉H₁₁ClF₃N] 225.64 g/mol (M)

¹H NMR (300 MHz, DMSO-d₆, 296 K): δ = 8.75 (s, 3H), 7.82-7.76 (m, 4H), 4.53-4.48 (m, 1H), 3.75 (s, 3H), 1.54-1.53 (d, J = 7.03 Hz, 3H) ppm.

¹³C NMR (75 MHz, DMSO-d₆, 296 K): δ = 144.00, 127.84, 125.60, 125.57, 125.46, 49.52, 20.62 ppm.

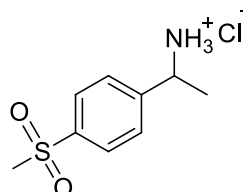
10:

1-(3,4-Dimethylphenyl)ethanaminium chloride

[C₁₀H₁₆ClN] 185.69 g/mol (M)

¹H NMR (300 MHz, DMSO-d₆, 296 K): δ = 7.43 (s, 3H), 7.23-7.12 (m, 3H), 4.23-4.16 (m, 1H), 2.22-2.20 (d, J = 4.69 Hz, 6H), 1.43-1.41 (d, J = 7.03 Hz, 3H) ppm.

¹³C NMR (75 MHz, DMSO-d₆, 296 K): δ = 136.81, 136.40, 136.32, 129.64, 127.95, 124.13, 49.81, 20.82, 19.49, 19.08 ppm.

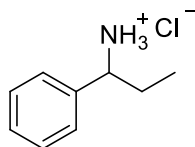
11:

1-(4-(Methylsulfonyl)phenyl)ethanaminium chloride

[C₉H₁₄ClNO₂S] 235.73 g/mol (M)

¹H NMR (300 MHz, DMSO-d₆, 296 K): δ = 8.97 (s, 3H), 7.98-7.95 (d, J = 7.61 Hz, 2H), 7.87-7.84 (m, J = 7.61 Hz, 2H), 4.53-4.49 (m, 1H), 3.23 (s, 3H), 1.56-1.54 (d, J = 7.03 Hz, 3H) ppm.

¹³C NMR (75 MHz, DMSO-d₆, 296 K): δ = 145.19, 140.61, 128.05, 127.26, 49.58, 43.42, 20.74 ppm.

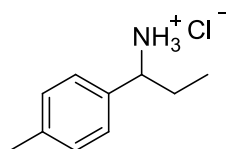
12:

1-Phenylpropan-1-aminium chloride

[C₉H₁₄ClN] 171.67 g/mol (M)

¹H NMR (300 MHz, DMSO-d₆, 296 K): δ = 8.70 (s, 3H), 7.53-7.51 (m, 2H), 7.44-7.38 (m, 3H), 4.11-4.06 (m, 1H), 2.05-1.98 (m, 1H), 1.86-1.76 (m, 1H), 0.76-0.71 (t, 3H) ppm.

¹³C NMR (75 MHz, DMSO-d₆, 296 K): δ = 137.80, 128.65, 128.44, 127.55, 55.87, 27.52, 10.05 ppm.

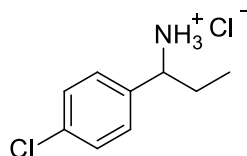
13:

1-(p-Tolyl)propan-1-aminium chloride

[C₁₀H₁₆ClN] 185.69 g/mol (M)

¹H NMR (400 MHz, DMSO-d₆, 296 K): δ = 8.68 (s, 3H), 7.40-7.38 (d, J = 8.2 Hz, 2H), 7.21-7.19 (d, J = 7.81 Hz, 2H), 4.02 (m, 1H), 2.29 (s, 3H), 2.05-2.00 (m, 1H), 1.81-1.77 (m, 1H), 0.74-0.70 (t, J = 7.42 Hz, 3H) ppm.

¹³C NMR (100 MHz, DMSO-d₆, 296 K): δ = 137.66, 134.75, 129.11, 127.48, 55.63, 27.42, 20.73, 10.05 ppm.

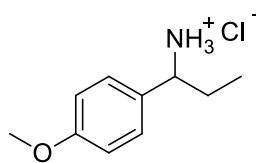
14:

1-(4-Chlorophenyl)propan-1-aminium chloride

[C₉H₁₃Cl₂N] 206.11 g/mol (M)

¹H NMR (400 MHz, DMSO-d₆, 296 K): δ = 8.80 (s, 3H), 7.58-7.56 (d, J = 8.59 Hz, 2H), 7.48-7.46 (d, J = 8.2 Hz, 2H), 4.13 (m, 1H), 2.06-2.00 (m, 1H), 1.82-1.78 (m, 1H), 0.74-0.70 (t, J = 7.42 Hz, 3H) ppm.

¹³C NMR (100 MHz, DMSO-d₆, 296 K): δ = 136.80, 133.03, 129.63, 128.58, 55.12, 27.35, 9.98 ppm.

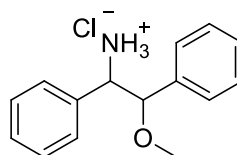
15:

1-(4-Methoxyphenyl)propan-1-aminium chloride

[C₁₀H₁₆ClNO] 201.69 g/mol (M)

¹H NMR (400 MHz, DMSO-d₆, 296 K): δ = 8.60 (s, 3H), 7.40-7.38 (d, J = 8.59 Hz, 2H), 6.92-6.90 (d, J = 8.2 Hz, 2H), 3.96 (m, 1H), 3.70 (s, 3H), 2.00-1.93 (m, 1H), 1.79-1.70 (m, 1H), 0.68-0.64 (t, J = 7.42 Hz, 3H) ppm.

¹³C NMR (100 MHz, DMSO-d₆, 296 K): δ = 159.20, 129.60, 128.92, 113.93, 55.38, 55.17, 27.39, 10.10 ppm.

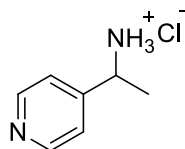
16:

2-Methoxy-1,2-diphenylethanaminium chloride

[C₁₅H₁₈ClNO] 263.76 g/mol (M)

¹H NMR (300 MHz, DMSO-d₆, 296 K): δ = 8.96 (s, 3H), 7.49-7.45 (m, 1H), 7.31-7.16 (m, 7H), 7.09-7.01 (m, 2H), 5.04-5.03 (d, J = 4.1 Hz, 0.8 H), 4.73-4.70 (d, J = 10.5 Hz, 0.2H), 4.49-4.48 (d, J = 4.7 Hz, 0.2H), 4.45-4.43 (d, J = 4.1 Hz, 0.8 H), 3.24-3.22 (d, J = 5.2 Hz, 3H) ppm.

¹³C NMR (75 MHz, DMSO-d₆, 296 K): δ = 137.13, 136.69, 133.39, 129.23, 128.98, 128.56, 128.39, 128.24, 128.13, 127.92, 127.67, 126.83, 84.14, 82.17, 59.28, 58.84, 57.04, 55.88 ppm.

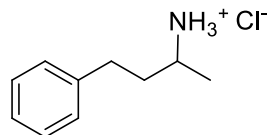
17:

1-(Pyridin-4-yl)ethanaminium chloride

[C₇H₁₁ClN₂] 158.63 g/mol (M)

¹H NMR (300 MHz, DMSO-d₆, 296 K): δ = 9.21 (s, 3H), 8.97-8.95 (m, 2H), 8.19-8.17 (m, 2H), 4.71-4.68 (m, 1H), 1.58-1.56 (d, J = 7.03 Hz, 3H) ppm.

¹³C NMR (75 MHz, DMSO-d₆, 296 K): δ = 156.77, 143.33, 124.73, 49.06, 20.15 ppm.

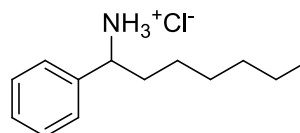
18:

4-Phenylbutan-2-aminium chloride

[C₁₀H₁₆ClN] 185.69 g/mol (M)

¹H NMR (300 MHz, DMSO-d₆, 296 K): δ = 8.29 (s, 3H), 7.30-7.16 (m, 5H), 3.11-3.10 (m, 1H), 2.68-2.62 (m, 2H), 1.96-1.92 (m, 1H), 1.76-1.73 (m, 1H), 1.25-1.23 (d, J = 6.24 Hz, 3H) ppm.

¹³C NMR (75 MHz, DMSO-d₆, 296 K): δ = 141.03, 128.40, 128.22, 125.96, 46.38, 35.84, 30.85, 18.01 ppm.

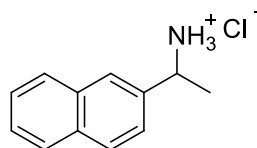
19:

1-Phenylheptan-1-aminium chloride

[C₁₃H₂₂ClN] 227.77g/mol (M)

¹H NMR (300 MHz, DMSO-d₆, 296 K): δ = 8.73 (s, 3H), 7.55-7.36 (m, 5H), 4.15-4.13 (m, 1H), 2.02-1.97 (m, 2H), 1.22-1.17 (m, 8H), 0.83-0.79 (t, J = 7.02 Hz, 3H) ppm.

¹³C NMR (75 MHz, DMSO-d₆, 296 K): δ = 138.06, 128.60, 128.37, 127.52, 54.52, 34.21, 30.97, 28.14, 24.98, 21.91, 13.86 ppm.

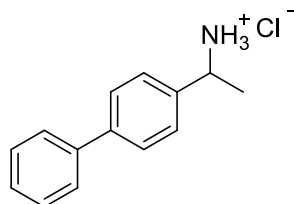
20:

1-(Naphthalen-2-yl)ethanaminium chloride

[C₁₂H₁₄ClN] 207.70 g/mol (M)

¹H NMR (400 MHz, DMSO-d₆, 296 K): δ = 8.81(s, 3H), 8.03-7.91 (m, 4H), 7.74-7.72 (m, 1H), 7.56-7.53 (m, 2H), 4.55-4.52 (m, 1H), 1.62-1.61 (d, J = 6.64 Hz, 3H) ppm.

¹³C NMR (100 MHz, DMSO-d₆, 296 K): δ = 136.91, 132.61, 128.36, 127.85, 127.62, 126.59, 126.48, 125.81, 124.68, 50.14, 20.73 ppm.

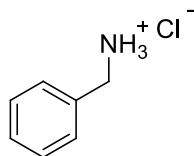
21:

1-([1,1'-Biphenyl]-4-yl)ethanaminium chloride

[C₁₄H₁₆ClN] 233.74 g/mol (M)

¹H NMR (400 MHz, DMSO-d₆, 296 K): δ = 8.77 (s, 3H), 7.72-7.63 (m, 5H), 7.48-7.45 (m, 3H), 7.39-7.35 (m, 1H), 4.45-4.39 (m, 1H), 1.58-1.56 (d, J = 6.64 Hz, 3H) ppm.

¹³C NMR (100 MHz, DMSO-d₆, 296 K): δ = 140.14, 139.56, 138.63, 128.99, 127.65, 127.54, 126.89, 126.71, 49.73, 20.79 ppm.

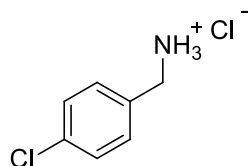
22:

Phenylmethanaminium chloride

[C₇H₁₀ClN] 143.61 g/mol (M)

¹H NMR (300 MHz, DMSO-d₆, 296 K): δ = 8.55 (s, 3H), 7.53-7.51 (m, 2H), 7.41-7.34 (m, 3H), 3.97 (s, 2H) ppm.

¹³C NMR (75 MHz, DMSO-d₆, 296 K): δ = 134.46, 128.94, 128.47, 128.24, 42.16 ppm.

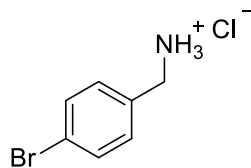
23:

(4-Chlorophenyl)methanaminium chloride

[C₇H₉Cl₂N] 178.06 g/mol (M)

¹H NMR (300 MHz, DMSO-d₆, 296 K): δ = 8.76 (s, 3H), 7.59-7.56 (m, 2H), 7.46-7.43 (m, 2H), 4.00 (s, 2H) ppm.

¹³C NMR (75 MHz, DMSO-d₆, 296 K): δ = 133.15, 133.09, 131.11, 128.45, 41.39 ppm.

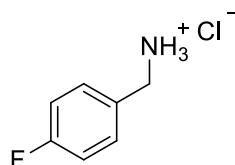
24:

(4-Bromophenyl)methanaminium chloride

[C₇H₉BrClN] 222.51 g/mol (M)

¹H NMR (300 MHz, DMSO-d₆, 296 K): δ = 8.71 (s, 3H), 7.61-7.58 (m, 2H), 7.50-7.48 (m, 2H), 3.98-3.96 (m, 2H) ppm.

¹³C NMR (75 MHz, DMSO-d₆, 296 K): δ = 133.58, 131.35, 121.66, 41.39 ppm.

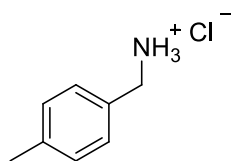
25:

(4-Fluorophenyl)methanaminium chloride

[C₇H₉ClFN] 161.60 g/mol (M)

¹H NMR (300 MHz, DMSO-d₆, 296 K): δ = 8.68 (s, 3H), 7.61-7.56 (m, 2H), 7.26-7.20 (m, 2H), 4.01-3.96 (m, 2H) ppm.

¹³C NMR (75 MHz, DMSO-d₆, 296 K): δ = 163.68, 160.45, 131.50, 130.46, 115.45, 115.18, 41.34 ppm.

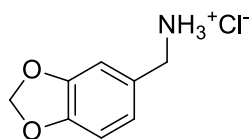
26:

p-tolylmethanaminium chloride

[C₈H₁₂ClN] 157.64 g/mol (M)

¹H NMR (300 MHz, DMSO-d₆, 296 K): δ = 9.05 (s, 3H), 7.57-7.54 (m, 2H), 7.27-7.25 (m, 2H), 4.85 (m, 2H), 2.34 (s, 3H) ppm.

¹³C NMR (75 MHz, DMSO-d₆, 296 K): δ = 163.68, 160.45, 131.50, 130.46, 115.45, 115.18, 41.34 ppm.

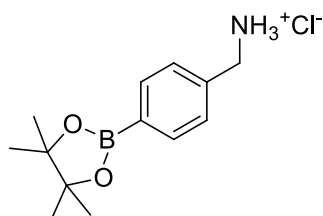
27:

Benzo[d][1,3]dioxol-5-ylmethanaminium chloride

[C₈H₁₀ClNO₂] 187.62 g/mol (M)

¹H NMR (400 MHz, DMSO-d₆, 296 K): δ = 8.61 (s, 3H), 7.16 (m, 1H), 6.99-6.96 (m, 1H), 6.92-6.90 (m, 1H), 6.01 (s, 2H), 3.89 (s, 2H) ppm.

¹³C NMR (100 MHz, DMSO-d₆, 296 K): δ = 147.25, 127.75, 122.95, 109.61, 108.22, 101.21, 41.94 ppm.

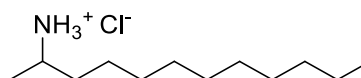
28:

4-(4,4,5,5-Tetramethyl-1,3,2-dioxaborolan-2-yl)phenylmethanaminium chloride

[C₁₃H₂₁BClNO₂] 269,58 g/mol (M)

¹H NMR (400 MHz, DMSO-d₆, 296 K): δ = 8.69 (s, 3H), 7.69-7.67 (d, J = 7.81 Hz, 2H), 7.52-7.51 (d, J = 7.81 Hz, 2H), 4.01 (s, 2H), 1.28 (s, 12H) ppm.

¹³C NMR (100 MHz, DMSO-d₆, 296 K): δ = 137.34, 134.49, 128.34, 83.74, 42.00, 24.66 ppm.

29:

Dodecan-2-aminium chloride

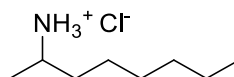
[C₁₂H₂₅ClN] 221.81 g/mol (M)

¹H NMR (300 MHz, DMSO-d₆, 296 K): δ = 8.18 (s, 3H), 3.08-3.05 (m, 1H), 1.23-1.16 (m, 18H), 0.85-0.82 (m, 3H) ppm.

¹³C NMR (75 MHz, DMSO-d₆, 296 K): δ = 46.71, 34.02, 31.32, 29.02, 28.90, 28.83, 28.75, 28.73, 24.83, 22.12, 17.99, 13.91 ppm.

30:

Octan-2-aminium chloride

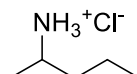
[C₈H₂₀ClN] 165.70 g/mol (M)

¹H NMR (300 MHz, DMSO-d₆, 296 K): δ = 8.19 (s, 3H), 3.09-3.04 (m, 1H), 1.64-1.58 (m, 1H), 1.43-1.36 (m, 1H), 1.17-1.16 (d, J = 6.64 Hz, 3H), 0.86-0.83 (m, 3H) ppm.

¹³C NMR (75 MHz, DMSO-d₆, 296 K): δ = 47.14, 34.41, 31.48, 28.86, 25.16, 22.40, 18.40, 14.32 ppm.

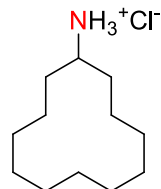
31:

Pentan-2-aminium chloride

[C₅H₁₄ClN] 123.62 g/mol (M)

¹H NMR (300 MHz, DMSO-d₆, 296 K): δ = 8.19 (s, 3H), 3.11-3.06 (m, 1H), 1.62-1.58 (m, 1H), 1.39-1.29 (m, 3H), 1.17-1.16 (d, J = 6.64 Hz, 3H), 0.87-0.83 (t, J = 7.03 Hz, 3H) ppm.

¹³C NMR (75 MHz, DMSO-d₆, 296 K): δ = 46.51, 36.18, 18.15, 18.03, 13.72 ppm.

32:

Cyclododecanaminium chloride

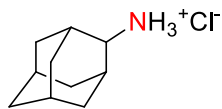
[C₂₂H₃₈ClN] 219.79 g/mol (M)

¹H NMR (300 MHz, DMSO-d₆, 296 K): δ = 8.18 (s, 3H), 3.08-3.05 (m, 1H), 1.23-1.16 (m, 18H), 0.85-0.82 (m, 3H) ppm.

¹³C NMR (75 MHz, DMSO-d₆, 296 K): δ = 46.71, 34.02, 31.32, 29.02, 28.90, 28.83, 28.75, 28.73, 24.83, 22.12, 17.99, 13.91 ppm.

33:

Adamantan-2-aminium chloride

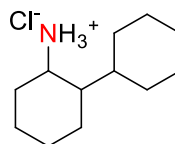
[C₁₀H₁₈ClN] 187.71 g/mol (M)

¹H NMR (300 MHz, DMSO-d₆, 296 K): δ = 8.37 (s, 3H), 3.24 (m, 1H), 2.32 (m, 1H), 2.08-2.01 (m, 3H) 1.82-1.68 (m, 8H), 1.53-1.50 (m, 2H) ppm.

¹³C NMR (75 MHz, DMSO-d₆, 296 K): δ = 54.66, 36.86, 36.15, 29.93, 29.49, 26.43, 26.34 ppm.

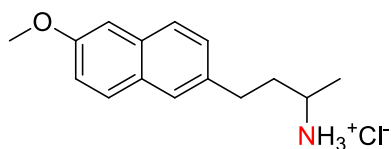
34:

[1,1'-bi(cyclohexan)]-2-aminium chloride

[C₁₂H₂₄ClN] 217.78 g/mol (M)

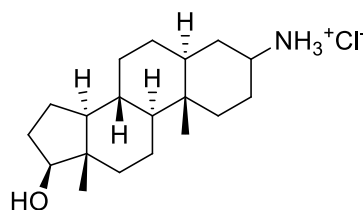
¹H NMR (300 MHz, DMSO-d₆, 296 K): δ = 8.06 (s, 3H), 3.46 (m, 1H), 2.22-0.74 (m, 20H) ppm.

¹³C NMR (75 MHz, DMSO-d₆, 296 K): δ = 55.26, 47.27, 44.00, 41.37, 35.59, 35.51, 30.84, 30.05, 29.28, 28.77, 28.65, 27.38, 26.07, 25.90, 25.82, 23.65, 22.13, 18.83 ppm.

35:Nabutmetone- NH₃⁺Cl⁻[C₁₅H₂₀ClNO] 265.78 g/mol (M)

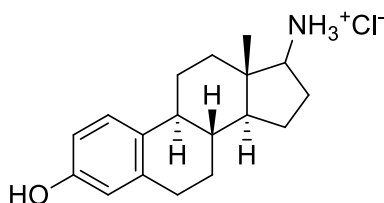
¹H NMR (300 MHz, DMSO-d₆, 296 K): δ = 8.22 (s, 3H), 7.78-7.66 (m, 3H), 7.38-7.29 (m, 2H), 7.17-7.13 (m, 1H), 3.87 (s, 3H), 3.16 (m, 1H), 2.86-2.77 (m, 2H), 2.12-1.77 (m, 2H), 1.29-1.27 (d, J = 6.44 Hz, 3H) ppm.

¹³C NMR (75 MHz, DMSO-d₆, 296 K): δ = 156.83, 136.06, 132.81, 128.79, 128.56, 127.55, 126.86, 125.95, 118.58, 105.75, 55.15, 46.42, 35.80, 30.80, 18.09 ppm.

36:Stanolone-NH₃⁺Cl⁻[C₁₉H₃₄ClNO] 327.93 g/mol (M)

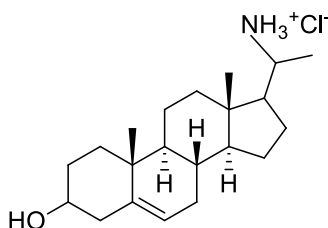
¹H NMR (300 MHz, DMSO-d₆, 296 K): δ = 8.08 (s, 3H (2 H)), 4.44-4.43 (m, 1H), 3.45-3.41 (m, 1H), 2.93 (m, 1H), 1.79-0.76 (m, 25H), 0.61 (s, 3H) ppm.

¹³C NMR (75 MHz, DMSO-d₆, 296 K): δ = 80.01, 53.62, 50.56, 49.43, 44.12, 42.55, 36.58, 36.02, 35.10, 32.32, 31.13, 29.84, 27.96, 25.82, 23.06, 20.33, 11.82, 11.33 ppm.

37:Estrone-NH₃⁺Cl⁻[C₁₈H₂₆ClNO] 307.86 g/mol (M)

¹H NMR (300 MHz, DMSO-d₆, 296 K): δ = 9.02 (s, 3H (1.4H)), 7.69-7.67 (m, 1H), 7.05-7.03 (m, 1H), 6.53-6.46 (m, 2H), 4.20 (m, 1H), 2.74-2.73 (m, 2H), 2.41-2.29 (m, 2H), 2.08-1.93 (m, 4H), 1.75-1.72 (m, 1H), 1.54-1.43 (m, 2H), 1.37-1.22 (m, 4H), 0.81 (s, 3H) ppm.

¹³C NMR (75 MHz, DMSO-d₆, 296 K): δ = 155.51, 137.49, 130.37, 126.54, 115.43, 113.28, 59.90, 51.25, 50.06, 47.83, 43.94, 42.49, 38.68, 38.45, 35.87, 31.84, 29.54, 26.62, 26.04, 23.54, 21.62, 14.02, 12.08 ppm.

38:Pregnenolone-NH₃⁺Cl⁻[C₂₂H₃₈ClNO] 369.00 g/mol (M)

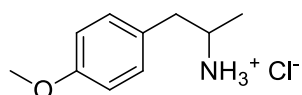
^1H NMR (300 MHz, DMSO- d_6 , 296 K): δ = 7.96 (s, 3H), 5.26 (m, 1H), 3.27-3.22 (m, 1H), 3.10-3.03 (m, 1H), 2.16-0.64 (m, 30H) ppm.

^{13}C NMR (75 MHz, DMSO- d_6 , 296 K): δ = 141.28, 120.27, 69.97, 55.84, 53.86, 50.11, 49.47, 49.39, 48.20, 42.20, 41.68, 41.38, 38.38, 36.93, 36.06, 31.40, 31.26, 26.23, 25.49, 23.76, 23.55, 20.44, 19.15, 18.89, 18.77, 11.63, 11.49 ppm.

39:

1-(4-methoxyphenyl)propan-2-aminium chloride

[$\text{C}_{10}\text{H}_{16}\text{ClNO}$] 201.69 g/mol (M)



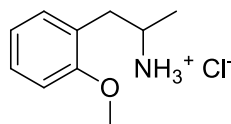
^1H NMR (300 MHz, DMSO- d_6 , 296 K): δ = 8.26 (s, 3H), 7.16-7.14 (m, 2H), 6.89-6.87 (m, 2H), 3.72 (s, 3H), 3.30 (m, 1H), 3.02-2.98 (m, 1H), 2.62-2.57 (m, 1H), 1.10-1.09 (d, J = 6.25 Hz, 3H) ppm.

^{13}C NMR (75 MHz, DMSO- d_6 , 296 K): δ = 158.06, 130.26, 128.67, 113.96, 55.02, 48.18, 39.14, 17.38 ppm.

40:

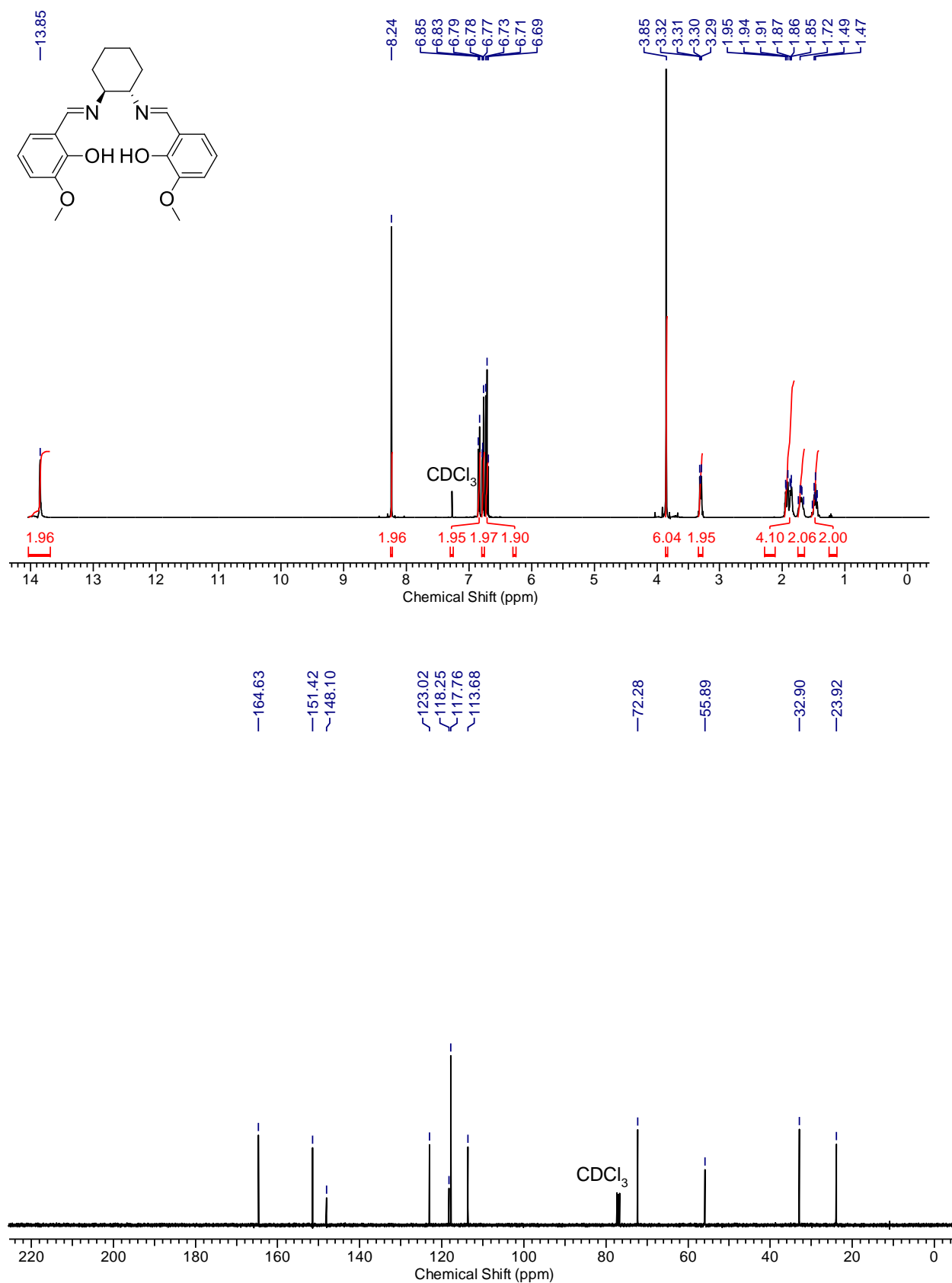
1-(2-methoxyphenyl)propan-2-aminium chloride

[$\text{C}_{10}\text{H}_{16}\text{ClNO}$] 201.69 g/mol (M)

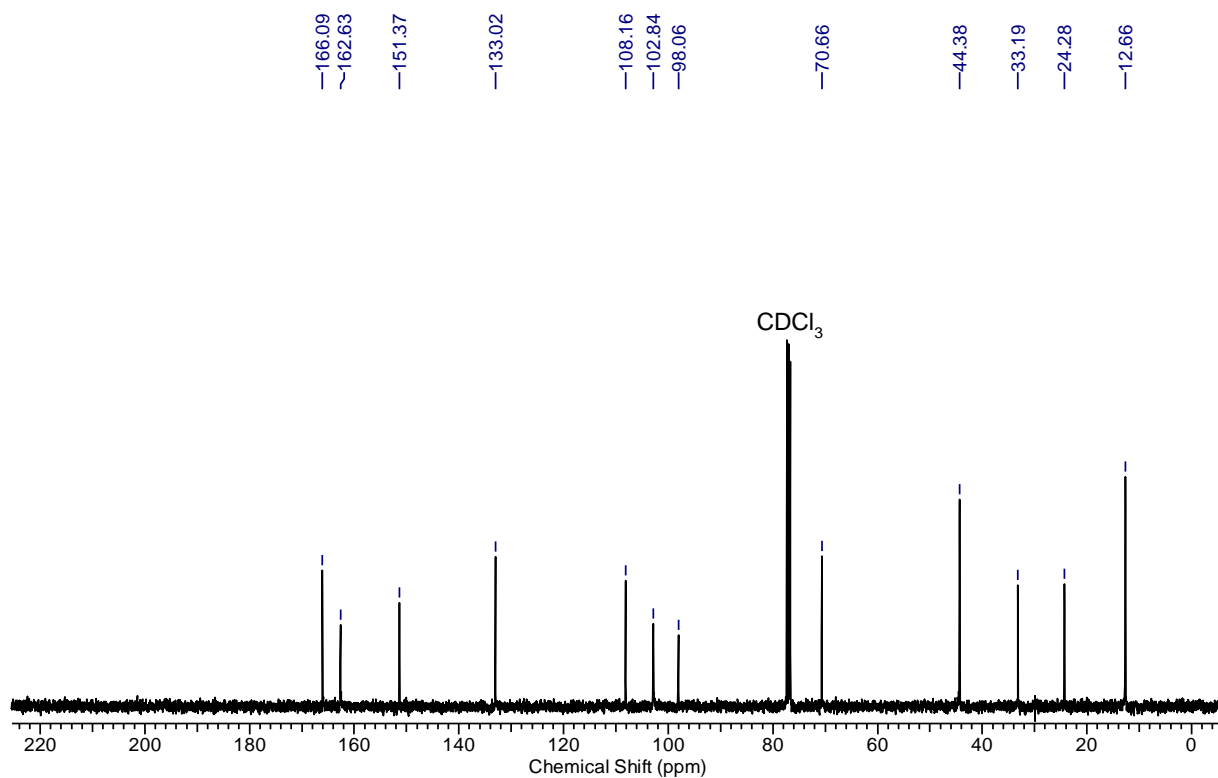
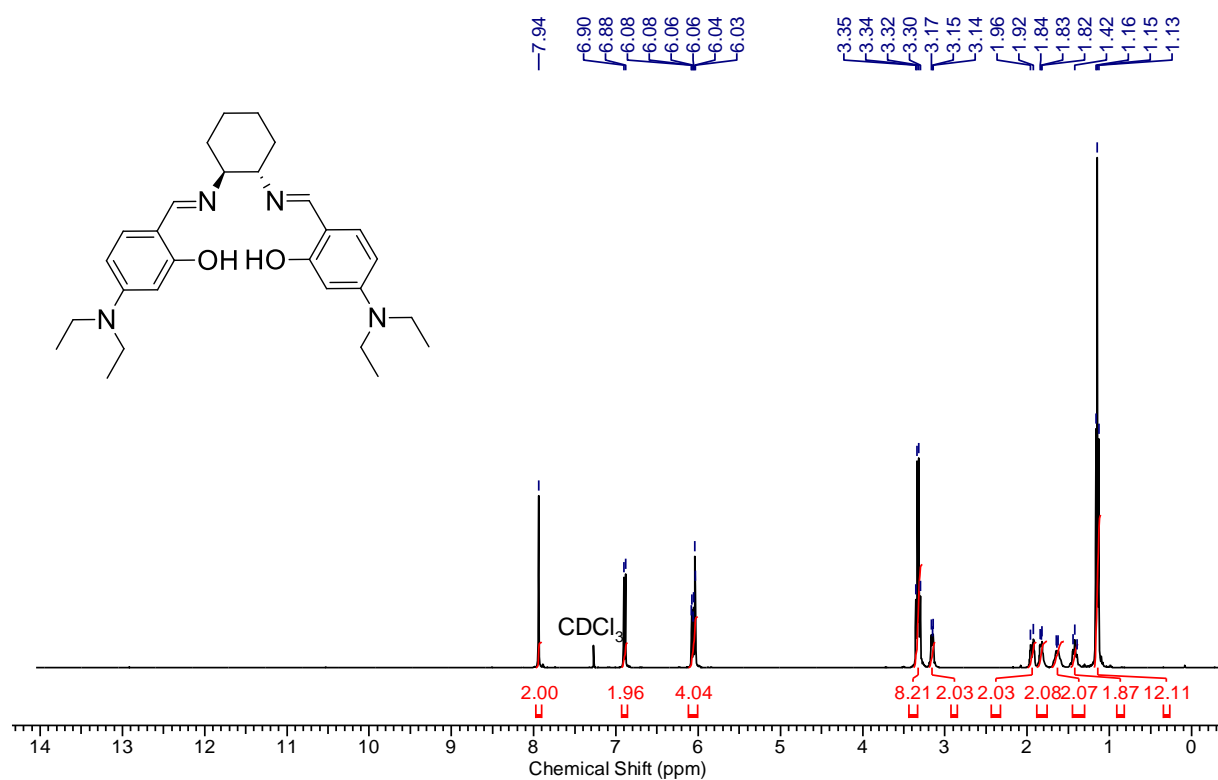


^1H NMR (300 MHz, DMSO- d_6 , 296 K): δ = 8.07 (s, 3H), 7.28-7.24 (m, 1H), 7.17-7.15 (m, 1H), 7.01-6.99 (m, 1H), 6.93-6.89 (m, 1H), 3.79 (s, 3H), 3.40-3.39 (m, 1H), 2.99-2.94 (m, 1H), 2.71-2.66 (m, 1H), 1.09-1.07 (d, J = 6.64 Hz, 3H) ppm.

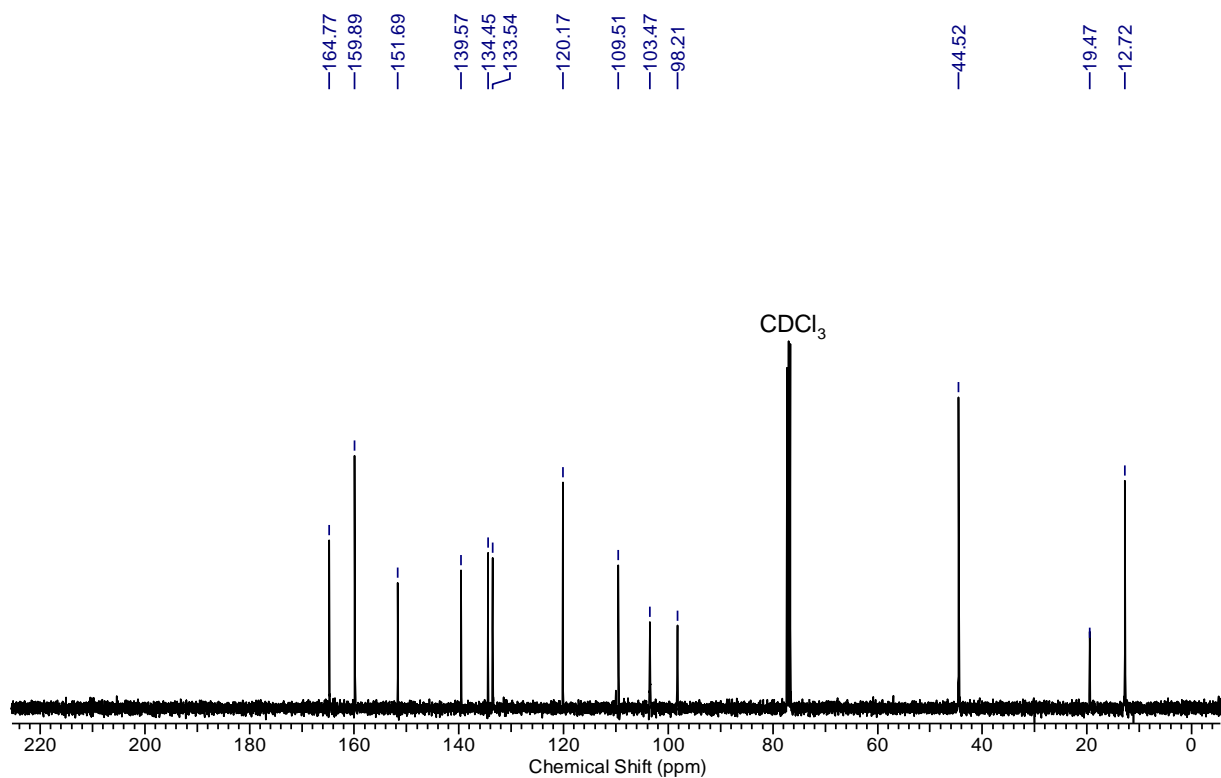
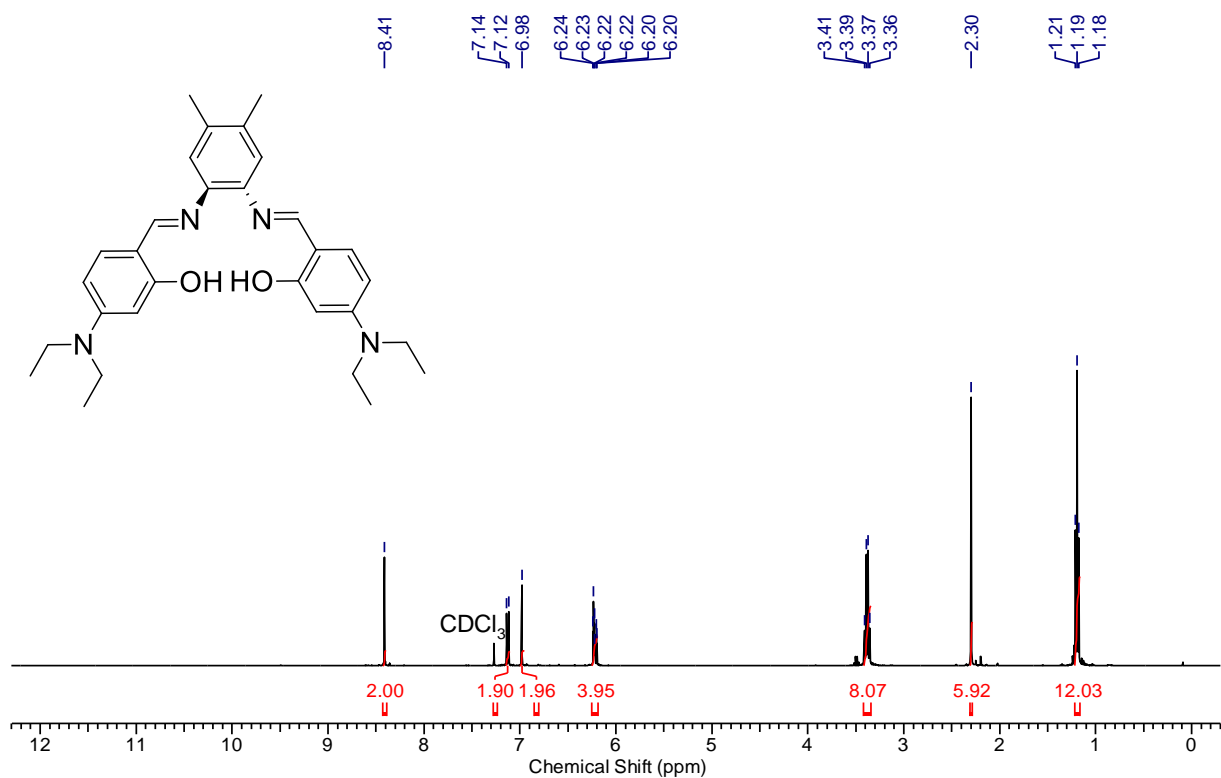
^{13}C NMR (75 MHz, DMSO- d_6 , 296 K): δ = 157.28, 130.93, 128.43, 124.48, 120.40, 110.94, 55.34, 46.71, 34.92, 17.75 ppm.

NMR spectra**Ligand I:**

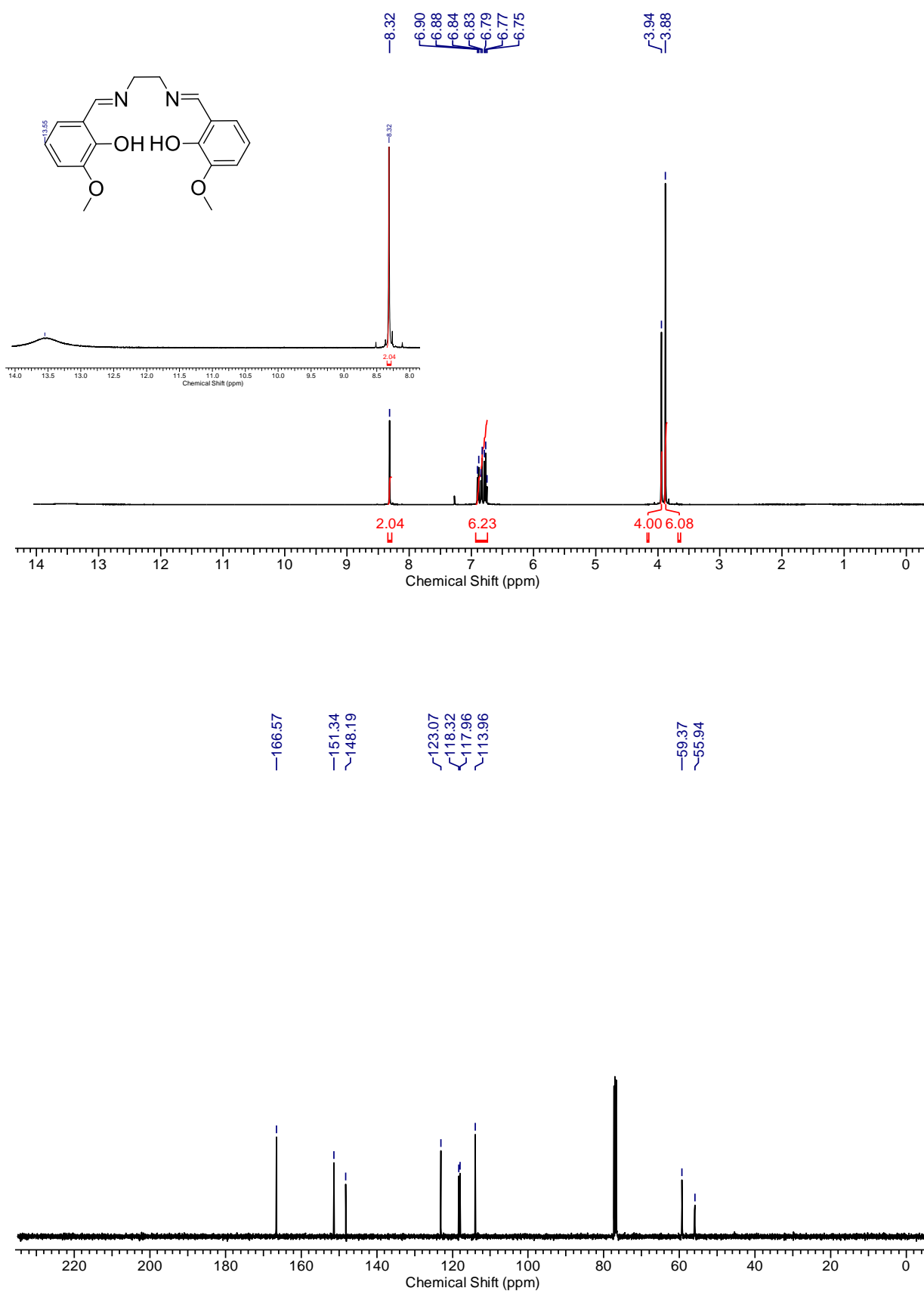
Ligand II



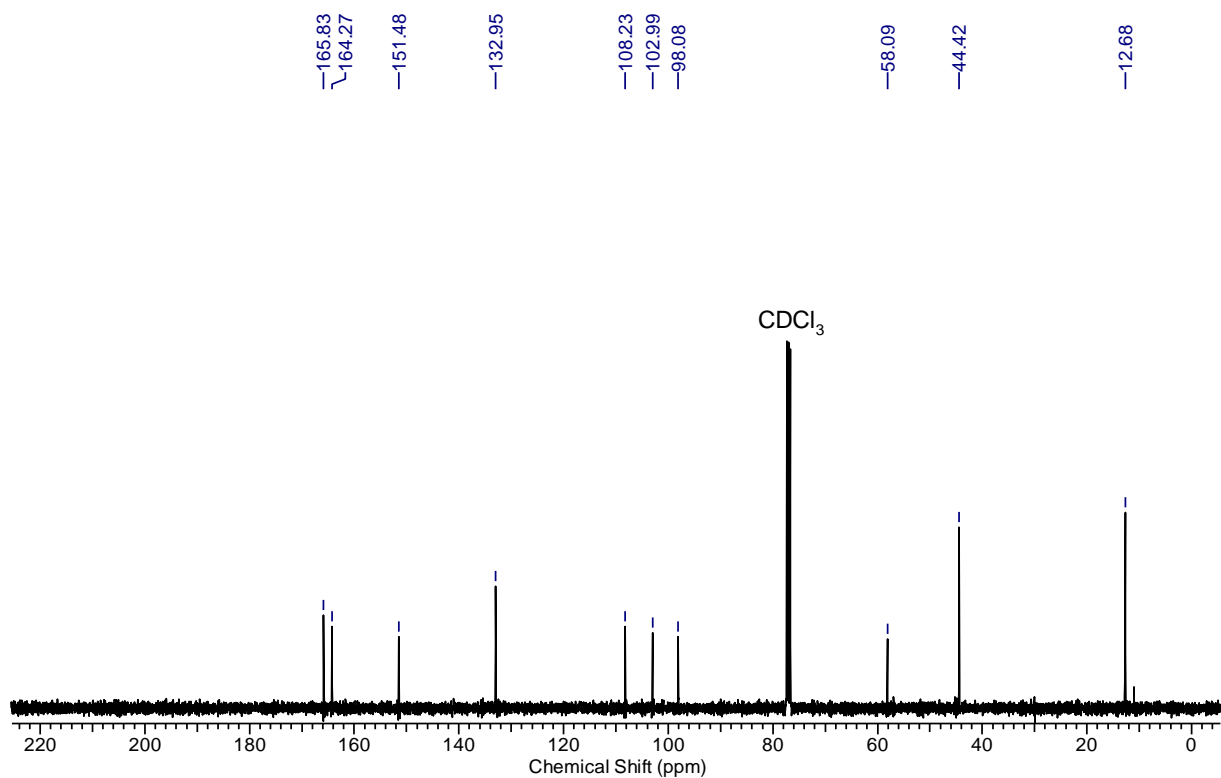
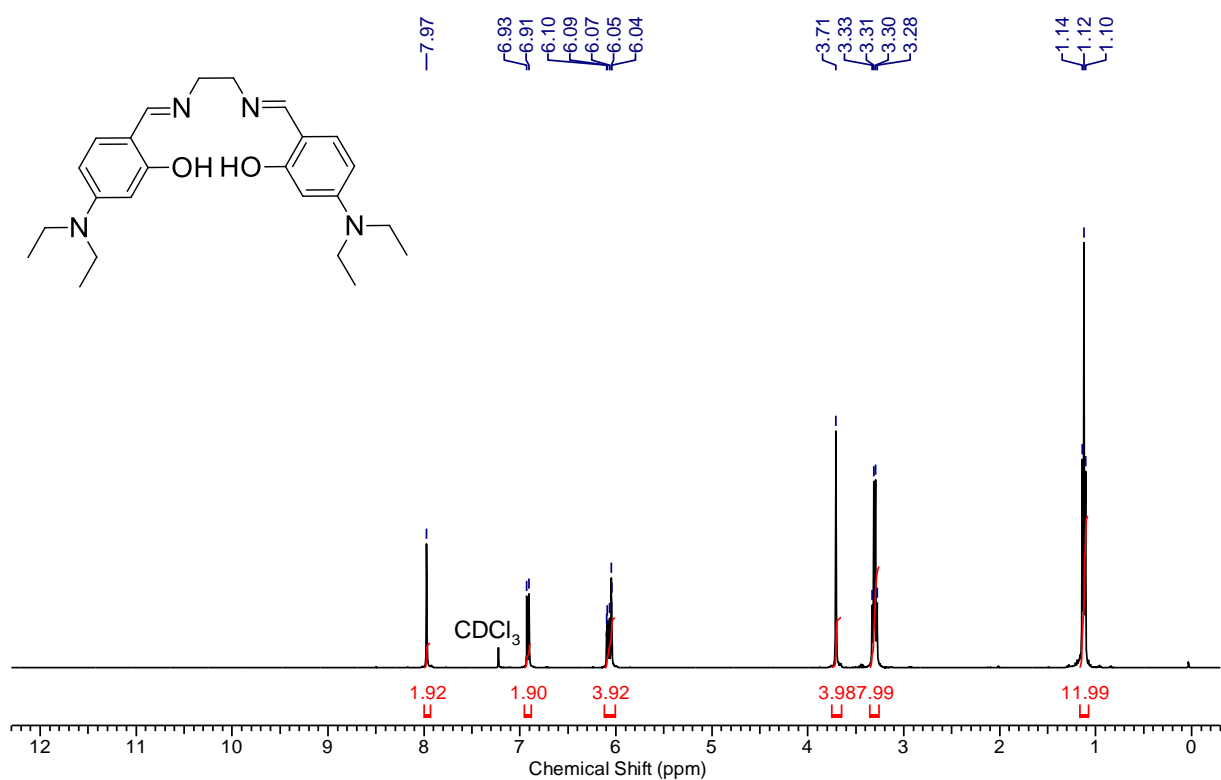
Ligand III



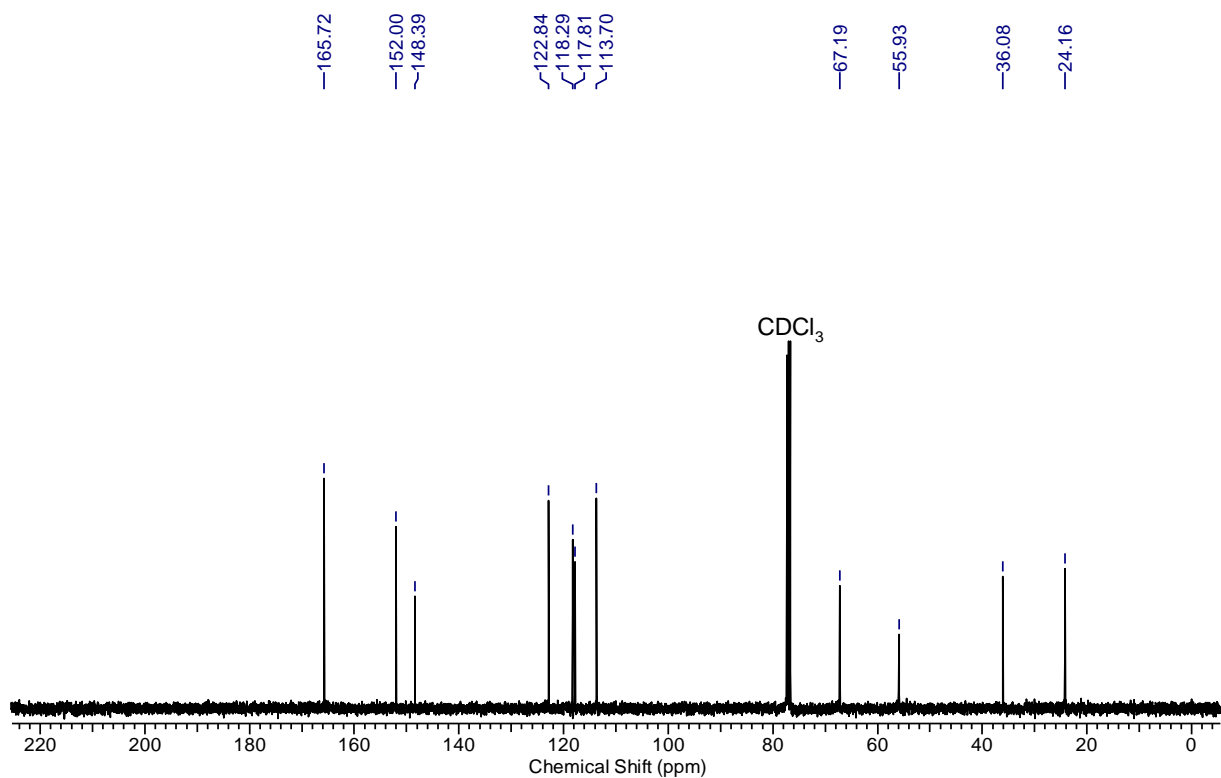
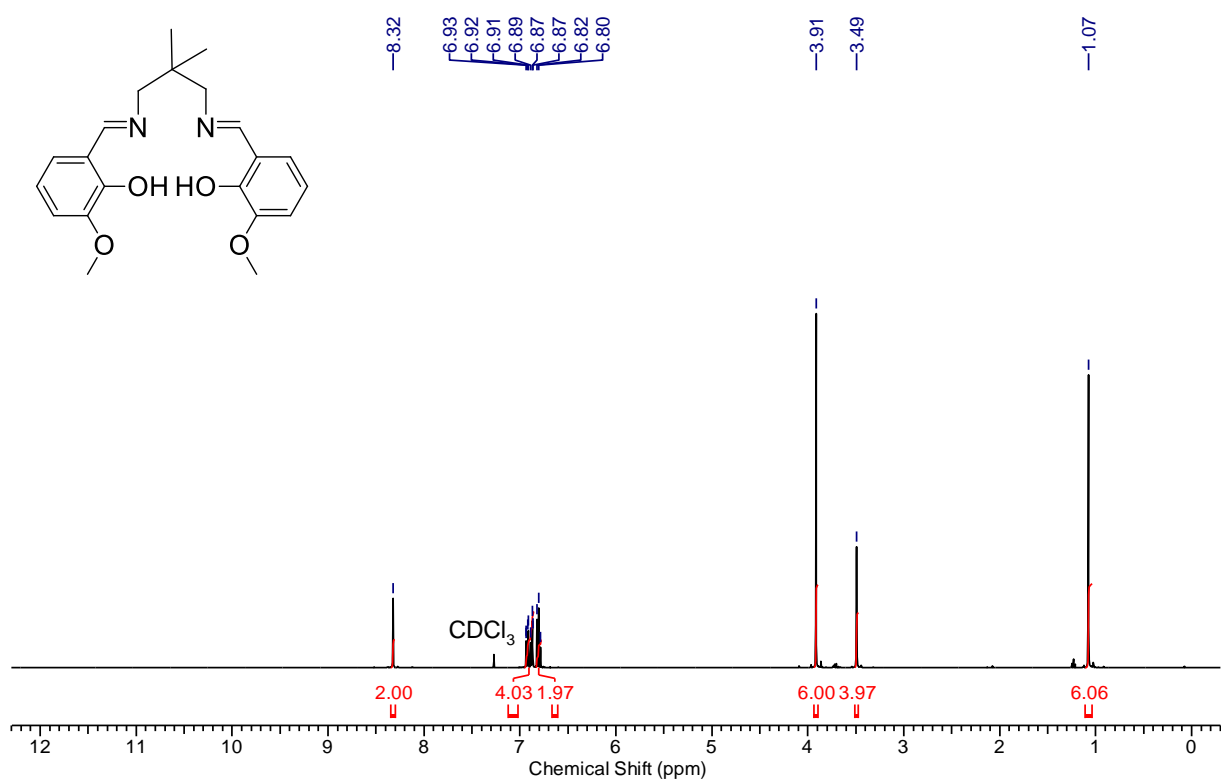
Ligand IV

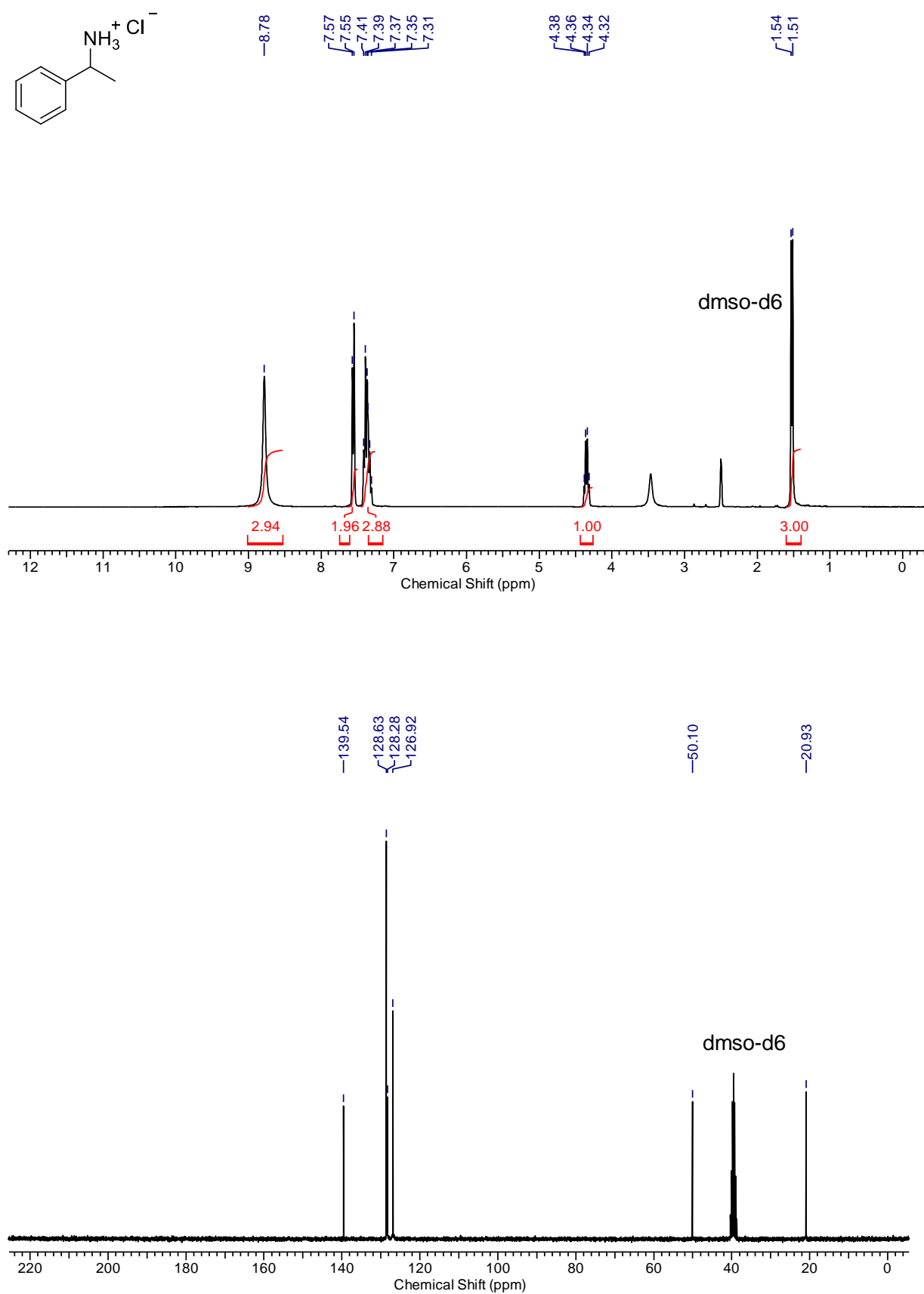


Ligand V

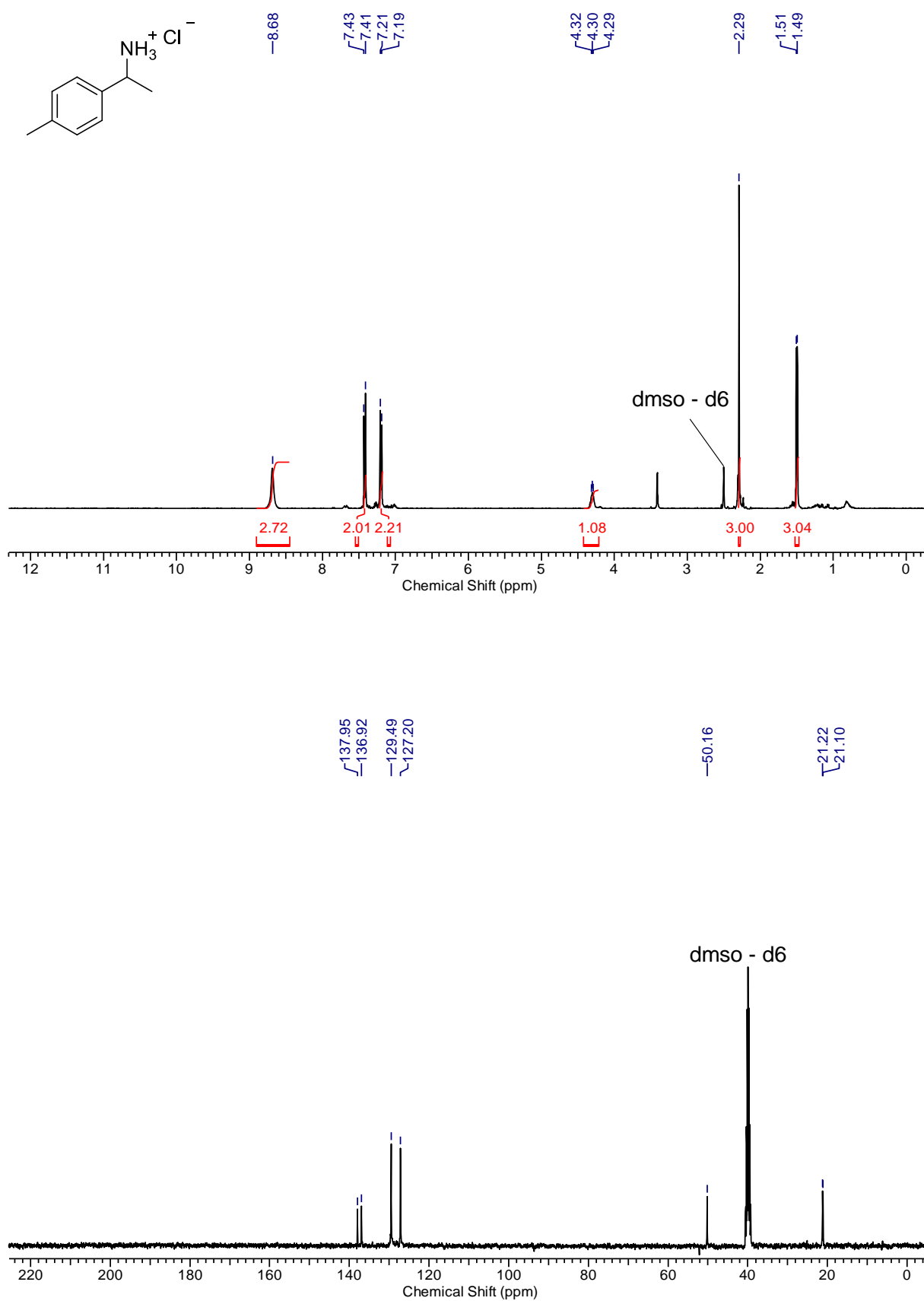


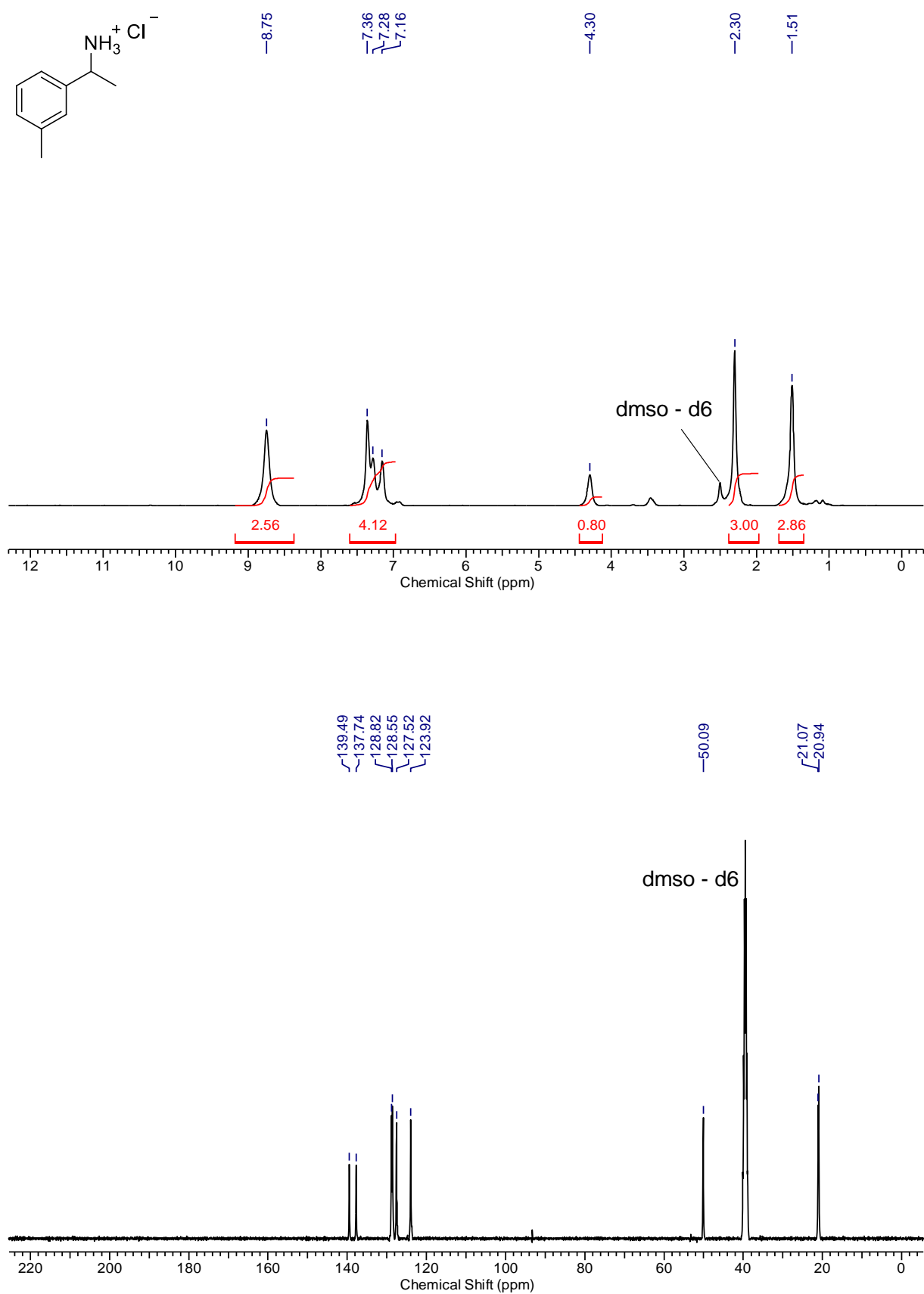
Ligand VI



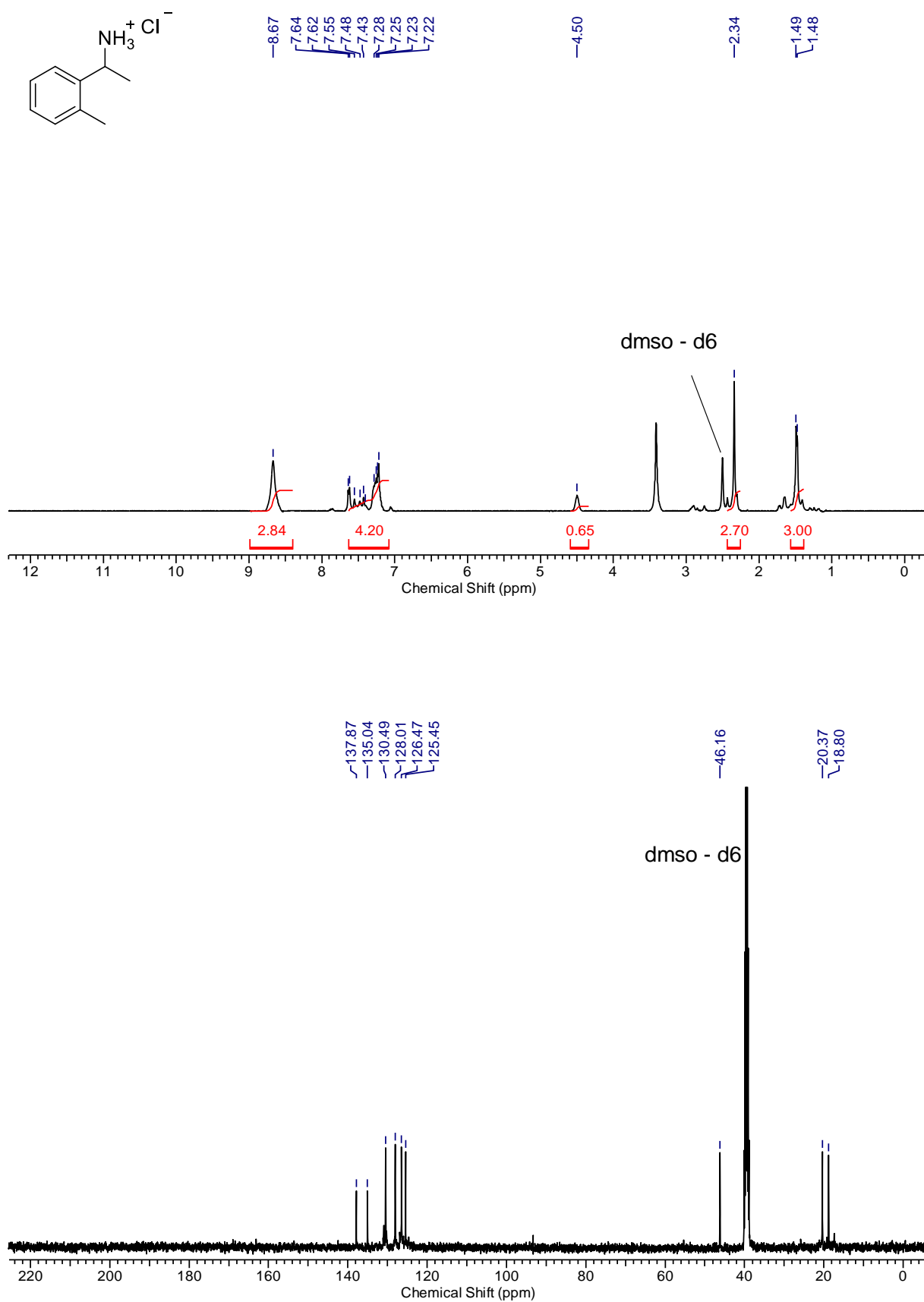
1:

2:

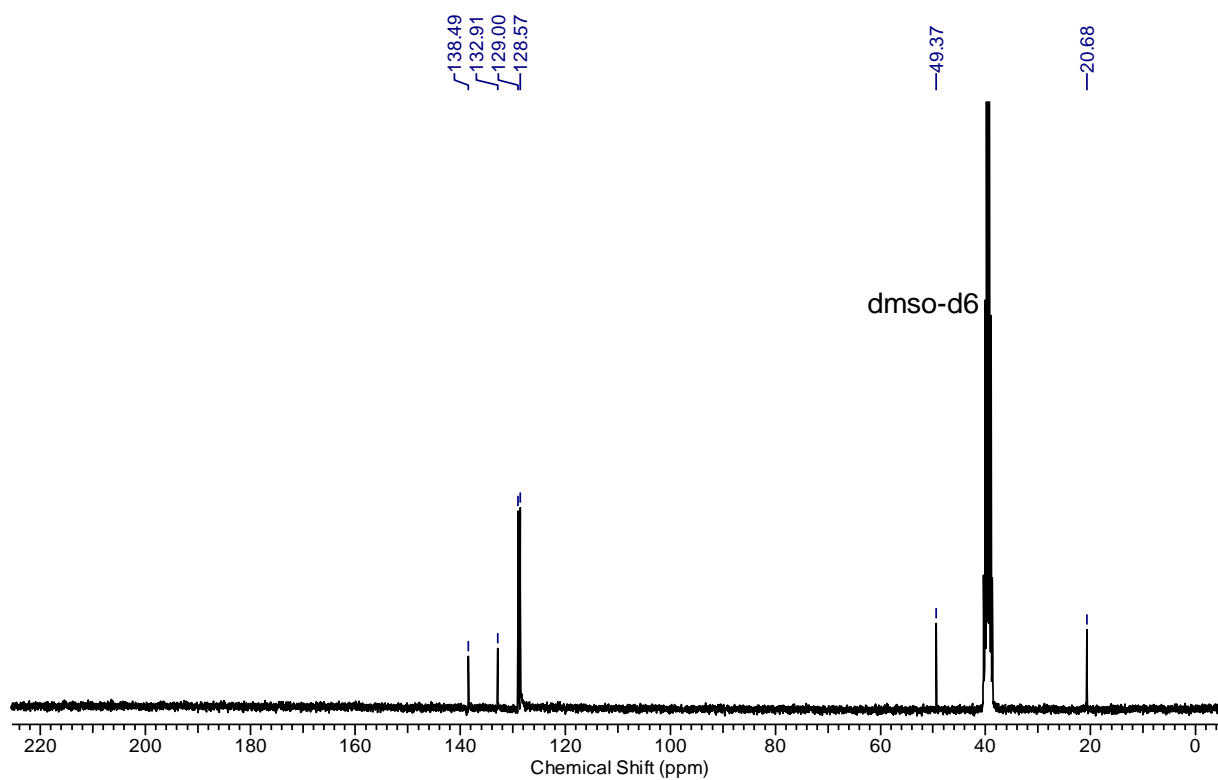
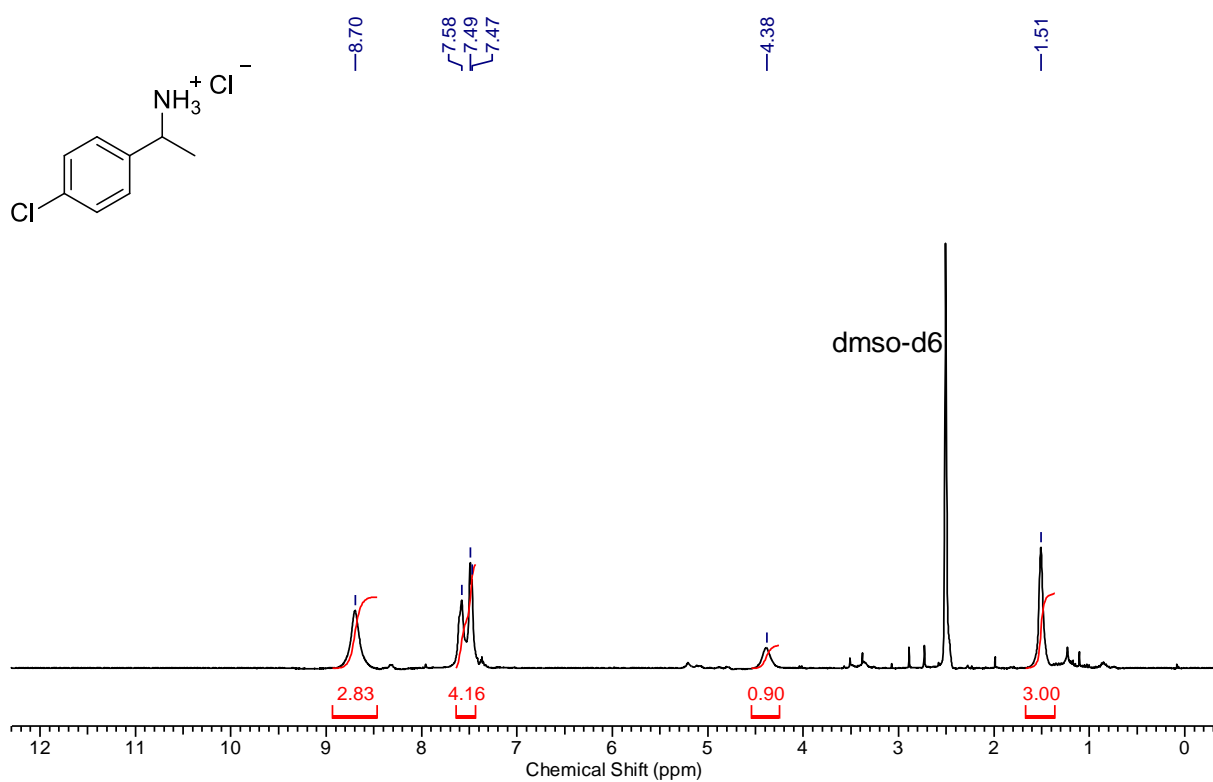


3:

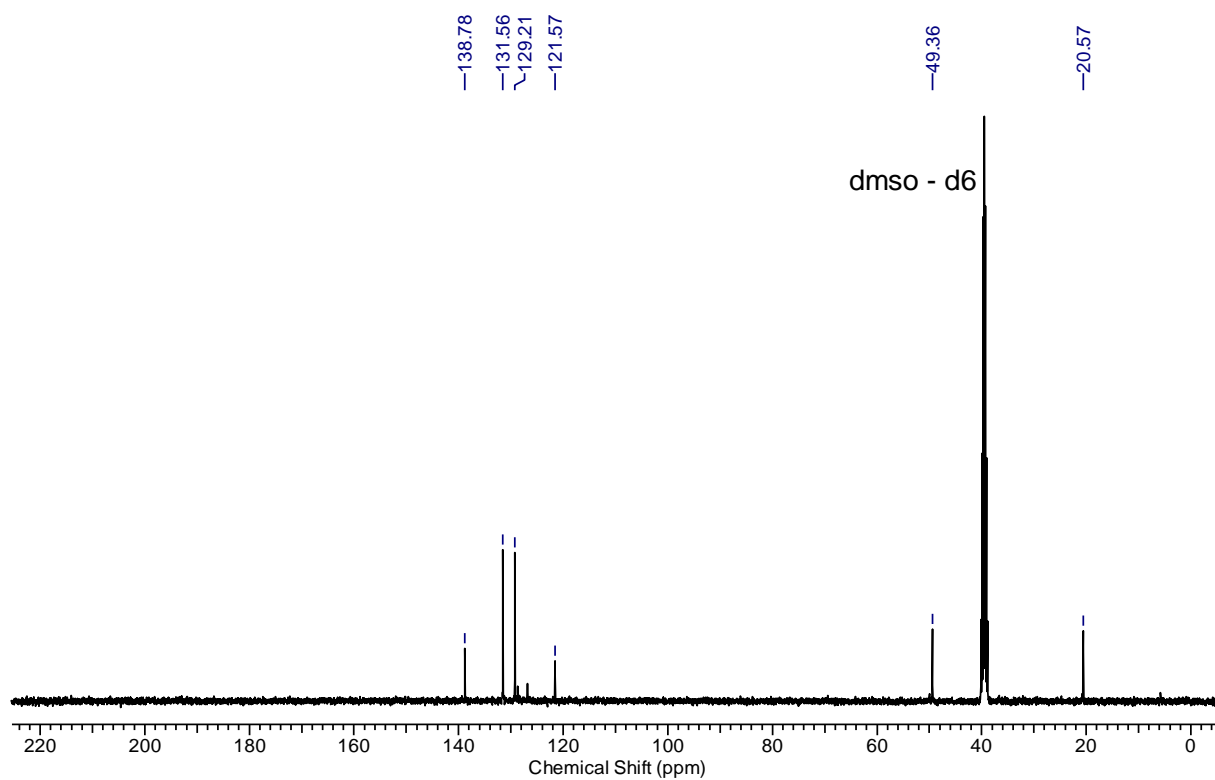
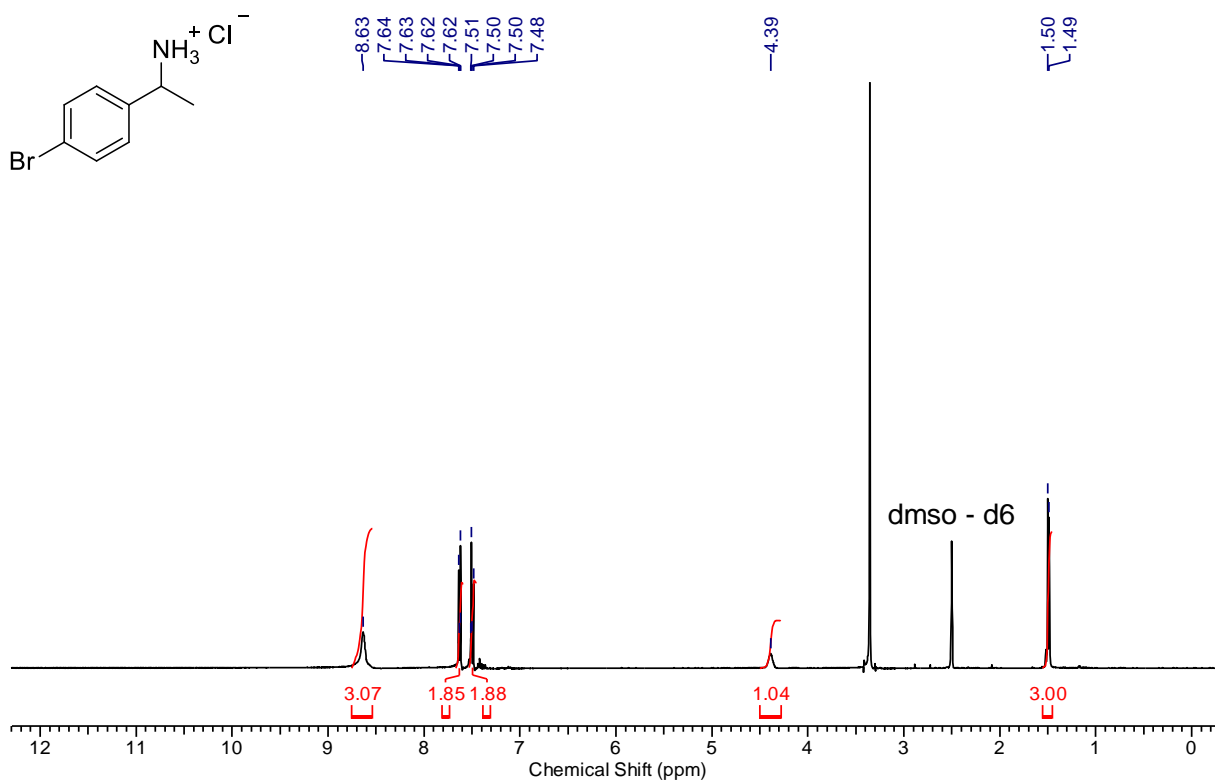
4:



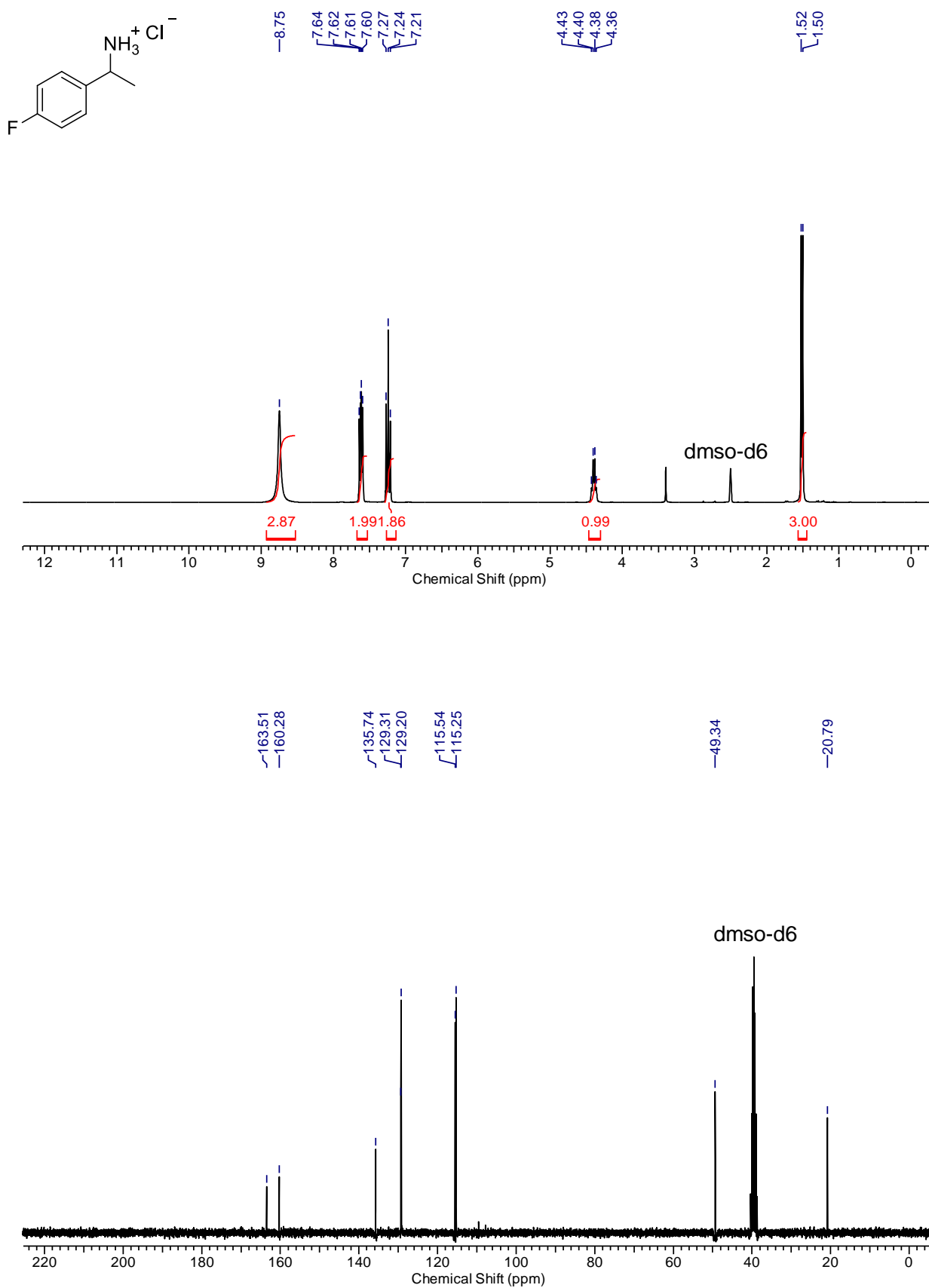
5:

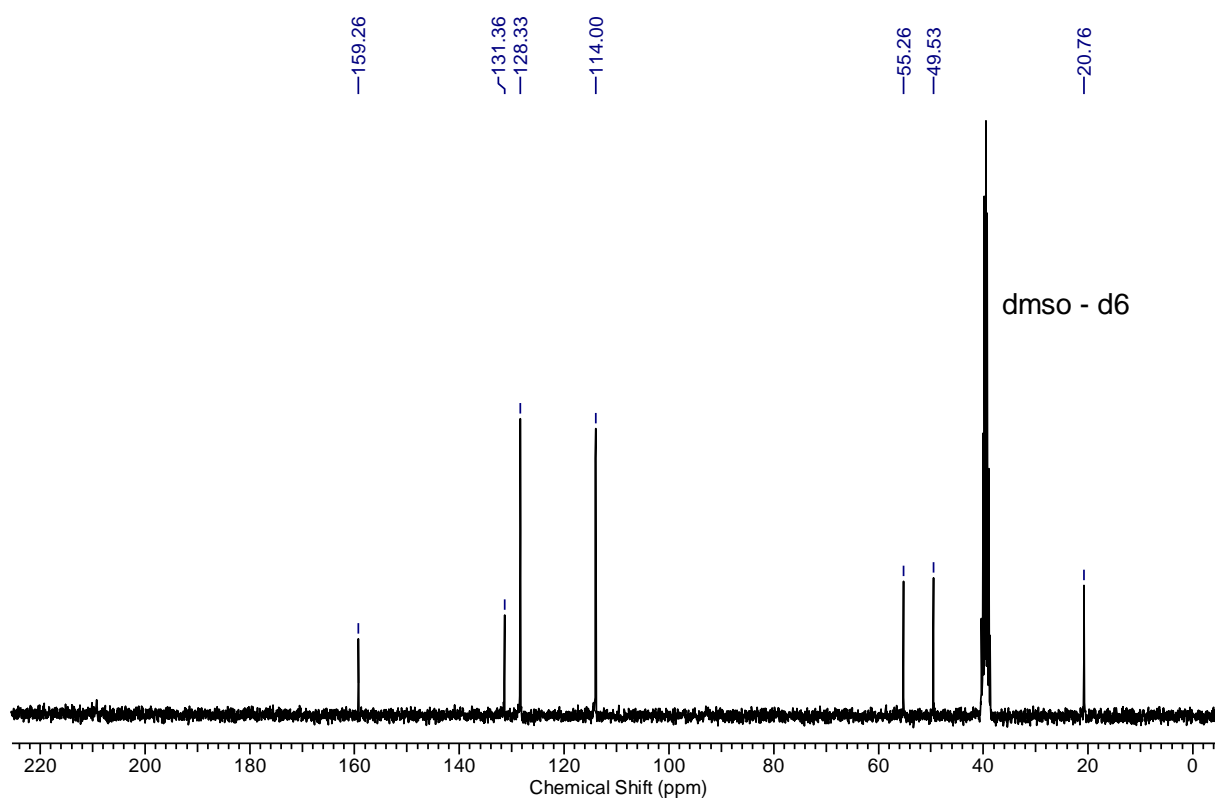
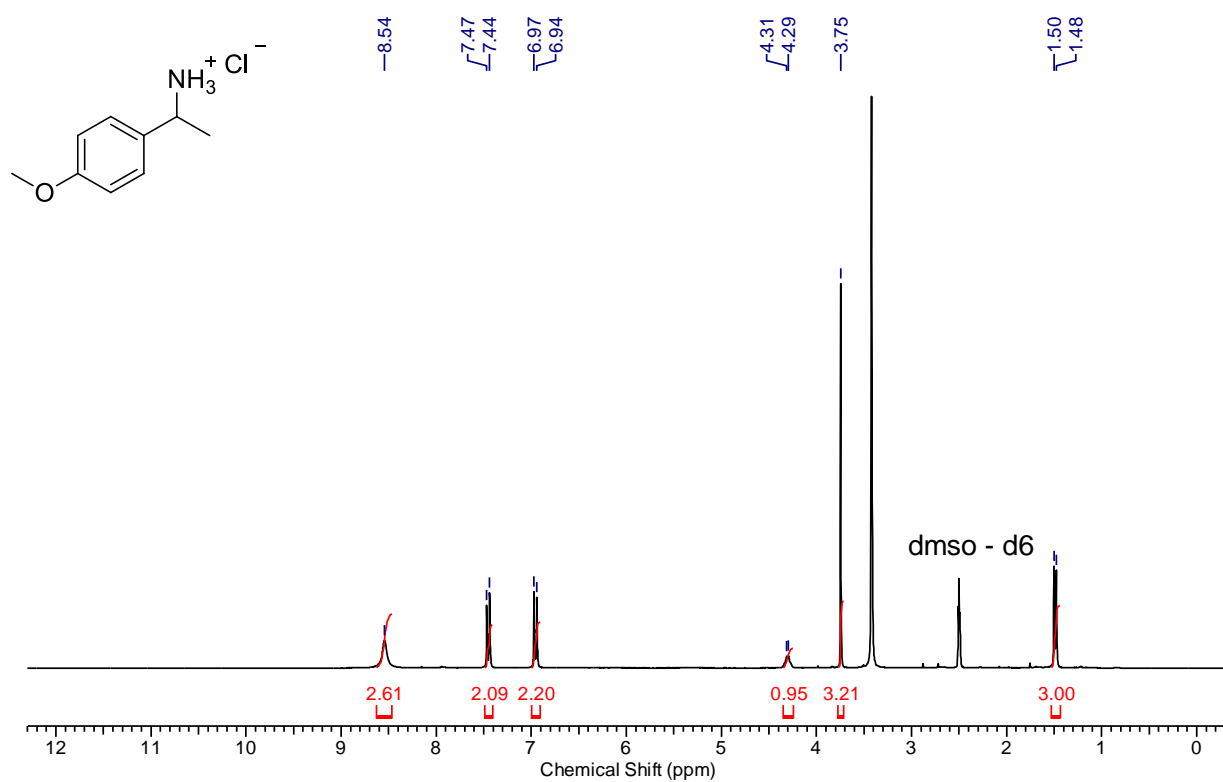


6:

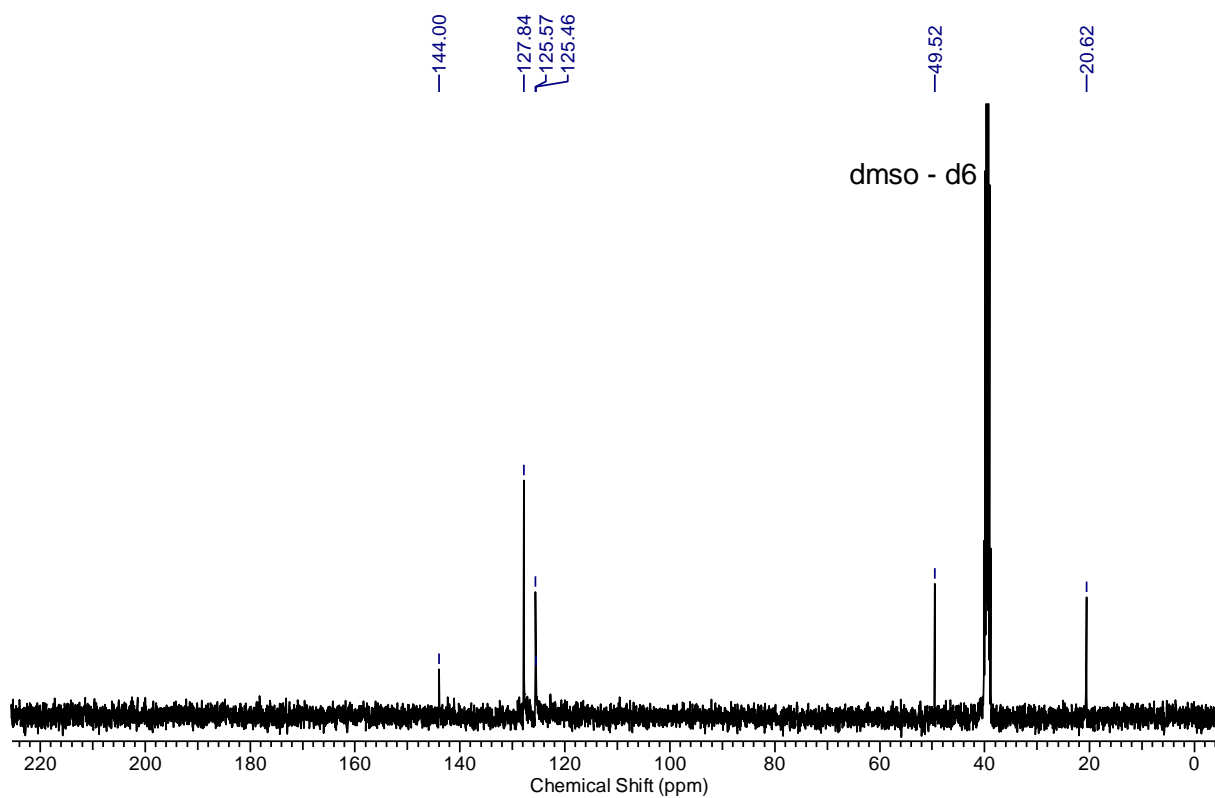
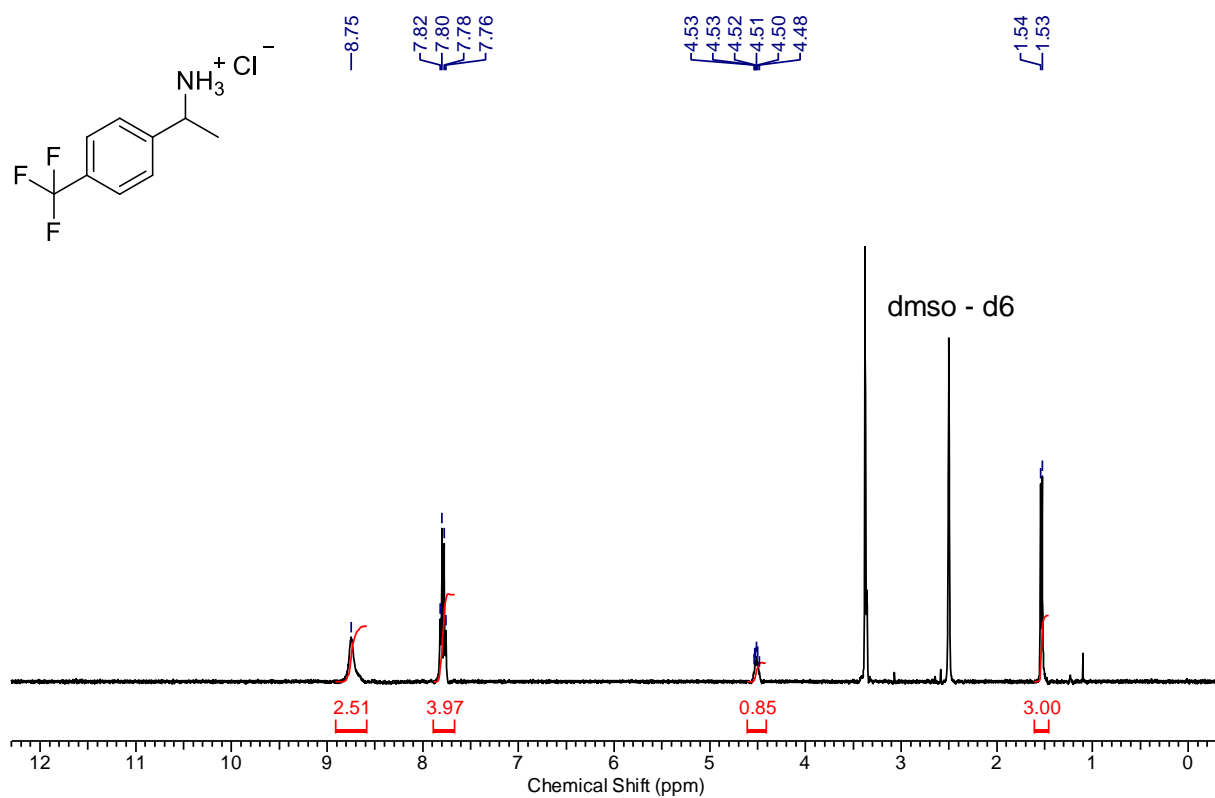


7:

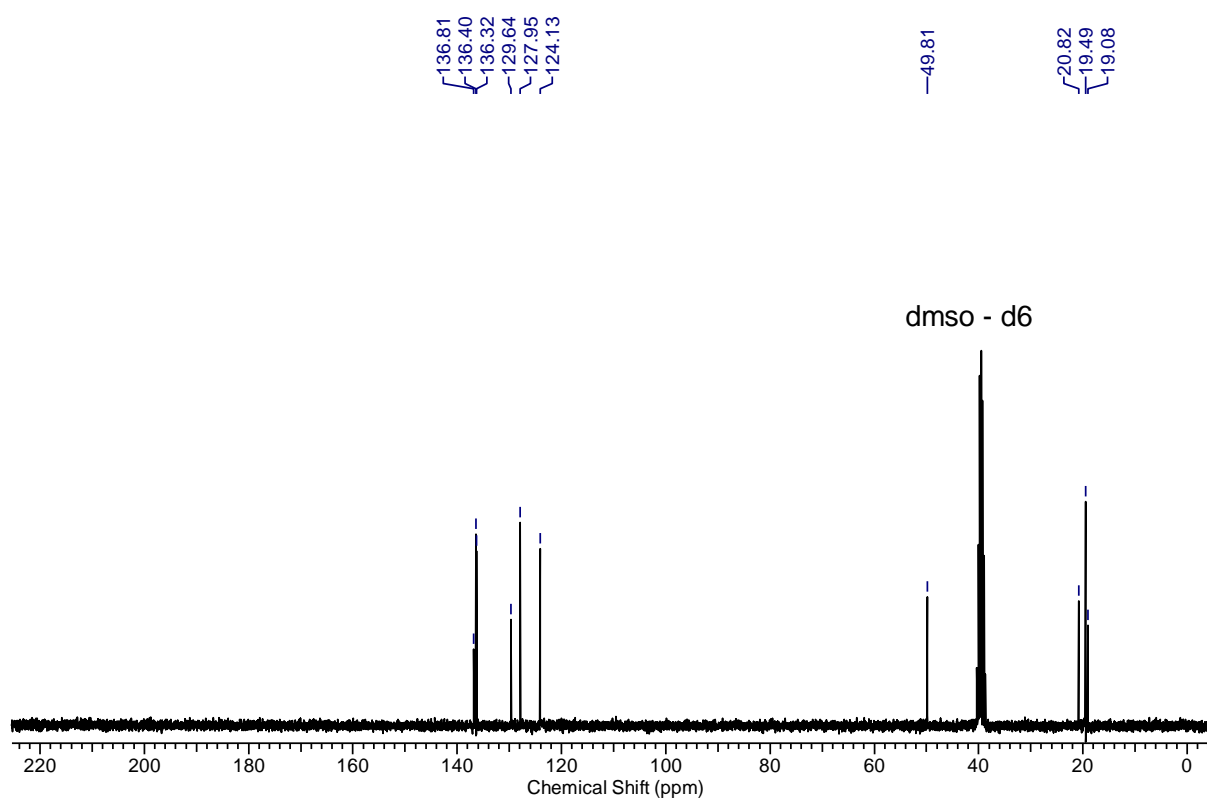
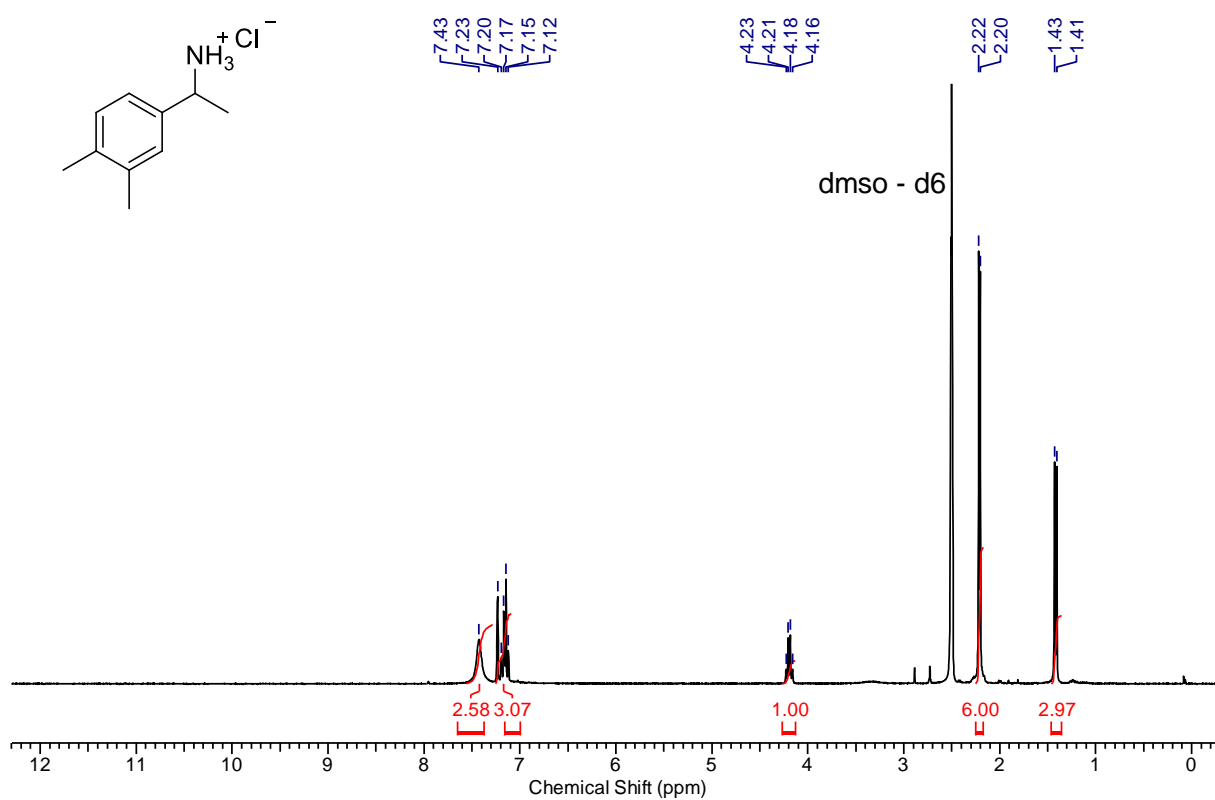


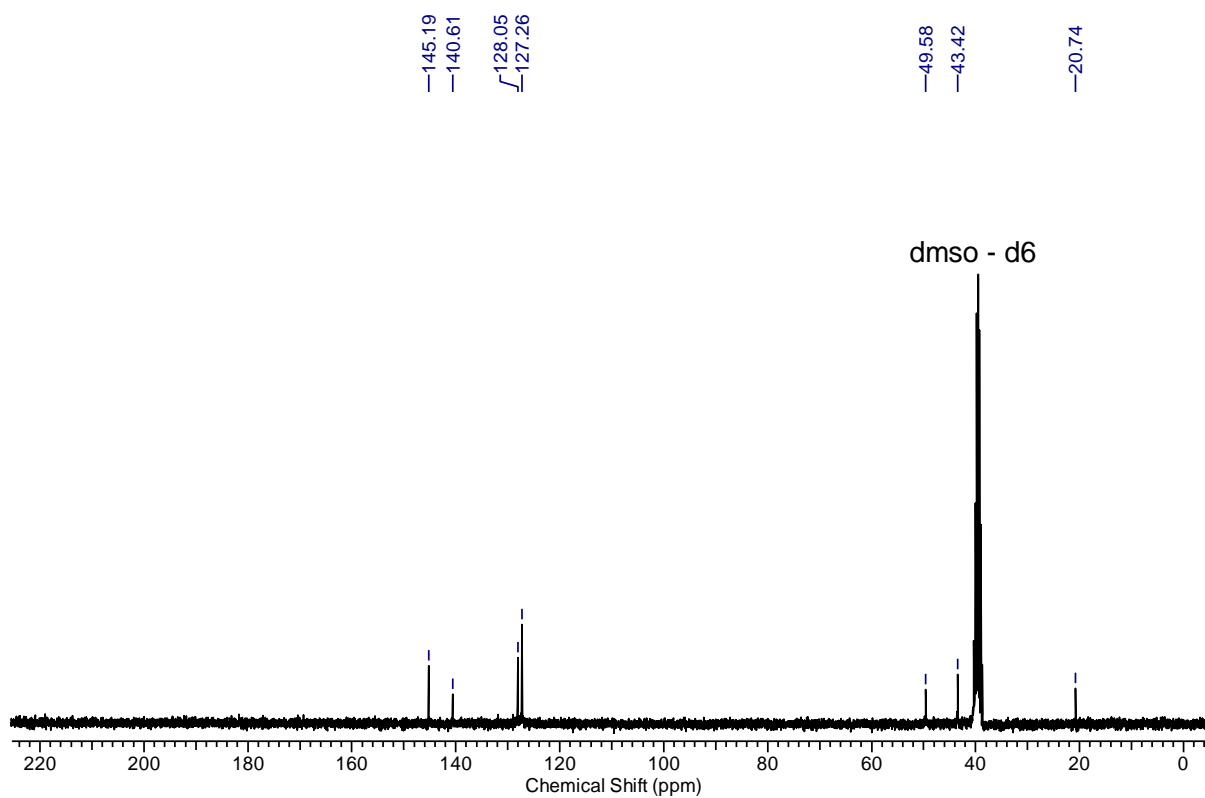
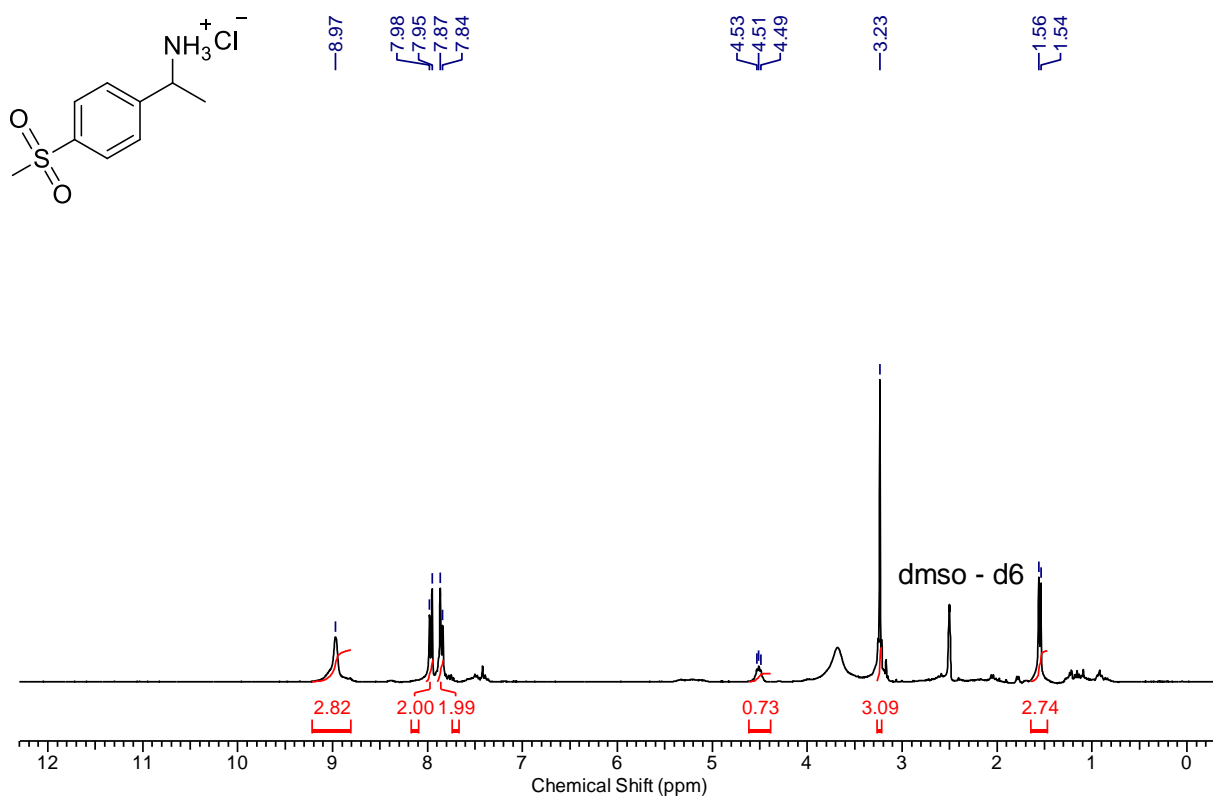
8:

9:

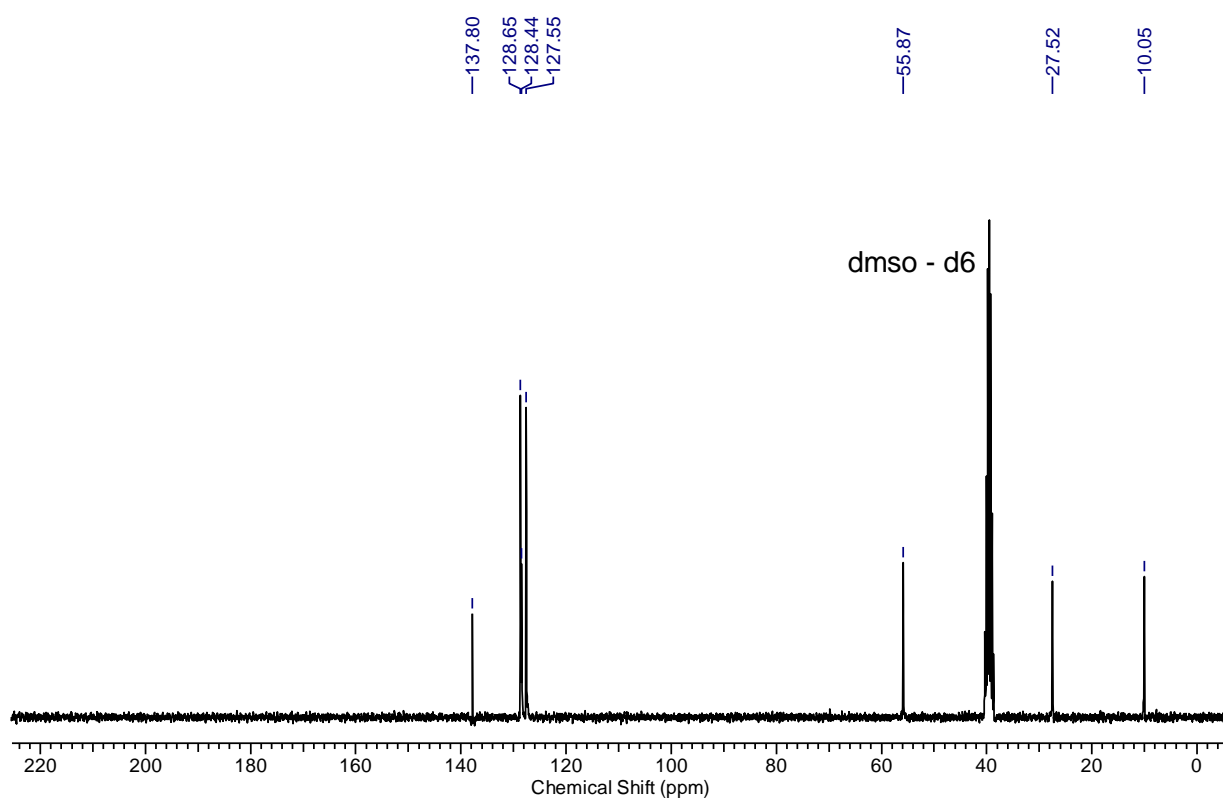
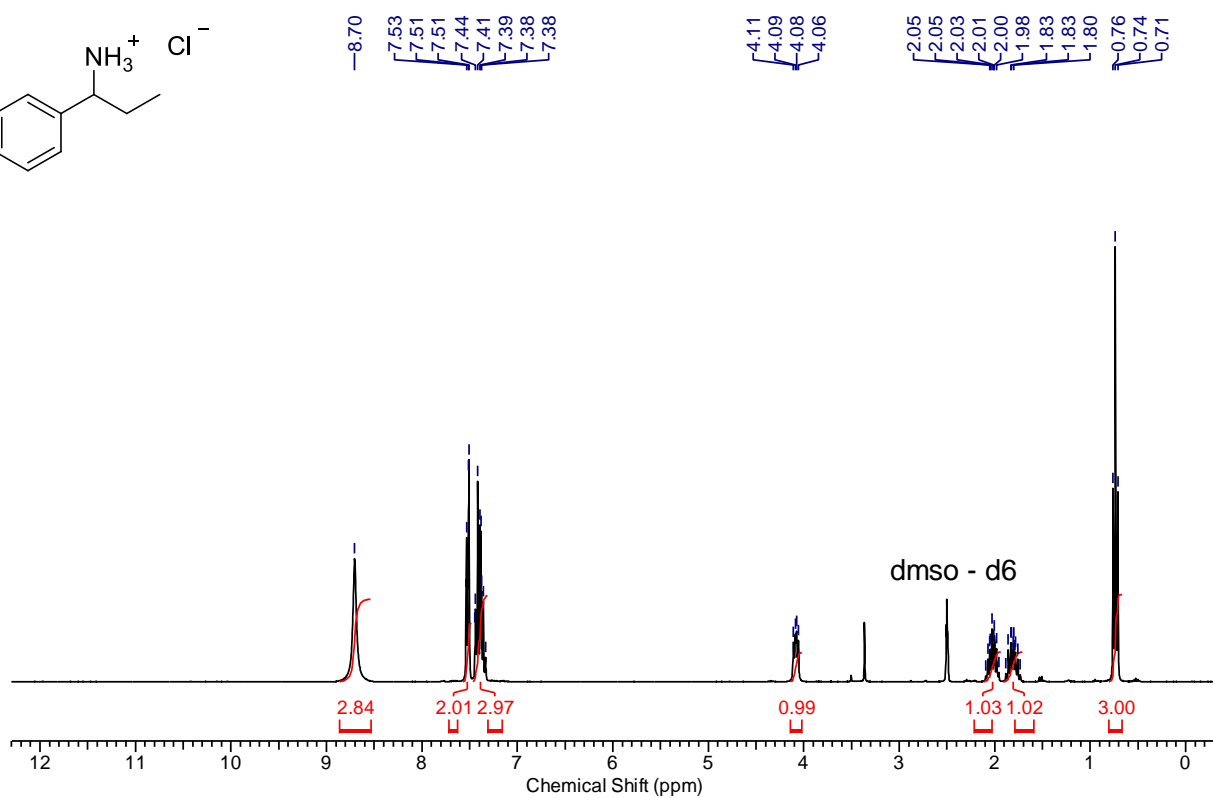
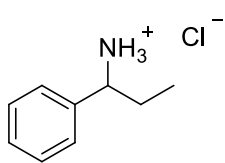


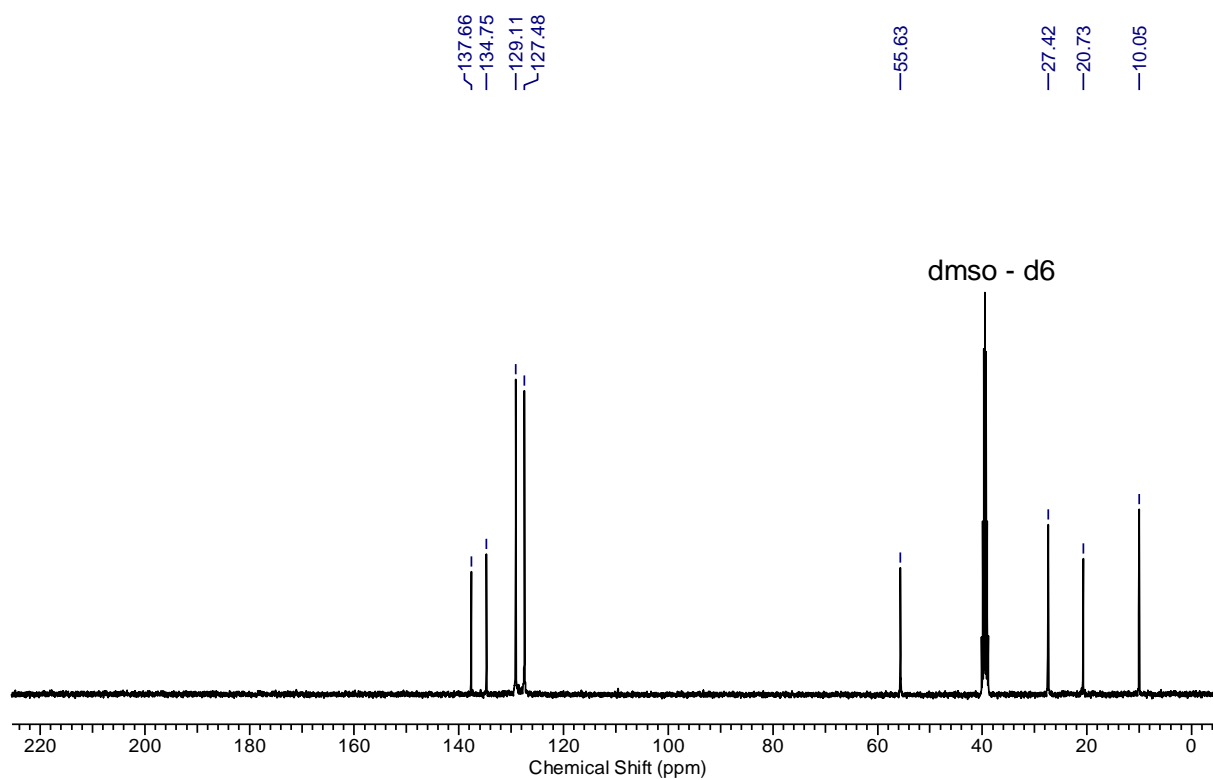
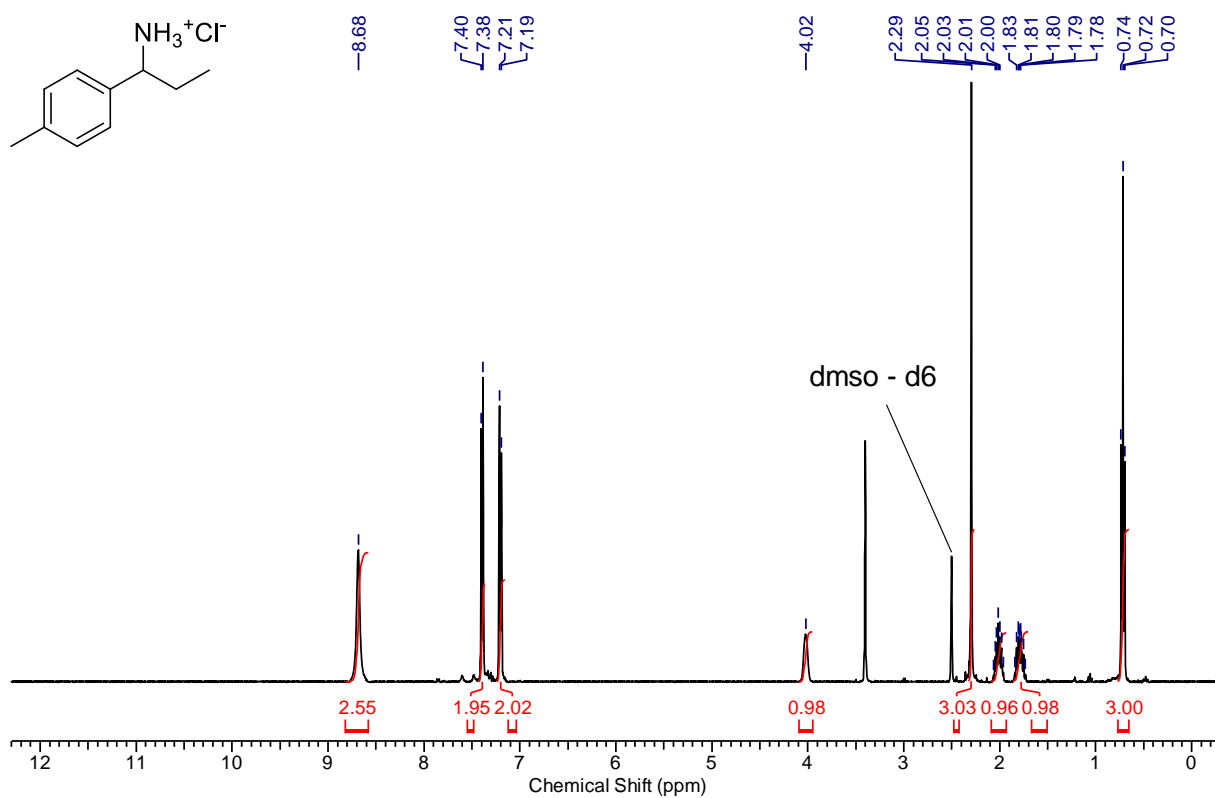
10:

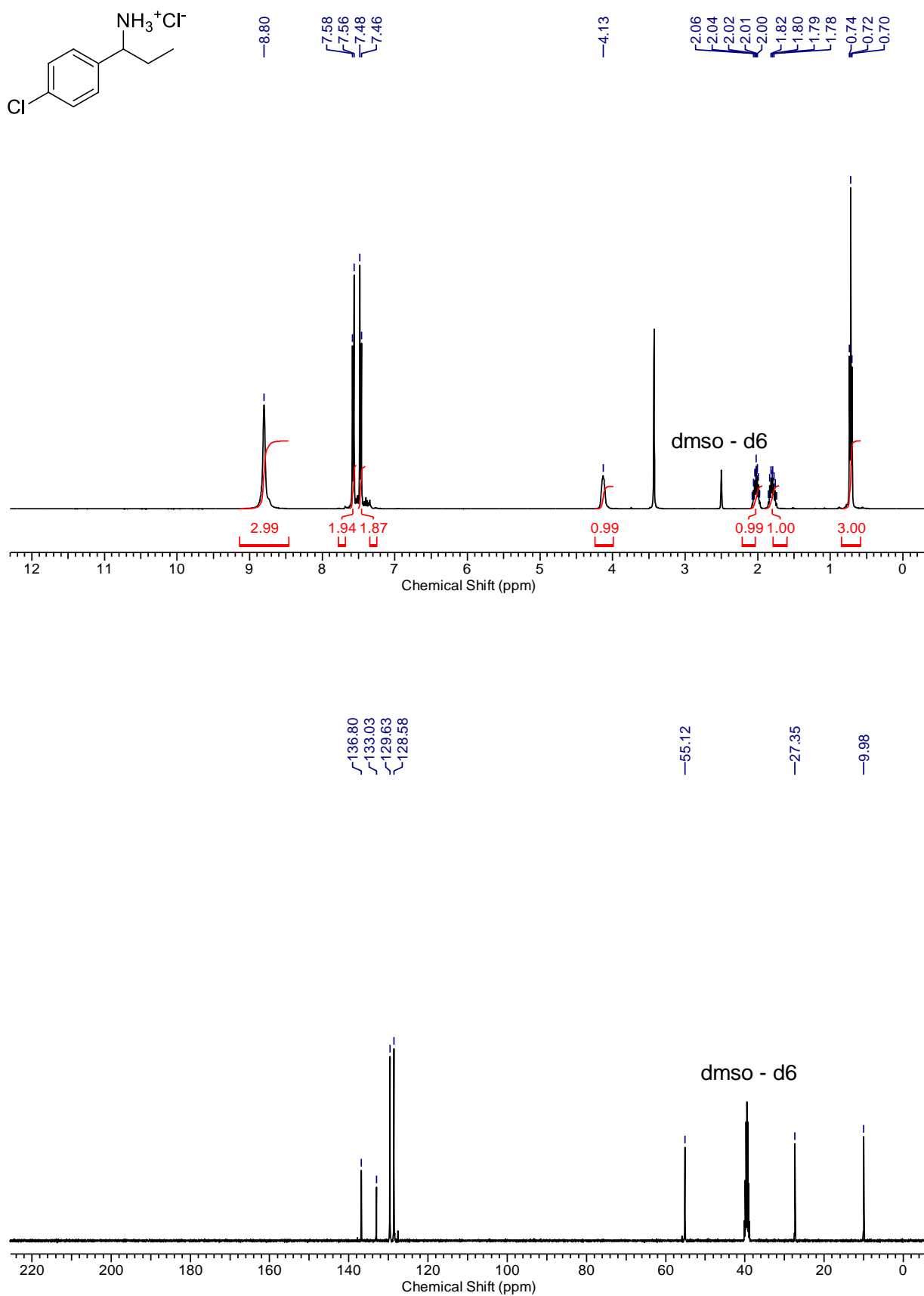


11:

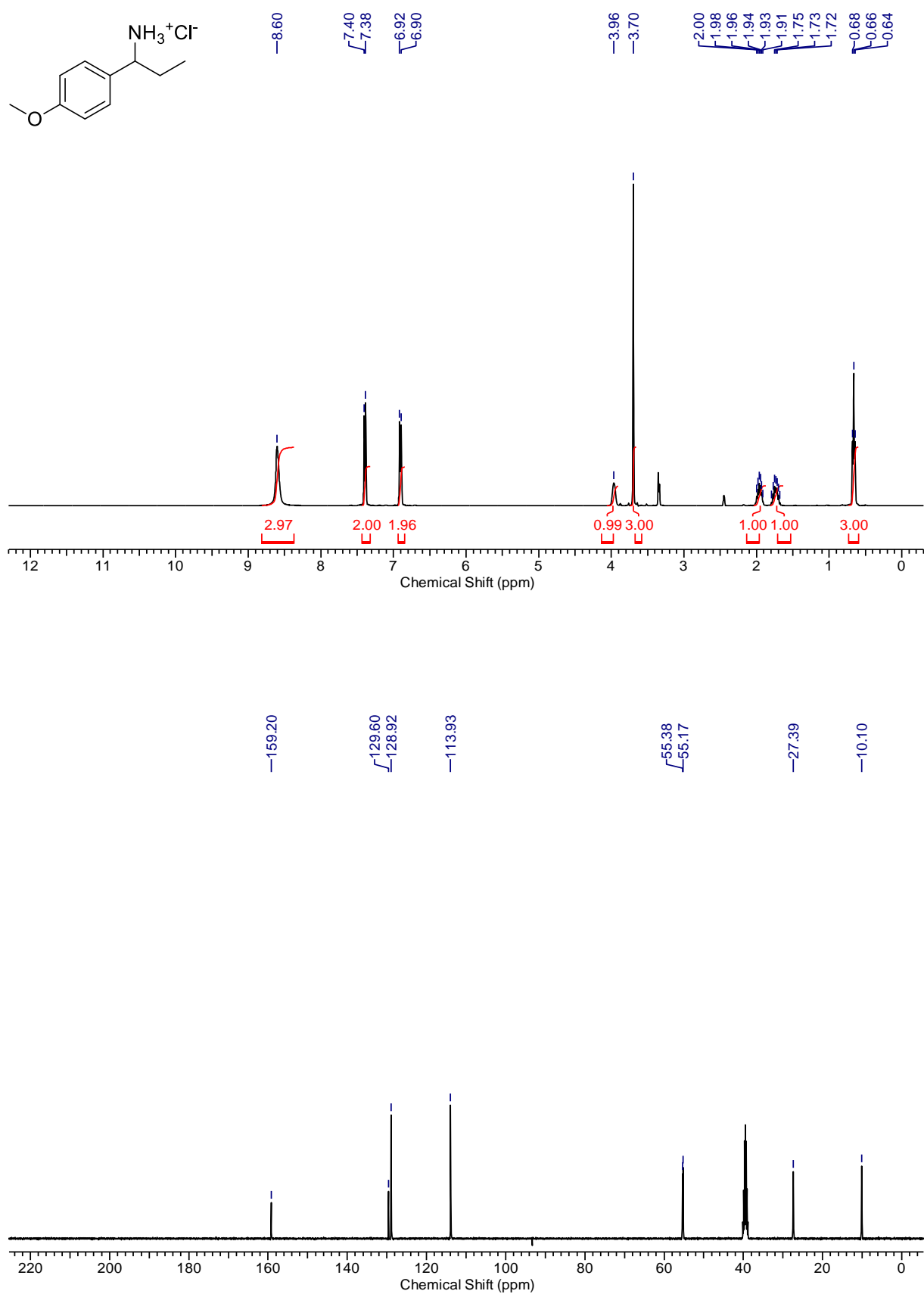
12:



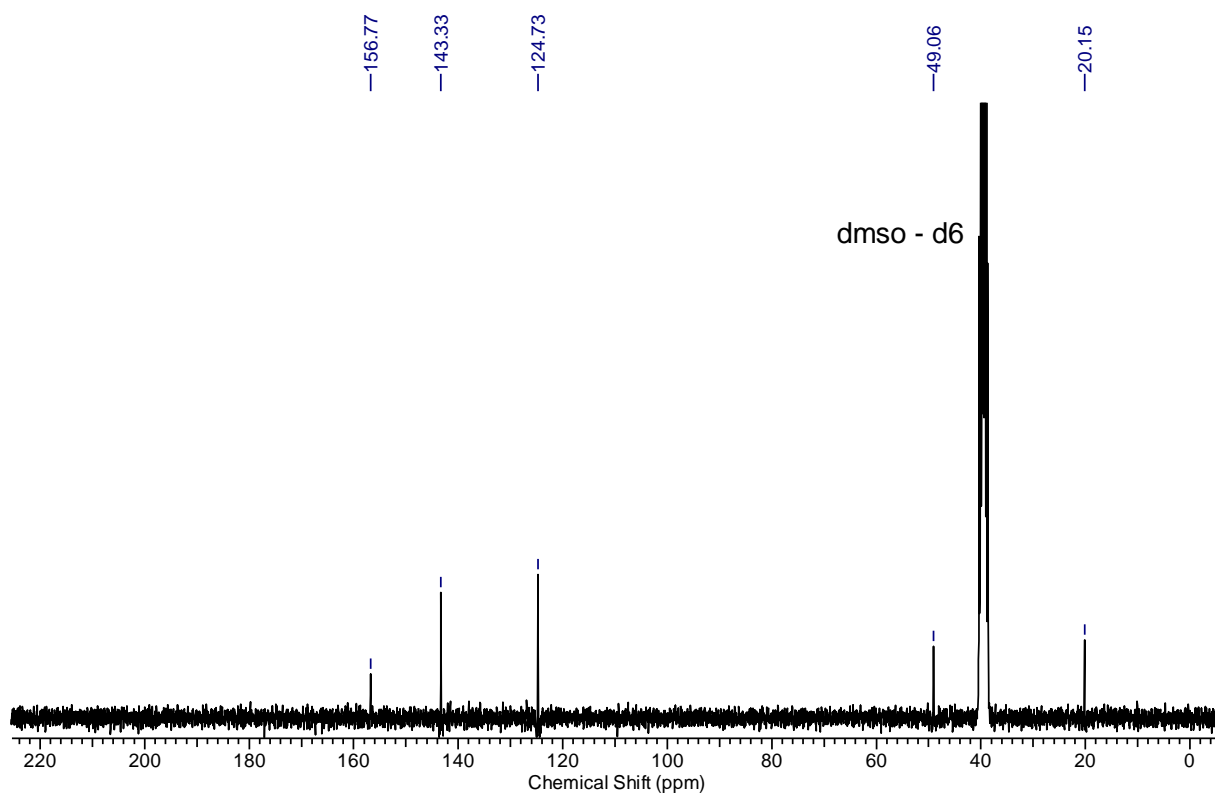
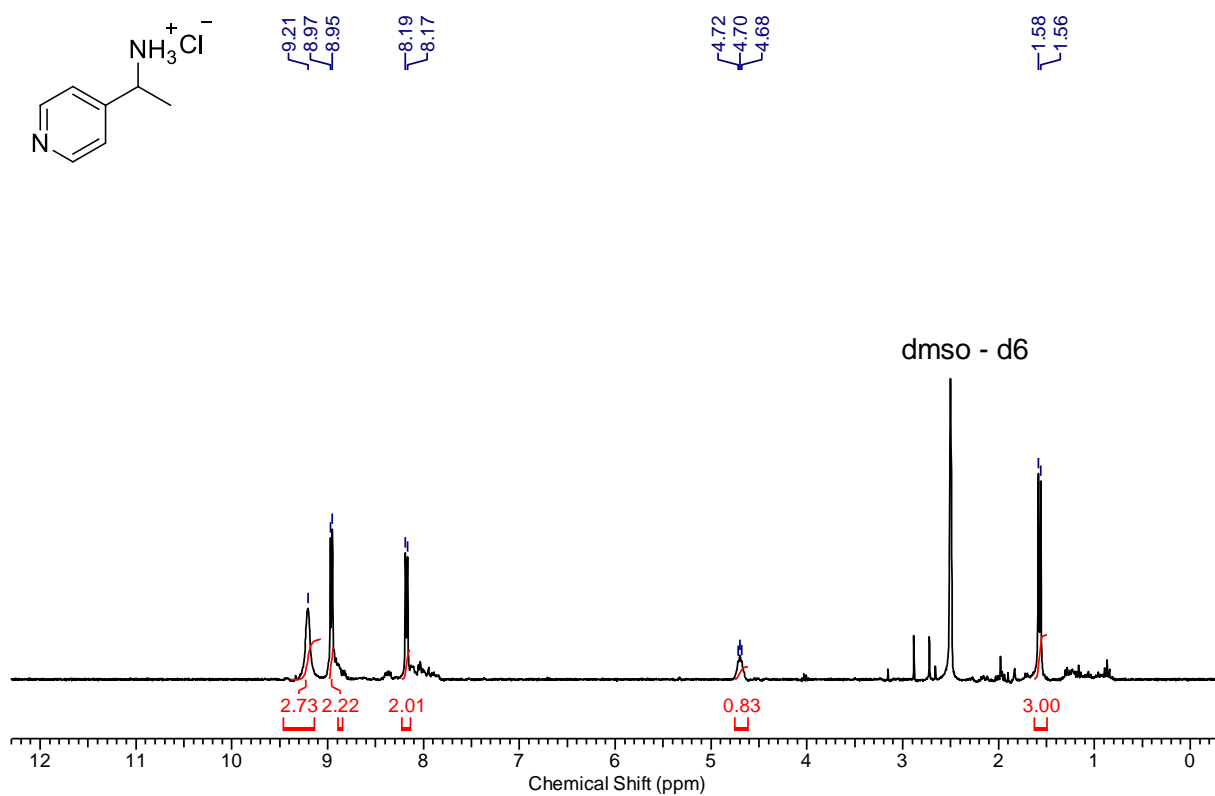
13:

14:

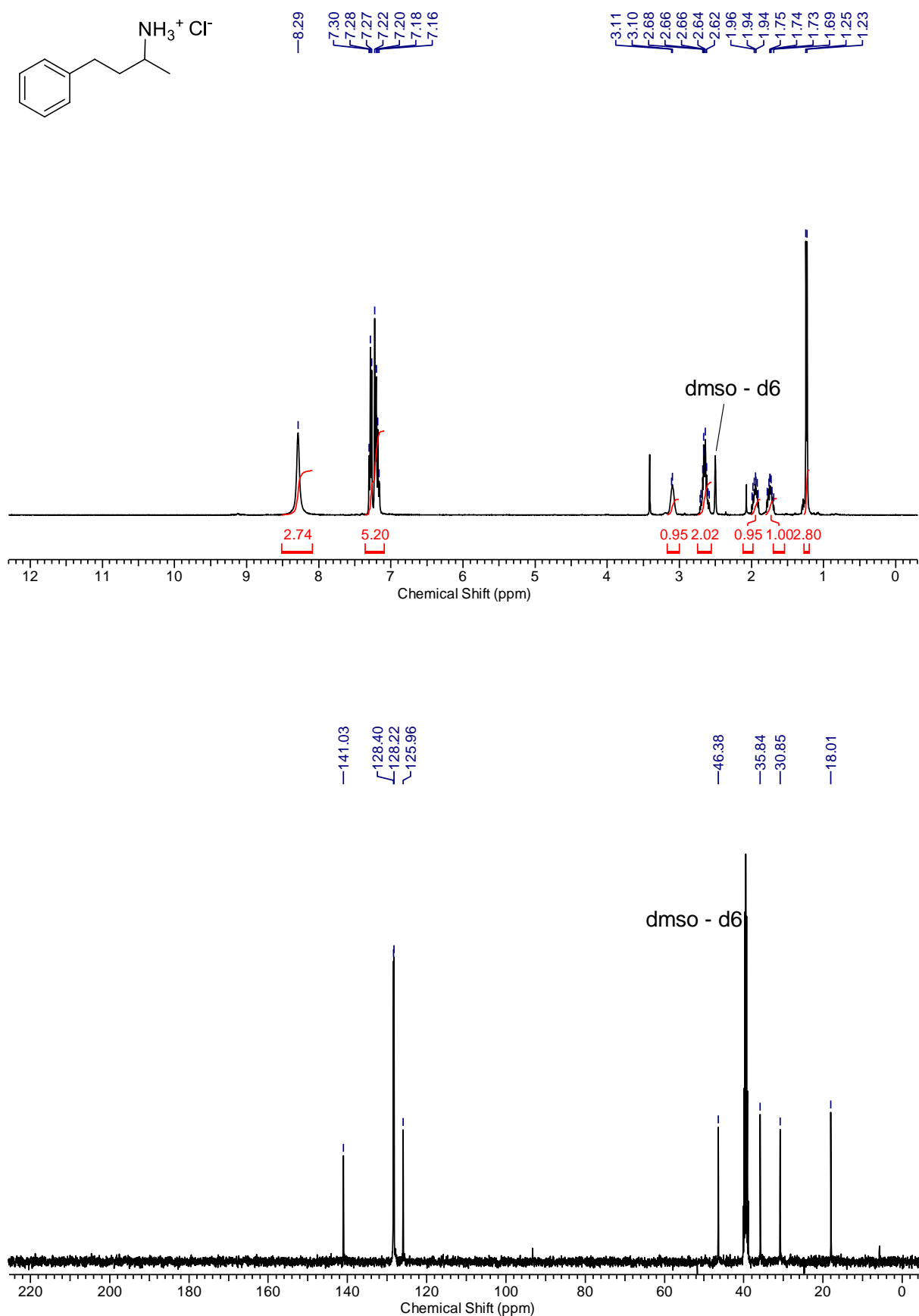
15:

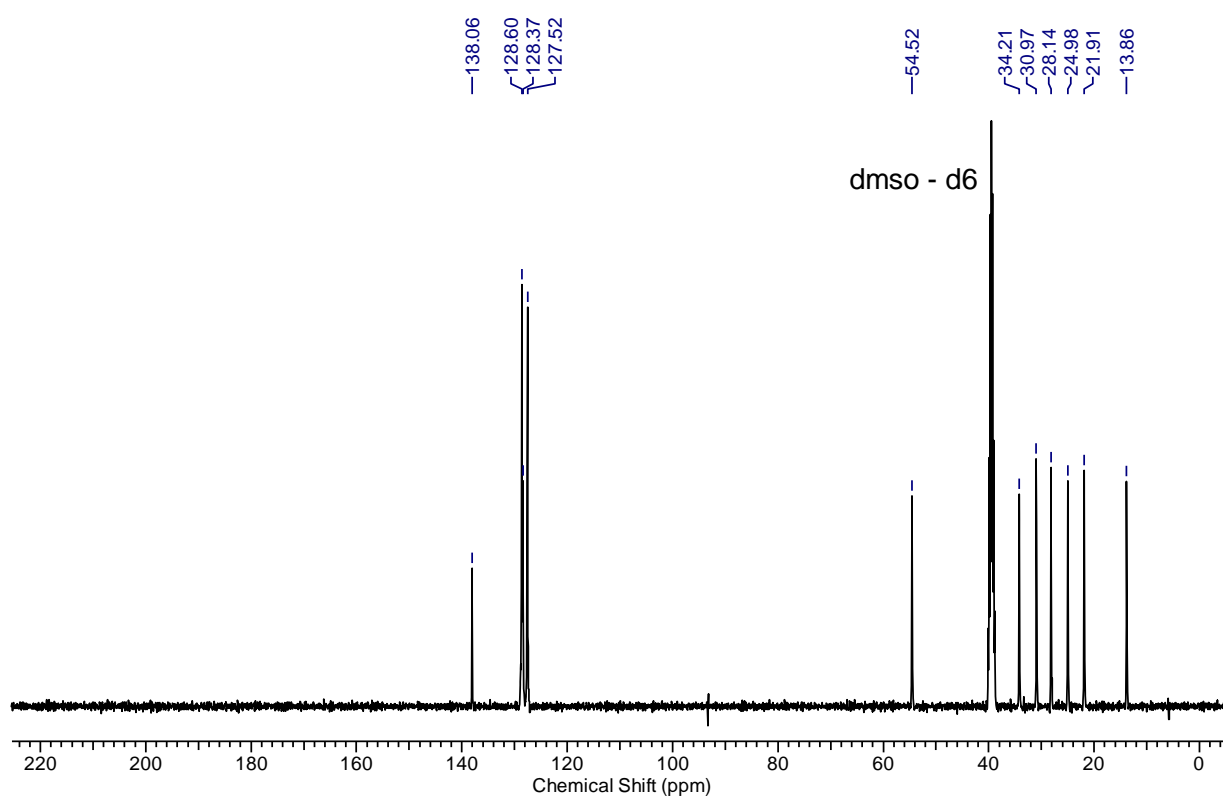
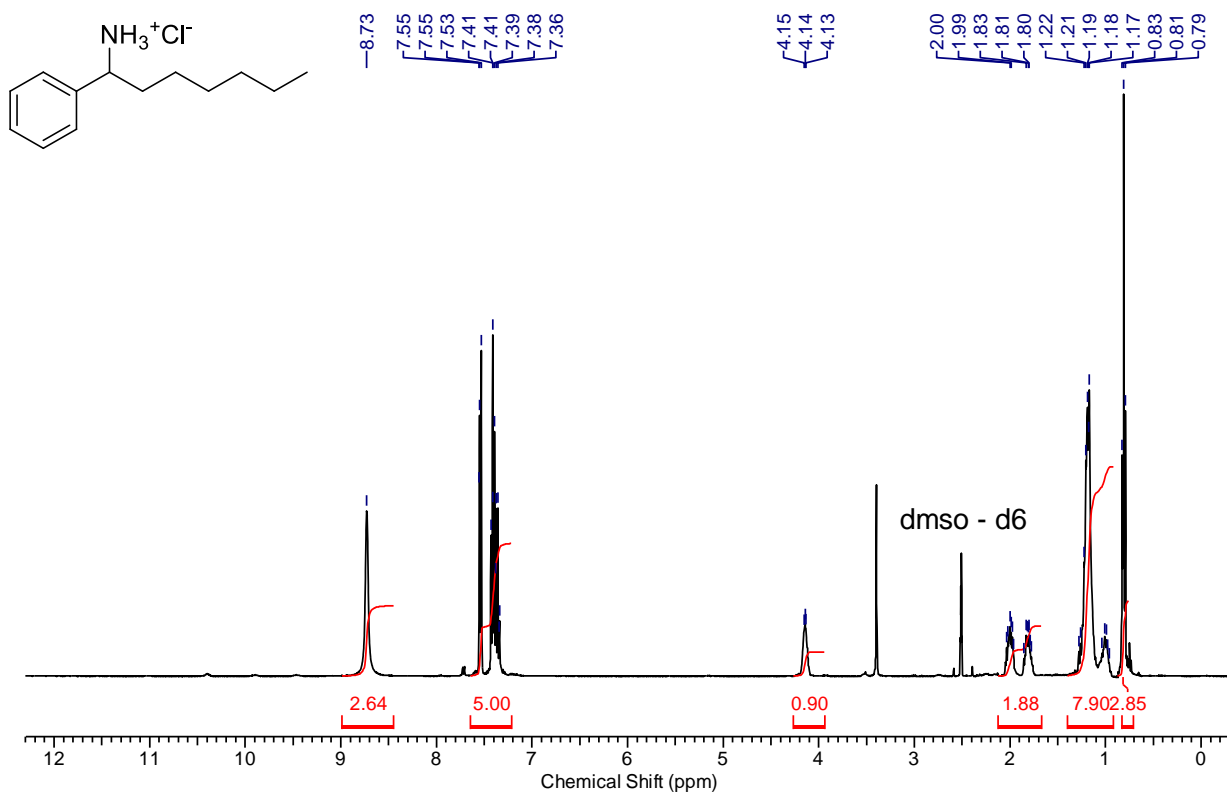


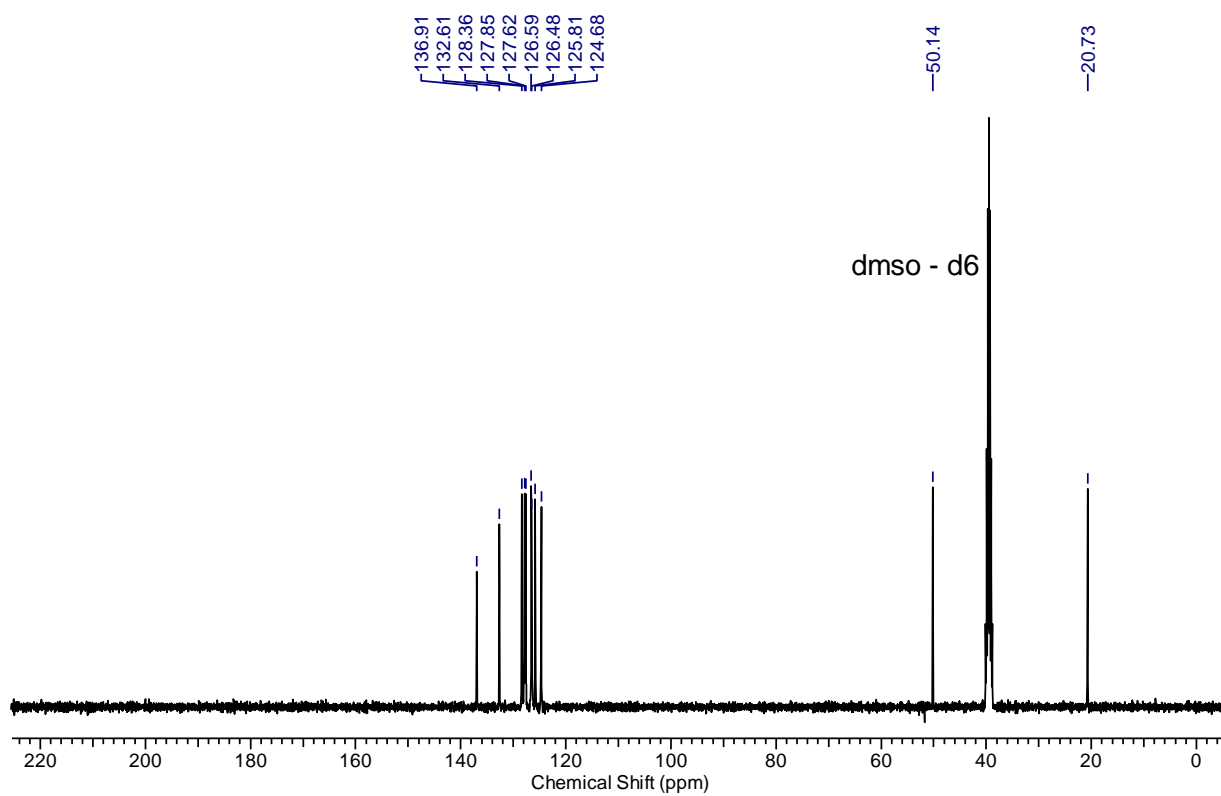
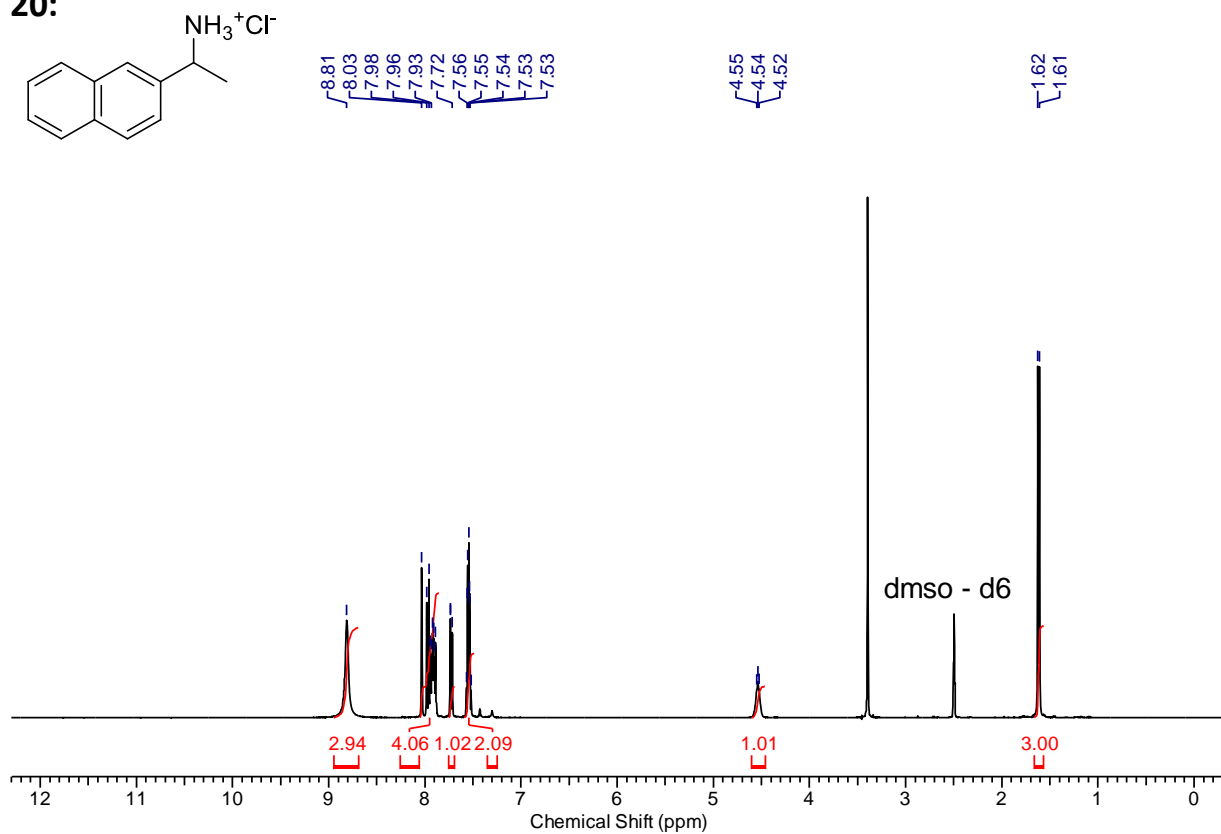
17:

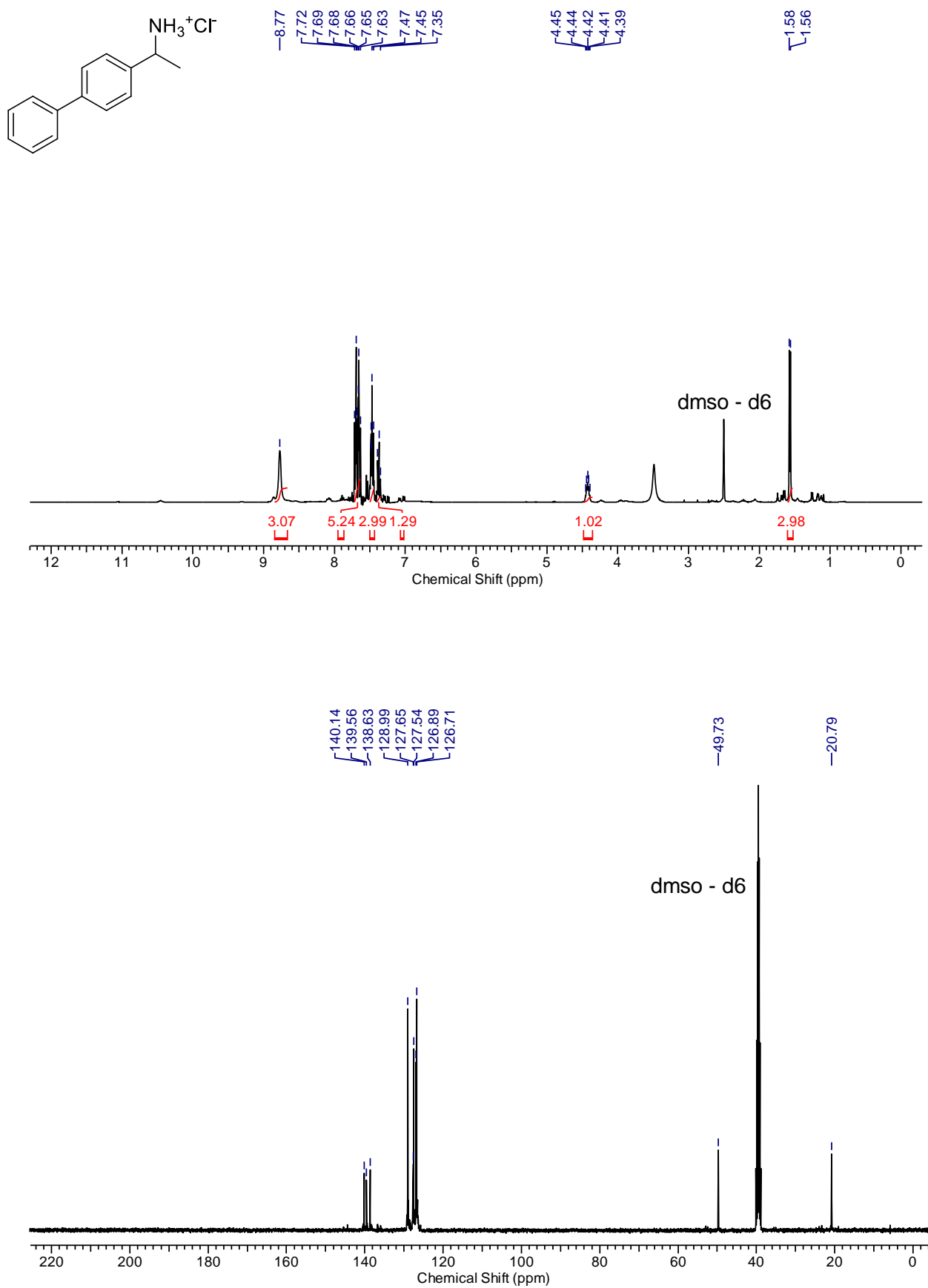


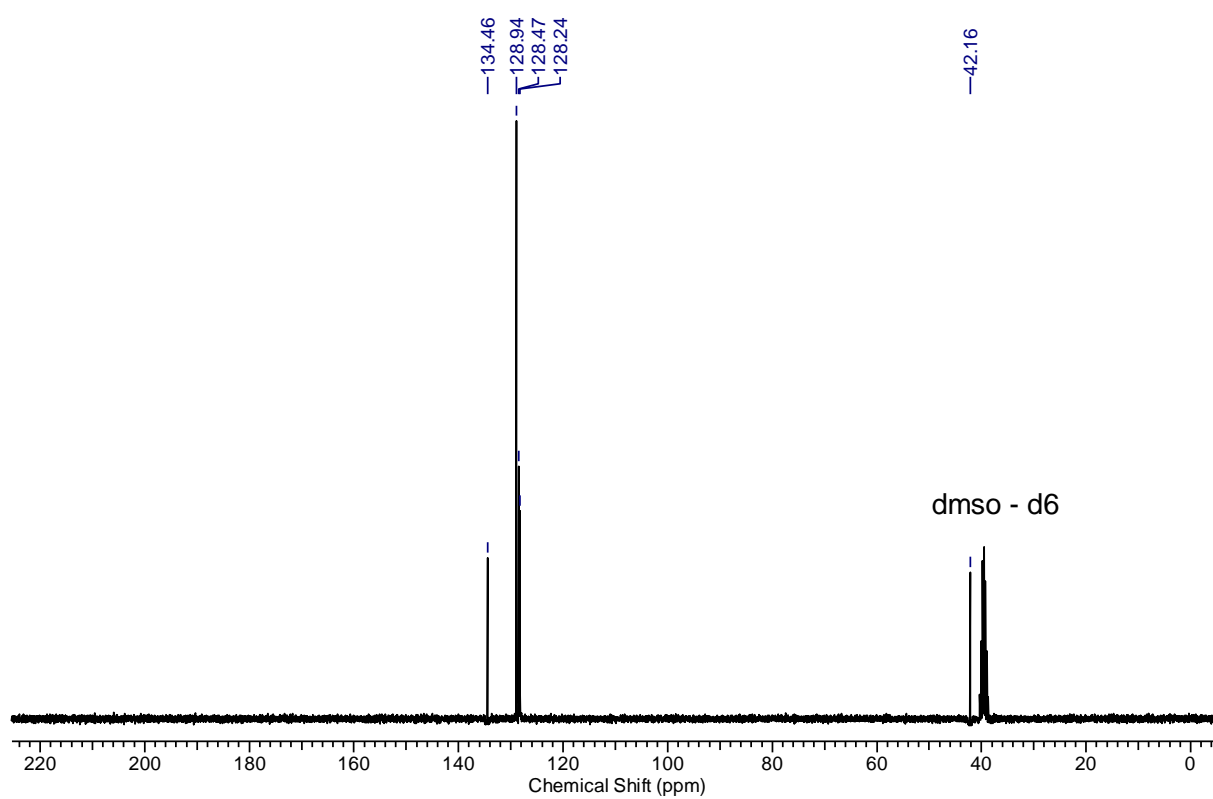
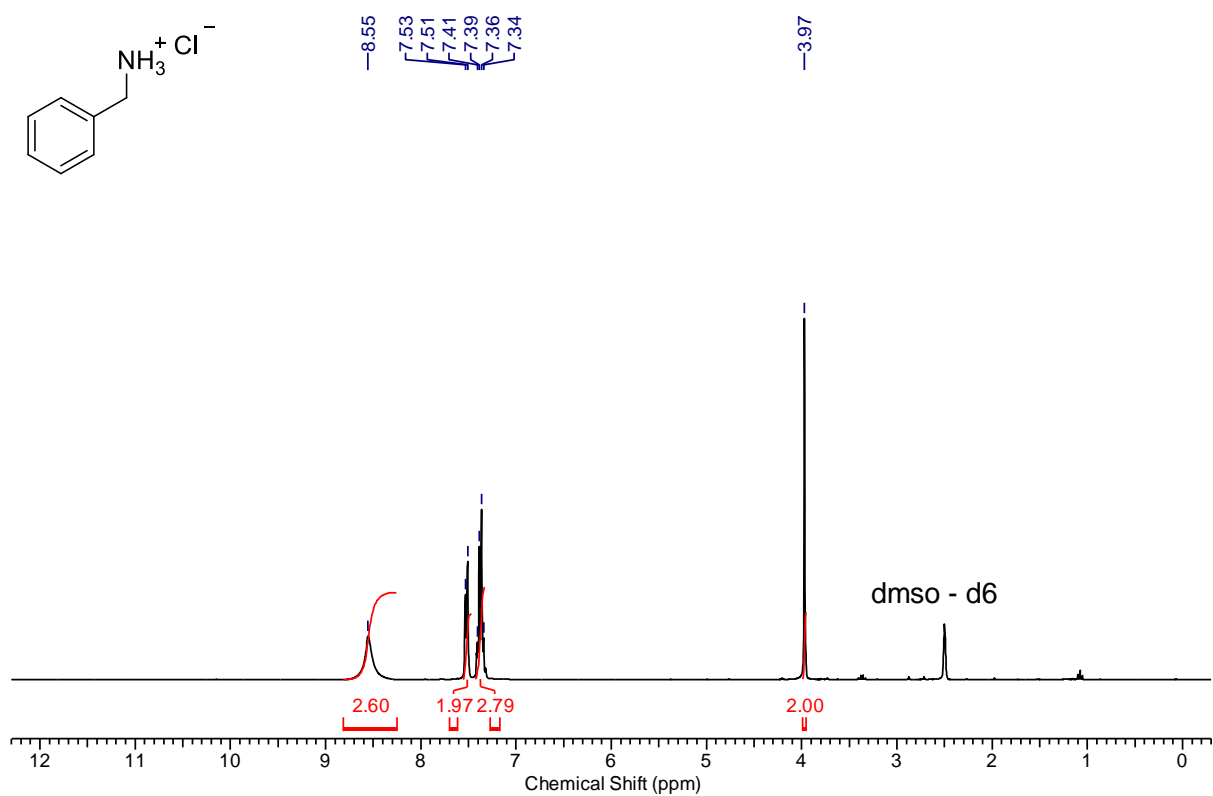
18:

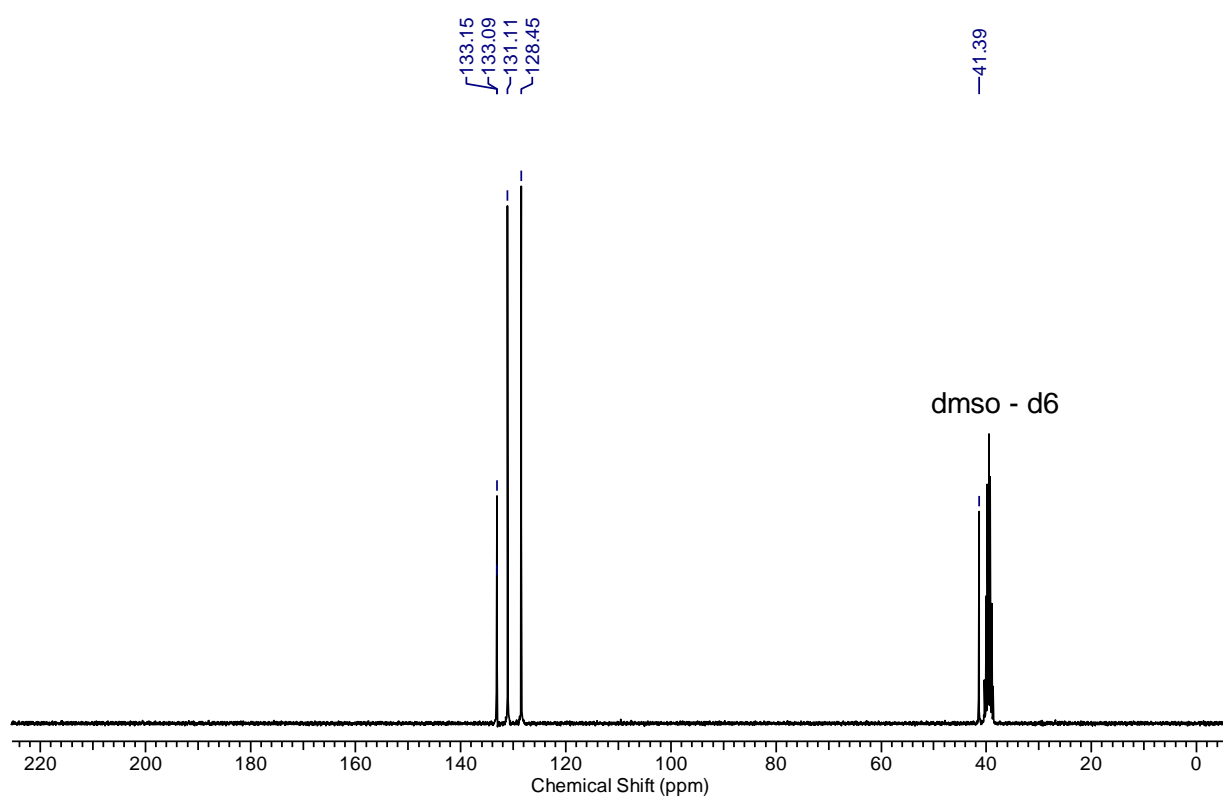
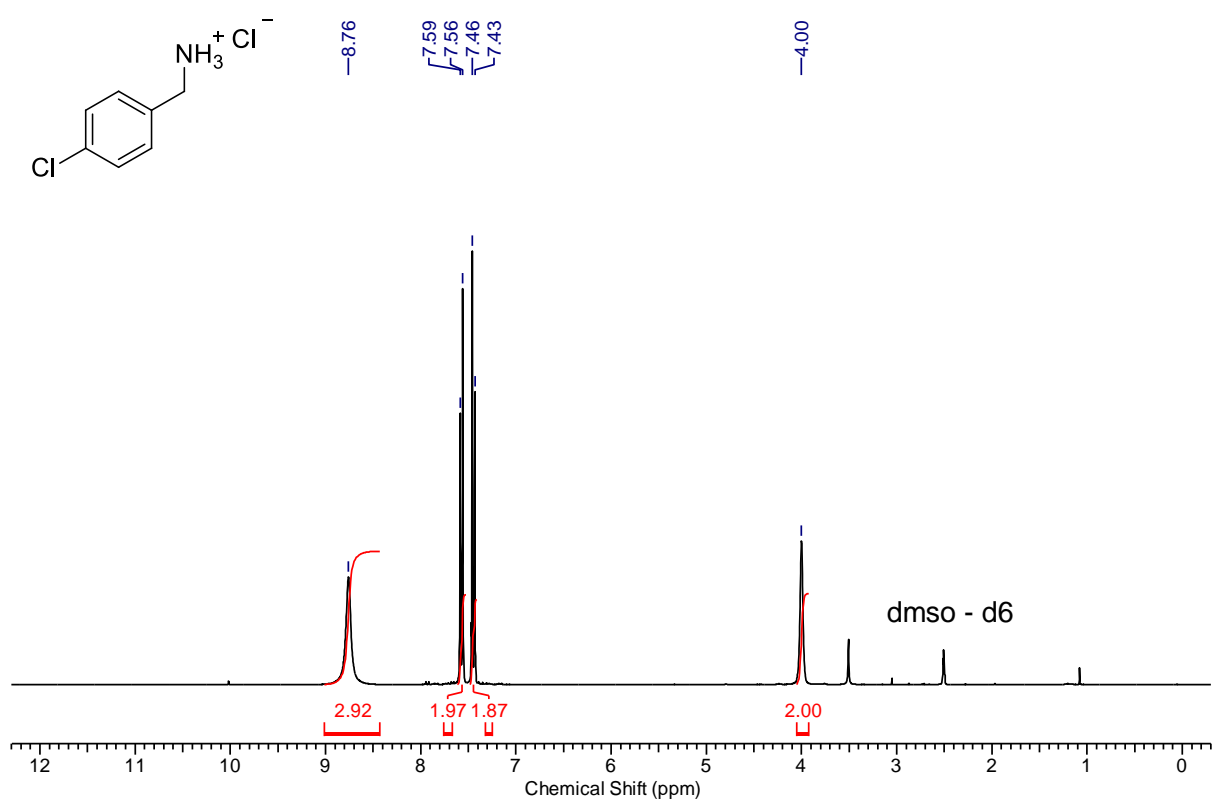


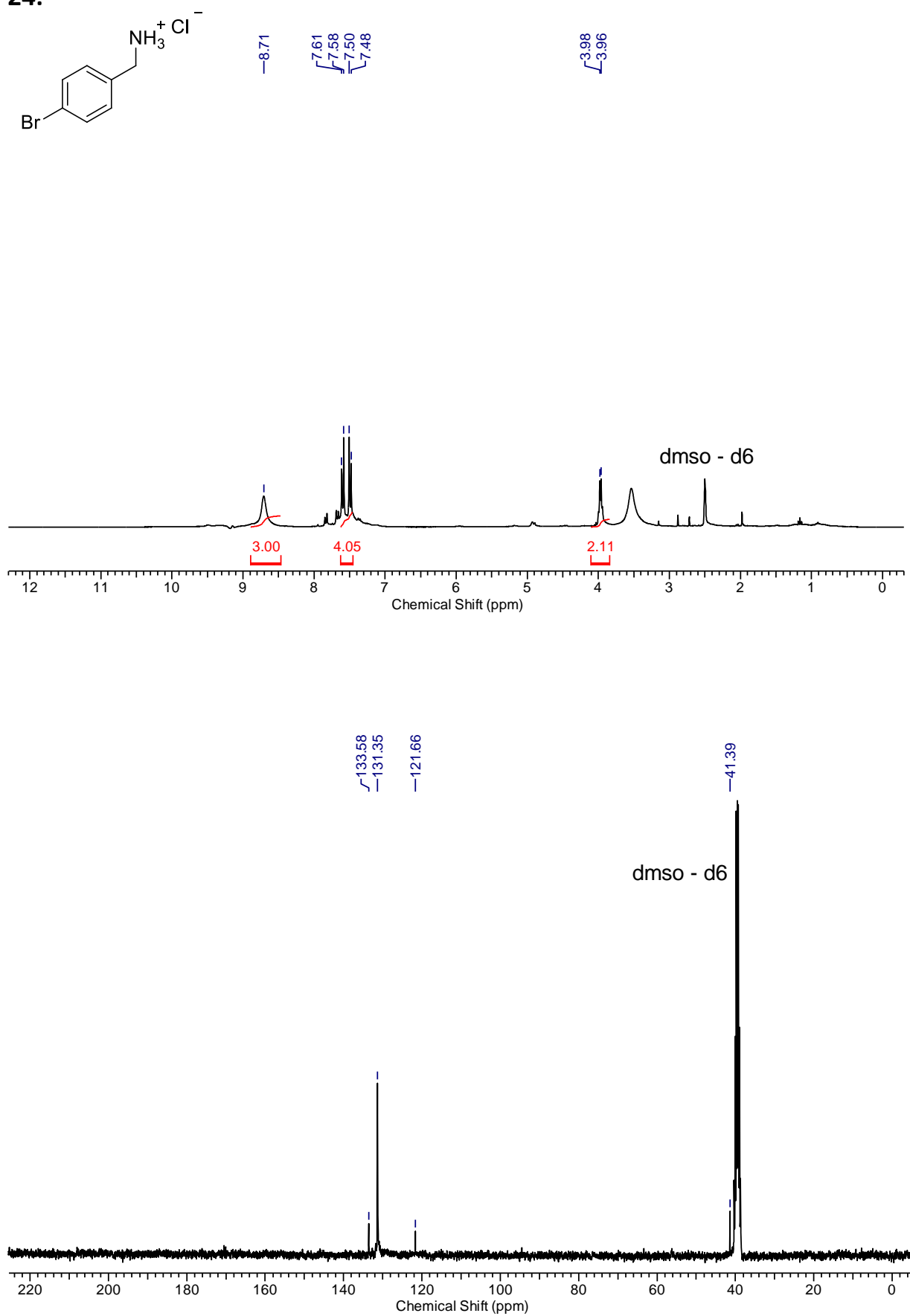
19:

20:

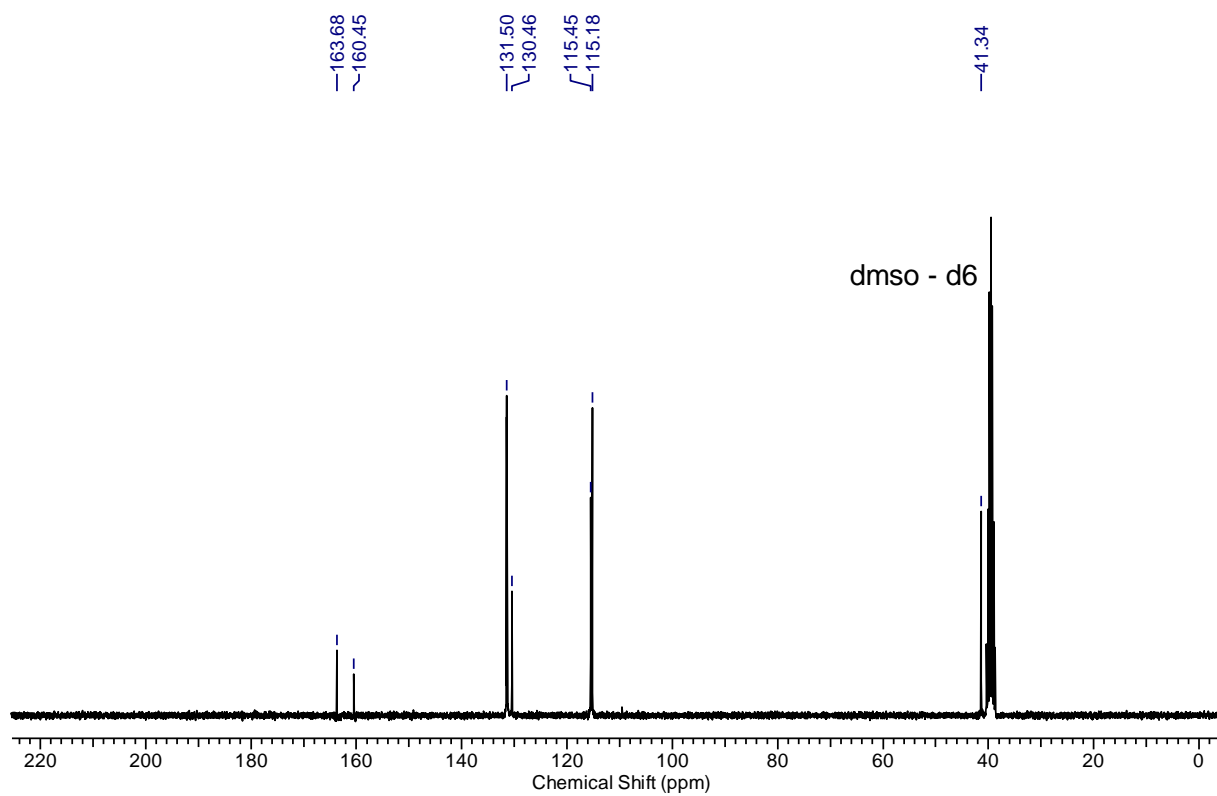
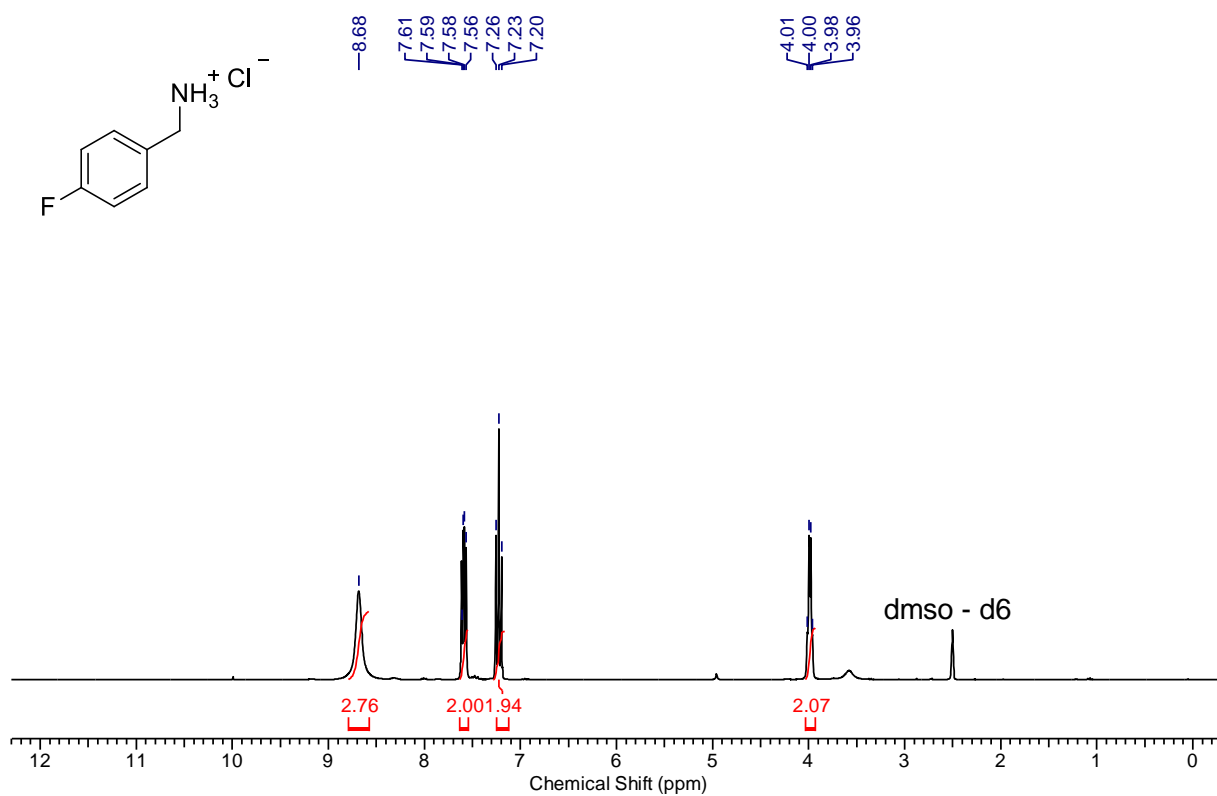
21:

22:

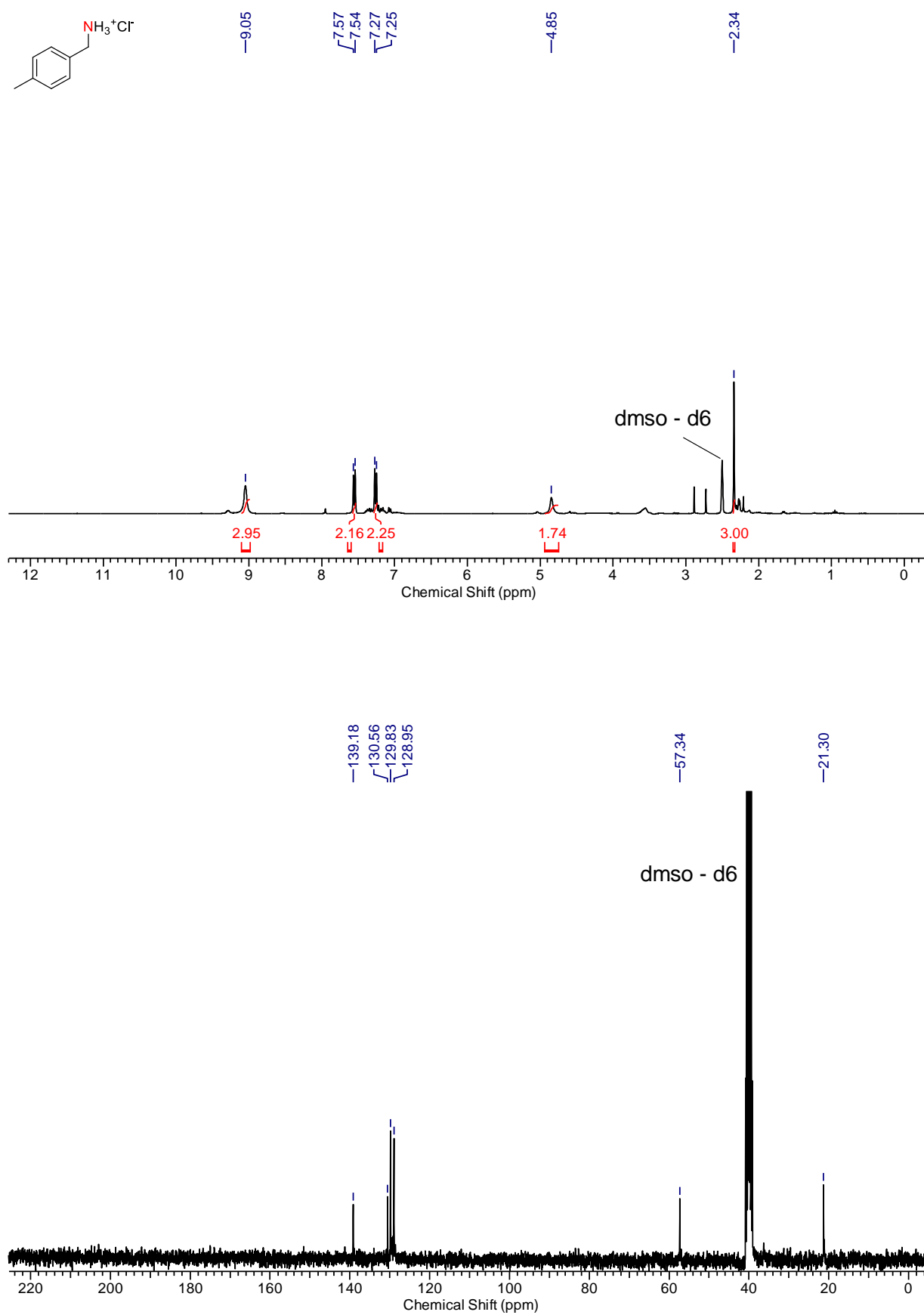
23:

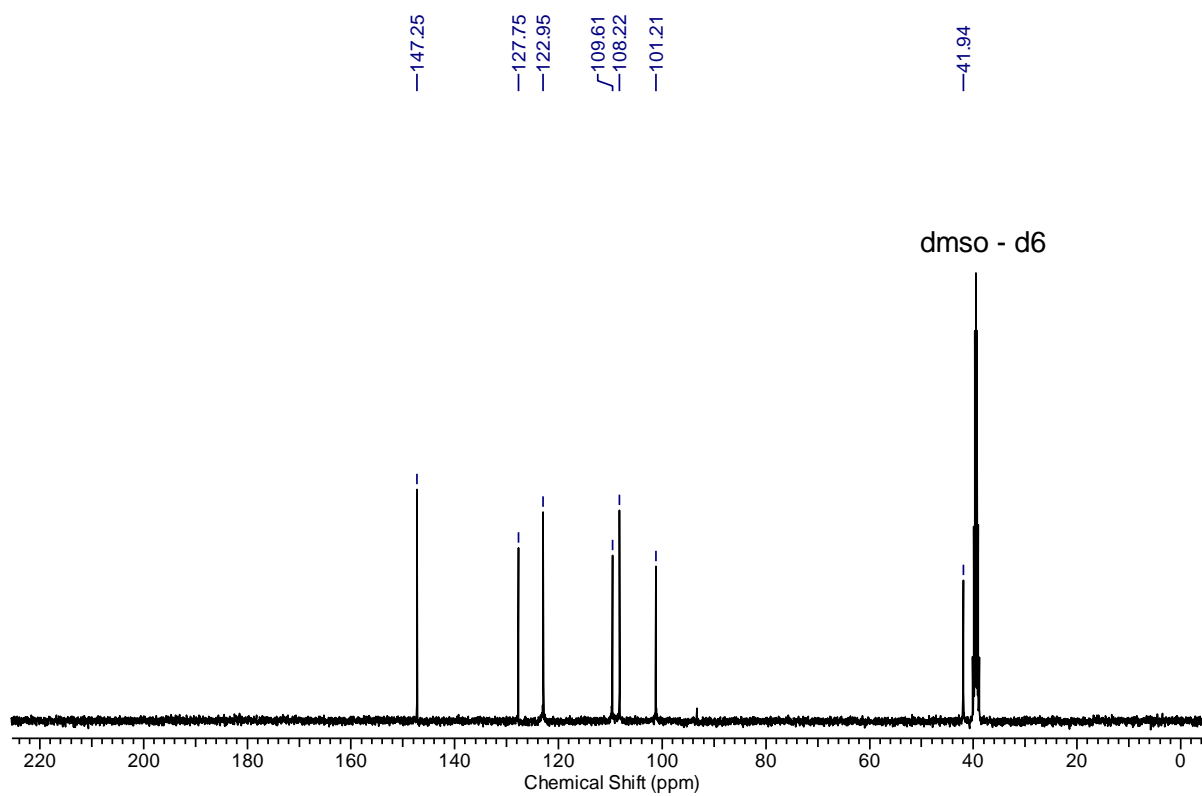
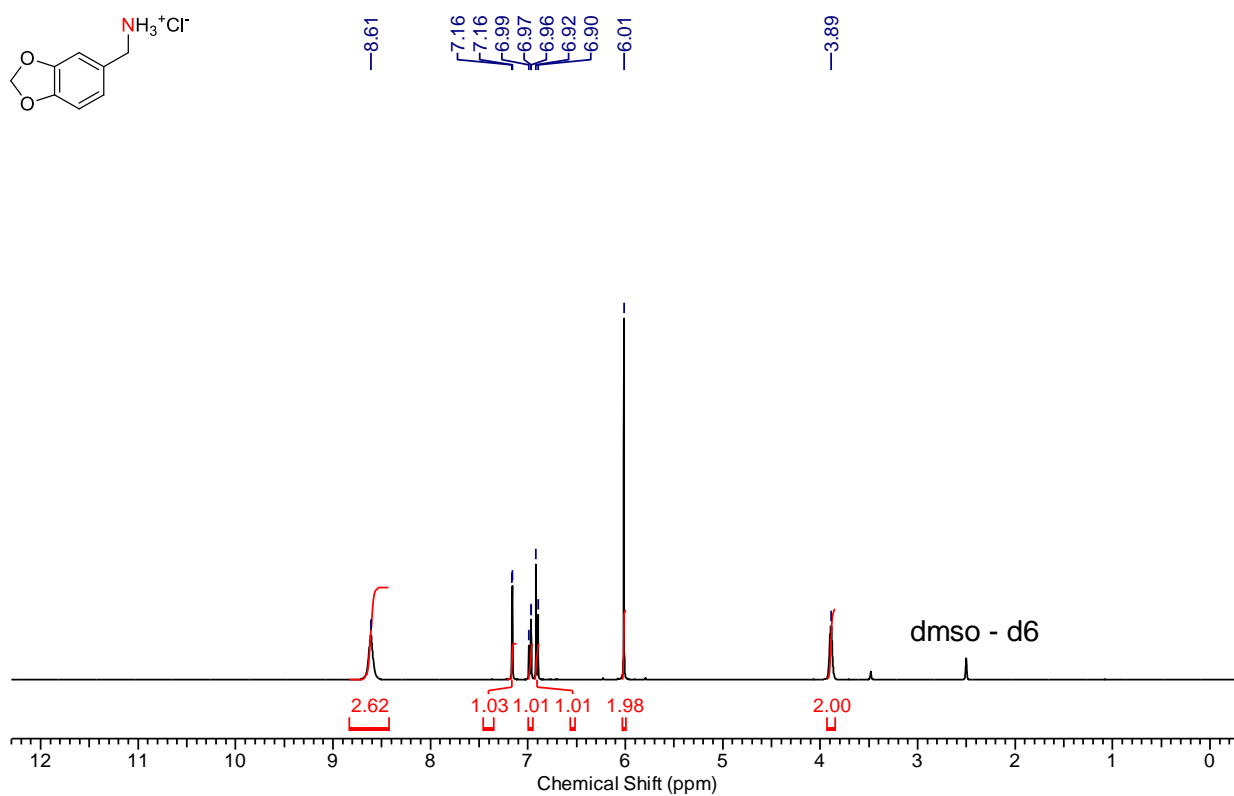
24:

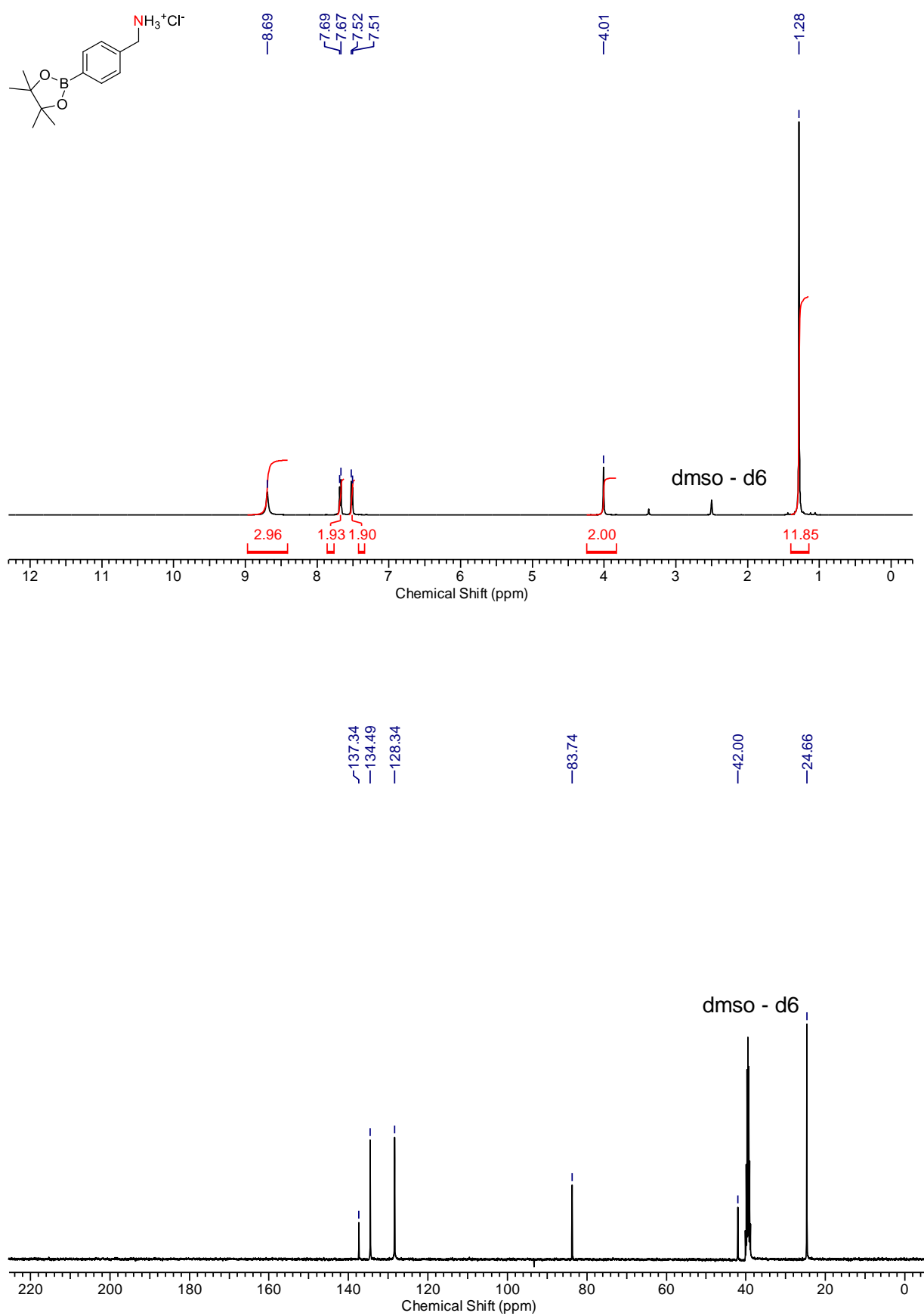
25:



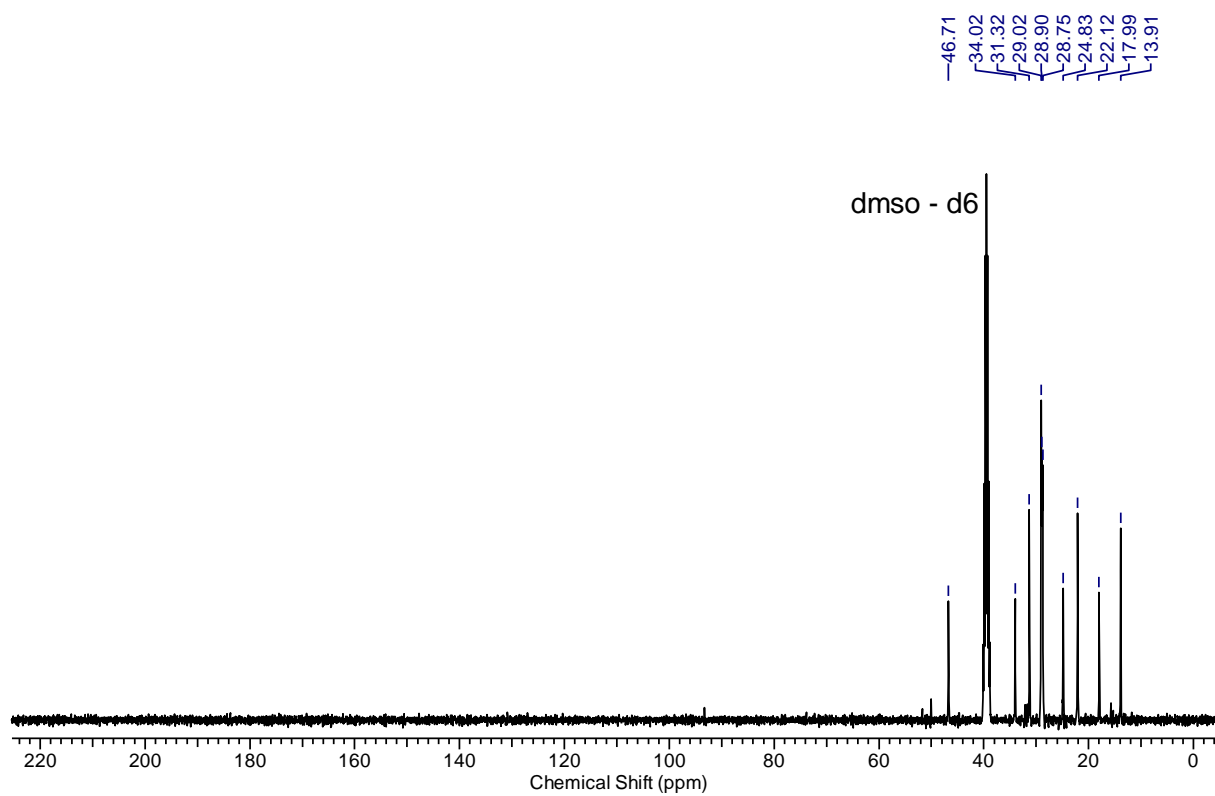
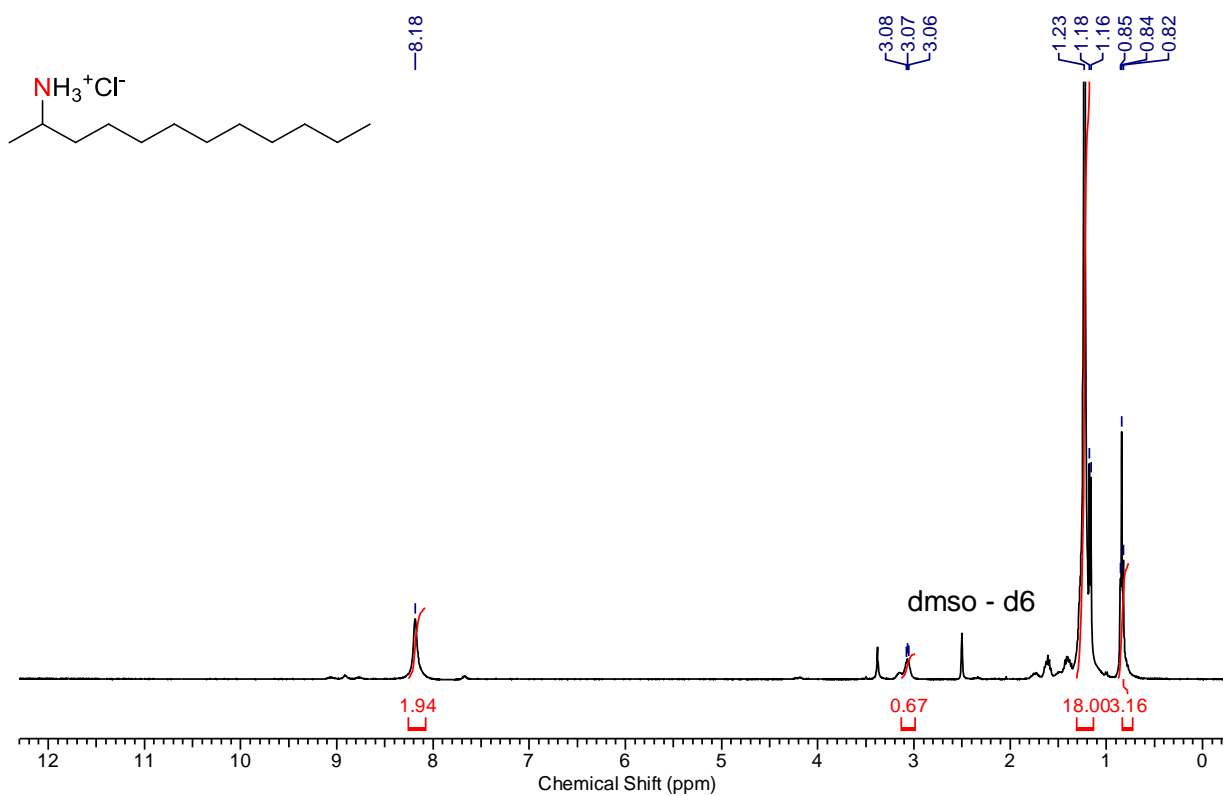
26:

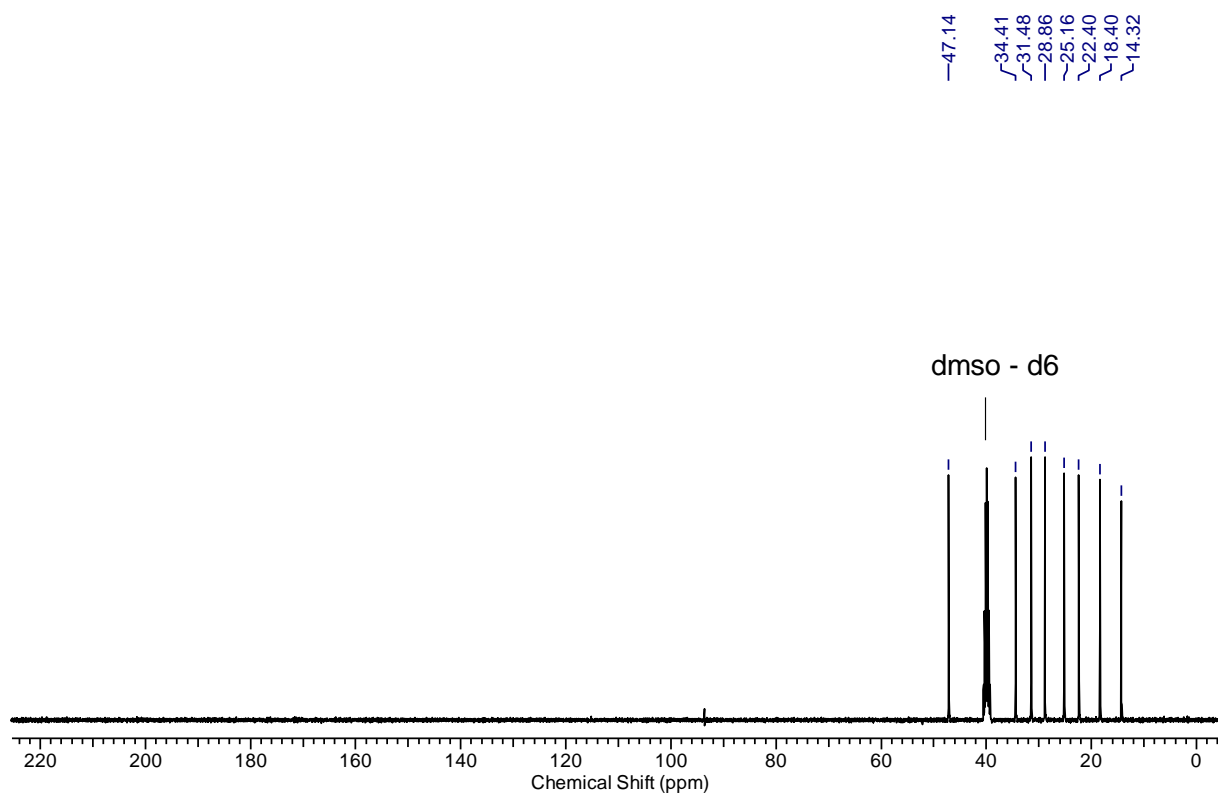
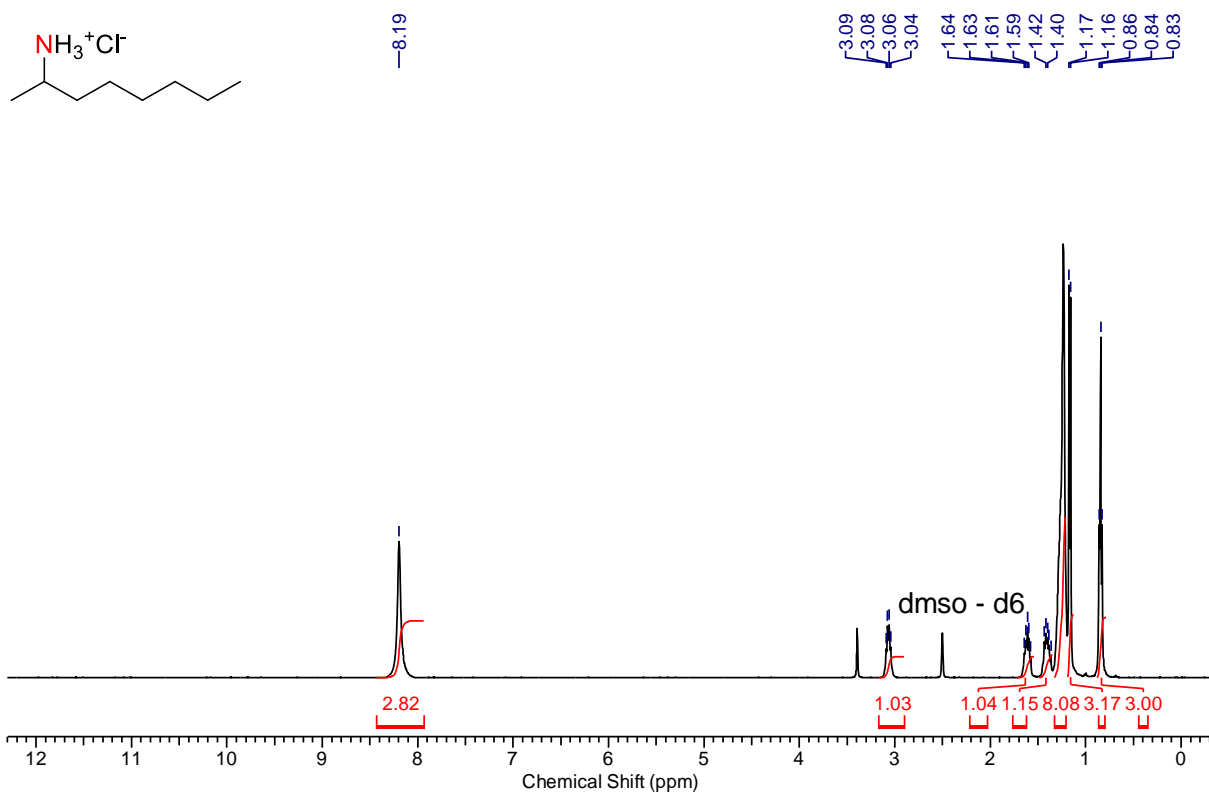


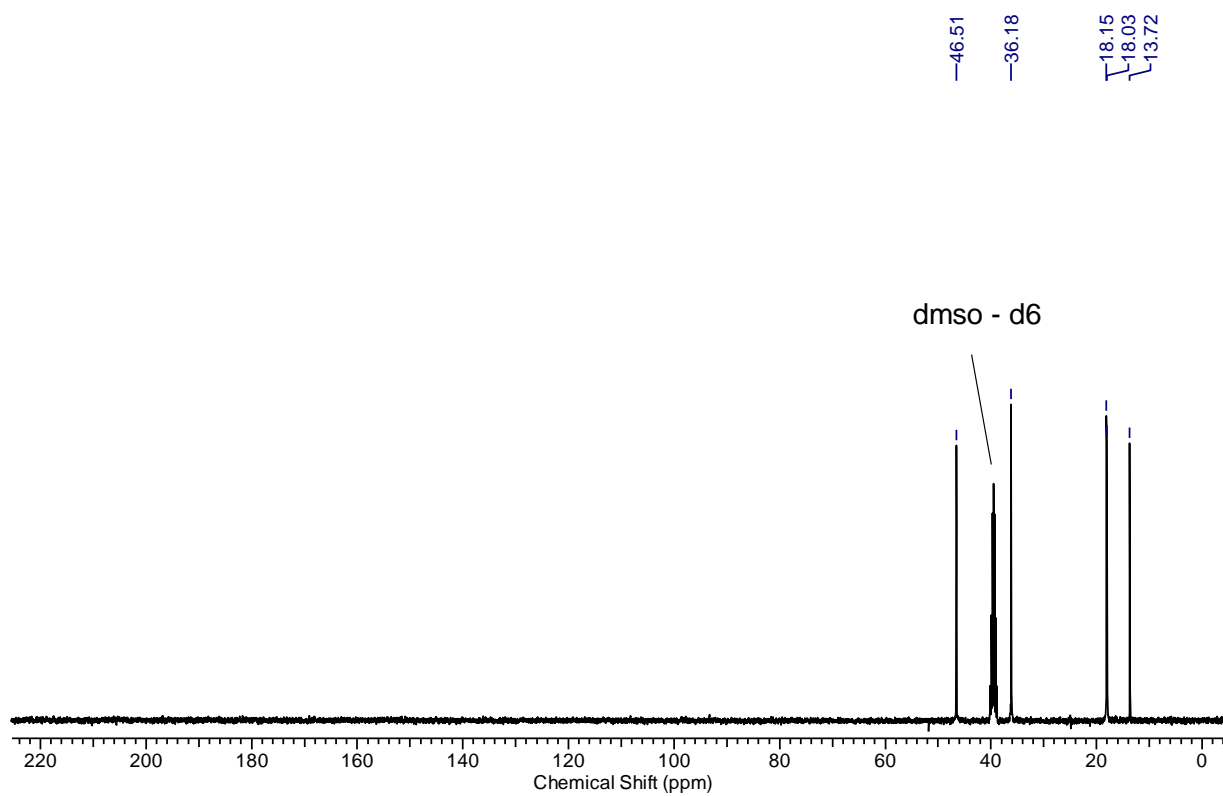
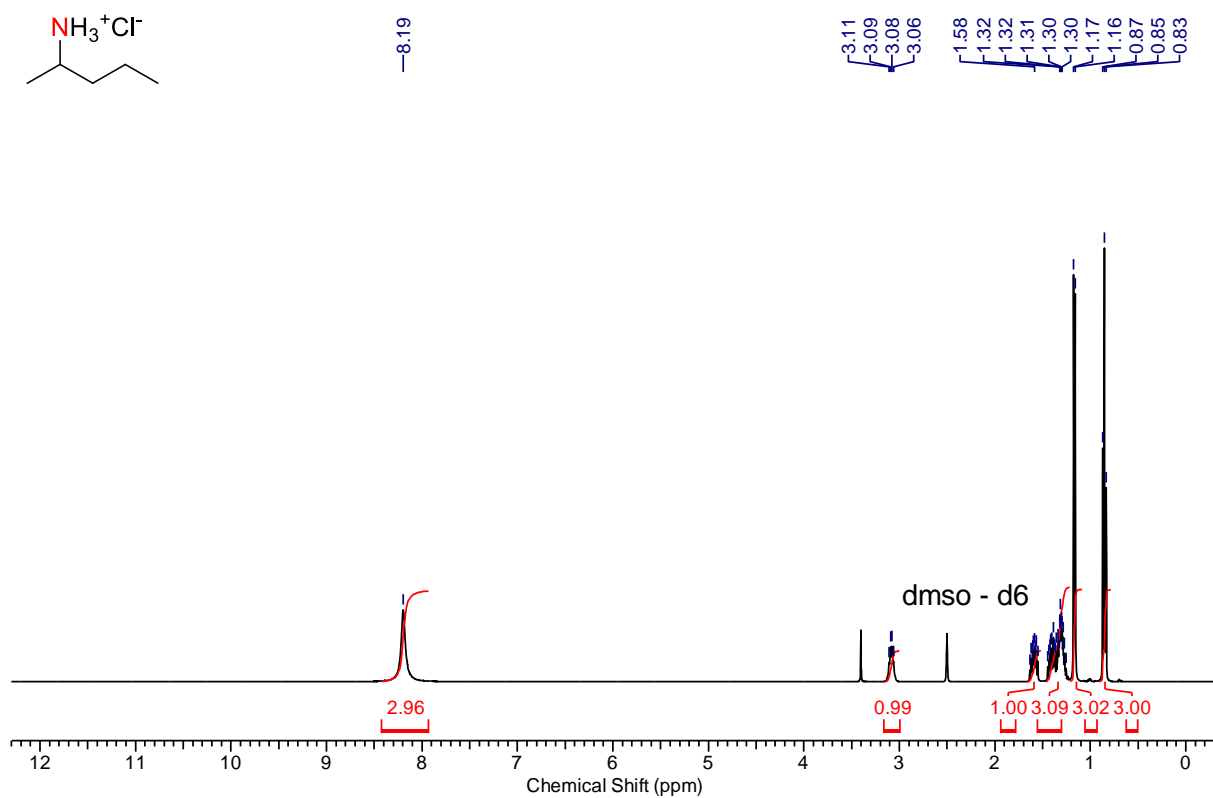
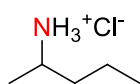
27:

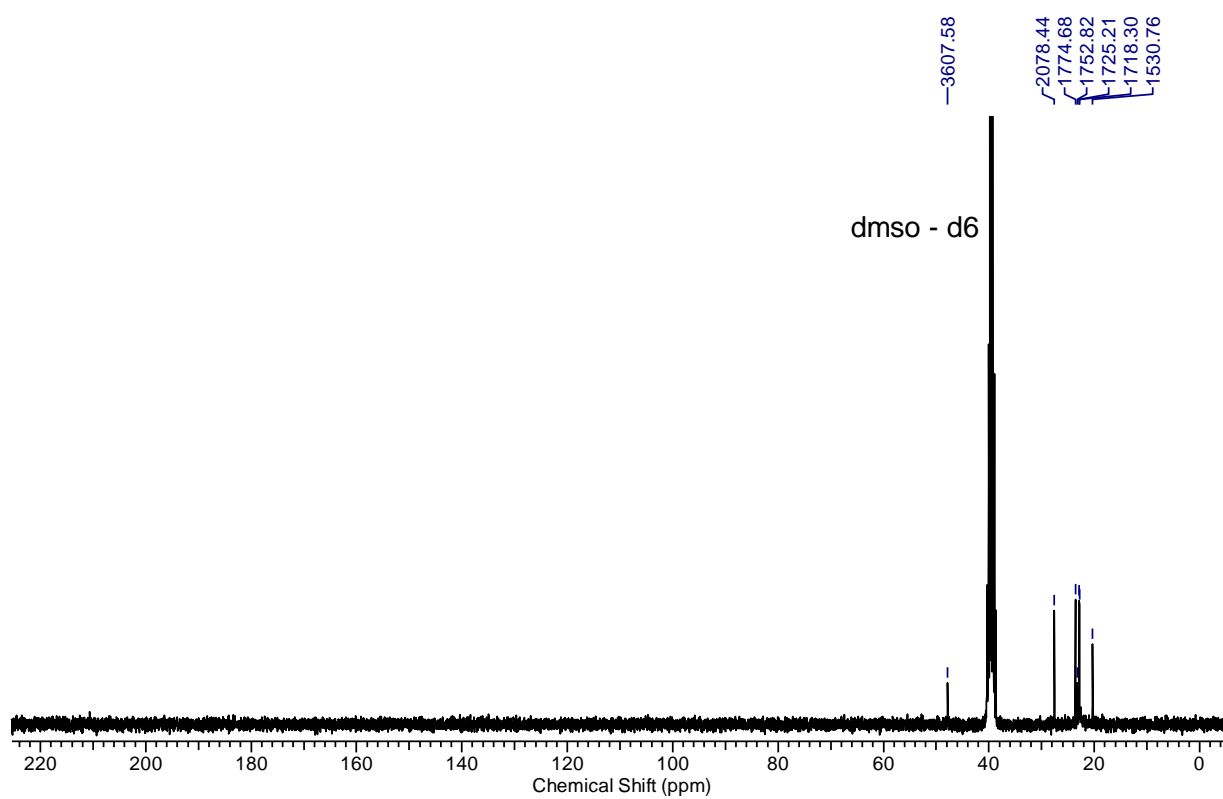
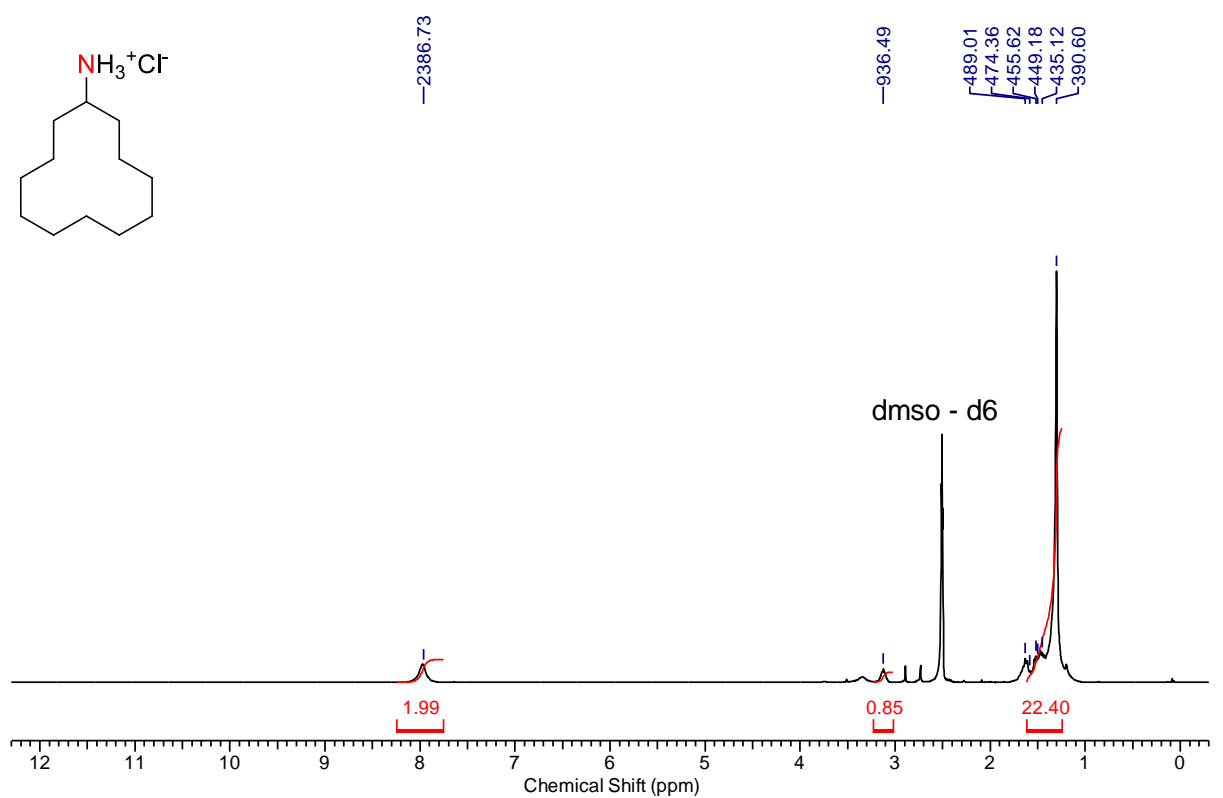
28:

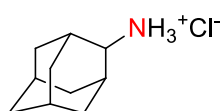
29:



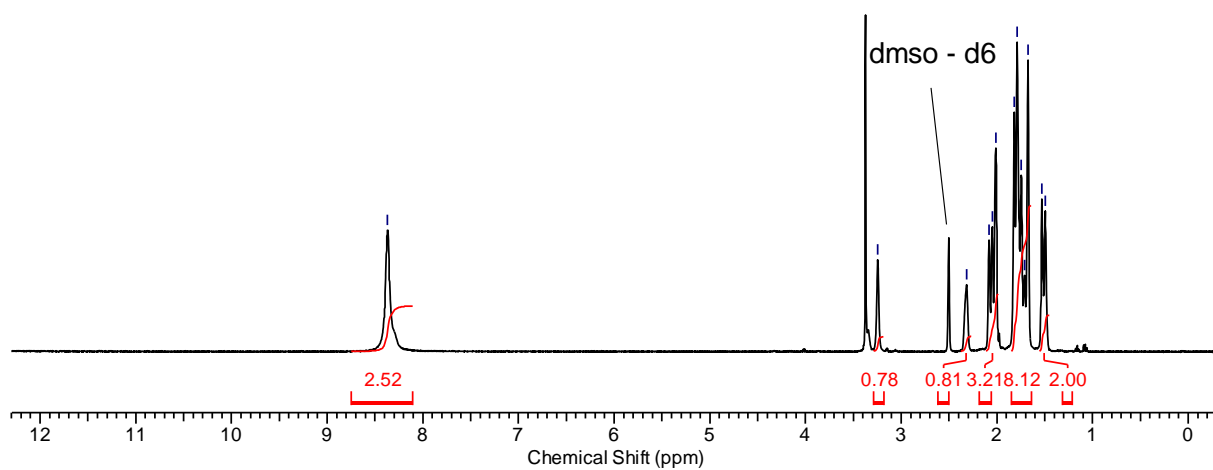
30:

31:

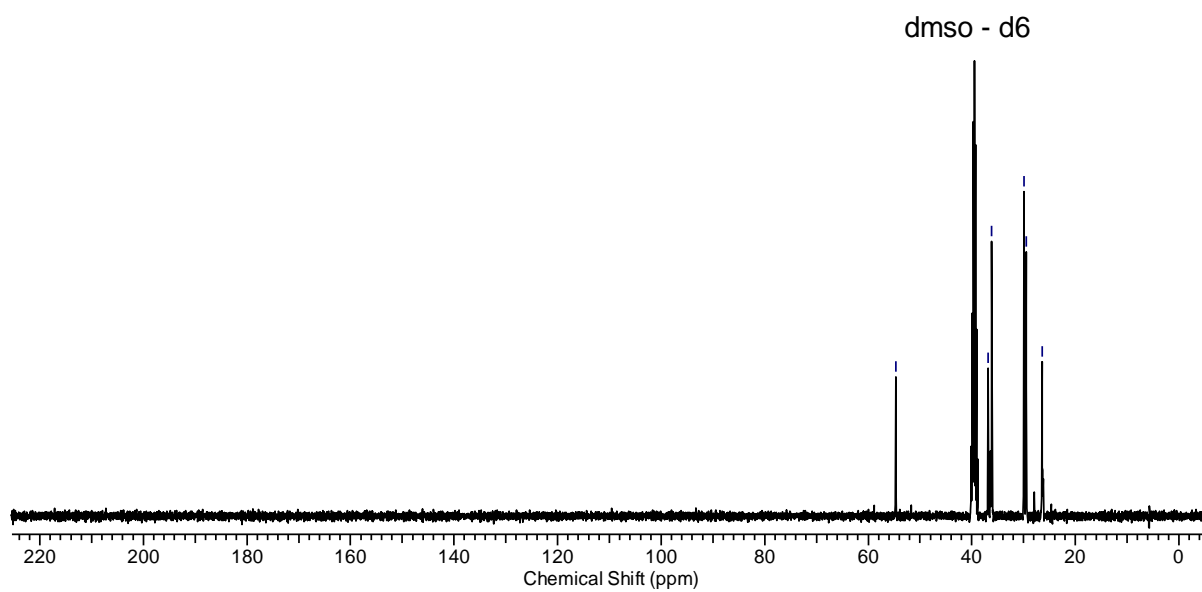
32:

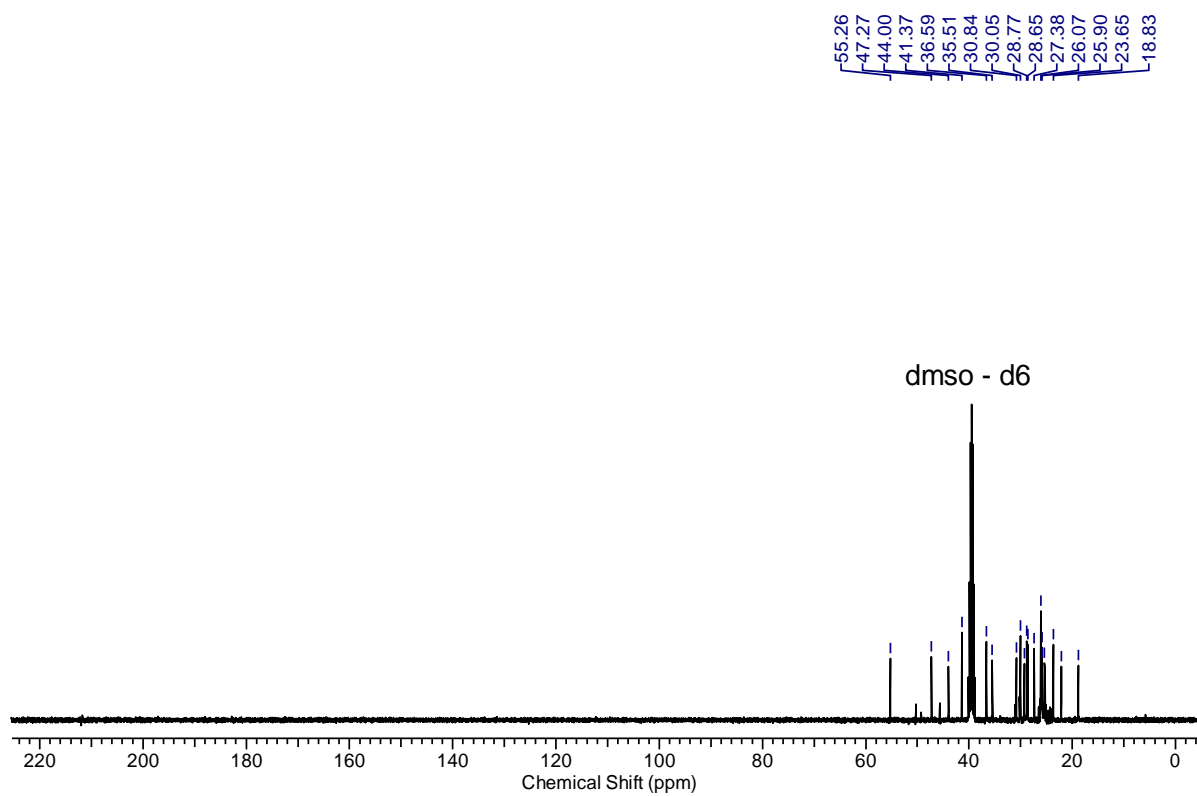
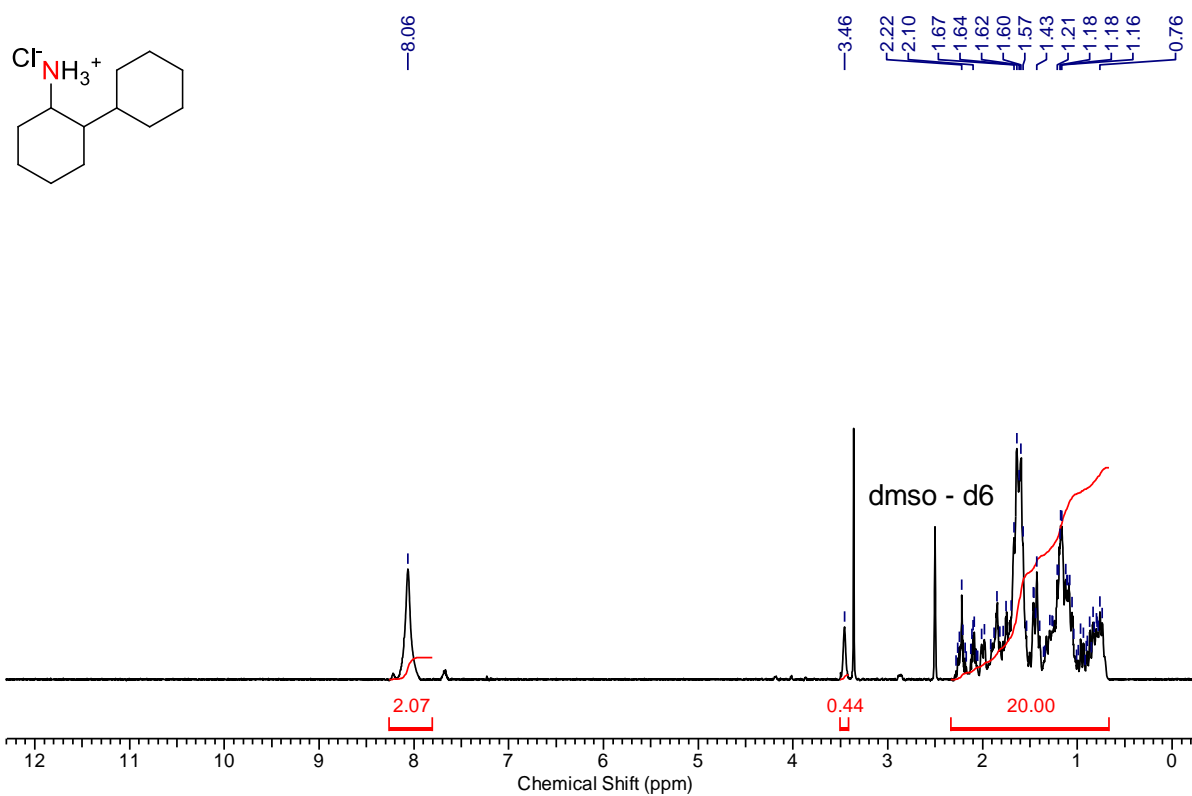
33:

-8.37

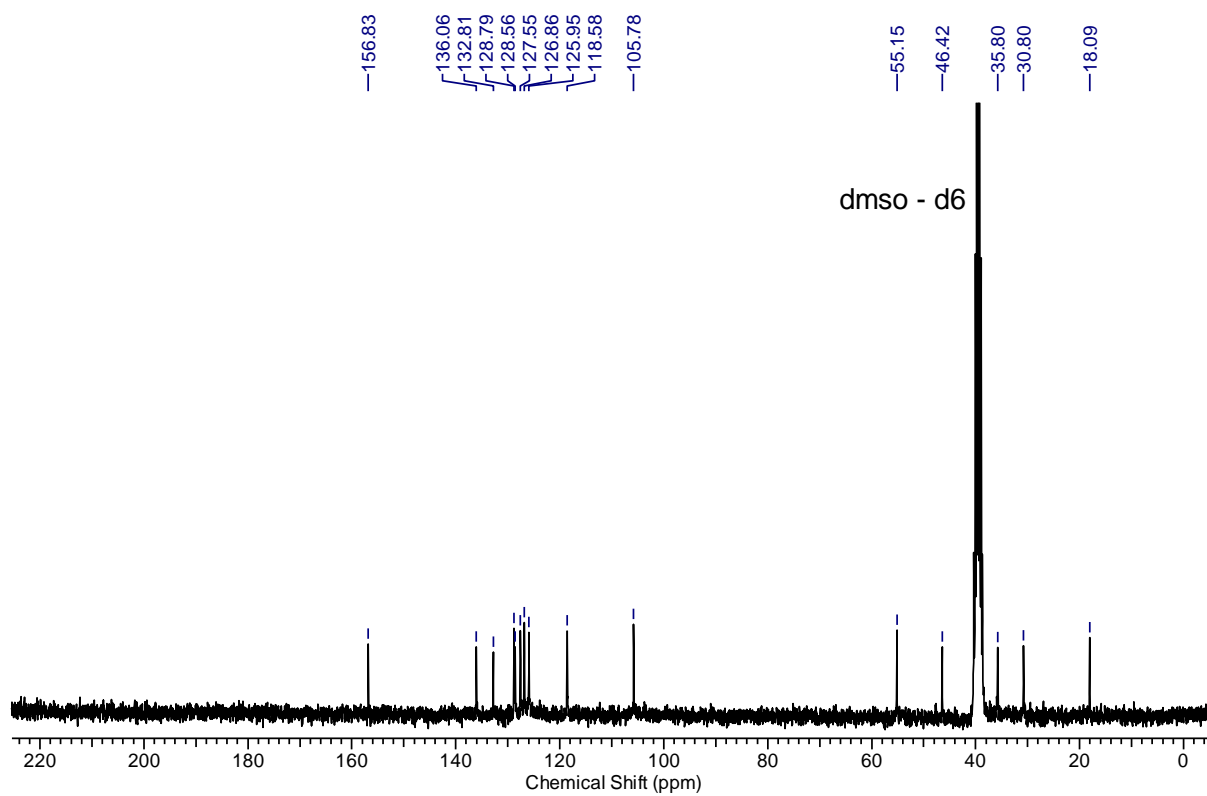
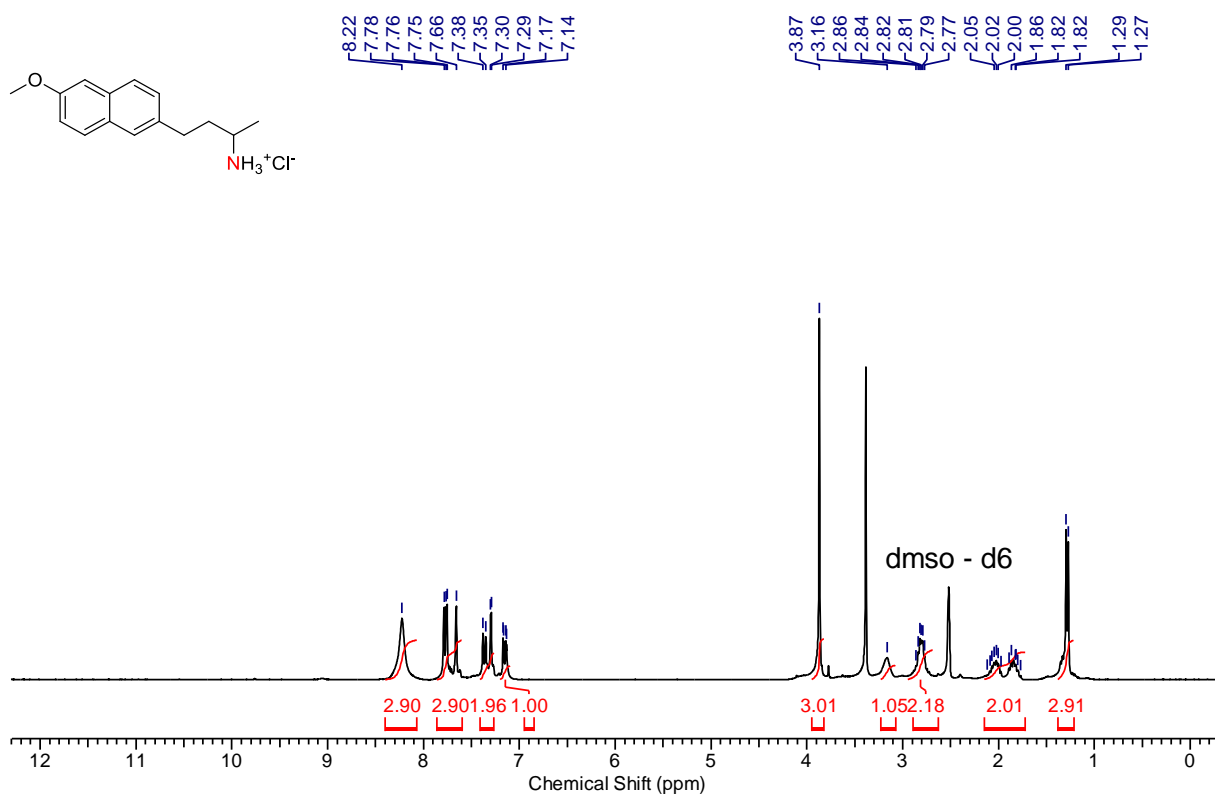
-3.24
-2.32
-2.08
-2.05
-2.01
-1.82
-1.79
-1.74
-1.71
-1.68
-1.53
-1.50

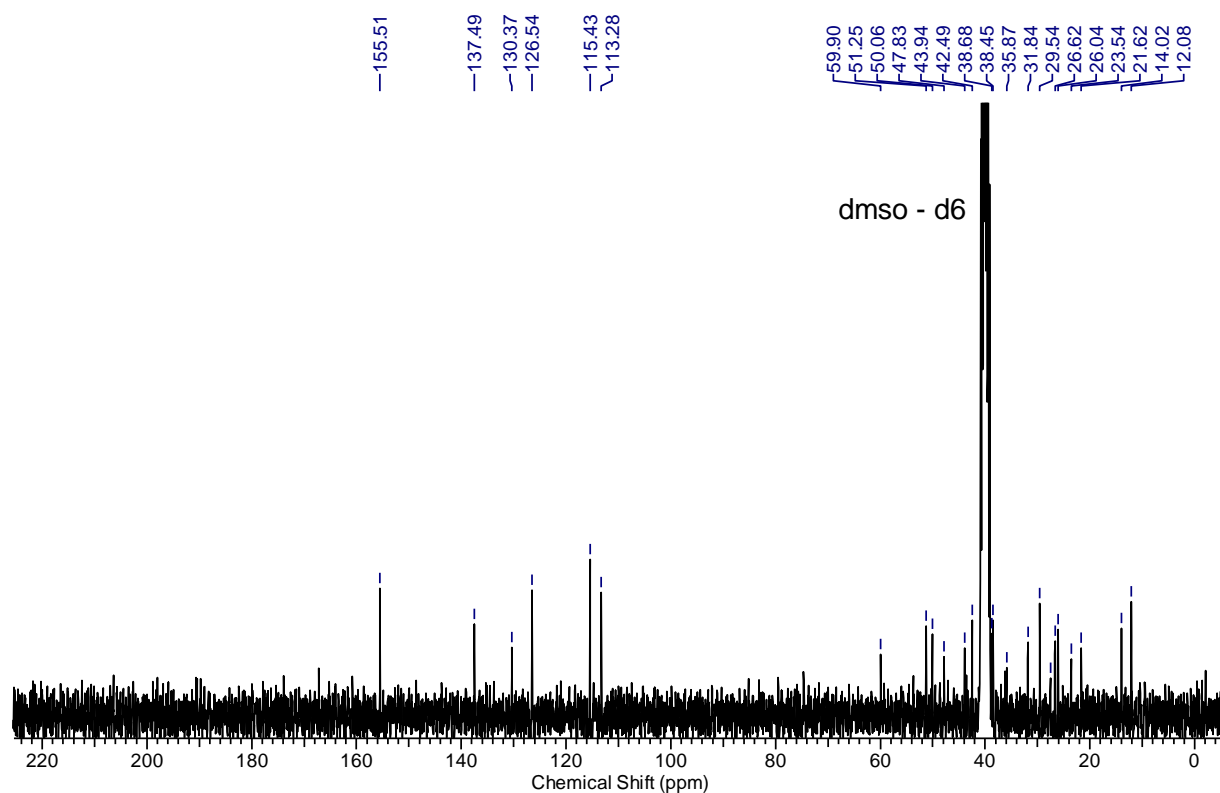
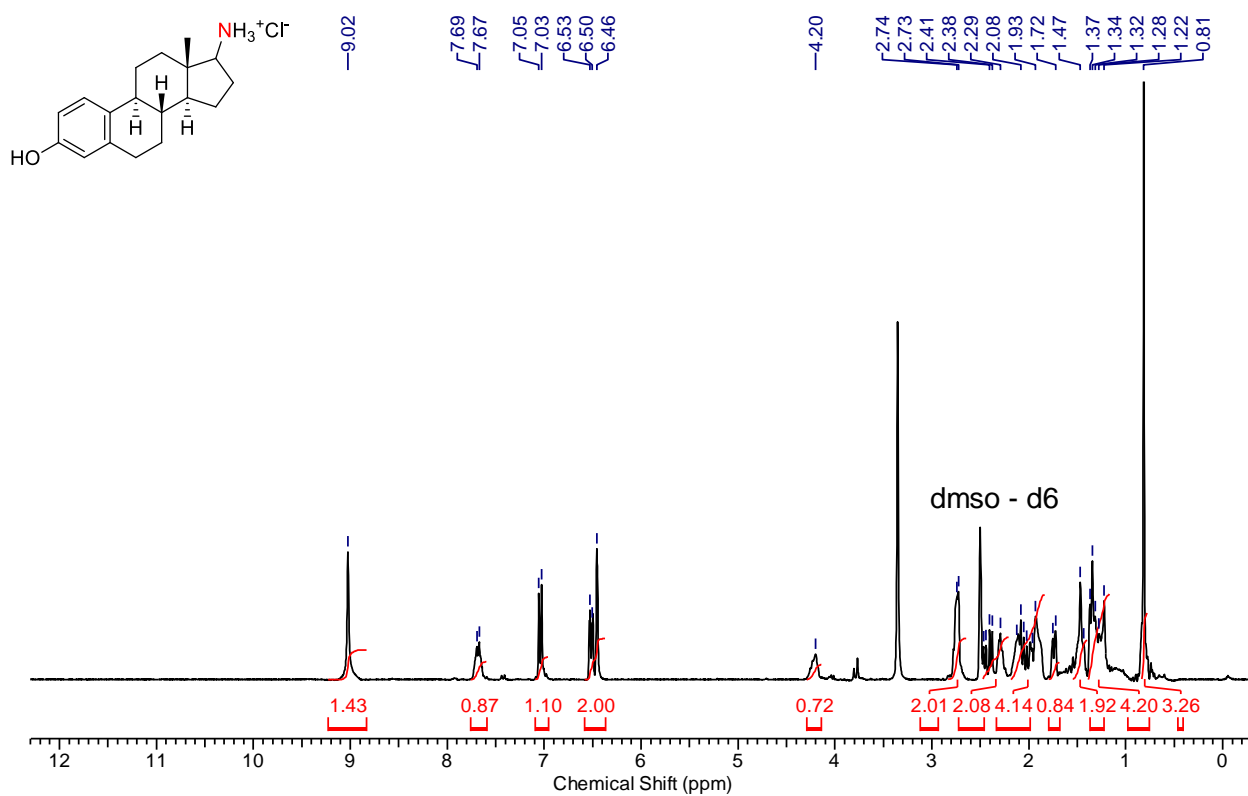
-54.66

-36.86
-36.15
-29.93
-29.49
-26.43

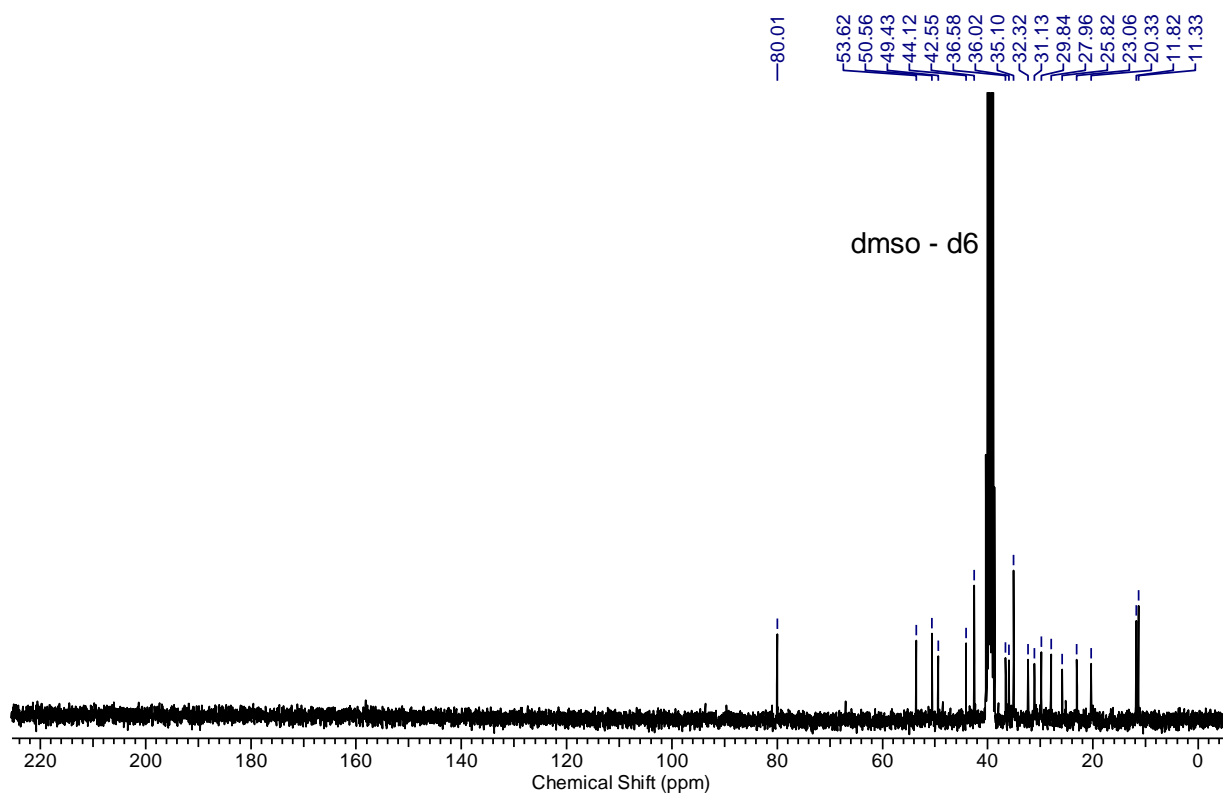
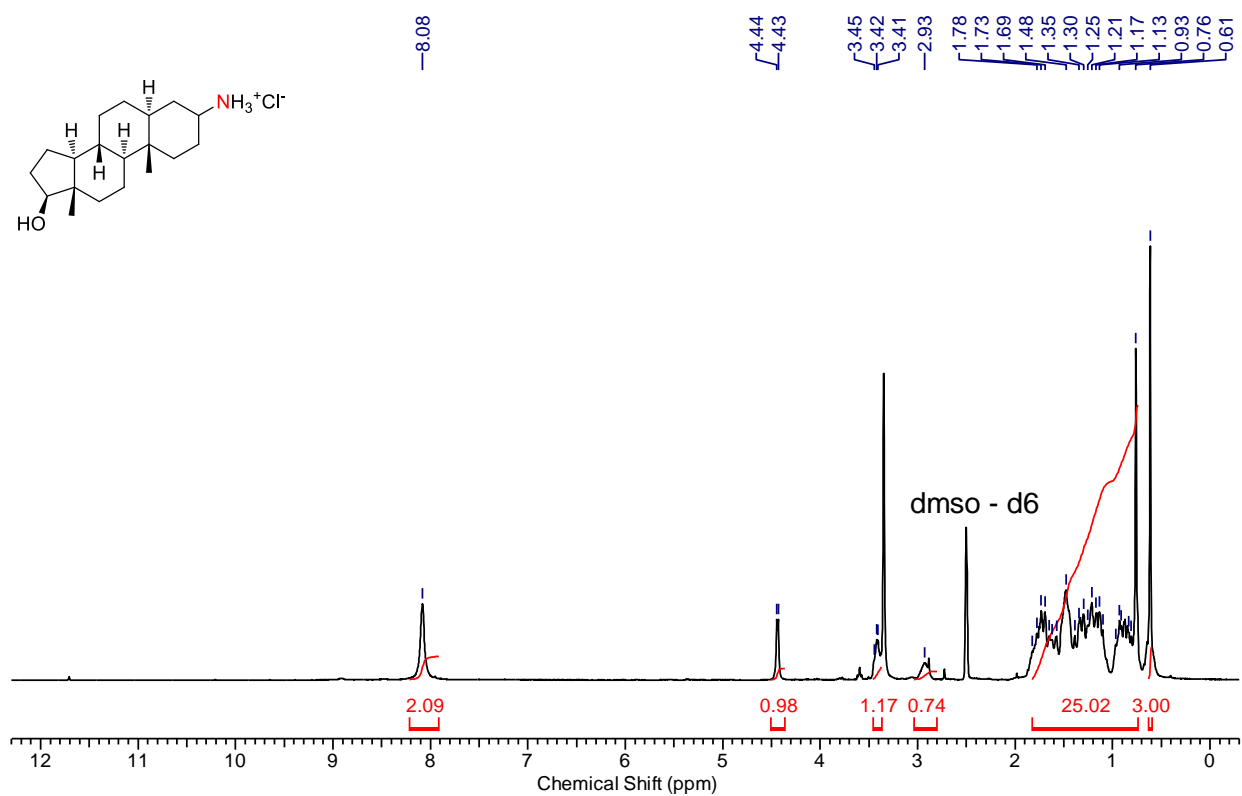
34:

35:

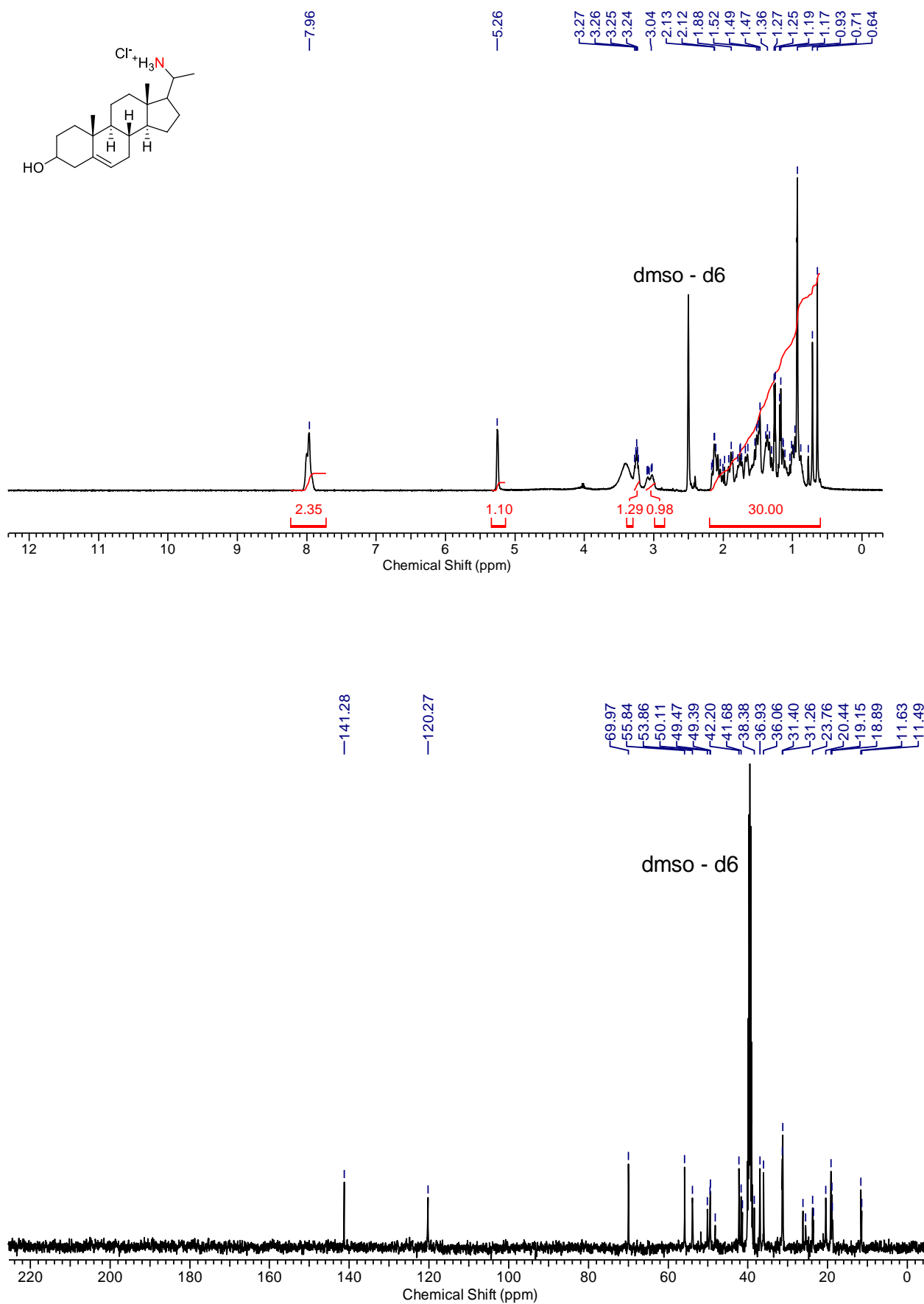


36:

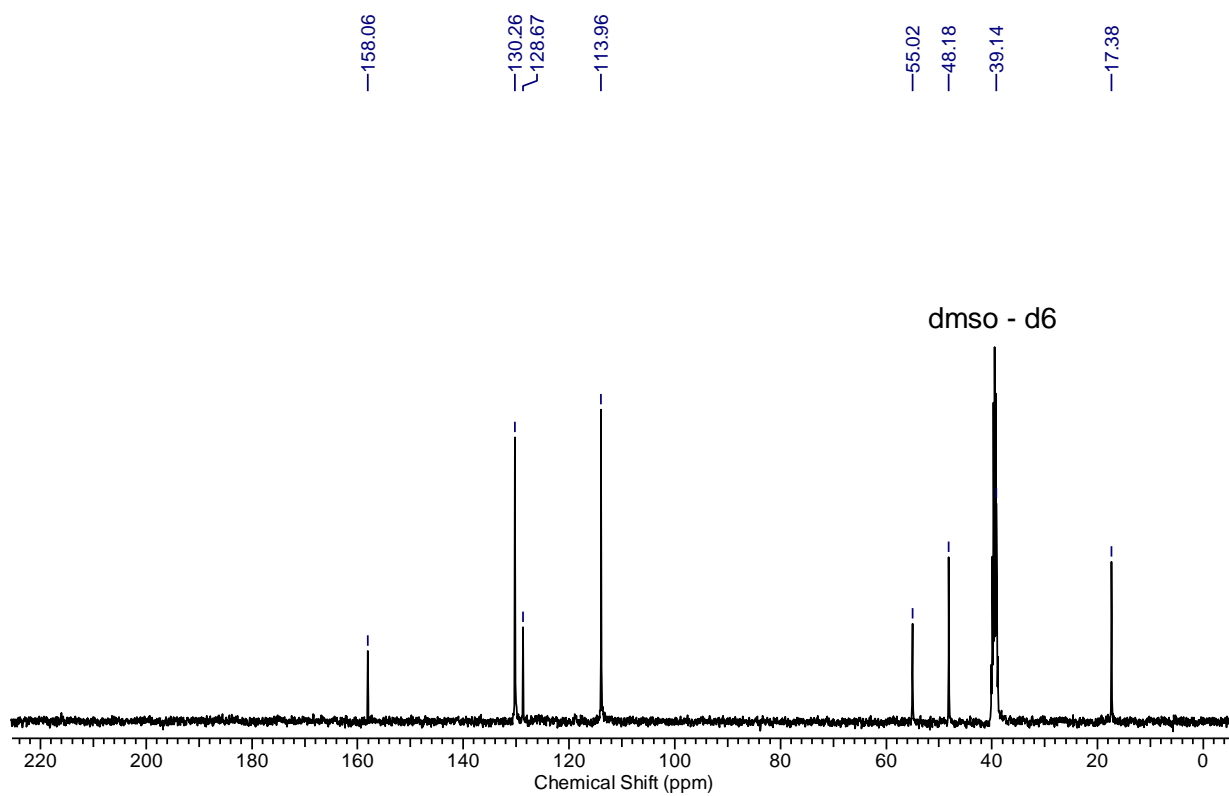
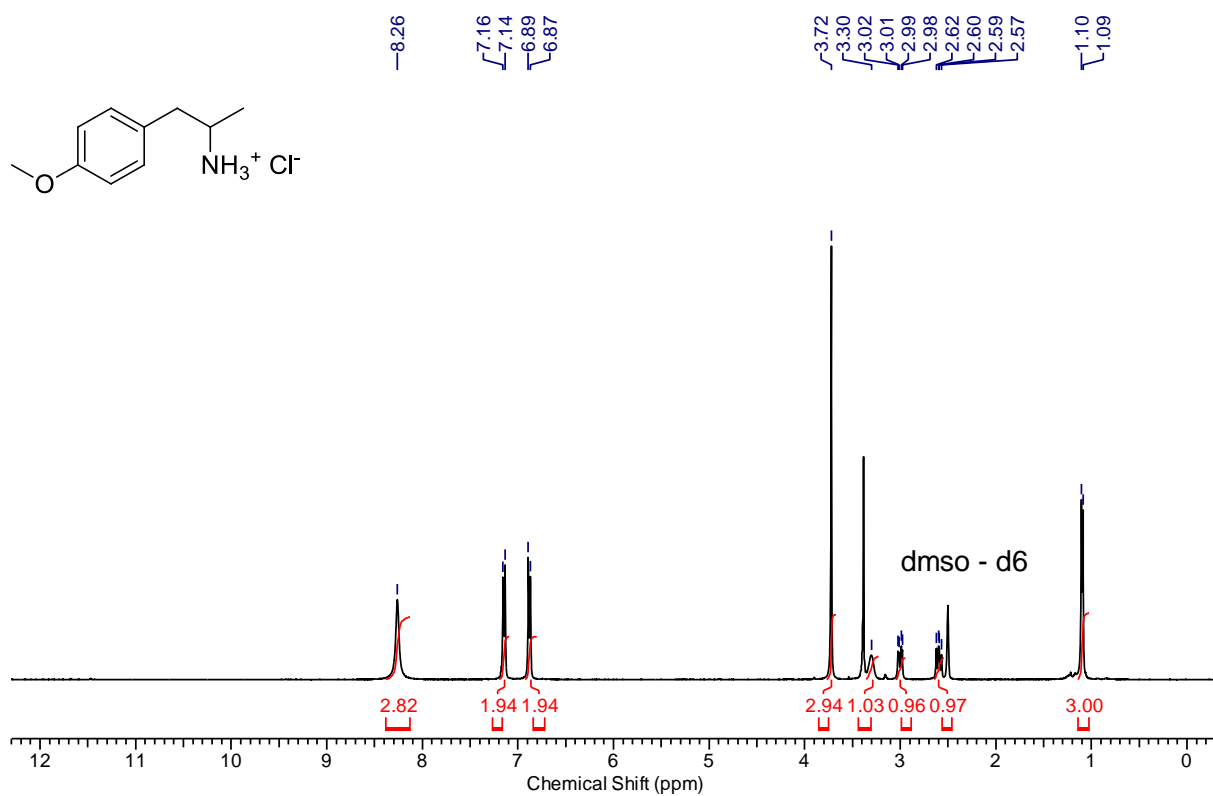
37:



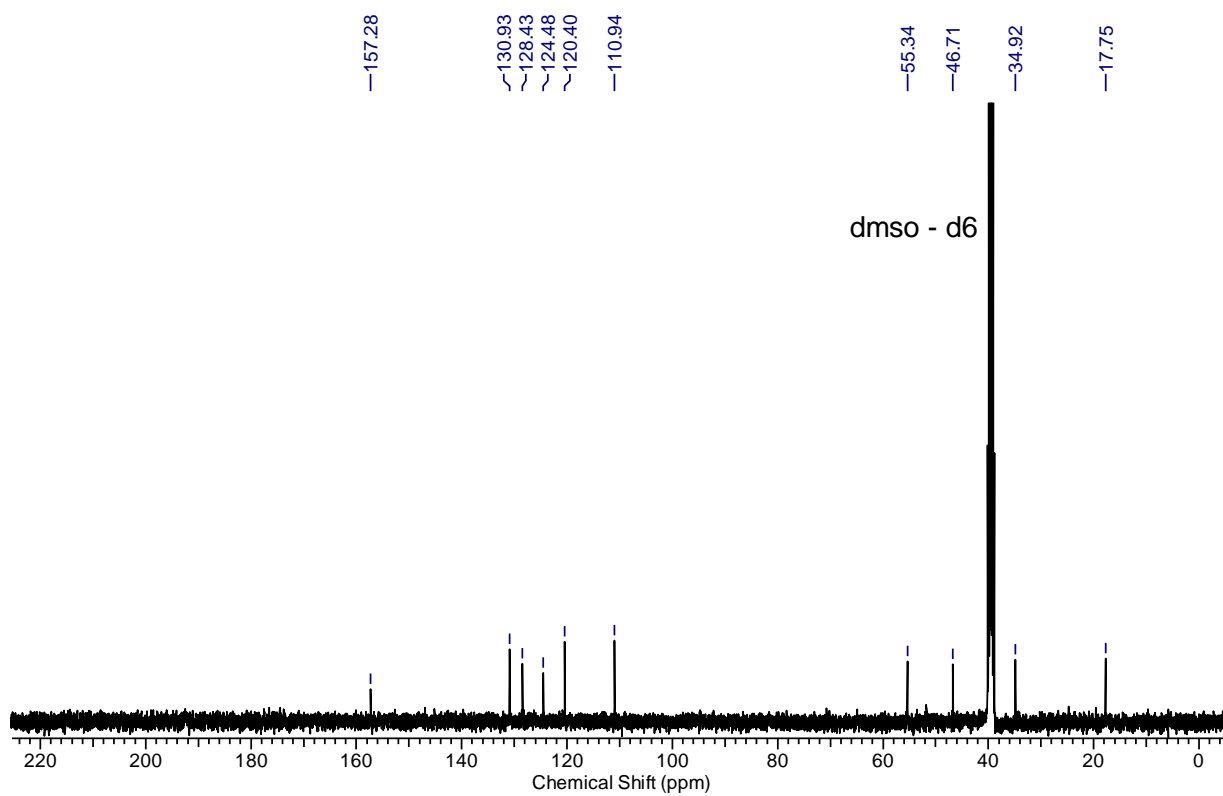
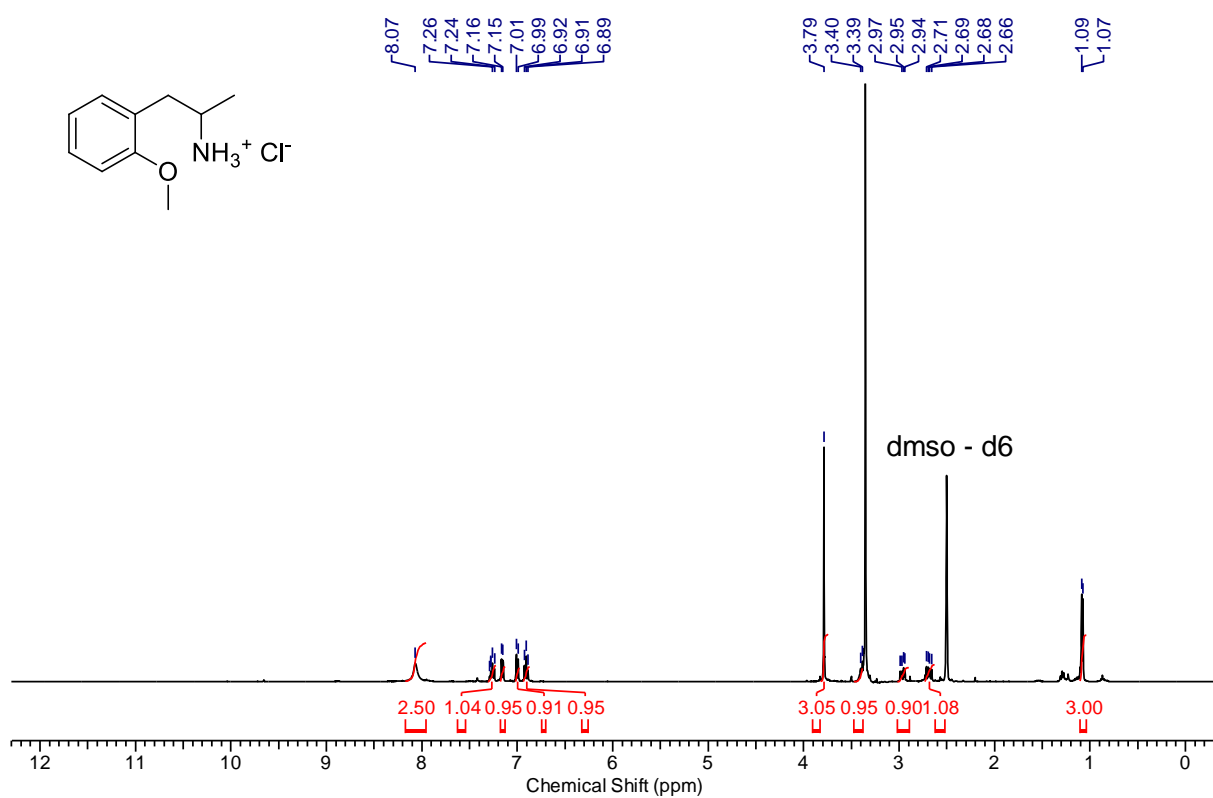
38:

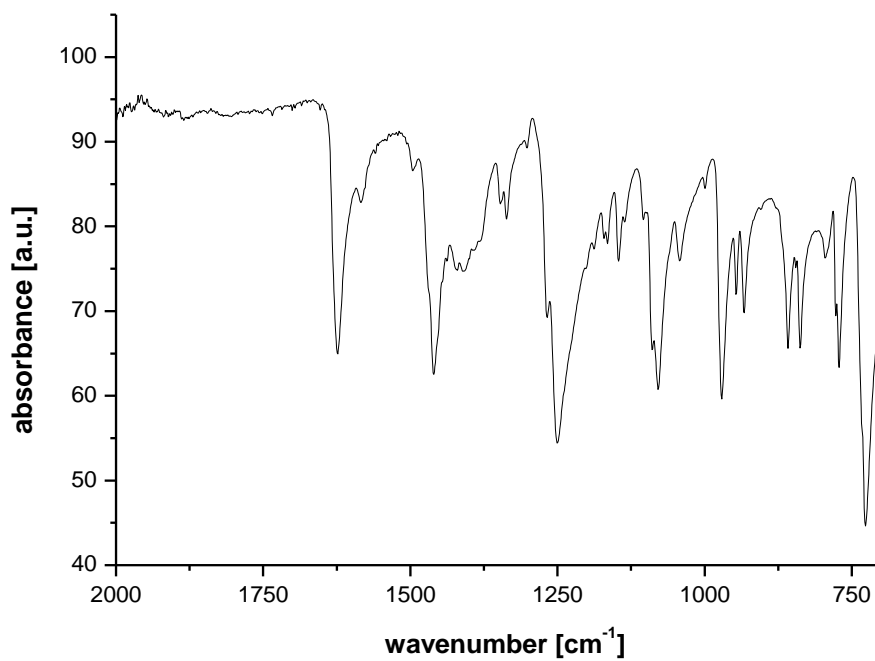
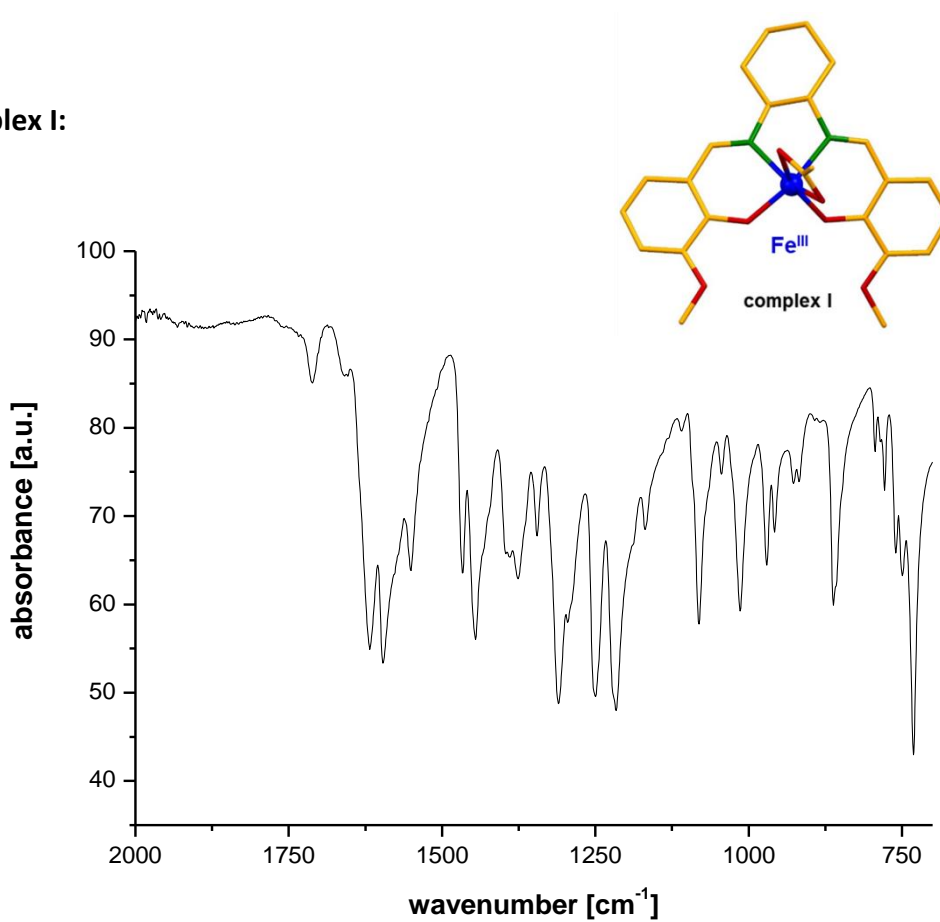


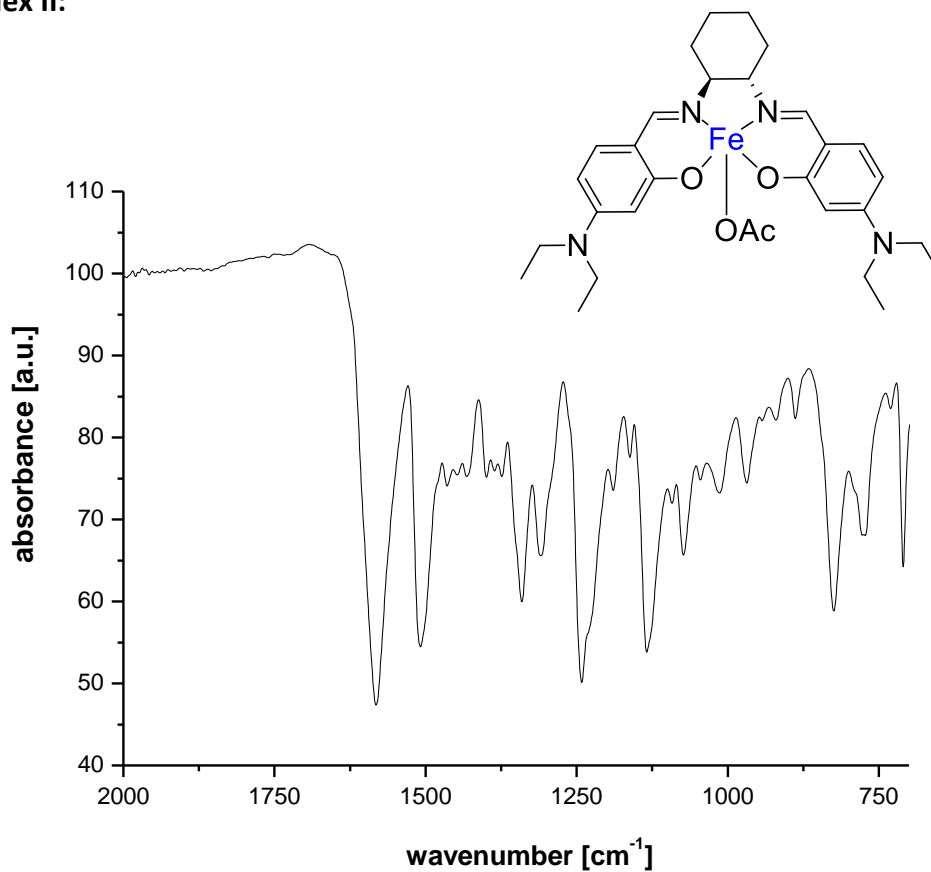
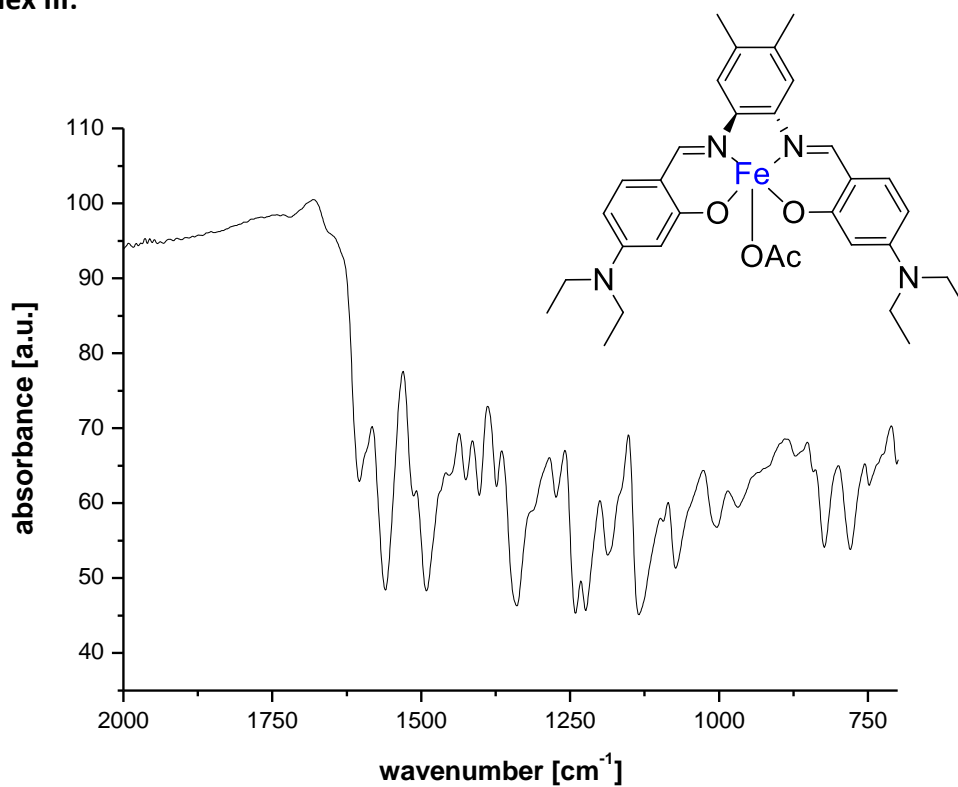
39:



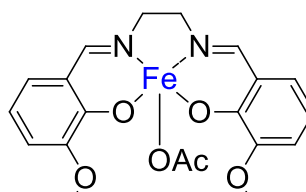
40:

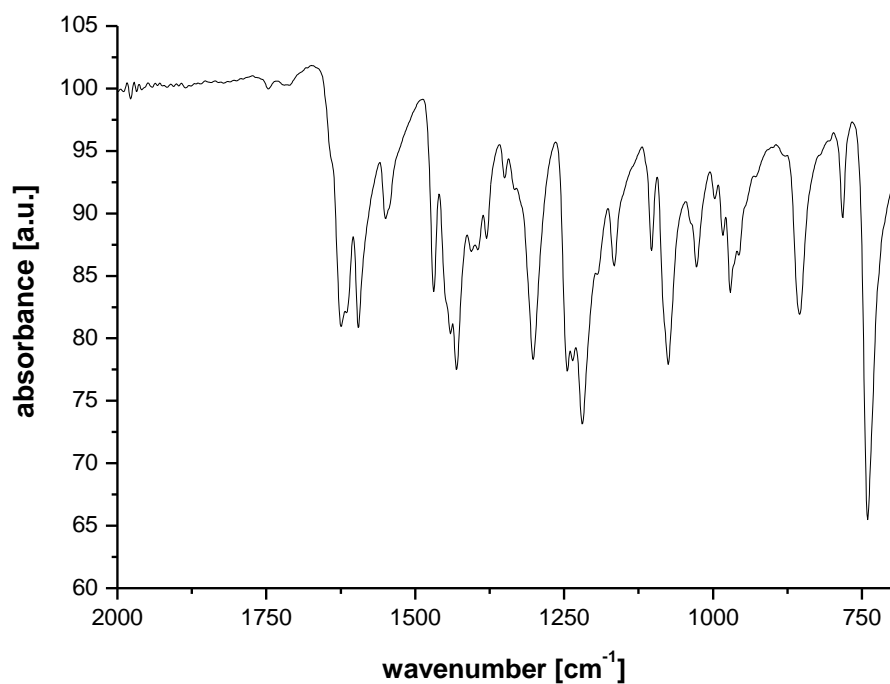


FTIR spectroscopy**Ligand I:****Complex I:**

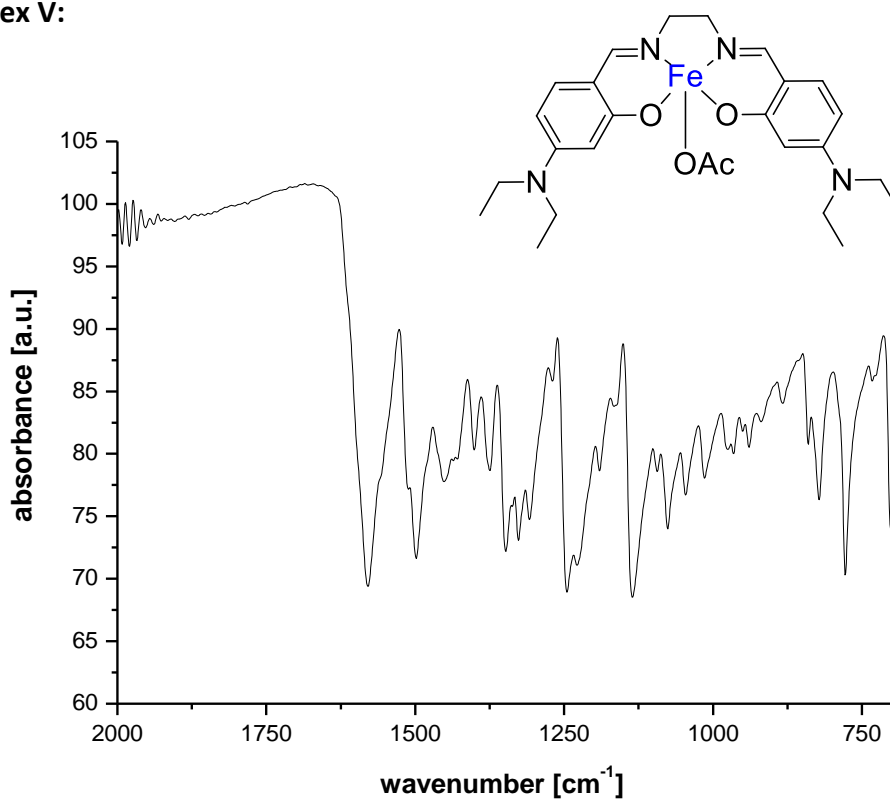
Complex II:**Complex III:****Complex IV:**

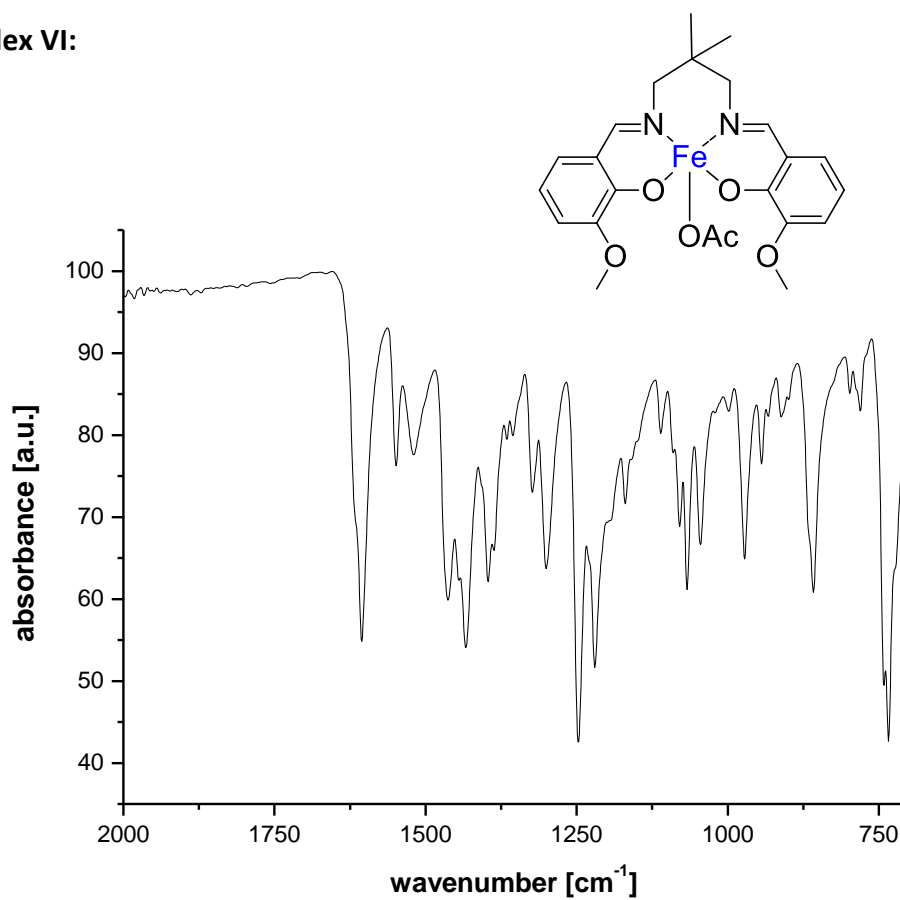
186





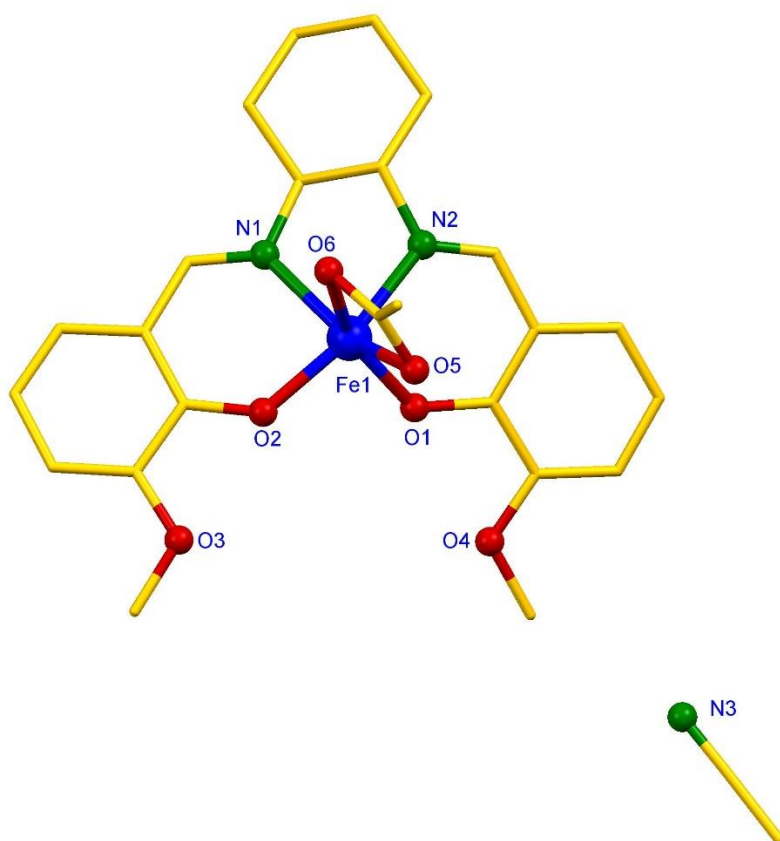
Complex V:



Complex VI:

Crystallographic data of complex I

The Fe complex I was dissolved in acetonitrile and crystallized by -32 °C (purple needles).

**checkCIF/PLATON (basic structural check)**

Structure factors have been supplied for datablock(s) sv_452_p21n

THIS REPORT IS FOR GUIDANCE ONLY. IF USED AS PART OF A REVIEW PROCEDURE FOR PUBLICATION, IT SHOULD NOT REPLACE THE EXPERTISE OF AN EXPERIENCED CRYSTALLOGRAPHIC REFEREE.

No syntax errors found. CIF dictionary [Interpreting this report](#)

Structure	factor	report
-----------	--------	--------

Datablock: sv_452_p21n

Bond precision:	C-C = 0.0020 Å		Wavelength=0.71073
Cell:	a=12.048(2)	b=12.534(3)	c=16.704(3)
	alpha=90	beta=98.75(3)	gamma=90
Temperature: 133 K			
	Calculated	Reported	
Volume	2493.1(9)	2493.1(9)	

Space group	P 21/n	P 1 21/n 1
Hall group	-P 2yn	-P 2ybc (x-
Moiety formula	C24 H27 Fe N2 O6, C2 H3 N	C24 H27 Fe N2 O6, C2 H3 N
Sum formula	C26 H30 Fe N3 O6	C26 H30 Fe N3 O6
Mr	536.38	536.39
Dx,g cm-3	1.429	1.429
Z	4	4
Mu (mm-1)	0.652	0.652
F000	1124.0	1125.9
F000'	1125.86	
h,k,lmax	16,16,22	16,16,22
Nref	6324	6084
Tmin,Tmax	0.978,0.991	0.981,0.995
Tmin'	0.945	

Correction method= # Reported T Limits: Tmin=0.981 Tmax=0.995 AbsCorr =
NUMERICAL

Data completeness= 0.962

Theta(max)= 28.510

R(reflections)= 0.0272(5097)

wR2(reflections)= 0.0943(6084)

S = 0.746

Npar= 329

The following ALERTS were generated. Each ALERT has the format

test-name_ALERT_alert-type_alert-level.

Click on the hyperlinks for more details of the test.

Alert level C

GOODF01_ALERT_2_C The least squares goodness of fit parameter lies
outside the range 0.80 <> 2.00

Goodness of fit given = 0.746

PLAT029_ALERT_3_C _diffn_measured_fraction_theta_full value Low . 0.962 Why?

PLAT126_ALERT_1_C Error in or Uninterpretable Hall Symbol -P 2YBC (X-Z,Y

PLAT911_ALERT_3_C Missing FCF Refl Between Thmin & STh/L= 0.600 31 Report

Alert level G

PLAT066_ALERT_1_G Predicted and Reported Tmin&Tmax Range Identical ? Check
PLAT073_ALERT_1_G H-atoms ref, but _hydrogen_treatment Reported as constr Check
PLAT232_ALERT_2_G Hirshfeld Test Diff (M-X) Fe1 --O5 . 8.2 s.u.

And 3 other PLAT232 Alerts

PLAT232_ALERT_2_G Hirshfeld Test Diff (M-X) Fe1 --O6 . 6.6 s.u.
PLAT232_ALERT_2_G Hirshfeld Test Diff (M-X) Fe1 --N1 . 6.0 s.u.
PLAT232_ALERT_2_G Hirshfeld Test Diff (M-X) Fe1 --N2 . 5.6 s.u.
PLAT790_ALERT_4_G Centre of Gravity not Within Unit Cell: Resd. # 2 Note

C2 H3 N

PLAT793_ALERT_4_G Model has Chirality at C8 (Centro SPGR) S Verify
PLAT793_ALERT_4_G Model has Chirality at C13 (Centro SPGR) S Verify
PLAT794_ALERT_5_G Tentative Bond Valency for Fe1 (III) . 2.97 Info
PLAT912_ALERT_4_G Missing # of FCF Reflections Above STh/L= 0.600 211 Note
PLAT960_ALERT_3_G Number of Intensities with I < -2*sig(I) ... 1 Check
PLAT978_ALERT_2_G Number C-C Bonds with Positive Residual Density. 16 Info
PLAT982_ALERT_1_G The Fe-f' = 0.3582 Deviates from IT-value = 0.3463 Check
PLAT983_ALERT_1_G The Fe-f'' = 0.8493 Deviates from IT-Value = 0.8444 Check

0 **ALERT level A** = Most likely a serious problem - resolve or explain

0 **ALERT level B** = A potentially serious problem, consider carefully

4 **ALERT level C** = Check. Ensure it is not caused by an omission or oversight

15 **ALERT level G** = General information/check it is not something unexpected

5 ALERT type 1 CIF construction/syntax error, inconsistent or missing data

6 ALERT type 2 Indicator that the structure model may be wrong or deficient

3 ALERT type 3 Indicator that the structure quality may be low

4 ALERT type 4 Improvement, methodology, query or suggestion

1 ALERT type 5 Informative message, check

It is advisable to attempt to resolve as many as possible of the alerts in all categories. Often the minor alerts point to easily fixed oversights, errors and omissions in your CIF or refinement strategy, so attention to these fine details can be worthwhile. In order to resolve some of the more serious problems it may be necessary to carry out additional measurements or structure refinements. However, the purpose of your study may justify the reported deviations and the more serious of these should

normally be commented upon in the discussion or experimental section of a paper or in the "special_details" fields of the CIF. checkCIF was carefully designed to identify outliers and unusual parameters, but every test has its limitations and alerts that are not important in a particular case may appear. Conversely, the absence of alerts does not guarantee there are no aspects of the results needing attention. It is up to the individual to critically assess their own results and, if necessary, seek expert advice.

Publication of your CIF in IUCr journals

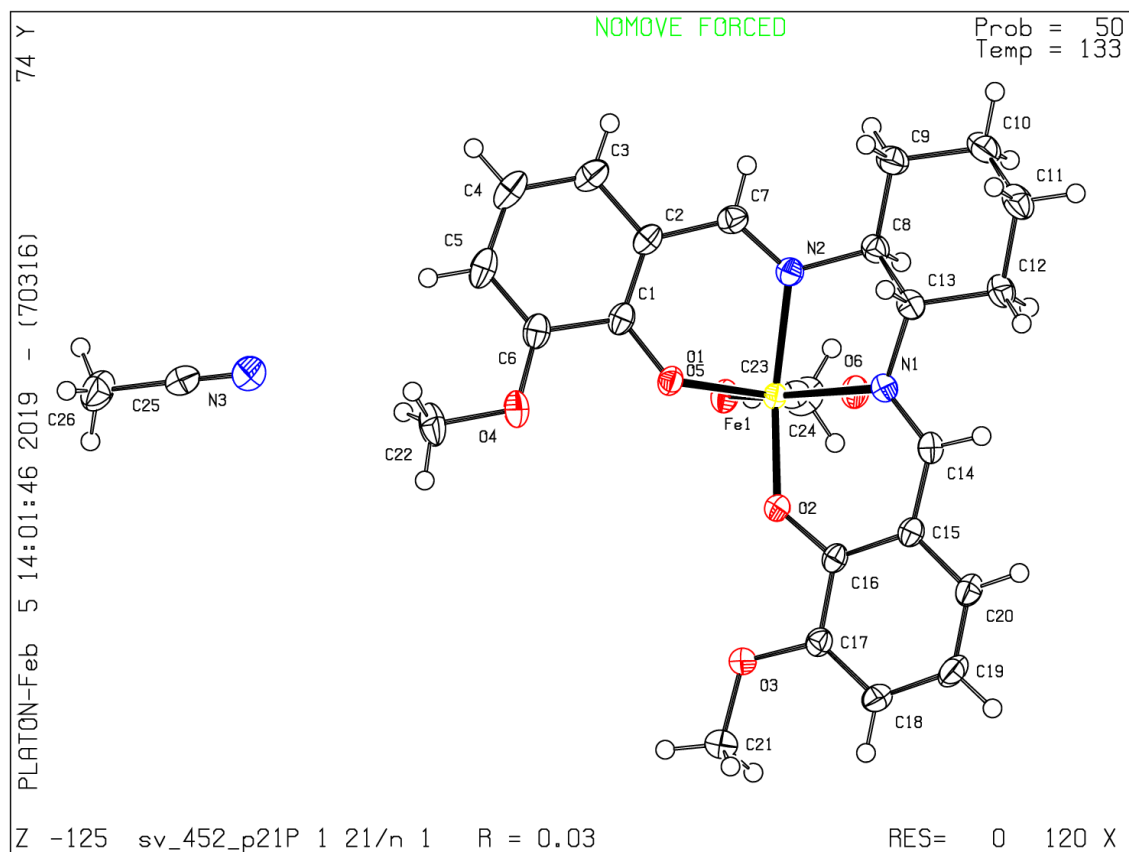
A basic structural check has been run on your CIF. These basic checks will be run on all CIFs submitted for publication in IUCr journals (*Acta Crystallographica*, *Journal of Applied Crystallography*, *Journal of Synchrotron Radiation*); however, if you intend to submit to *Acta Crystallographica Section C* or *E* or *IUCrData*, you should make sure that full publication checks are run on the final version of your CIF prior to submission.

Publication of your CIF in other journals

Please refer to the *Notes for Authors* of the relevant journal for any special instructions relating to CIF submission.

PLATON version of 06/01/2019; check.def file version of 19/12/2018

Datablock sv_452_p21n - ellipsoid plot



5.5.5 References

- [1] a) H.-R. Wen, S.-J. Liu, X.-R. Xie, J. Bao, C.-M. Liu and J.-L. Chen, *Inorg. Chim. Acta* **2015**, *435*, 274–282; b) J. S. Elia, M. Risch, L. Giordano, A. N. Mansour and Y. Shao-Horn, *J. Am. Chem. Soc.* **2014**, *136*, 17193–17200.
- [2] L. F. B. Ribeiro, O. Flores, P. Furtat, C. Gervais, R. Kempe, R. A. F. Machado and G. Motz, *J. Mater. Chem. A* **2017**, *5*, 720-729.

6. Hydrogenation of various N-heterocycles Employing an Heterogeneous Iron Catalyst

Christoph Bäumler^[a], and Rhett Kempe^{*[a]}

[a] Anorganische Chemie II – Katalysatordesign, Universität Bayreuth, 95440 Bayreuth.

To be submitted

Keywords: Iron • N-heteroarenes • quinolines • quinoxalines • hydrogenation

Abstract: The selective hydrogenation of N-heteroarenes is a challenging reaction in organic synthesis. The use of reusable catalysts based on earth-abundant metals, especially iron, is similarly appealing. Herein, we report on a reusable iron catalyst for the selective hydrogenation of various N-heteroarenes including quinolines and quinoxalines. The key to the high activity lies in the combination of a N-doped SiC material and a specific iron salen complex. The robust Fe/(N)SiC catalyst convinces with high activity and high selectivity. The application of this iron catalyst in hydrogenation reactions, enables the production of important building blocks for bioactive-, natural- or pharmaceutical products.

6.1 Introduction

The reduction of N-heteroarenes to their corresponding partially or completely saturated derivatives has attracted more attention due to their immense utility as building blocks and key intermediates in the manufacture of pharmaceuticals, agrochemicals, and other fine chemicals.^[1] Therefore, the synthesis of reusable catalysts, based on low cost and low toxic earth-abundant 3d metals, represents an enormous issue in the green chemistry. The first progresses in the hydrogenation of N-heterocycles were achieved by homogeneous catalysts based on noble metals (e.g. Ru, Ir, Pd, Au, Rh).^[2] In general, the molecular well-defined catalysts need to be activated in advance to generate the active species and stored in an inert gas atmosphere. The need of co-catalysts and additives is a problem, especially, the difficulties in the catalyst recycling.^[3] Despite several advantages like high activity, selectivity and atom efficiency the use of homogeneous catalysts is less desirable in the chemical industry. Conversely, heterogeneous catalysts seem to be the perfect alternative, cause its easy handling and the possibility of large-scale processes in respect to their perfect recycling properties. Catalysts based on noble metals are well researched whereby problems with stereo selectivity and functional group tolerance are known.^[4] In the last years, in respect of sustainability

and environment concerns, the focus of the researchers was set on earth-abundant 3d base metals (e.g. Ni, Co, Fe). Reports about the application in the hydrogenation of *N*-heteroarenes are quite limited so far.^[5,6] The low cost and the possibility of generating unique selectivity pattern is one of the decisive facts why the use of base metals is of great interest. Regarding the relative frequency of the 3d metals in the earth's crust and relating price developments the prime choice should be iron.^[7] The first iron based heterogeneous work were published by Shaw et al., converting quinaldine by very harsh conditions at 300 °C.^[8] Also, Beller and coworkers introduced a system based on Fe (2018) with a broad spectrum and great selectivity.^[9]

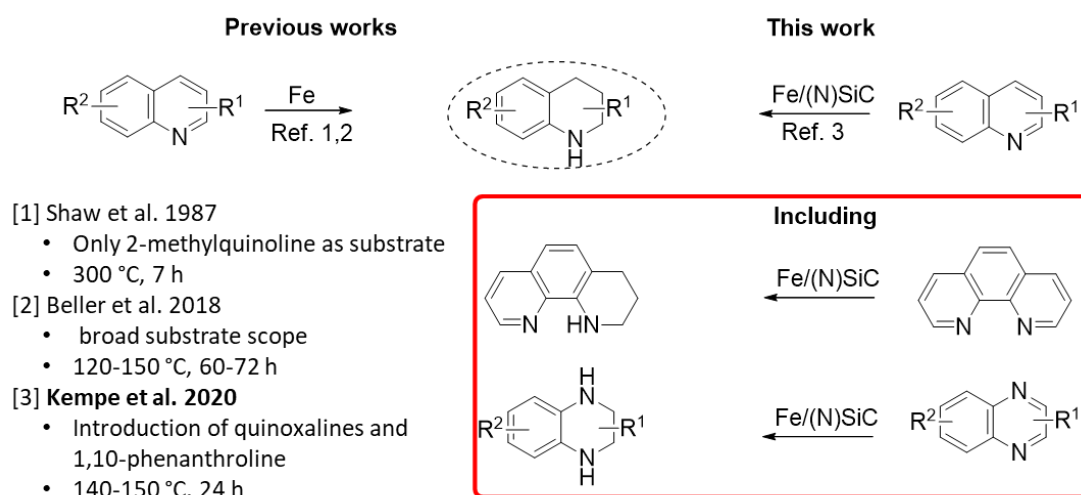


Figure 1: Heterogeneous iron catalysts for the hydrogenation of *N*-heteroarenes.

To the best of my knowledge, there is no report on iron based heterogeneous catalysts which can convert other *N*-heteroarenes without the quinoline motive, which was well researched by Beller et al.. Moreover, it is very desirable to hydrogenate other *N*-heteroarenes like quinoxalines, regarding the potential for an application in the pharmaceutical manufacturing. Substituted tetrahydroquinoxalines are important structure motives for the synthesis of tetrahydrofolic acids^[10] and as cholesteryl ester transfer protein inhibitors for different treatments like for atherosclerosis.^[11] Consequently, the synthesis of well-defined iron based heterogeneous catalysts for the hydrogenation of *N*-heteroarenes is of great interest concerning the aforementioned advantages like abundance, price and the good biocompatibility. The use of molecular hydrogen as a clean reducing agent is also highly attractive in combination with iron which is known in nature to be active as iron-iron hydrogenases in bio organisms in H₂ activation and transport.^[12] We have recently introduced a variety of homogeneous earth-abundant metal catalysts^[13,14], reusable nanostructured catalysts for energy storage^[15], novel organic reactions^[16] and earth-abundant metal catalysts with a broad applicability in organic synthesis.^[17,18]

6.2 Results and Discussion

Previously, the herein presented Fe/(N)SiC catalyst was successfully tested in the reductive amination of carbonyl compounds and completely characterized.^[18] Therefore, the great hydrogenation properties were already known and tested in the hydrogenation of N-heteroarenes. The catalyst is easy to synthesize whereby the combination of support material and the iron salen complex are the essential for the high activity. The (N)SiC support material was synthesized by modifying a known literature procedure^[19] and was impregnated with a specific iron salen complex dissolved in acetonitrile (Figure 2). After removal of the solvent, the sample was pyrolyzed under a nitrogen atmosphere at 750 °C followed by a treatment under a reductive atmosphere (N₂/H₂ 90/10) at 550 °C. Transmission electron microscopy (TEM) indicated the existence of homogeneously distributed nanoparticles with an average particle size of 10 nm (Figure 2).

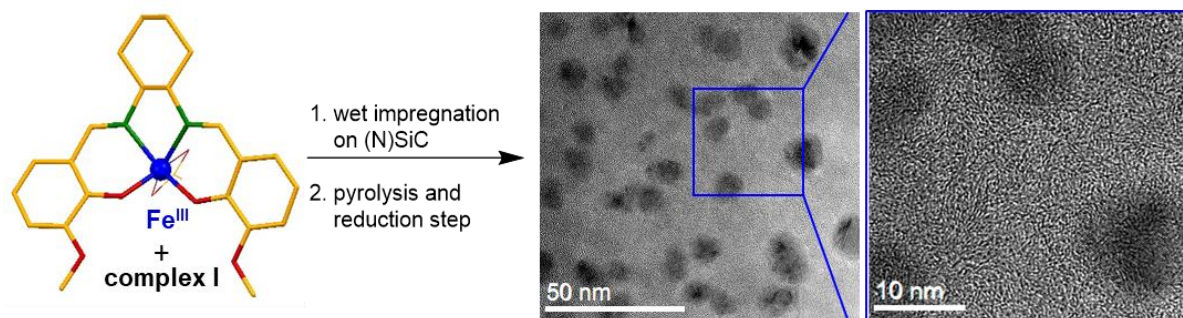
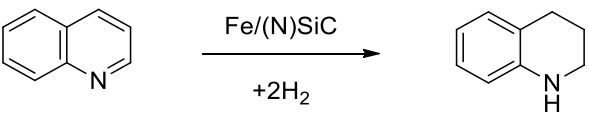


Figure 2: Synthesis and characterization of the Fe catalyst: Synthesis of the iron catalyst by wet impregnation of complex I (molecular structure determined by X-ray single crystal structure analysis, color code: green = N, red = O, orange = C) on the (N)SiC support, followed by pyrolysis and hydrogen treatment. TEM analysis suggested the presence of homogeneously distributed Fe nanoparticles with an average particle size of 10 nm.

Next, the catalyst was applied in the hydrogenation of quinolines and quinoxalines. The reduction of quinoline to 1,2,3,4-tetrahydroquinoline was chosen as benchmark reaction for optimizing the reaction conditions. The solvent screening showed that higher yields were generated with increasing polarity of the solvent with exception of water. Hence, methanol achieved the best yields in comparison to other solvents with a volume of 3 mL. Longer reaction times achieved better results, but the reduced reaction time is more desirable. In summary, the catalyst showed the best performance applying 3 mL methanol, 150 °C and 6.5 MPa H₂ for 24 h (Table 1).

Table 1: Screening of the reaction conditions.

				
Solvent	Volume [mL]	Reaction time [h]	Temperature [°C]	Yield [%]
MeOH	4	24	150	90
H ₂ O	4	24	150	56
H ₂ O/MeOH (1:1)	4	24	150	60
H ₂ O/MeOH (1:4)	4	24	150	72
EtOH	4	24	150	84
<i>i</i> -PrOH	4	24	150	77
MtBE	4	24	150	9
Toluol	4	24	150	2
THF	4	24	150	29
Digylme	4	24	150	25
MeOH	3	24	150	97
MeOH	4	24	150	90
MeOH	5	24	150	83
MeOH	3	8	140	32
MeOH	3	24	140	79
MeOH	3	40	140	96

Reaction conditions: 10 mol% Fe (70 mg Fe/(N)SiC, 4.0 wt% Fe, 0.05 mmol Fe, 2.8 mg Fe), 0.5 mmol quinoline, 6.5 MPa H₂.

Yields were determined by GC using *n*-dodecane as an internal standard.

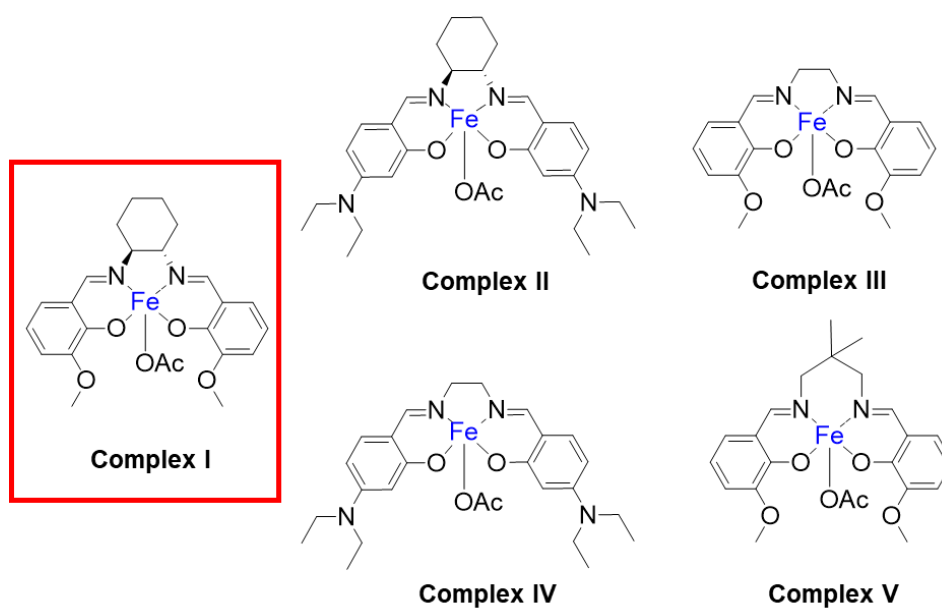
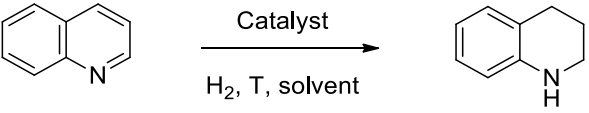


Figure 3: Different synthesized iron complexes used as metal source for the catalyst screening. The acetate molecule bonds as a chelating ligand (OAc = acetate).

The complexes depicted in Figure 3 (see Supporting Information for more details) originate all from the same structure motive and were tested as metal source in the catalyst synthesis. The obtained Fe/(N)SiC catalysts achieved yields in the range of 65 % (complex I) and 38 % in the case of complex IV (Table 2, Entries 3, 5-9). The *ortho*-vanillin structure in combination with a not sterically demanding aliphatic diamino-building block seems to be essential for the high activity of complex I. The use of a common salt Fe(III) nitrate ($\text{Fe}(\text{NO}_3)_3 \cdot 9\text{H}_2\text{O}$) as metal source lead to a decrease of yield compared to complex I (Table 2, Entry 13). The (N)SiC support without metal source shows no activity (Table 2, Entry 12). Common support materials like SiO_2 or $\gamma\text{-Al}_2\text{O}_3$ in combination with complex I are not suitable for this reaction (Table 2, Entries 9,11). In case of TiO_2 only traces of product were detectable (Table 2, Entry 10). Consequently, the combination of the iron complex I and the (N)SiC support material used is crucial for the high activity of our catalyst.

Table 2: Catalyst screening for the hydrogenation of quinoline.

				
Entry	Metal source	Support material	Pyrolysis temperature [°C]	Yield [%]
1^[a]	Complex I	(N)SiC	750	97
2	Complex I	(N)SiC	650	58
3	Complex I	(N)SiC	750	65
4	Complex I	(N)SiC	850	56
5	Complex II	(N)SiC	750	54
6	Complex III	(N)SiC	750	49
7	Complex IV	(N)SiC	750	38
8	Complex V	(N)SiC	750	60
9	Complex I	SiO_2	750	0
10	Complex I	TiO_2	750	4
11	Complex I	$\gamma\text{-Al}_2\text{O}_3$	750	0
12 ^[b]	-	(N)SiC	1000	0
13	$\text{Fe}(\text{NO}_3)_3$	(N)SiC	750	40

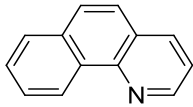
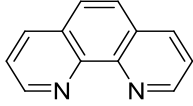
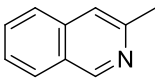
Reaction conditions: 10 mol% Fe (70 mg Fe/(N)SiC with 4.0 wt% Fe loading, 0.05 mmol Fe, 2.8 mg Fe), 0.5 mmol quinoline, 135 °C, 20 h, 6.5 MPa H_2 , 3 mL MeOH. Yields were determined by GC using *n*-dodecane as an internal standard. [a] 150 °C, 24 h. [b] 60 mg (N)SiC.

In the next step we were interested in the substrate scope of the hydrogenation of *N*-heteroarenes. Quinolines with various substituents were hydrogenated in good yields. Electron-donating methyl or methoxy substituents were well tolerated and the corresponding 1,2,3,4-tetrahydroquinoline could be achieved in yields up to 99 % (Table 3, Entries 1-4, 7). The position of the substituent was very influential. 2-Methyl and 3-methyl substituents lead to yields higher than 90 % in contrast to 8-methylquinoline. Also challenging substrates like 8-hydroxyquinoline with a free hydroxy substituent was transformed into the corresponding 1,2,3,4-tetrahydroquinoline-8-ol (Table 3, Entry 5). Also, quinolines with an electron-withdrawing substituent like 6-chloroquinoline could be converted in 81 % yield (Table 3, Entry 6). In the next step other *N*-heteroarenes with structural similarity to the quinoline motive were hydrogenated. The selective hydrogenation of benzo[*h*]quinoline to 1,2,3,4-tetrahydrobenzo[*h*]quinoline was very demanding and achieved a yield of 41 % (Table 3, Entry 8). Interestingly, the selective hydrogenation of 1,10-phenanthroline to the partly hydrogenated 1,2,3,4-tetrahydro-1,10-phenanthroline was accomplished with an excellent yield of 96 %. Additionally, 3-methylisoquinoline was converted into the corresponding hydrogenated product in good yield (Table 3, Entry 9).

Table 3: Hydrogenation of quinolines and other quinoline based *N*-heteroarenes; substrate scope.

$ \begin{array}{c} \text{R}^2 \text{---} \text{C}_6\text{H}_3\text{---} \text{N} \text{---} \text{R}^1 \\ \xrightarrow[24 \text{ h, MeOH}]{6.5 \text{ MPa H}_2, 140 \text{ }^\circ\text{C, Fe/(N)SiC}} \\ \text{R}^2 \text{---} \text{C}_6\text{H}_3\text{---} \text{NH} \text{---} \text{R}^1 \end{array} $			
Entry	Substrate	Product	Yield [%]
1		$\text{R}^1/\text{R}^2 = \text{H}$	97
2		$\text{R}^1 = 2\text{-CH}_3; \text{R}^2 = \text{H}$	99
3		$\text{R}^1 = 3\text{-CH}_3, \text{R}^2 = \text{H}$	90
4		$\text{R}^2 = 8\text{-CH}_3, \text{R}^1 = \text{H}$	70
5			40
6			81
7			86

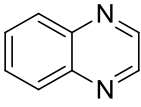
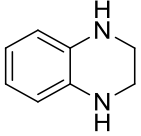
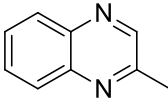
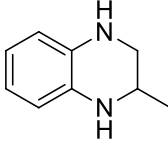
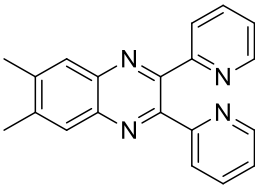
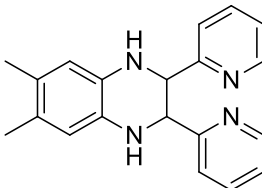
Other quinoline based N-heteroarenes:

8		41
9		96
10		86

Reaction conditions: 0.5 mmol substrate, 10 mol % catalyst (2.8 mg Fe, 0.05 mmol, 70 mg), 3 mL MeOH. Yields were determined by GC using *n*-dodecane as an internal standard.

In the next step, we were interested in the hydrogenation of catalytic more demanding quinoxaline derivatives. The reaction-time and -temperature had to be increased to ensure good yields. The conversion of quinoxaline to the corresponding 1,2,3,4-tetrahydroquinoxaline yielded in 86 % (Table 4, Entry 1). Also, an electron-donating methyl substituent was introduced with a great yield of the hydrogenated product (Table 4, Entry 2). The introduction of sterically demanding substituents including a pyridine motive was accomplished with 75 % yield (Table 4, Entry 3).

Table 4: Hydrogenation of quinoxalines; substrate scope.

$ \text{R}^1\text{-}\text{C}_6\text{H}_3\text{(N)}_2\text{-R}^2 \xrightarrow[155\text{ }^\circ\text{C, 36 h, MeOH, 6.5 MPa H}_2]{\text{Fe (12 mol \%)}} \text{R}^1\text{-}\text{C}_6\text{H}_3\text{(NH)}_2\text{-R}^2 $			
Entry	Substrate	Product	Yield [%]
1			96
2			88
3			75

Reaction conditions: 0.5 mmol quinoxaline, 10 mol % catalyst (2.8 mg Fe, 0.05 mmol, 70 mg), 3 mL MeOH. Yields were determined by GC using *n*-dodecane as an internal standard.

In summary, the already known catalyst was successfully introduced in the hydrogenation of different *N*-heteroarenes with molecular hydrogen. Various quinolines with different substituents could be selectively hydrogenated to the corresponding products in good yields. Also, benzo[*h*]quinoline and 3-methylisoquinoline could be smoothly hydrogenated. Herein, we report on the first heterogeneous iron catalyst for the selective reduction of quinoxalines to 1,2,3,4-tetrahydroquinoxalines in good yields. The great selectivity of the catalyst towards different types of *N*-heterocycles was proven in the case of 1,10-phenanthroline and 6,7-dimethyl-2,3-di(pyridin-2-yl)quinoxaline. This selectivity pattern could enable further applications in the synthesis of bioactive compounds.

6.3 Acknowledgements

We thank the DFG for financial support.

6.4 References

- [1] a) T. J. Donohoe, R. Garg and C. A. Stevenson, *Tetrahedron: Asymmetry* **1996**, 7, 317-344. b) A. Gualandi, D. Savoia, *RSC Adv.* **2016**, 6, 18419-18451. c) Z. Wei, F. Shao, J. Wang, *Chin. J. Chem.* **2019**, 40, 980-1002.
- [2] a) X.-F. Tu, L.-Z. Gong, *Angew. Chem. Int. Ed.* **2012**, 51, 11346-11349. b) G. E. Dobereiner, A. Nova, N. D. Schley, N. Hazari, S. J. Miller, O. Eisenstein, R. H. Crabtree, *J. Am. Chem. Soc.* **2011**, 133, 7547-7562. c) T. Wang, L.-G. Zhuo, Z. Li, F. Chen, Z. Ding, Y. He, Q.-H. Fan, J. Xiang, Z.-X. Yu, A. S. C. Chan, *J. Am. Chem. Soc.* **2011**, 133, 9878 d) S. Urban, N. Ortega, F. Glorius, *Angew. Chem. Int. Ed.* **2011**, 50, 3803-3806. e) R. Kuwano, Y. Hashiguchi, R. Ikeda, K. Ishizuka, *Angew. Chem. Int. Ed.* **2015**, 54, 2393-2396. f) Z. Yang, F. Chen, S. Zhang, Y. He, N. Yang, Q.-H. Fan, *Org. Lett.* **2017**, 19, 1458-1461. g) Á. Vivancos, M. Beller, M. Albrecht, *ACS Catal.* **2018**, 8, 17-21.
- [3] a) R. H. Fish, A. D. Thormodsen, G. A. Cremer, *J. Am. Chem. Soc.* **1982**, 104, 5234-5237. b) C. Y. Legault, A. B. Charette, *J. Am. Chem. Soc.* **2005**, 127, 8966-8967.
- [4] a) N. A. Beckers, S. Huynh, X. Zhang, E. J. Luber, J. M. Buriak, *ACS Catal.* **2012**, 2, 1524-1534. b) D. Ren, L. He, L. Yu, R.-S. Ding, Y.-M. Liu, Y. Cao, H.-Y. He, K.-N. Fan, *J. Am. Chem. Soc.* **2012**, 134, 17592-17598. c) M. Fang, R. A. Sánchez-Delgado, *J. Catal.* **2014**, 311, 357-368. d) A. Karakulina, A. Gopakumar, I. Akçok, B. L. Roullet, T. LaGrange, S. A. Katsyuba, S. Das, P. J. Dyson, *Angew. Chem. Int. Ed.* **2016**, 55, 292-296. e) X. Wang, W. Chen, L. Zhang, T. Yao, W. Liu, Y. Lin, H. Ju, J. Dong, L. Zheng, W. Yan, X. Zheng, Z. Li, X. Wang, J. Yang, D. He, Y. Wang, Z. Deng, Y. Wu, Y. Li, *J. Am. Chem. Soc.* **2017**, 139, 9419-9422. f) S. Zhang, Z. Xia, T. Ni, Z. Zhang, Y. Ma and Y. Qu, *J. Catal.*

- 2018**, 359, 101-111. g) Y. Wu, H. Yu, Y. Guo, X. Jiang, Y. Qi, B. Sun, H. Li, J. Zheng, X. Li, *Chem. Sci.* **2019**, 10, 10459-10465.
- [5] Selected examples for homogeneous catalysts: a) S. Chakraborty, W. W. Brennessel, W. D. Jones, *J. Am. Chem. Soc.* **2014**, 136, 8564-8567. b) R. Xu, S. Chakraborty, H. Yuan, W. D. Jones, *ACS Catal.* **2015**, 5, 6350-6354. c) R. Adam, J. R. Cabrero-Antonino, A. Spannenberg, K. Junge, R. Jackstell, M. Beller, *Angew. Chem. Int. Ed.* **2017**, 56, 3216-3220. d) V. Papa, Y. Cao, A. Spannenberg, K. Junge, M. Beller, *Nat. Catal.* **2020**, 3, 135-142.
- [6] Selected examples for heterogeneous catalysts: a) C. Liu, Z. Rong, Z. Sun, Y. Wang, W. Du, Y. Wang, L. Lu, *RSC Adv.* **2013**, 3, 23984-23988. b) F. Chen, A.-E. Surkus, L. He, M.-M. Pohl, J. Radnik, C. Topf, K. Junge, M. Beller, *J. Am. Chem. Soc.* **2015**, 137, 11718-11724. c) Z. Wei, Y. Chen, J. Wang, D. Su, M. Tang, S. Mao, Y. Wang, *ACS Catal.* **2016**, 6, 5816-5822. d) J. Li, G. Liu, X. Long, G. Gao, J. Wu, F. Li, *J. Catal.* **2017**, 355, 53-62. e) F. Chen, W. Li, B. Sahoo, C. Kreyenschulte, G. Agostini, H. Lund, K. Junge, M. Beller, *Angew. Chem.* **2018**, 130, 14696-14700. f) G. Jaiswal, M. Subaramanian, M. K. Sahoo, E. Balaraman, *ChemCatChem* **2019**, 11, 2449-2457.
- [7] ABUNDANCE OF ELEMENTS IN THE EARTH'S CRUST AND IN THE SEA, *CRC Handbook of Chemistry and Physics*, 97th edition (**2016–2017**). b) Aktuelle Edelmetallpreise available at <https://www.gold.de/kurse/> (04.05.2020). c) Pig iron price available at <https://www.metal.com/> (04.05.2020).
- [8] J. E. Shaw and P. R. Stapp, *J. Heterocycl. Chem.* **1987**, 24, 1477-1483.
- [9] B. Sahoo, C. Kreyenschulte, G. Agostini, H. Lund, S. Bachmann, M. Scalone, K. Junge, M. Beller, *Chem. Sci.* **2018**, 9, 8134-8141.
- [10] a) S. J. Benkovic, P. A. Benkovic, D. R. Comfort, *J. Am. Chem. Soc.* **1969**, 91, 5270-5279. b) M. P. Mertes, A. J. Lin, *J. Med. Chem.* **1970**, 13, 77-82.
- [11] C. T. Eary, Z. S. Jones, R. D. Groneberg, L. E. Burgess, D. A. Mareska, M. D. Drew, J. F. Blake, E. R. Laird, D. Balachari, M. O'Sullivan, A. Allen, V. Marsh, *Bioorg. Med. Chem. Lett.* **2007**, 17, 2608-2613.
- [12] J. G. De Vries, C. J. Elsevier, *Handbook of Homogeneous Hydrogenation*; Wiley- VCH, Weinheim, Germany, 2007.
- [13] a) S. Rösler, J. Obenauf, R. Kempe, *J. Am. Chem. Soc.* **2015**, 137, 7998–8001. b) S. Rösler, M. Ertl, T. Irrgang, R. Kempe, *Angew. Chem. Int. Ed.* **2015**, 54, 15046–15050. c) N. Deibl, R. Kempe, *J. Am. Chem. Soc.* **2016**, 138, 10786–10789.
- [14] a) F. Kallmeier, T. Irrgang, T. Dietel, R. Kempe, *Angew. Chem. Int. Ed.* **2016**, 55, 11806–11809. b) N. Deibl, R. Kempe, *Angew. Chem. Int. Ed.* **2017**, 56, 1663–1666. c) F. Kallmeier, B. Dudziec, T. Irrgang, R. Kempe, *Angew. Chem. Int. Ed.* **2017**, 56, 7261–7265. d) G. Zhang, T. Irrgang, T. Dietel, F. Kallmeier, R. Kempe, *Angew. Chem. Int. Ed.* **2018**, DOI: 10.1002/anie.201801573. e) F. Freitag,

- T. Irrgang, R. Kempe, *J. Am. Chem. Soc.* **2019**, *141*, 11677–11685. f) R. Fertig, T. Irrgang, F. Freitag, J. Zander, R. Kempe, *ACS Catal.* **2018**, *8*, 8525–8530.
- [15] D. Forberg, T. Schwob, M. Zaheer, M. Friedrich, N. M. Iyajima, R. Kempe, *Nat. Commun.* **2016**, *7*, 13201–13206.
- [16] D. Forberg, T. Schwob, R. Kempe, *Nat. Commun.* **2018**, *9*, 1751–1757.
- [17] a) T. Schwob, R. Kempe, *Angew. Chem. Int. Ed.* **2016**, *55*, 15175–15179. b) T. Schwob, M. Ade, R. Kempe, *ChemSusChem* **2019**, *12*, 3013–3017. c) C. Bäuml, R. Kempe, *Chem. Eur. J.* **2018**, *24*, 8989–8993. d) G. Hahn, P. Kunnas, N. de Jonge and R. Kempe, *Nat. Catal.* **2019**, *2*, 71–77.
- [18] C. Bäuml, C. Bauer, R. Kempe, *ChemSusChem* **2020**, *13*, doi.org/10.1002/cssc.202000856.
- [19] L. F. B. Ribeiro, O. Flores, P. Furtat, C. Gervais, R. Kempe, R. A. F. Machado and G. Motz, *J. Mater. Chem. A* **2017**, *5*, 720–729.

6.5 *Supporting Information*

6.5.1 General considerations

All air- and moisture sensitive reactions were performed under dry argon or nitrogen atmosphere using standard Schlenk and glove box techniques. All dried solvents were obtained from a solvent purification system (activated alumina cartridges) or purchased from Acros. Deuterated solvents were dried via molecular sieves. All chemicals were acquired from commercial sources with purity over 95 % and used without further purification. The precursor SMP 10 was purchased from Starfire Systems, New York, USA.

Hydrogen chemisorption measurements were performed by using a ChemBET Pulsar TPR/TPD instrument from Quantachrome.

Pyrolysis and reduction were performed under nitrogen or forming gas (90/10) atmosphere in a high temperature furnace (EHA 12/450B200, Carbolite) or in a ChemBET Pulsar TPR/TPD instrument from Quantachrome.

Fourier transform infrared (FTIR) spectroscopy measurements were performed with a Cary 630 FTIR spectrometer (Agilent Technologies) over a range from 2000 cm⁻¹ to 700 cm⁻¹.

NMR measurements were carried out with a Varian INOVA 300 and 400 (300 MHz for ¹H, 75 MHz for ¹³C; 400 MHz for ¹H, 100 MHz for ¹³C) at 296 K. Chemical shifts are reported in ppm relative to the residual solvent signal (DMSO-d₆: 7.26 ppm (¹H), 77.16 ppm (¹³C); DMSO-d₆: 2.50 ppm (¹H), 39.51 ppm (¹³C)), coupling constants (J) are reported in Hz.

All tested reactions were determined via GC and GC-MS analysis. GC analyses were carried out on an Agilent 6850 GC system equipped with an Optima 17 column (30 m x 0.32 mm x 0.25 μm). GC-MS analyses were carried out on an Agilent 7890A GC system equipped with a HP-5MS column (30 m x 0.32 mm x 0.25 μm) and a 5975C inert MSD.

The hydrogenation experiments were carried out with Parr Instrument stainless steel autoclaves N-MT5 300 mL equipped with heating mantles and temperature controller.

6.5.2 General catalytic procedures

Hydrogenation of N-Heteroarenes

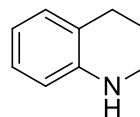
A magnetic stirring bar, 0.5 mmol substrate, 3.5 mL methanol and 10 mol % Fe catalyst (2.8 mg Fe, 0.05 mmol, 70 mg) were filled in a 5 mL reaction vial. The vial was placed in a high-pressure autoclave (Parr Instruments) and the autoclave was flushed three times with 2.0 MPa of hydrogen. The autoclave was pressured with 6.5 MPa of hydrogen and the reaction was stirred for 20 h at 140-150 °C. The autoclave was cooled to room temperature and the hydrogen pressure was released. Yields were determined by either GC using *n*-dodecane as an internal standard in combination with GC-MS analysis or by isolation of the product. Then, the solution was centrifugated to remove the catalyst and column chromatography (silica, ethyl acetate-methanol mixture as eluent) was executed for purification and for isolating the products. The obtained hydrogenated N-heterocycles were further analyzed by ^1H and ^{13}C spectroscopy.

6.5.3 Characterization of isolated products

1:

1,2,3,4-tetrahydroquinoline

[C₉H₁₁N₁] 133.09 g/mol (M)



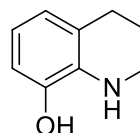
^1H NMR (400 MHz, CDCl₃, 296 K): δ = 6.85-6.80(m, 2H), 6.43-6.37 (m, 2H), 5.55 (s, 1H), 3.18-3.14 (t, 2H), 2.66-2.62 (t, 2H), 1.82-1.74 (q, 2H) ppm.

^{13}C NMR (100 MHz, CDCl₃, 296 K): δ = 145.34, 128.89, 126.33, 119.80, 114.99, 113.31, 40.82, 26.74, 21.60 ppm.

5:

1,2,3,4-tetrahydroquinolin-8-ol

[C₉H₁₁NO] 149.08 g/mol (M)



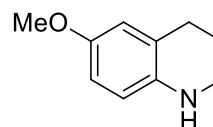
^1H NMR (400 MHz, CDCl_3 , 296 K): δ = 8.94 (s, 1H), 6.48-6.25 (m, 3H), 4.65 (s, 1H), 3.21-3.18 (t, 2H), 2.66-2.61 (t, 2H), 1.82-1.74 (q, 2H) ppm.

^{13}C NMR (100 MHz, CDCl_3 , 296 K): δ = 143.25, 133.88, 120.41, 119.98, 114.78, 111.47, 40.97, 26.56, 21.87 ppm.

7:

6-methoxy-1,2,3,4-tetrahydroquinoline

$[\text{C}_{10}\text{H}_{13}\text{NO}]$ 163.10 g/mol (M)



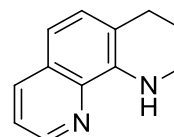
^1H NMR (400 MHz, CDCl_3 , 296 K): δ = 6.51-6.47(m, 2H), 6.38-6.35 (m, 1H), 5.14 (s, 1H), 3.60 (s, 3H), 3.12-3.08 (t, 2H), 2.65-2.61 (t, 2H), 1.80-1.72 (q, 2H) ppm.

^{13}C NMR (100 MHz, CDCl_3 , 296 K): δ = 150.27, 139.56, 121.04, 114.54, 114.31, 112.67, 55.24, 41.17, 26.89, 21.89 ppm.

8:

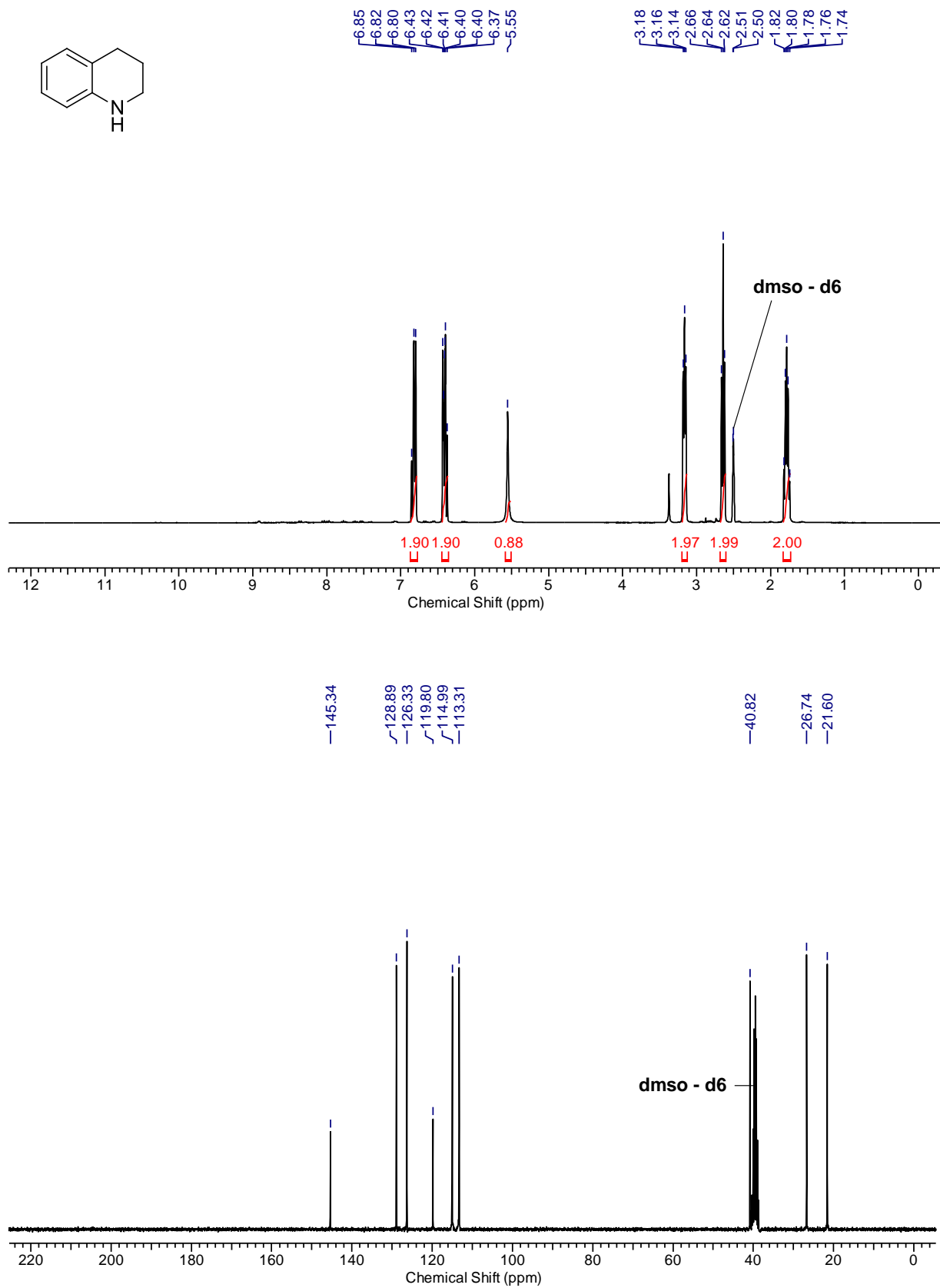
1,2,3,4-tetrahydro-1,10-phenanthroline

$[\text{C}_{12}\text{H}_{12}\text{N}_2]$ 184.1 g/mol (M)

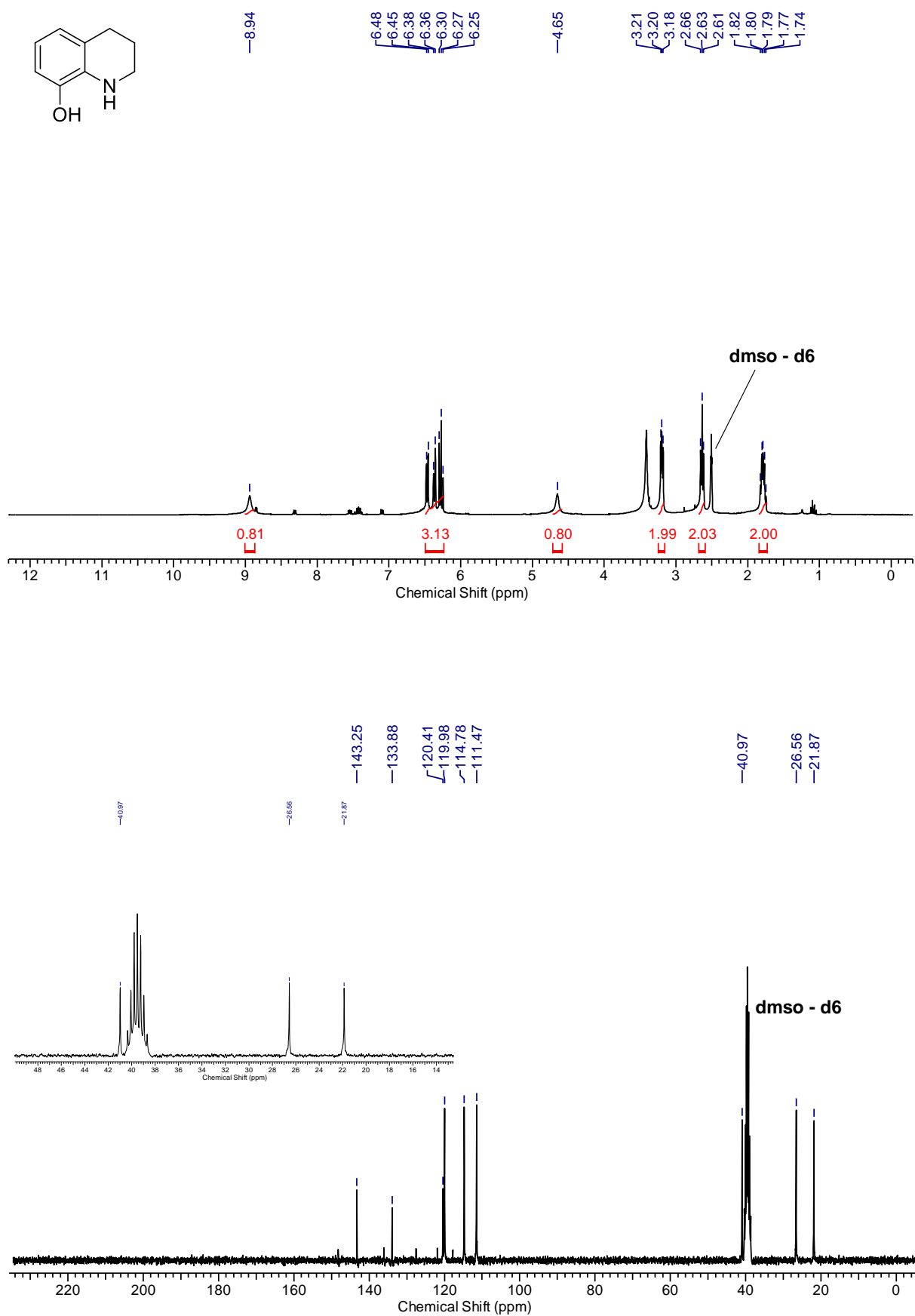


^1H NMR (300 MHz, CDCl_3 , 296 K): δ = 8.67-8.66 (d, 1H), 8.13-8.10 (d, 1H), 7.41-7.37 (m, 1H), 7.14-7.11 (d, 2H), 6.96-6.93 (d, 1H), 6.40 (s, 1H), 3.43-3.39 (t, J = 5.86 Hz, 2H), 2.85-2.81 (t, J = 5.86, 2H), 1.95-1.87 (q, J = 5.86, 2H) ppm.

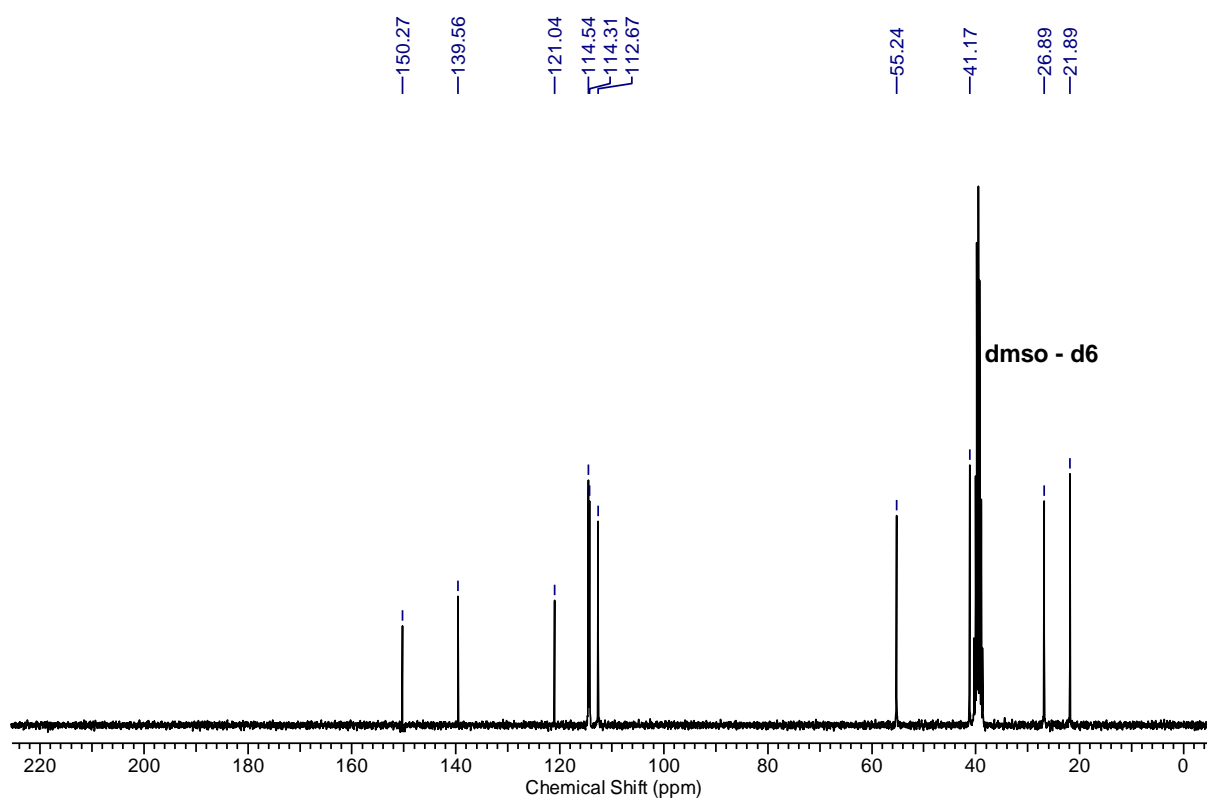
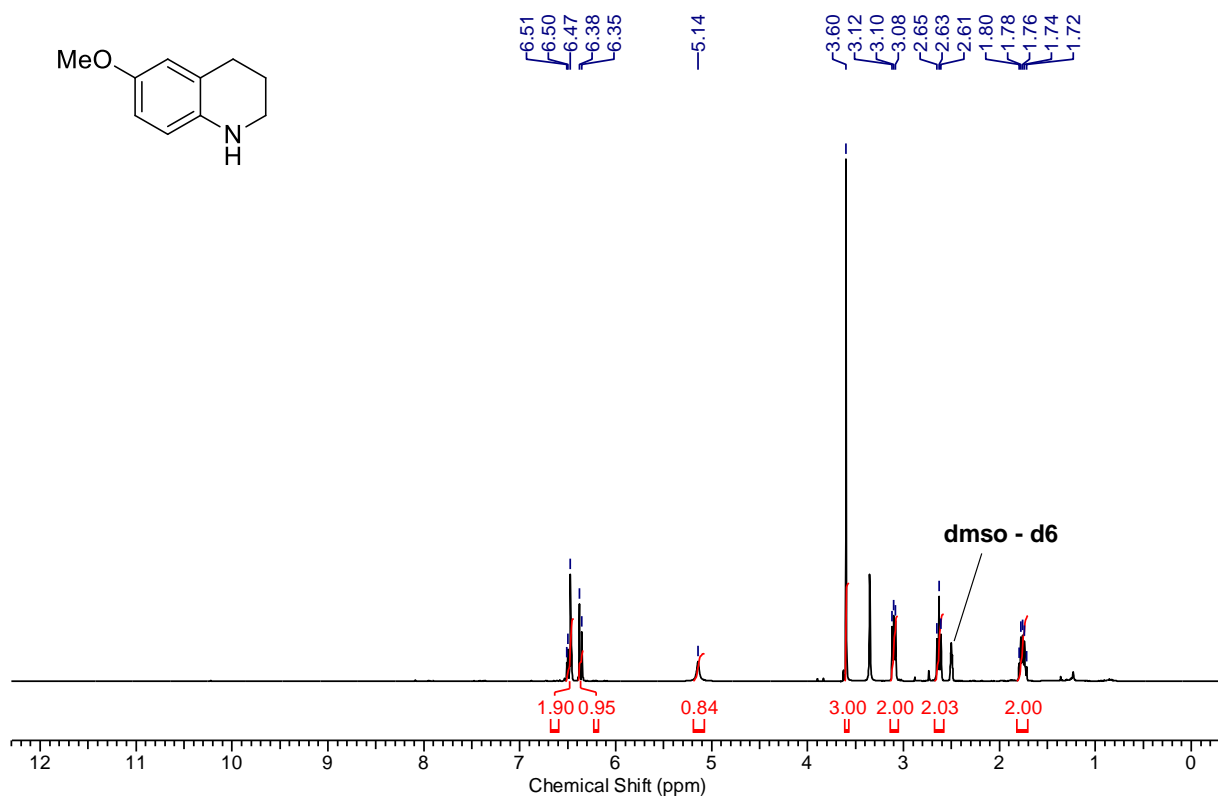
^{13}C NMR (75 MHz, CDCl_3 , 296 K): δ = 160.42, 151.98, 136.13, 131.35, 129.11, 128.77, 125.90, 120.84 ppm.

NMR spectra**1**

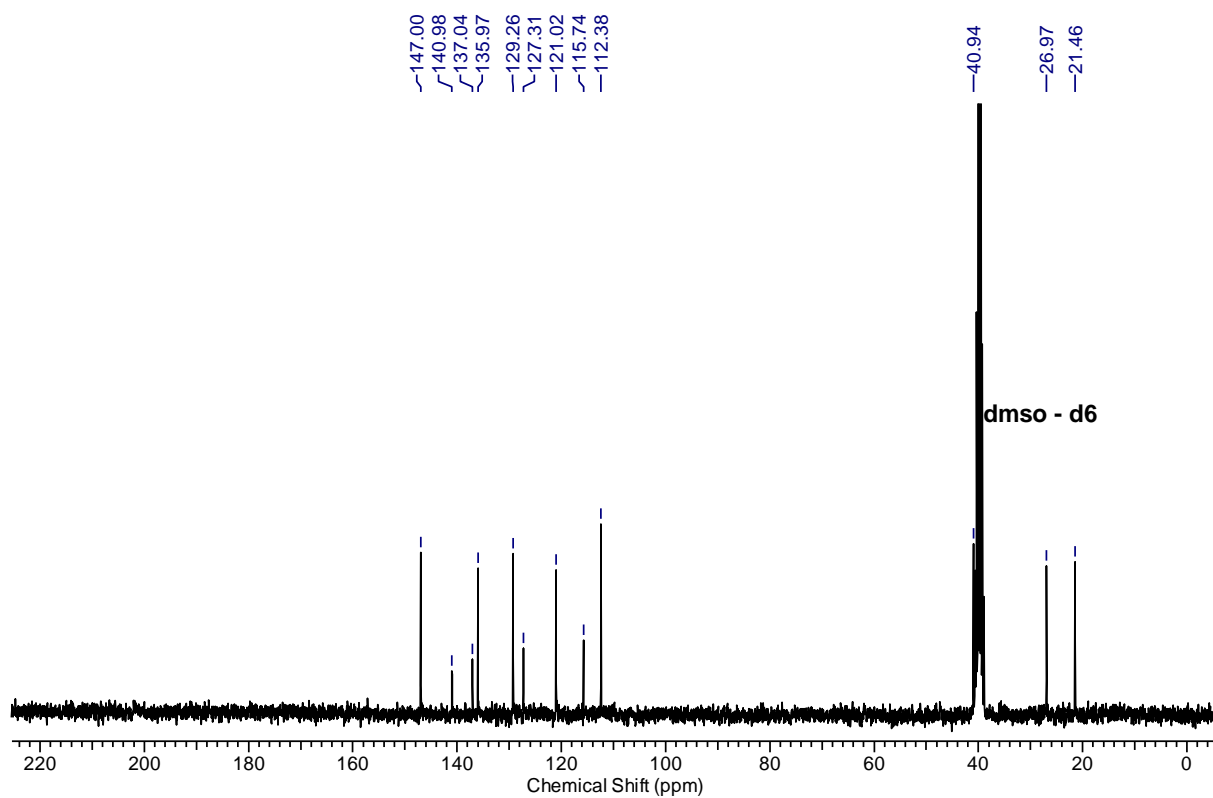
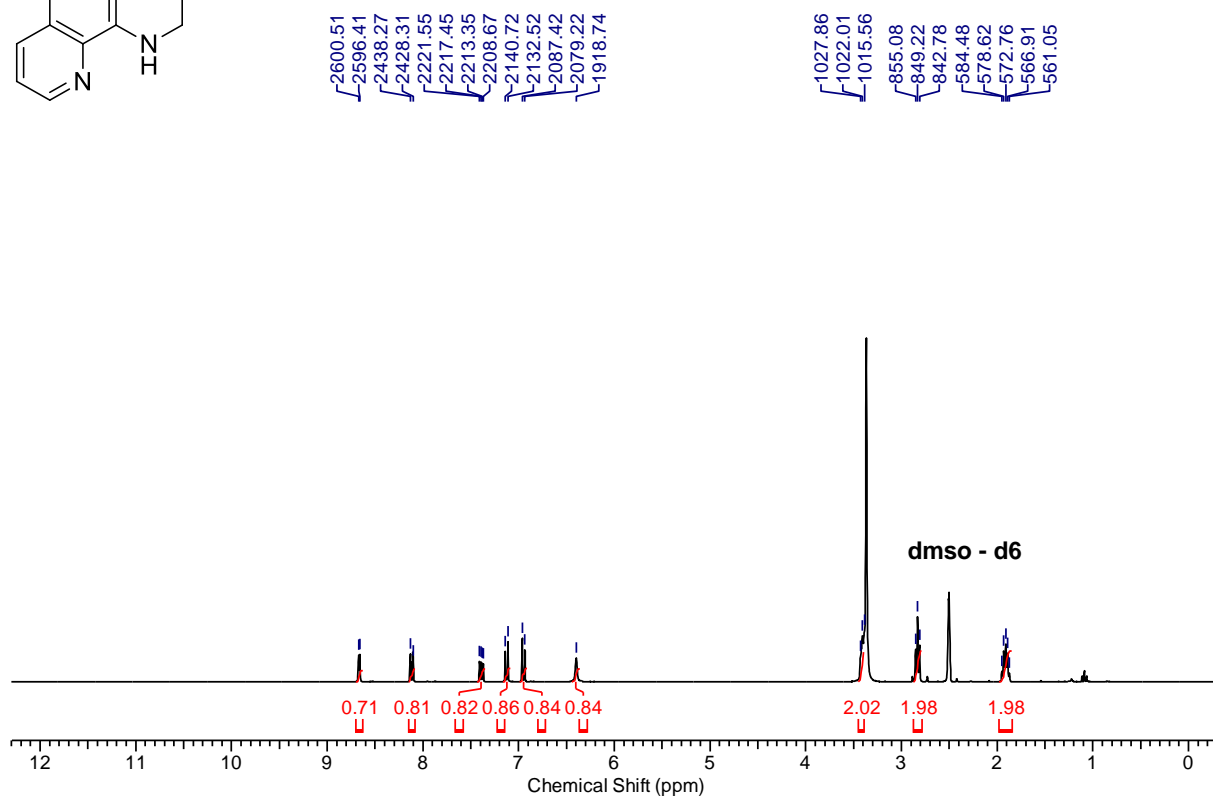
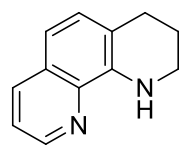
5



7



8



7. List of publications

The following publications were published or are to be submitted.

1. C. Bäumlér, R. Kempe, *Chem. Eur. J.* **2018**, 24, 8989-8993.
"The Direct Synthesis of Imines, Benzimidazoles and Quinoxalines from Nitroarenes and Carbonyl Compounds by Selective Nitroarene Hydrogenation Employing a Reusable Iron Catalyst"
2. C. Bäumlér, C. Bauer, R. Kempe, *ChemSusChem* **2020**, 13, 3110-3114.
"The Synthesis of Primary Amines through Reductive Amination Employing an Iron Catalyst"
3. C. Bäumlér, R. Kempe, to be submitted.
"Hydrogenation of various N-heterocycles Employing an Heterogeneous Iron Catalyst"

8. Acknowledgements

First, I want to thank my academic supervisor,

Prof. Rhett Kempe,

for giving me the opportunity to do my PhD on this very interesting topic. I am very grateful for his confidence, which enabled me to work under great scientific freedom. Also, I would like to thank him for his constant interest in the progress of the work and for the numerous constructive scientific discussions.

I want to thank Dr. Christine Denner for the excellent supervision over the last years, the REM and EDX measurements and for her very friendly, positive and professional support.

A special thank goes to all my lab-mates, Daniel Forberg, Sonja Fehn, Stefan Schwarz, Mirco Eckardt, Gabriela Wietzel, Tobias Schwob, Timon Schönauer, Mara Klarner, Leah Kaiser, Christina Thiersch, Annalena Engelhard, Barbara Klausfelder, Matthias Elfinger, for the great and friendly atmosphere and the good support in lab. In particular, I would like to thank you for your professional support and for your constant willingness to help with questions and problems. Furthermore, I want to thank all the members of the AC II chair for the great time and the helpful practical advices: Tony Hille, Nicklas Deibl, Dr. Winfried Kretschmer, Dr. Torsten Irrgang, Andreas Gollwitzer, Thomas Dietel, Dominik Tilgner, Frederick Freitag, Fabian Kallmeier, Robin Fertig, Martin Schlagbauer, Tobias Schwarz, Alexander Goller and Patrick Wolff.

Thanks to all my students, especially Annalena Engelhard and Christof Bauer, for their practical support during their thesis work or various internships. You were a great help.

Also, I want to thank Anna-Maria Dietel, Heidi Maisel, Marlies Schilling and Christine Fell for their special support regarding administration matters. A special thanks goes to Marlies Schilling, which was a person you always could ask for help and did it with a smile.

My warmest thanks go to my parents, which were significantly responsible for doing my PhD. The constant motivation and support were incredible, and I would like to thank you for this.

A very special thanks goes to my girlfriend Ann-Katrin Watkins, for her ongoing emotional support, her big understanding and above all, her love.

9. Declaration / Erklärung

Eidesstattliche Versicherungen und Erklärungen

(§ 8 Satz 2 Nr. 3 PromO Fakultät)

Hiermit versichere ich eidesstattlich, dass ich die Arbeit selbstständig verfasst und keine anderen als die von mir angegebenen Quellen und Hilfsmittel benutzt habe (vgl. Art. 64 Abs. 1 Satz 6 BayHSchG).

(§ 8 Satz 2 Nr. 3 PromO Fakultät)

Hiermit erkläre ich, dass ich die Dissertation nicht bereits zur Erlangung eines akademischen Grades eingereicht habe und dass ich nicht bereits diese oder eine gleichartige Doktorprüfung endgültig nicht bestanden habe.

(§ 8 Satz 2 Nr. 4 PromO Fakultät)

Hiermit erkläre ich, dass Hilfe von gewerblichen Promotionsberatern bzw. -vermittlern oder ähnlichen Dienstleistern weder bisher in Anspruch genommen wurde noch künftig in Anspruch genommen wird.

(§ 8 Satz 2 Nr. 7 PromO Fakultät)

Hiermit erkläre ich mein Einverständnis, dass die elektronische Fassung der Dissertation unter Wahrung meiner Urheberrechte und des Datenschutzes einer gesonderten Überprüfung unterzogen werden kann.

(§ 8 Satz 2 Nr. 8 PromO Fakultät)

Hiermit erkläre ich mein Einverständnis, dass bei Verdacht wissenschaftlichen Fehlverhaltens Ermittlungen durch universitätsinterne Organe der wissenschaftlichen Selbstkontrolle stattfinden können.

Bayreuth,

Christoph Bäumler

